Development of an equation of state for nematic liquid crystals

Towards a molecular-based description

Development of an equation of state for nematic liquid crystals

Towards a molecular-based description

Proefschrift

ter verkrijging van de graad van doctor
aan de Technische Universiteit Delft,
op gezag van de Rector Magnificus prof. ir. K. C. A. M. Luyben,
voorzitter van het College voor Promoties,
in het openbaar te verdedigen op Vrijdag, 11 September, 2015 om 15:00 uur

door

Thijs van Westen

Master of Science, Delft University of Technology,
geboren te Middelharnis, Nederland.

Dit proefschrift is goedgekeurd door de promotoren:

Prof. Dr. -Ing. Joachim Gross
Prof. dr. ir. Thijs J. H. Vlugt

Samenstelling promotiecommissie:

Rector Magnificus,	voorzitter
Prof. Dr. -Ing. J. Gross,	Universität Stuttgart, promotor
Prof. dr. ir. T. J. H. Vlugt,	Technische Universiteit Delft, promotor

Onafhankelijke leden:

Prof. dr. G. Jackson,	Imperial College London
Prof. dr. B. Mulder,	Universiteit Wageningen
Prof. dr. S. Calero,	Universidad-Pablo de Olavide Sevilla
Prof. dr. S. J. Picken,	Technische Universiteit Delft
Prof. dr. D. J. E. M. Roekaerts,	Technische Universiteit Delft

This research is supported by the Stichting voor Technische Wetenschappen (Dutch Technology Foundation, STW), applied science division of the Nederlandse organisatie voor Wetenschappelijk Onderzoek (Netherlands Organization for Scientific Research, NWO) and the Technology Program of the Ministry of Economic Affairs. In addition, this work was sponsored by the Stichting Nationale Computerfaciliteiten (National Computing Facilities Foundation, NCF) for the use of supercomputing facilities, with financial support from NWO-EW.

Keywords: Liquid crystals, nematic, equation of state, chain molecules, perturbation theory

Printed by: XXX

Front & Back: T. van Westen

ISBN/EAN 978-94-6186-509-0

An electronic version of this dissertation is available at
`http://repository.tudelft.nl/`.

Contents

1

Introduction

In this thesis I aim to contribute to a molecular understanding and -description of the phase behaviour of liquid crystalline materials. In particular, I aim at the development of a molecular-based equation of state (EoS) for describing nematic (only orientationally ordered) liquid crystals (LCs) and their mixtures. Special emphasis is put on the role of intra-molecular flexibility on the liquid crystalline phase behaviour. Also, the solubility of small gases in nematic solvents is studied—an area that could be important for potential applications of LCs as novel solvents in gas-absorption processes. In the first part of this introductory chapter, the reader is provided with some background on the liquid crystalline state of matter, the status of LC research, and common and potential applications of LCs (Sections 1.1 and 1.2). Subsequently, available theories for the nematic state are briefly reviewed, and the foundations of the perturbation methodology which is at the basis of the EoS developed in this work are discussed (Section 1.3). Finally, an outline of the work performed in this thesis is presented (Section 1.4).

1

1.1 Background

Most matter can exist in a solid, liquid, or gaseous state. Whereas molecules in the solid state are arranged following a strict, long-ranged positional and orientational ordering, in the liquid state all ordering randomizes over a few molecular diameters. Some substances can enter liquid crystalline states, commonly referred to as mesophases, which are characterized by a molecular ordering that is in between that of a liquid and a perfectly ordered crystal [1–4]. Many ordering structures are possible; each structure corresponding to a certain liquid crystalline phase. Some examples are included in Fig. 1.1, where I show a nematic (N) phase and a smectic (Sm) phase, each characterized by, respectively, long-ranged partial orientational ordering, and long-ranged partial orientational and -positional ordering.

A key characteristic of molecules/particles that form mesophases (in this work referred to as LC molecules or mesogens) is a certain *anisotropy* in their shape or interactions with other molecules/particles. As an example, a nearly spherical molecule like methane will not form any mesophases. But how about hexane? Clearly, being a chain molecule, the molecular shape of hexane can be regarded as anisotropic. Nonetheless, mesophases of hexane are not observed. The reason is that the carbon atoms forming the backbone of a hexane molecule are sp^3 hybridized and therefore form a bond with neighbouring atoms that is relatively flexible to bending and torsional rotations. As a result, the atoms in the chain are free to visit many different chain conformations, thereby diminishing much of the anisotropy of the molecular shape. Some examples of organic molecules that do show mesophase behaviour are depicted in Fig. 1.2. As can be observed, the shape of the molecules is characterized by a rigid, anisotropic molecular core (the ring structures linked by rigid sp^2 bonds) and a semi-flexible alkyl tail. Given the importance of the rigid anisotropic core for inducing the formation of mesophases, this part of a LC molecule is usually referred to as the mesogenic unit. I should stress however, that anisotropic attractive interactions, such as those arising from the dipolar nitrile-group (R-CN) at the head of the PCH5 molecule, are also an important factor to be considered. I further note, that besides elongated molecules (Fig. 1.2) also oblate (*i.e.* sheet-like, or disk-like) molecules form liquid crystalline phases. In Section 1.3.2, I further discuss molecular attributes to liquid crystalline phase formation.

Due to the importance of temperature on the formation of mesophases of low-molecular-weight organic molecules such as those drawn in Fig. 1.2, these substances are generally referred to as thermotropic LCs. A different class of LCs arises, however, if the characteristic length scale of a mesogen becomes large compared to the atomistic length scale. For such systems, the effect of temperature is usually far less important, and the phase behaviour is primarily determined by the density (or concentration) of the mesogens. These systems are referred to as lyotropic LCs. Some examples of systems exhibiting lyotropic liquid crystalline phase behaviour are solutions of polymers, amphiphilic molecules, or colloids [6–8]. In principle, the classification of a liquid crystal as being either thermotropic or lyotropic is somewhat artificial since most real nematogens display features of both. Although even today it is common to describe a LC by a theory developed for either one of these classes (*i.e.* the theory of Onsager for lyotropic LCs [9] vs. the theory of Maier and Saupe

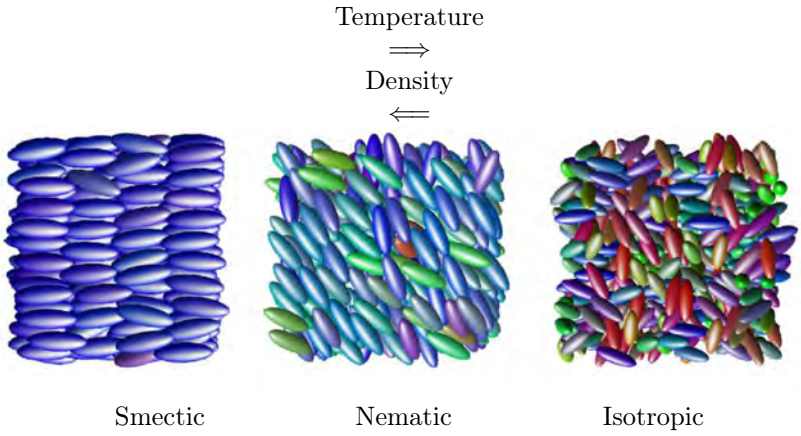

Figure 1.1: Schematic representation of different ordering structures found in liquid crystalline materials. Included are a smectic phase (characterized by partial orientational ordering and partial 1-dimensional positional ordering), a nematic phase (characterized by partial orientational ordering) and an isotropic liquid phase. The colour of the particles is a measure for their orientation. (Part of this image was taken from Figure 1 of Ref. [5]. © IOP Publishing. Reproduced by permission of IOP Publishing. All rights reserved.)

for thermotropic LCs [10–12]), from early on (for example in the work of Flory [13], Gelbart and Baron [14, 15], or Cotter [16, 17]) there has been an awareness that the description of both should originate from one unified theoretical framework. Recent theoretical effort (by for example the group of Jackson [18–21]) is along this line. In Section 1.3.2, I will provide some more background on this point.

As a result of the ordering of molecules in a LC material, many of the material's physical properties (*e.g.* index of refraction, elastic modulus, etc.) are anisotropic. Although, at first sight, this is no different than in crystalline solids, the fluidity of LC materials offers an advantage in that the ordering of molecules—and thus the physical properties of the material—can be easily tuned by external stimuli such as temperature, fields (shear, electric or magnetic) or a change in chemical environment [4]. This coupled effect of (1) easily tunable-, and (2) anisotropic material properties has led to a large number of technological applications. For example, due to the anisotropy that is induced by the orientational ordering of molecules, nematic phases are birefringent; meaning that light linearly polarized along one axis of a certain reference frame has a different speed of travelling through the material than light polarized along another axis. This combined with the possibility of influencing the degree of ordering (and thus the birefringence) by the application of an electric field has laid the basis for the now ubiquitous liquid crystalline display (LCD) technology used for example in laptops and television screens [2, 4]. Besides LCDs, one can think of numerous other examples of LC technology, such as switchable windows, highly accurate LC thermometers, ultra-strong polymer fibres (such as Kevlar), and chemical/biological sensors [4].

While the study of the opto-electronic properties of LCs for LCD purposes remains a dominant research area, the past few decades have shown the emergence of

(a) $C_{18}H_{25}N$

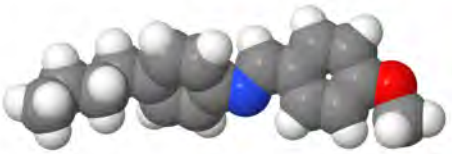

(b) $C_{18}H_{21}NO$

Figure 1.2: A schematic representation of two typical thermotropic liquid crystal molecules. In (a) I show 4-(trans-4'pentylcyclohexyl)-benzonitrile (PCH5), whereas in (b) I show N-(4-Methoxybenzylidene)-4-butylaniline (MBBA). White denotes hydrogen, gray denotes carbon, blue denotes nitrogen, and red denotes oxygen.

other interesting fields in which LCs could play a vital role. An example is the use of LCs as *structured solvents*. In the materials- and nano sciences, for example, the self-organizing mechanisms observed in liquid crystalline systems have been identified as a promising route to develop new, smart nanostructured materials or to produce nanoparticles of controlled sizes. As an example, the supramolecular ordering observed in certain mesophases can be utilized as a template for the production of mesoporous materials. Moreover, the partitioning of space as observed in certain lyotropic LCs (*e.g.* micelles) can be used to produce nanoparticles of well-defined sizes. In a subsequent step, LCs can provide the means to organize these nanoparticles into structured arrangements, thereby enabling a transferring of the properties of the nanoparticles to macroscopic scales. For a recent review on the use of LCs in materials- and nanosciences, the reader is referred to Ref. [22].

Recently, the use of LCs as structured solvents has also made its way into process technology. In a recent patent application [23], LCs were proposed as novel solvents for gas-absorption processes. It has been shown that the orientational ordering induced by the isotropic-to-nematic transition leads to a step-wise decrease in solubility of small solutes [24–26]. Therefore, when using a nematic LC as the solvent in a gas-absorption process, the phase transition could in many respects be utilized as a solubility switch. This potential application of LCs has been one of the main motivations for carrying out the work performed in this thesis.

Clearly, whether one is interested in developing new LC materials for specific tasks or designing new processes based on LCs, proper knowledge on the thermophysical properties of LCs—specifically on the link of molecular aspects to thermodynamic properties—is essential. Despite a long history of liquid-crystalline-state theory, it seems fair to say that analytical models (or equations of state) with such capabilities are still not fully developed. The work performed in this thesis is meant to contribute to such developments.

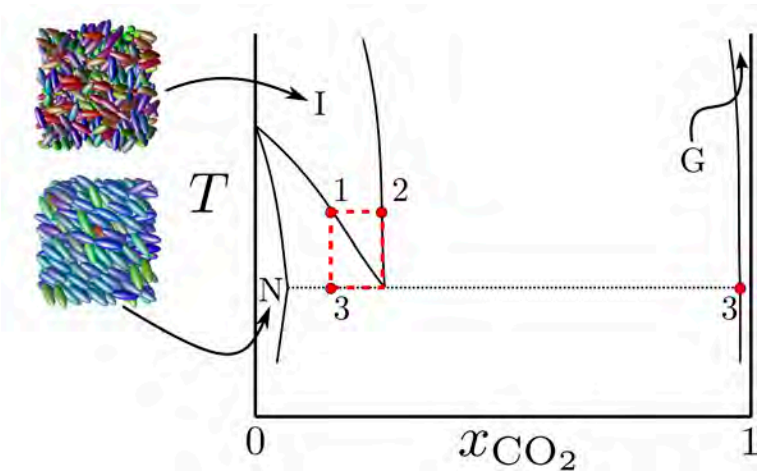

Figure 1.3: A schematic representation of a binary phase diagram of a LC with CO_2 [23, 24] , showing an isotropic (I), nematic (N) and gaseous (G) phase. The three-phase NIG equilibrium is denoted by the dotted line. The red box shows a possible absorption-desorption cycle for the removal of CO_2 from a process gas stream. At step 1-2, the solvent (in its isotropic liquid phase) is loaded with solute until saturation. After that, at step 2-3, the solvent is cooled down a few degrees to reach the NIG equilibrium. The decreased solubility of CO_2 in the nematic phase results in a desorption of CO_2 to a gas phase. Due to the low vapour pressure of the LC, the gas phase is almost pure in CO_2. Finally, at step 3-1, the nematic solvent is heated a few degrees until the initial isotropic solvent is regenerated. (Part of this image was taken from Figure 1 of Ref. [5].)

1.2 Liquid crystals as absorption liquids

One of the main motivations for the work performed in this thesis is a recent proposal for the use of nematic, thermotropic liquid crystals as novel solvents for gas-absorption processes [23]. Given that the phase transition from a normal (isotropic) liquid phase to a nematic phase is of first order, it results in a step-change of certain thermodynamic properties. The basic idea of the proposal from Ref. [23], is to utilize this phase transition to induce a step-wise decrease in the solubility of gases in the solvent.

To explain the principle, a schematic of a binary phase diagram of a LC with a small solute such as CO_2 is included in Fig. 1.3. In going through the diagram in a sequence 1-2 (loading), 2-3 (desorption), 3-1 (regeneration), a possible absorption-desorption cycle for a process based on a nematic LC solvent is pointed out. Whereas in conventional processes the lowering of the solubility required at the desorption step is accomplished by a substantial heating of the solvent (think of for example the amine-based process for carbon capture [27–29]), the scheme in Fig. 1.3 shows a possibility for *desorption upon cooling*. Moreover, since a phase transition (from isotropic to nematic) is employed to induce the change in solubility, the desorption takes place over a very narrow range in temperature and pressure. This should be placed in sharp contrast to the relatively large temperature and pressure swings used in common industrial absorption processes [30]. These insights combined with the

notion that the I-N transition generally involves a relatively small phase transition enthalpy, indicate that the use of LC solvents could potentially lead to a drastic decrease in the energy consumption of absorption-desorption processes.

For a successful implementation of a process such as that being sketched here, the nematic LC solvent should (1) have a relatively low viscosity (for low pressure drop and sufficiently high transport properties), (2) be selective towards the compound that needs to be absorbed (think of CO_2/CH_4 selectivity in natural gas sweetening [31]), (3) be stable to impurities, (4) have a suitable thermal operating window (stability of nematic phase), and, above all, (5) have a large maximum loading of solute. Given the large variety of thermotropic LCs [32], a suitable choice of functional groups within a LC molecule could possibly lead to fulfilment of the above criteria. Such a tailoring of LC molecules for specific tasks could in principle be done experimentally, but in practise the large number of molecular structures makes this approach infeasible. If one takes into account that the optimal LC solvent might well be a mixture of different LCs [33–35], the experimental burden becomes especially unrealistic. The systematic optimisation of LC solvents thus requires a predictive molecular model. When used in a solvent design method [36–40], this could allow for a rapid, targeted screening of LC molecules and their mixtures, thereby facilitating evaluation and (possible) implementation of the absorption-desorption process. The work performed in this thesis is meant to contribute to the development of a predictive equation of state for LCs and their mixtures.

I should note that the situation sketched above is not unique in materials science. Also for zeolites, metal-organic frameworks (MOFs), and ionic liquids, the design space is large; and novel molecular modelling techniques are usually required for finding optimal molecules or molecular structures for specific tasks. Some recent examples involve the use of GPU accelerated molecular simulations for screening of zeolites and MOFs for carbon and methane capture applications [41, 42], or the use of COSMO-RS for screening of ionic liquids for carbon capture [42].

1.3 Theory of anisotropic fluids

1.3.1. Describing orientational order

The orientational ordering of the molecules in a liquid crystal is imperfect. Since the properties of a liquid crystal critically depend on the degree of ordering, it is evident some sort of quantification is required. For this purpose, let us assume an (idealized) system of cylindrically symmetric, anisotropic molecules. I introduce the director ($\boldsymbol{n}$), which is defined as the average direction of all molecules in a phase. For a nematic phase, the director points in the direction of preferred orientation of the molecules; therefore, it is convenient to define the orientation ($\boldsymbol{\omega} = (\theta, \phi)$) of a single molecule with respect to this director (Fig. 1.4).

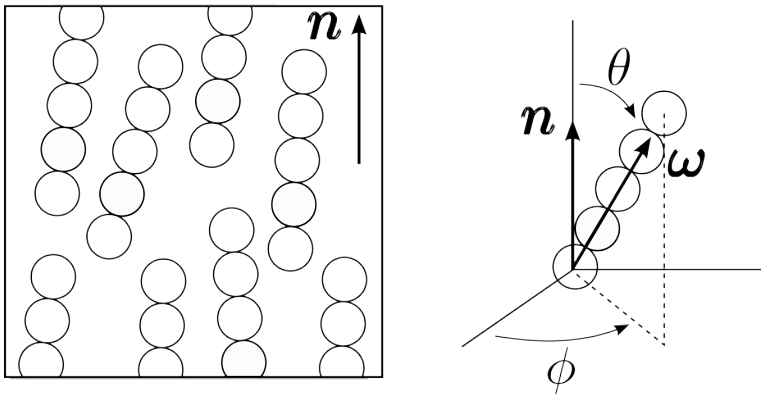

Figure 1.4: Definition of the orientation of a molecule. The director $\boldsymbol{n}$ is a vector pointing in the preferred direction of the molecules in a phase. The orientation $\boldsymbol{\omega} = (\theta, \phi)$ of a molecule is defined as the polar angle θ and azimuthal angle ϕ with respect to this director. Due to the cylindrical symmetry of the nematic phase, the state of orientational ordering is independent of ϕ.

For the cylindrically symmetric molecules considered here, the probability for a molecule to be in a certain orientation $\boldsymbol{\omega}$ solely depends on the polar angle θ. Therefore, the distribution of all molecular orientations can be described by the probability density $f(\boldsymbol{\omega}) = f(\theta)$. In the remainder of this thesis this probability density will be referred to as the orientational distribution function (ODF). Clearly, for a nematic phase the ODF will be peaked for molecular orientations close to the director ($\theta \approx 0$). For an isotropic phase, all molecular orientations have equal probability and the ODF is a constant. In fact, on imposing the normalization condition $\int f(\boldsymbol{\omega})\mathrm{d}\boldsymbol{\omega} = 1$, I can write

$$f_{\mathrm{iso}}(\boldsymbol{\omega}) = \frac{1}{\int \mathrm{d}\boldsymbol{\omega}} = \frac{1}{\int_0^{2\pi}\int_0^{\pi} \sin(\theta)\mathrm{d}\theta\mathrm{d}\phi} = \frac{1}{4\pi} \tag{1.1}$$

Although the ODF contains all the information needed for describing the *state* of ordering in a material, it is often sufficient to specify a scalar valued measure for the *degree* of ordering. For nematic phases, the degree of ordering is characterized by an orientational average of the second order Legendre polynomial of $\cos(\theta)$, according to [3]

$$\begin{aligned} S_2 &= \langle P_2(\cos\theta)\rangle_{\boldsymbol{\omega}} \\ &= \frac{1}{2}\left\langle 3\cos^2(\theta) - 1\right\rangle_{\boldsymbol{\omega}} \\ &= \frac{1}{2}\int \left(3\cos^2(\theta) - 1\right) f(\boldsymbol{\omega})\mathrm{d}\boldsymbol{\omega} \\ &= \pi \int_{-1}^{1} \left(3\cos^2(\theta) - 1\right) f(\theta)\mathrm{d}\cos(\theta) \end{aligned} \tag{1.2}$$

The so-obtained scalar S_2 is usually referred to as the nematic order parameter. To

appreciate this definition, let us look at the limiting cases of an isotropic- and a perfect nematic phase. For the isotropic phase, substitution of Eq. (1.1) in Eq. (1.2) leads to

$$S_{2,\,\mathrm{iso}} = \frac{1}{4}\int_{-1}^{1}\left(3\cos^2(\theta)-1\right)\mathrm{d}\cos(\theta) = 0 \tag{1.3}$$

For a perfect nematic phase, the ODF is zero everywhere except for $\theta = 0$ and $\theta = \pi$. Therefore, given the normalization condition $\int f(\boldsymbol{\omega})\mathrm{d}\boldsymbol{\omega} = 1$, the ODF can be defined as a sum of two Dirac-delta functions, according to

$$f_{\mathrm{perfect\ nem}}(\boldsymbol{\omega}) = \frac{1}{2\pi}\left\{\delta(\cos(\theta)-1)+\delta(\cos(\theta)+1)\right\} \tag{1.4}$$

Substituting the above result for the ODF in Eq. (1.2), leads to the nematic order parameter of a perfect nematic phase:

$$\begin{aligned} S_{2,\,\mathrm{perfect\ nem}} &= \frac{1}{2}\int_{-1}^{1}\left(3\cos^2(\theta)-1\right)\left\{\delta(\cos(\theta)-1)+\delta(\cos(\theta)+1)\right\}\mathrm{d}\cos(\theta) \\ &= \frac{1}{2}\left\{(3\times 1^2-1)\times\frac{1}{2}+(3\times(-1)^2-1)\times\frac{1}{2}\right\} \\ &= 1 \end{aligned} \tag{1.5}$$

For imperfect orientational ordering, as observed in systems of real mesogens, the nematic order parameter typically takes on a value between 0.3 and 0.9 [4]. A typical course of S_2 with temperature is presented in Fig. 1.5.

Historically, the nematic order parameter has been of great importance from both a practical- and theoretical point of view. Due to a large number of experimental methods for measuring the order parameter (*e.g.* X-ray analysis, NMR, etc. [43]), it is one of the primary quantities used for comparison to results from nematic-state theories. For this reason some phenomenological theories, such as the Landau-deGennes theory [3, 44], consider the order parameter as a theoretical input. On the contrary, several molecular-based approaches result in a Helmholtz energy functional for nematic fluids described in terms of the order parameter (see Ref. [19] for a recent review). In such theories the order parameter is not invoked from the outset (as in the Landau-deGennes theory), thereby clearly showing its fundamental nature.

1.3.2. Theory of the nematic state

To start this brief discussion on nematic-state theory, let me first answer the following question: Why should a fluid form a nematic phase? After all, the orientational ordering of molecules leads to a decrease in orientational entropy—why would a fluid pay the price of a decreased entropy? Well, the stability of a system with given temperature T and volume V is determined by a minimum of the Helmholtz energy, which is defined as a balance between an energetic term U and an entropic term TS, according to $A = U - TS$. There are thus two possible answers, and both are valid:

1. there is (either) an energetic incentive. With $U = U^{\mathrm{ig}} + U^{\mathrm{intermol}}$, we know that it is a lower (more negative) average intermolecular potential energy (U^{intermol})

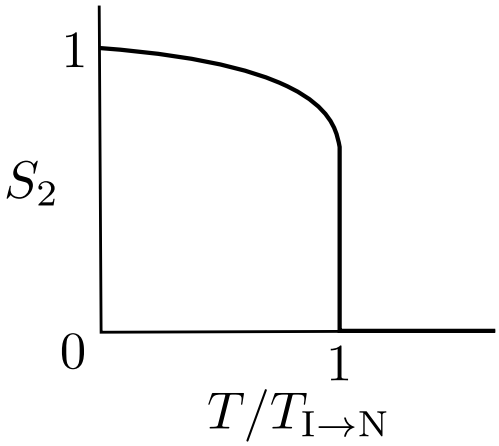

Figure 1.5: A typical course of the nematic order parameter S_2 with temperature T. The temperature is displayed relative to the temperature at the isotropic-nematic phase transition $T_{\mathrm{I}\to\mathrm{N}}$. For $T/T_{\mathrm{I}\to\mathrm{N}} < 1$, the phase is nematic, resulting in an order parameter larger than zero. For $T/T_{\mathrm{I}\to\mathrm{N}} > 1$, the phase is isotropic, corresponding to an order parameter equal to zero. It is important to note that at the transition, the change of the order parameter is discontinuous, corresponding to a first-order phase transition.

that causes a nematic phase to form. The lowering of the intermolecular potential can be understood from angle-dependent attractive intermolecular forces that favour the alignment of molecules. If the temperature is lowered, the relative effect of these attractions with respect to the loss in orientational entropy grows until at some point these forces become the dominant feature, leading to a (thermotropic) transition to a nematic phase. Maier and Saupe (1959) were the first to give a molecular-based description of this effect [10–12].

2. (or) there is a compensating entropic effect. For systems of molecules with anisotropic shape, the alignment of molecules—and the more efficient molecular packing that results from it—leads to an increase in the free volume (*i.e.* configurational entropy) of the system. If the density of nematogens increases, the gain in configurational entropy can become so large that it exceeds the loss in orientational entropy. If this is the case, a (lyotropic) phase transition to an orientationally ordered (nematic) phase results. In a landmark paper from 1949 [9], Lars Onsager laid the foundation for a statistical-mechanical treatment of such entropy-driven ordering transitions.

Clearly, in systems of real nematogens, both entropic effects (due to the repulsion between hard molecular cores) and energetic effects (due to attractive intermolecular interactions) can work as a driving force for mesophase formation. A molecular theory intended to describe mesophase behaviour should therefore encompass both effects. Before I discuss the general framework (*i.e.* molecular perturbation theory) needed to develop such a theory, let me elaborate on the two basic theories of the nematic state: the Maier-Saupe theory, and the theory of Onsager.

The Maier-Saupe theory

In its original form, the Maier-Saupe (MS) theory leads to the following mean-field potential for the orientation-dependent (anisotropic) part of the interaction energy of a molecule with all other molecules in a nematic fluid [10–12]

$$\Psi \propto -\rho^2 S_2 P_2(\cos\theta) \tag{1.6}$$

Here, ρ is the density of the system, $P_2(\cos\theta)$ is the second order Legendre polynomial of $\cos\theta$, and S_2 is the nematic order parameter (defined by Eq. (1.2)). The total energy due to the anisotropic part of the interactions U_{aniso} can be obtained from an ensemble average of this mean-field potential. Accordingly, it follows that

$$\begin{aligned} U_{\text{aniso}} &= \frac{1}{2} N \frac{\int \Psi \exp\left(-\beta\Psi\right) \mathrm{d}\cos\theta}{\int \exp\left(-\beta\Psi\right) \mathrm{d}\cos\theta} \\ &= -\frac{1}{2} N \epsilon^{\text{LC}} \rho^2 S_2 \frac{\int P_2(\cos\theta) \exp\left(-\beta\Psi\right) \mathrm{d}\cos\theta}{\int \exp\left(-\beta\Psi\right) \mathrm{d}\cos\theta} \\ &= -\frac{1}{2} N \epsilon^{\text{LC}} \rho^2 S_2^2 \end{aligned} \tag{1.7}$$

where N is the number of molecules, and ϵ^{LC} is a (positive) pure-component parameter independent of temperature, density or pressure. In principle, it can be shown that the mean-field potential as introduced in Eq. (1.6) follows from an underlying angle-dependent intermolecular potential of the form $u(r) = -\epsilon(1/r^6)\cos^2(\gamma)$ [14], where r is the separation between the molecular centres of mass, and γ is the angle between the molecular axes. It is possible, therefore, to relate the mean-field parameter ϵ^{LC} to the underlying energy parameter ϵ of this anisotropic intermolecular potential, thereby constituting a clear molecular basis of the MS approach.

The orientational entropy of the system can be obtained from the Boltzmann equation $S = -Nk\sum_i p_i \ln p_i$ which relates the entropy S to the probability p_i of a certain distribution of molecular orientations [45]. In our case, the probability is defined by $f(\boldsymbol{\omega})$; leading to the following anisotropic contribution to the entropy of the system

$$S_{\text{aniso}} = -Nk \int f(\boldsymbol{\omega}) \ln(4\pi f(\boldsymbol{\omega})) \mathrm{d}\boldsymbol{\omega} \tag{1.8}$$

Please note the introduction of the normalization constant 4π (cf. Eq. (1.1)) to ensure the anisotropic contribution goes to zero for an isotropic distribution of molecular orientations. Combining energetic and entropic terms, one obtains the following functional for the anisotropic Helmholtz energy contribution resulting from the MS theory

$$\frac{A_{\text{aniso}}[f(\boldsymbol{\omega})]}{NkT} = \int f(\boldsymbol{\omega}) \ln(4\pi f(\boldsymbol{\omega})) \mathrm{d}\boldsymbol{\omega} - \frac{1}{2} \frac{\epsilon^{\text{LC}}}{kT} \rho^2 S_2^2[f(\boldsymbol{\omega})] \tag{1.9}$$

Generally, $f(\boldsymbol{\omega})$ is found self-consistently from the EoS by ensuring it minimizes the total Helmholtz energy of the system. Typically, the pure-component parameter ϵ^{LC} is regressed to experimental PVT-data of a nematic phase, data for the phase transition temperature ($T^{\text{N}\to\text{I}}$), or to data for the nematic order parameter. For a limited number of mesogens, this leads to reasonable correlation of isotropic-nematic transition temperatures or the temperature dependence of the nematic order parameter [46]. The fact that the MS theory does not include any entropic driving force for mesophase formation, however, generally results in a rather poor description of density-dependent properties (such as $S_2(\rho)$) [1]. Furthermore, when using a realistic magnitude of the anisotropic attractive interactions (which are related to ϵ^{LC}), predicted isotropic-nematic transition temperatures are significantly too low

(see Ref. [14] and references therein), indicating an underestimation of the driving force for the phase transition. To improve on such shortcomings, many empirical extensions of the MS theory have been developed [46]. Probably the one with the most physical appeal is the following

$$\epsilon^{\mathrm{LC}} = \epsilon_E^{\mathrm{LC}} + T\epsilon_S^{\mathrm{LC}} \tag{1.10}$$

With this extension, one obtains two independent pure-component parameters: one for the energetic driving force for mesophase formation (ϵ_E^{LC}), and one for the entropic driving force (ϵ_S^{LC}). Clearly, the regression of these two parameters provides great flexibility in correlating experimental results, which is probably one of the reasons the MS theory has found such widespread use. Moreover, when coupled to an accurate EoS for describing the properties of the isotropic phase, quite accurate correlation of for example isotropic-nematic transition temperatures, the density difference at the phase transition, and the nematic order parameter, can be obtained [47]. Having that said, I should stress that the incorporation of the entropic driving force is purely empirical, leading to a theory with little predictive value. Moreover, due to this extension, part of the energetic parameter (ϵ_E^{LC}) implicitly includes a coupling between entropic and energetic effects [14, 15, 19]. As a result, in Eq. (1.10), ϵ_E^{LC} is not only related to the parameters of the attractive intermolecular potential underlying the mean-field potential of Eq. (1.6), but also to the geometrical features of the molecules. The fact that the extended MS theory does not provide one with these dependencies adds to the empirical nature of the approach. For practically relevant applications, the MS model is more a phenomenological theory, incapable of providing a link to details of the molecular model or intermolecular potential. For the purposes aimed at in this thesis (*i.e.* the development of a molecular-based EoS for LCs that is suitable for use in solvent design methods), such a theory is inadequate.

The Onsager theory

A more rigorous route towards a molecular description of mesophases is provided by the Onsager theory. Although the Onsager theory will be discussed in depth in Chapter 4 of this thesis, it is instructive to give a brief overview of the theory at this point.

Onsager showed that by treating molecules of different orientation as different chemical species, one can reformulate the virial expansion of Mayer and Mayer [48] (which at the time was developed for isotropic fluids only) to anisotropic fluids [9]. Although Onsager considered the specific case of hard rods, his results can be generalized to systems of hard, purely repulsive molecules of general anisotropic shape, leading to the following general Helmholtz energy functional

$$\frac{A[f(\boldsymbol{\omega})]}{NkT} = A_{\mathrm{iso}}^{\mathrm{id}} + \int f(\boldsymbol{\omega}) \ln(4\pi f(\boldsymbol{\omega})) \mathrm{d}\boldsymbol{\omega} + B_2[f(\boldsymbol{\omega})]\rho + B_3[f(\boldsymbol{\omega})]\rho^2 + \ldots \tag{1.11}$$

Here, $\rho = N/V$ is the homogeneous number density, and B_2, B_3, and so on, are the virial coefficients. Onsager suggested to cut off the virial expansion after the first term, resulting in a second virial theory that is only exact in the low density

limit. To obtain the orientation-dependence of the second virial coefficient $B_2[f(\boldsymbol{\omega})]$ of two hard, purely repulsive molecules, he provided a relation to their orientation-dependent pair-excluded volume $V_{\mathrm{ex}}(\boldsymbol{\omega}_1, \boldsymbol{\omega}_2)$ (*i.e.* the volume inaccessible to the center of mass of a molecule 1 due to the presence of a molecule 2), according to

$$\begin{aligned} B_2[f(\boldsymbol{\omega})] &= \frac{1}{2} \int \int V_{\mathrm{ex}}(\boldsymbol{\omega}_1, \boldsymbol{\omega}_2) f(\boldsymbol{\omega}_1) f(\boldsymbol{\omega}_2) \mathrm{d}\boldsymbol{\omega}_1 \mathrm{d}\boldsymbol{\omega}_2 \\ &= \frac{1}{2} \left\langle V_{\mathrm{ex}}(\boldsymbol{\omega}_1, \boldsymbol{\omega}_2) \right\rangle_{\boldsymbol{\omega}_1, \boldsymbol{\omega}_2} \end{aligned} \tag{1.12}$$

Fig. 1.6 shows the pair-excluded volume for some typical model mesogens of aspect ratio $L^* = L/D > 2$, where L and D are the molecular length and diameter, respectively. What should be clear from this figure is that the pair-excluded volume of two anisotropic molecules in an aligned orientation ($V_{\mathrm{ex}} \propto 2L$) is smaller than that of two molecules in a perpendicular orientation ($V_{\mathrm{ex}} \propto L^2$). Accordingly, upon orientational ordering of molecules the second virial coefficient decreases, thereby constituting a clear driving force for mesophase formation. With this simple second virial theory, Onsager was able to show that the isotropic-nematic transition of purely repulsive molecules can be understood from a competition between two entropic terms: on the one hand an orientational-entropy term, favouring an isotropic distribution of molecular orientations; and on the other hand an excluded-volume term, favouring an aligned distribution of molecular orientations.

The fact that the excluded-volume term is weighted by density leads to the insight that the only system capable of forming a stable nematic phase at zero density is one of infinitely long rods. Therefore, the 2nd virial approximation as suggested by Onsager is only valid for such systems. To extend the approach to molecules of more moderate anisotropy, the effect of higher virial coefficients needs to be incorporated. Since the orientational dependence of these coefficients is usually difficult to obtain, it is common to use decoupling approximations [49–52] or Scaled Particle Theory [16, 53] to approximate the effect of higher virial coefficients by a non-linear dependence on density as

$$\frac{A^{\mathrm{res}}[f(\boldsymbol{\omega})]}{NkT} \approx \frac{A^{\mathrm{res}}(B_2[f(\boldsymbol{\omega})], \rho)}{NkT} \tag{1.13}$$

For a detailed discussion of how decoupling approximations or Scaled Particle Theory can be applied to obtain the density dependence of Eq. (1.13), the reader is referred to Chapter 4 of this thesis.

What should be apparent at this point is that, through the pair-excluded volume, the theory of Onsager explicitly considers the anisotropic shape of molecules. Therefore, in contrast to the MS theory, the approach of Onsager provides a rigorous link between molecular parameters and the entropic driving force for mesophase formation. For a system of hard spherocylinders (which is very similar to the hard rods considered by Onsager), for example, one obtains $V_{\mathrm{ex}} = C_1 + C_2 \sin(\gamma)$ with $C_1 = (4/3)\pi D^3 + 2\pi D^2 L$ and $C_2 = 2L^2 D$, where L and D are the length and diameter of the spherocylinders, respectively [9]. Furthermore, the Onsager approach can be extended to mesogens with attractive interactions by means of molecular perturbation theory [19, 54]. By taking appropriate limits for molecular size parameters,

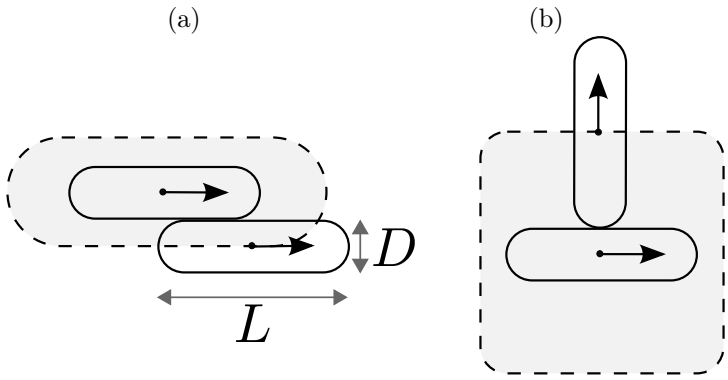

Figure 1.6: A 2-D schematic representation of the pair-excluded volume (denoted by the area between dashed lines) of two model mesogens of aspect ratio $L^* = L/D > 2$, where L and D are the molecular length and diameter, respectively. In (a) I show a parallel orientation, and in (b) a perpendicular orientation. For the parallel orientation $V_{\text{ex}} \propto 2L$, whereas for the perpendicular orientation $V_{\text{ex}} \propto L^2$.

such a theory can be reformulated to a form equivalent with the original theory of Maier and Saupe (cf. Eq. 1.9) [19], clearly showing the generality of the Onsager approach.

In the following sections, I will discuss the basics of molecular perturbation theory. Furthermore, I point out one of its major successes, *i.e.* the SAFT-family of equations of state for isotropic fluids. After that, I elaborate on possible routes to couple such a formalism to the theory of Onsager for developing a fluid theory for nematic fluid mixtures.

1.3.3. Molecular perturbation theory

Let's suppose one would like to describe the thermodynamics of a system in which the molecules interact by a given intermolecular pair-potential $u(r)$. Let's call this system the target system. If obtaining the properties of the target system is problematic, one could consider a system with a different intermolecular potential of which the thermodynamic properties are known. Let's call that system the reference system. If one could somehow link the target system to the reference system, the problem is solved. If the two systems are similar (where similarity will be defined later in this section), molecular perturbation theory provides this link.

If we denote the reference system by a subscript '0', the pair-potential of the target fluid can be written as

$$u_\lambda(r) = u_0(r) + \lambda u^{\text{pert}}(r) \tag{1.14}$$

where $u^{\text{pert}}(r) = u_\lambda(r) - u_0(r)$ is the difference between the potential of the target fluid and the reference fluid. The parameter λ couples the two systems; for $\lambda = 1$ we obtain the target fluid, whereas for $\lambda = 0$ the reference fluid is retained. The Helmholtz energy (and thus all other macroscopic thermodynamic properties) for a

system with an intermolecular potential defined by Eq. (1.14) can be obtained from

$$A = A_0 + \int_0^1 \left(\frac{\partial A}{\partial \lambda}\right)_{NTV} \mathrm{d}\lambda \tag{1.15}$$

Using the relation of the Helmholtz energy to the partition function, one can rewrite the derivative to λ as an ensemble average of the perturbation-part of the potential energy over the configurations of the target system. For a homogeneous, isotropic system, such an ensemble average can be written in terms of the radial distribution function (rdf) of the target system $g_\lambda(r)$, according to

$$\left(\frac{\partial A}{\partial \lambda}\right)_{NTV} = \left\langle \sum_{i=1}^{N} \sum_{j>i}^{N} u_{ij}^{\mathrm{pert}} \right\rangle_{\lambda} \tag{1.16}$$

$$= 2\pi N \rho \int_0^\infty u^{\mathrm{pert}}(r) g_\lambda(r) r^2 dr \tag{1.17}$$

To proceed, the rdf of the target system can be expanded around that of the reference system as

$$g_\lambda(r) \approx g_0(r) + \left(\frac{\partial g_\lambda(r)}{\partial \lambda}\right)_{NTV}\Bigg|_{\lambda=0} \lambda + \ldots \tag{1.18}$$

Provided *similarity* between the rdf of the reference- and the target system, the expansion is rapidly convergent. When truncated after the first term, a first order perturbation theory results

$$A = A_0 + 2\pi N \rho \int_0^\infty u^{\mathrm{pert}}(r) g_0(r) r^2 dr \tag{1.19}$$

$$= A_0 + A_1 \tag{1.20}$$

Clearly, to provide the required similarity, a proper choice for the reference system is critical. It turns out that at densities typical for the liquid state, molecular structure (and thus the rdf) is primarily determined by the repulsion between hard molecular cores [54]. Therefore, a good approximation for the reference system can usually be obtained from purely repulsive systems, such as a system of hard spheres. The properties of such purely repulsive fluids (think of rdf, Helmholtz energy) are relatively well developed and can be obtained from various statistical-mechanical techniques [54].

1.3.4. The SAFT approach

The development of molecular perturbation theory was revolutionary in some respects, since it for the first time allowed a quantitative molecular-based description of the fluid phase behaviour of simple, nearly spherical fluids, such as Argon [55]. Its application to molecules of more complicated architecture (*e.g.* chains and rings typical for many organic molecules), however, required another impressive theoretical development: Wertheim's thermodynamic perturbation theory (TPT) [56–60]. TPT provides one with a Helmholtz energy contribution for strongly associating

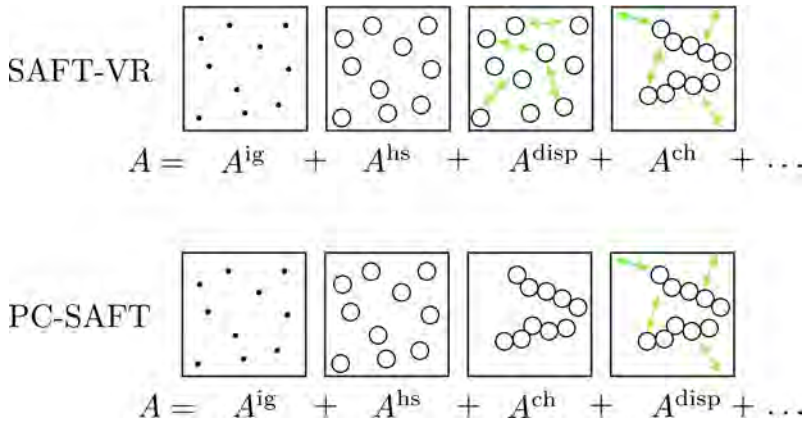

Figure 1.7: The perturbation scheme of some different versions of the SAFT theory. Included are the SAFT-VR theory [68–70, 73, 74], and the PC-SAFT approach of Gross and Sadowski [71, 72]. Contributions other than due to dispersion interactions (*e.g.* association [75, 76], polarity [77, 78], electrostatic [79, 80]) are left out for clarity.

(hydrogen-bonding) compounds, which, in the limit of infinite association strength, also provides the means to bond spherical segments into chains, thereby leading to a theory capable of describing the phase behaviour of chain fluids.

The framework of molecular perturbation theory and TPT have proven very powerful in predicting fluid properties. As pioneered by Chapman, Jackson and Gubbins [61–64], these two approaches form the basis of one of the most successful equations of state up to date: the Statistical-Associating-Fluid-Theory (SAFT) [65, 66]. In this approach, molecules are usually modelled as chains of freely-jointed spherical segments—the total interaction of which is described by different contributions, such as dispersion (*i.e.* Van der Waals attraction), polarity or association. It is common to use a fluid of hard spheres as a reference, and add the other contributions to the Helmholtz energy (dispersion, chain formation, etc.) as a perturbation. The Helmholtz energy of a fluid described by a SAFT approach can be written as

$$A = A^{\mathrm{ig}} + A^{\mathrm{hs}} + A^{\mathrm{disp}} + A^{\mathrm{ch}} + A^{\mathrm{polar}} + A^{\mathrm{ass}} + \ldots \tag{1.21}$$

Many versions of SAFT have been developed (*e.g.* SAFT [61–64], soft-SAFT [67], SAFT-VR [68–70], PC-SAFT [71, 72], etc.). Differentiation between the various versions is established by the choice of the perturbation scheme (*i.e.* the reference system used for each perturbation contribution), the perturbing potentials, or the theoretical treatment of the different perturbation contributions. For illustration, I graphically show the perturbation scheme of some typical SAFT theories in Fig. 1.7. For clarity, attractive contributions due to interactions other than dispersion are omitted [65, 66].

Due to the molecular basis (*i.e.* a well defined molecular model and intermolecular potential) of SAFT-type theories, they allow for a meaningful comparison to results obtained from molecular simulations. Since such a comparison can be made

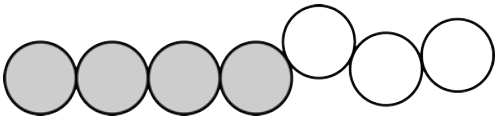

Figure 1.8: A partially flexible tangent hard-sphere chain molecule, or rod-coil molecule, as a model for mesogenic compounds. One part of the molecule is fixed in a rigid, linear conformation (gray segments) while the other part is full flexible.

at many different levels of theoretical development (for example for all perturbation contributions separately), it makes possible the development of a rigorous statistical-mechanical theory that, at least for the molecular model and potential under consideration, leads to an accurate description of thermodynamic properties. When applied to correlate the phase behaviour of real fluids, this provides one with the insight whether observed discrepancies are due to assumptions made for the molecular model/intermolecular potential or due to the theoretical treatment of this model/potential. Compared to non-molecular based methods, this allows for much more directed theoretical development.

Considering (1) its firm rooting in statistical mechanics, and (2) its success in describing the phase behaviour of isotropic fluids, the SAFT approach may serve as a rigorous platform from which to build an EoS for anisotropic fluids. In the following section I elaborate on a possible route for doing this.

1.3.5. Extending SAFT to anisotropic fluids

Although a model of freely-jointed spherical segments is certainly a coarse approximation for most real molecules (which commonly involve bond-bending, torsional potentials, ring structures, branching, etc.), the accurate representation of phase equilibria as generally obtained with SAFT-type theories [70, 72] strongly suggests such a coarse-grained representation captures essential parts of the underlying physics of isotropic fluids. Recent developments confirm that both, the molecular model is meaningful and the theory is sufficiently predictive. SAFT was for example shown to adequately correlate, extrapolate, and even predict results from molecular simulations, which allows for force field development [81–85].

An essential characteristic of mesogenic substances is a (partially) rigid, anisotropic molecular core. As a molecular model that captures this characteristic, I propose a partially flexible chain of spherical segments (see Fig. 1.8). In this study, molecules of this molecular model will be referred to as rod-coils. Although one could think of many other molecular models (*e.g.* rigid anisotropic particles such as spherocylinders [18, 19] or chains of such particles [86]), I feel the rod-coil model as proposed here may serve as a suitable starting point, since

1. it contains the most important difference between mesogenic and non-mesogenic compounds, namely a rigid, anisotropic core.

2. it maintains a certain degree of intra-molecular flexibility—a feature generally considered to be important for the (de)stabilization of mesophases.

3. it allows for a segment-based approach, leading to compatibility with available SAFT-type theories.

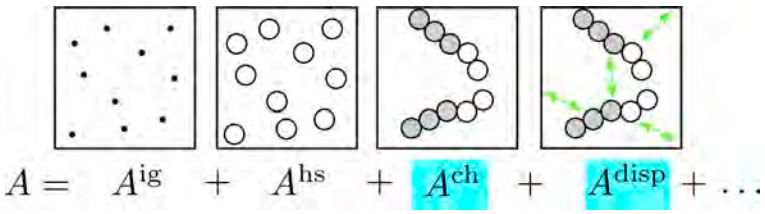

Figure 1.9: The proposed perturbation scheme for anisotropic, liquid crystalline fluids, based on the molecular model from Fig. 1.8. The Helmholtz energy contributions due to chain formation and dispersion interactions are developed in Chapters 2-5, and Chapters 6 and 7 of this thesis, respectively.

To allow for a theoretical description based on Onsager's approach (and especially the rescaling of higher virial coefficients as introduced in Chapter 4), it is best to treat the effects of chain connectivity and rigidity in the repulsive reference contribution to the EoS. Therefore I propose a perturbation scheme for anisotropic fluids as depicted in Fig. 1.9. The scheme is similar to that used in the PC-SAFT approach. The main difference is the incorporation of the effect of molecular rigidity in the repulsive reference- and attractive dispersion contribution.

1.4 Scope and outline of this thesis

The main goal of this thesis is to contribute to the development of a molecular-based equation of state for anisotropic fluids. More specifically, I make a first attempt to extend the SAFT formalism to nematic liquid crystals by developing a fluid theory via the perturbation scheme illustrated in Fig. 1.9. Accordingly, the work performed in this thesis can be divided in two parts, namely:

part A The development of an Onsager-based reference EoS that can describe the isotropic- and nematic fluid-phase behaviour of mixtures of hard, purely repulsive rod-coil molecules (Chapters 2-5).

part B The development of a perturbation contribution due to dispersion interactions of rod-coil molecules (Chapters 6 and 7).

Although other attractive interactions than dispersion (*e.g.* polarity, association) are also expected to be of importance for the formation of mesophases, these are not considered in this thesis. Moreover, a detailed comparison of the EoS to experimental data is left for future work; this thesis focuses on theory development, where the decisive evaluation is done by systematically comparing theory to results from molecular simulations.

Given the interest in the potential application of LCs as solvents for absorption processes (Section 1.2), it is desired the EoS developed in this thesis is applicable to mixtures of both mesogenic- and non-mesogenic compounds. Furthermore, the EoS should be of simple analytical form, suitable for use in engineering-oriented applications. A first step towards these goals was provided by the Phd work of

Franco-Melgar *et al.* [18, 19, 87]. In this comprehensive work, the Onsager-Trial-Function (OTF) approach was employed to develop a fully algebraic description of the isotropic-nematic transition of *pure-component systems* of *rigid* mesogens. The approach was generalized to rigid mesogens of many different shapes, the only requirement being a generic form of the pair-excluded volume (*i.e.* a series in $\sin(\gamma)$, where γ is the angle between the molecular axes). In this thesis, I aim at a theoretical approach of similar simplicity. However, in contrast to the work of Franco-Melgar *et al.*, I aim at a description of (1) *non-rigid* (rod-coil) molecules, and (2) *mixture systems*. As I show, these objectives pose considerable challenges.

The first problem is addressed in Chapter 2, which concerns the description of the pair-excluded volume. Due to intramolecular degrees of freedom, the pair-excluded volume of rod-coil molecules is not only a function of the angle (γ) between the overall molecular axes, but also of the molecular conformations. A rigorous description of the effect of conformational degrees of freedom on the excluded volume could in principle be achieved using MC simulations; however, this would result in a theory not suited for engineering applications. For the purposes aimed at in this thesis, a simpler treatment is required. Therefore, I propose a decoupling of the conformational distribution function which allows the internal degrees of freedom of the molecules to be averaged out. In the resulting theory, the orientation-dependent pair-excluded volume is obtained from an ensemble average over these internal degrees of freedom. Although the ensemble average needs to be obtained from MC simulations, I develop a general correlation which, when used in an Onsager-type theory, results in an analytical treatment of the effect of molecular flexibility on the isotropic-nematic transition. The correlation is cast in the general form of a series in $\sin(\gamma)$, thereby allowing an extension of the generalized Onsager approach of Franco-Melgar *et al.* to non-rigid molecules.

Apart from an accurate description of the excluded volume, a fluid theory for the isotropic-nematic transition relies on an accurate description of the isotropic phase. In Chapter 3, some commonly used equations of state (TPT2, GFD, SPT) are extended to rod-coil fluids. A novel EoS is developed that leads to a considerably improved description of the isotropic phase behaviour of rod-coil fluid mixtures.

In Chapter 4, the decoupling of the conformational distribution function (as proposed in Chapter 2) is used to extend Onsager's 2nd virial theory (as introduced in Section 1.3.2) to partially flexible (rod-coil) fluids. Several methods for treating molecules of moderate shape anisotropy (*i.e.* small chain length, large flexibility) are introduced. By combining the extended Onsager theory with the correlation for the pair-excluded volume from Chapter 2 and the novel EoS for the isotropic phase from Chapter 3, an analytical theory for the isotropic-nematic transition of rod-coil fluids is obtained. It is shown that the theory compares accurately to a wide range of results obtained from MC simulations. The effect of molecular shape and flexibility on the isotropic-nematic phase behaviour is thereby systematically examined. The theory is simplified to an algebraic EoS with a self-contained description of orientational ordering.

In Chapter 5, the Onsager theory from Chapter 4 is extended to mixtures. Considerable effort is put in reformulating the theory to analytical form. However, an

algebraic form as obtained for pure-component systems seems not possible. Theoretical results for the binary phase diagram are compared to results obtained from MC simulations. As for the pure-component case, excellent agreement is obtained. The EoS is used to study several phenomena. Most importantly, the solubility of small hard-sphere solutes in nematic rod-coil solvents is studied. It is shown that using a mixture of LCs as the solvent gives the possibility to maximize the solubility difference across the isotropic-nematic phase transition.

In part B of this thesis, the effect of attractive dispersion interactions is included in the reference model by means of the perturbation theory of Barker and Henderson. As for the reference case, an accurate EoS for the isotropic phase is important to obtain a reliable description of the isotropic-nematic equilibrium. Therefore, in Chapter 6, I first develop an EoS that can describe the isotropic (*i.e.* vapour and liquid) phase behaviour of rod-coil fluids, whose segments interact through a Lennard-Jones (LJ) 12-6 potential. In the course of the development I come to various new insights regarding the application of the Barker-Henderson perturbation theory to a hard-chain reference fluid. Most importantly, it is shown that in such a perturbed-chain approach an accurate description of the soft repulsion between the segments in LJ chain fluids can not be obtained by naively applying the conventional Barker-Henderson effective segment diameter. A new effective diameter is developed that depends on temperature, chain length and density. When used in the theory, a significantly improved description of the vapour-liquid phase behaviour is obtained.

In Chapter 7, the work of Chapters 2-6 is combined to develop an EoS for describing isotropic-nematic phase equilibria of LJ chain fluids. In addition, an anisotropic dispersion contribution is included to the EoS. The EoS is used to systematically study the effect of chain length, flexibility, and attractive dispersion interactions on the vapour-liquid-nematic phase behaviour. Theoretical results are compared to molecular simulations for isotropic-nematic equilibria of a system of rigid linear LJ 10-mers. Excellent agreement is obtained. The results indicate that the difference between the isotropic- and nematic dispersive Helmholtz energy contribution to the EoS is predominantly caused by the density difference at the isotropic-nematic phase transition. For LJ chain fluids, therefore, no anisotropic dispersion contribution is required. These results suggest a reliable description of the dispersion interactions of real LCs can be obtained from conventional theories that were developed for isotropic fluids.

part A

Equation of state for a purely repulsive reference fluid

2

An analytical approximation for the orientation-dependent pair-excluded volume of rod-coil fluids

A key ingredient in Onsager-like theories is the orientation-dependent excluded volume of two molecules. Although for convex molecular models this is generally known in analytical form, for more realistic molecular models that incorporate intramolecular flexibility, one usually has to rely on crude approximations or computationally expensive MC techniques. In this thesis, we aim at simple (approximate) analytical methods, while maintaining the theoretical rigour of the MC method. Therefore, we propose a decoupling of the conformational distribution function of a chain fluid into a part describing the orientation of the overall molecular axis and a part describing the internal degrees of freedom (bond- and torsion angles) of the molecules. This decoupling allows us to treat the orientation-dependent excluded volume of two partially flexible (rod-coil) molecules as an ensemble average over their internal degrees of freedom. We perform MC simulations to calculate this ensemble average for a wide range of different rod-coil molecules. An accurate, analytical approximation is developed by correlating the results. The correlation is valid over a large range of chain lengths and flexibilities; therefore when used in an Onsager-like theory for the isotropic-nematic transition (Chapter 4), it allows for an analytical treatment of the effects of molecular flexibility. The correlation is extended to mixtures by applying simple combining rules for the parameters involved. We have expressed the excluded volume as a second order power series in $\sin(\gamma)$, where γ is the angle between the molecular axes. Such a representation is appealing since the solution of the Onsager Helmholtz-energy functional usually involves an expansion of the excluded volume in Legendre coefficients. Moreover, when using the excluded-volume expression in an Onsager-type theory in the OTF approximation, it allows for an algebraic description of the nematic state (see Chapter 4). Both for pure components and mixtures, the correlation reduces to an exact expression in the limit of completely linear chains.

Parts of this chapter have been published as:
T. van Westen, T.J.H. Vlugt and J. Gross *J. Chem. Phys.* 137 (2012) 044906 [88].

2.1 Introduction

It is well recognized that theoretical descriptions of molecules that form liquid crystalline phases should go beyond the simple rigid models such as for example rods, disks, spherocylinders or ellipsoids [89–93]. Although these models play an important role in gaining understanding in the rich phase behaviour of liquid crystals [94–98], Flory already suggested in 1956 that a certain degree of intramolecular flexibility—a characteristic of any 'real' liquid crystal molecule—would have a considerable effect on the liquid crystalline phase behaviour [90]. Now, several molecular simulation studies [91–93, 99] have confirmed this hypothesis. For the isotropic-nematic phase transition in particular, one finds that introducing flexibility into the molecular model destabilizes the nematic phase (due to a decreased anisotropy of the molecules) and thereby shifts the phase transition to higher density and pressure.

Inspired by the seminal work of Flory and these more recent observations, several authors have worked towards incorporating the effects of molecular flexibility in a theoretical description of the isotropic-nematic transition [100–108]. The starting point for all of these studies is Onsager's theory [9, 109]. For a system of infinitely thin hard rods, Onsager showed that the isotropic-nematic phase transition can be understood from a competition between an orientational entropy, which is maximized by an isotropic distribution of molecular orientations, and a configurational entropy (free volume), which is maximized by aligning the molecules to minimize the excluded volume. To extend the theory of Onsager to molecules with a certain degree of intramolecular flexibility, an additional chain-conformational entropy has to be taken into account. The first to do this were Khoklov and Semenov [100–102]. In their analysis on worm-like chains, a correction to the orientational-entropy term of the Onsager Helmholtz-energy functional was introduced to account for the additional conformational degrees of freedom. The effect of these degrees of freedom on the excluded volume was approximated by breaking up a molecule into a number of uncorrelated rigid subsections of length equal to the molecule's persistence length. More recent theoretical efforts due to, for example, Fynewever and Yethiraj [103], suggest that a more rigorous treatment of the effect of chain flexibility on the excluded volume leads to a more accurate description of the isotropic-nematic transition of semi-flexible chain molecules. In such an approach, a MC simulation of two chain molecules is performed to calculate an ensemble average of the pair-excluded volume over all (relevant) molecular conformations. Although, in contrast to the Khoklov-Semenov theory, this allows an application of the method to other molecular models than the worm-like chain, the dependence on MC simulations renders a computationally expensive approach, not suited for the routine engineering applications aimed at in this thesis.

Given its good performance [103], it would be desirable to apply the method of Fynewever and Yethiraj to the rod-coil model laid out in Section 1.3.5 of this thesis. Therefore, in the present chapter, we develop a general correlation for the orientation-dependent pair-excluded volume of rod-coil molecules of arbitrary chain length and flexibility. The use of this correlation in Onsager-like theories for the isotropic-nematic phase transition eliminates the need to perform individual MC simulations for calculating the excluded volume while accurately, albeit in an average

way, covering the effects of intramolecular flexibility (see Chapter 4 for details).

This chapter is organized as follows. In Section 2.2, we discuss the rod-coil molecular model. After that, in Sec 2.3 some theoretical background is given on the second virial coefficient and pair-excluded volume of non-rigid chain molecules. Furthermore, we derive the method of Fynewever and Yethiraj based on a decoupling of the conformational distribution function. The algorithm for calculating the pair-excluded volume from MC simulations is presented in Section 2.4. In Section 2.5, the correlation for the pair-excluded volume of rod-coil molecules is developed and tested against MC simulations of two chain molecules. Our findings are summarized in Section 2.6.

2.2 Molecular model

The molecular architecture of typical (thermotropic) liquid crystal molecules of prolate type consists of a rather rigid, anisotropic core with one or more (semi-)flexible tail-groups attached to its end(s) [1, 89]. To mimic this architecture, we assume a chain of m tangent hard spheres of diameter σ, where one part of the chain is arranged in a linear conformation (referred to as 'rod') while the other part is fully flexible (referred to as 'coil'). This model will be referred to as rod-coil fluid. We employ a general m-m_R notation to denote a rod-coil with a total number of m segments and a number of m_R segments in the rigid block. A completely linear or flexible chain is simply referred to as a linear or flexible m-mer, respectively.

As a measure for the partial flexibility of a molecule, a dimensionless rigidity parameter is introduced, which is defined as the ratio of the total number of rigid bond-angles to the the total number of bond-angles in a molecule:

$$\chi_{\mathrm{R}} = \begin{cases} \dfrac{m_R - 2}{m - 2} & \text{for } m > 2 \\ 1 & \text{for } m \leq 2 \end{cases} \tag{2.1}$$

The rigidity parameter serves as an input for the excluded-volume expression developed in this chapter. The parameter varies conveniently from zero to unity between the completely flexible- and rigid chain limit, respectively.

In principle, the flexibility (and thus χ_{R}) of 'real' molecules is state-point (T, P and ρ) dependent (see for example the recent work of Dennison *et al.* [110, 111]). The fact that this state-point dependence is not included in the molecular model outlined above constitutes some degree of approximation. It is important to mention, however, that many accurate theories for the isotropic state (*e.g.* the SAFT family of equations of state [61–63, 65, 72]) have been developed based on similar approximations. In these theories, it is generally assumed that the intramolecular conformation is not affected by the density of the fluid. The temperature dependence of the non-bonded intramolecular interactions can then be considered in the ideal gas contribution to the Helmholtz energy. The same reasoning could be applied to liquid crystalline fluids. In doing this, the increase in the end-to-end distance of a chain molecule that is observed in simulation studies of the isotropic-nematic transition [92, 99] is neglected. The assumption of density independent molecular flexibility is in that respect analogous to the assumption made in SAFT theories, where

a comparable increase in end-to-end distance for vapour-liquid transitions [112] is neglected.

2.3 The second virial coefficient and pair-excluded volume of non-rigid chain fluids

As originally shown by Mayer and Mayer [48], the second virial coefficient of a system of spherical molecules whose interactions are governed by the pair-potential $u(r)$ can be written as an integral of the Mayer-f function $\Phi(\boldsymbol{r}_1, \boldsymbol{r}_2) = \exp(-\beta u(r)) - 1$ over configurational space

$$\begin{aligned} B_2 &= -\frac{1}{2V} \iint \Phi(\boldsymbol{r}_1, \boldsymbol{r}_2) \mathrm{d}\boldsymbol{r}_1 \mathrm{d}\boldsymbol{r}_2 \\ &= -\frac{1}{2} \iint \Phi(\boldsymbol{r}_{12}) \mathrm{d}\boldsymbol{r}_{12} \end{aligned} \tag{2.2}$$

Here, $\boldsymbol{r}_{12}$ is the vector between the center of mass of molecules 1 and 2. This result involves an exact extension to mixtures, according to

$$B_2 = \sum_i \sum_j x_i x_j B_{2,ij} \tag{2.3}$$

where x_i is the mole fraction of a chemical species i, and the double sum is over all possible pairs of chemical species in the mixture. By treating molecules of different orientations ($\boldsymbol{\omega}$) as different chemical species, Onsager argued one can replace the mole fractions x_i in the above equation by the orientational distribution function $f(\boldsymbol{\omega})$, leading to the following functional for the second virial coefficient of anisotropic, rigid molecules [9]

$$B_2[f(\boldsymbol{\omega})] = -\frac{1}{2} \iiint \Phi(\boldsymbol{r}_{12}, \boldsymbol{\omega}_1, \boldsymbol{\omega}_2) f(\boldsymbol{\omega}_1) f(\boldsymbol{\omega}_2) \mathrm{d}\boldsymbol{\omega}_1 \mathrm{d}\boldsymbol{\omega}_2 \mathrm{d}\boldsymbol{r}_{12} \tag{2.4}$$

Extrapolation to the case of non-rigid molecules is straightforward—now every molecule with a different conformation ($\tilde{\boldsymbol{\omega}}$) is treated as a different chemical species—and we can write the second virial coefficient as a functional of the conformational distribution function (CDF) $f(\tilde{\boldsymbol{\omega}})$

$$B_2[f(\tilde{\boldsymbol{\omega}})] = -\frac{1}{2} \iiint \Phi(\boldsymbol{r}_{12}, \tilde{\boldsymbol{\omega}}_1, \tilde{\boldsymbol{\omega}}_2) f(\tilde{\boldsymbol{\omega}}_1) f(\tilde{\boldsymbol{\omega}}_2) \mathrm{d}\tilde{\boldsymbol{\omega}}_1 \mathrm{d}\tilde{\boldsymbol{\omega}}_2 \mathrm{d}\boldsymbol{r}_{12} \tag{2.5}$$

For the hard, purely repulsive molecules considered here, the Mayer function is minus unity for molecular configurations that show overlap and zero otherwise. Therefore, minus the integral of the Mayer function over the separation $\boldsymbol{r}_{12}$ is equal to the volume inaccessible to the center of mass of molecule 2 due to the presence of molecule 1, *i.e.* the pair-excluded volume. As a result, the second virial coefficient can be written as a conformational average of the pair-excluded volume, according

to

$$B_2[f(\tilde{\boldsymbol{\omega}})] = \frac{1}{2}\iint V_{\mathrm{ex}}(\tilde{\boldsymbol{\omega}}_1,\tilde{\boldsymbol{\omega}}_2) f(\tilde{\boldsymbol{\omega}}_1) f(\tilde{\boldsymbol{\omega}}_2) \mathrm{d}\tilde{\boldsymbol{\omega}}_1 \mathrm{d}\tilde{\boldsymbol{\omega}}_2 \tag{2.6}$$

$$V_{\mathrm{ex}}(\tilde{\boldsymbol{\omega}}_1,\tilde{\boldsymbol{\omega}}_2) = -\int \Phi(\boldsymbol{r}_{12},\tilde{\boldsymbol{\omega}}_1,\tilde{\boldsymbol{\omega}}_2) \mathrm{d}\boldsymbol{r}_{12} \tag{2.7}$$

To apply the above result in an Onsager-type theory for the nematic phase, one needs not only the CDF of a chain fluid, but also the excluded volume of two molecules for all possible molecular conformations. Evidently, this would result in a theory of tremendous complexity.

In the present thesis, we aim at a simpler approach. We assume a molecule's CDF can be decoupled in a part depending only on the internal conformation $\boldsymbol{\omega}'$ (all bond and torsion angles) of the molecule and a part depending only on the overall molecular axis $\boldsymbol{\omega}$ (defined as the eigenvector corresponding to the smallest eigenvalue of the molecule's moment of inertia tensor), according to

$$f(\tilde{\boldsymbol{\omega}}) \approx f(\boldsymbol{\omega}') f(\boldsymbol{\omega}) \tag{2.8}$$

With this approximation we actually assume a molecule's internal conformation is unaffected by the density of the system (for a more detailed discussion on the consequences of this approximation, the reader is referred to Chapter 4). Due to the decoupling, the pair-excluded volume can be treated as an ensemble average $\langle \ldots \rangle$ over all internal conformations of molecules 1 and 2. Accordingly, the second virial coefficient can be written in the same form as proposed by Fynewever and Yethiraj [103]

$$B_2[f(\boldsymbol{\omega}] = \frac{1}{2}\iint \langle V_{\mathrm{ex}}(\tilde{\boldsymbol{\omega}}_1,\tilde{\boldsymbol{\omega}}_2)\rangle_{\boldsymbol{\omega}'_1,\boldsymbol{\omega}'_2} f(\boldsymbol{\omega}_1) f(\boldsymbol{\omega}_2) \mathrm{d}\boldsymbol{\omega}_1 \mathrm{d}\boldsymbol{\omega}_2 \tag{2.9}$$

The great virtue of this approach is that due to the averaging, the non-rigid molecules can be treated as if they are cylindrically symmetric. As a result, the ensemble average can be reduced to a function solely depending on the angle γ between the overall molecular axes, according to

$$\langle V_{\mathrm{ex}}(\tilde{\boldsymbol{\omega}}_1,\tilde{\boldsymbol{\omega}}_2)\rangle_{\boldsymbol{\omega}'_1,\boldsymbol{\omega}'_2} = V_{\mathrm{ex}}(\gamma) \tag{2.10}$$

In the present chapter, we calculate $V_{\mathrm{ex}}(\gamma)$ by means of MC simulations of two chain molecules and fit a general correlation to the results.

2.4 Simulation details

To calculate the orientation-dependent excluded volume of two molecules, a slightly altered version of the MC algorithm introduced by Fynewever and Yethiraj [103] is used:

1. Generate two isolated chain molecules independently using the Rosenbluth method [113–116]. This method is known to produce much better statistics compared to a random generation of chains. In this method, a molecule is grown by choosing the orientation of each new bead from a predefined number of trial directions. To remove the bias introduced by this and to recover correct Boltzmann sampling, each molecule is assigned a statistical weight equal to its Rosenbluth weight. The statistical weight W_{12} of the pair of molecules is then the product of the two Rosenbluth weights W_1 and W_2.

2. Calculate the orientation of each molecule as the eigenvector corresponding to the smallest eigenvalue of its moment of inertia tensor. Rotate chain 2 to the desired angle γ.

3. Put the first bead of chain 1 at the center of a cubical simulation box with volume V_{box} and box length equal to the sum of the chain lengths of molecule 1 and 2, *i.e.* $m_1 + m_2$.

4. Move chain 2 to N_{step} random positions and count the number of overlaps N_{overlap}. Typically $N_{\text{step}} = 10^5$ is sufficient for accurate sampling.

5. Repeat Steps 1-4 for N_{pair} different chain pairs and calculate the excluded volume as

$$V_{\text{ex}}(\gamma) = \frac{V_{\text{box}}}{N_{\text{step}}} \frac{\sum_{i=1}^{N_{\text{pair}}} \left(N_{\text{overlap}} W_{12}\right)_i}{\sum_{i=1}^{N_{\text{pair}}} \left(W_{12}\right)_i} \tag{2.11}$$

   Note that, at this step, all internal conformational dependencies of the excluded volume are averaged out. Additionally, we average out any up-down asymmetry, *i.e.* $V_{\text{ex}}(\gamma) = V_{\text{ex}}(\pi - \gamma)$. Typically, $N_{\text{pair}} = 2500$ leads to sufficiently accurate sampling.

6. Repeat Steps 1-5 N_{exp} different times and average the excluded volume over the independent calculations. The value of N_{exp} is chosen such that the standard deviation calculated from the independent calculations is sufficiently small ($\sim$0.5%).

7. Repeat Steps 1-6 for a number of different angles γ uniformly distributed between 0 and $\pi/2$. For small chains ($m < 20$) we typically use 19 different angles, for longer chains we reduce this to 7 different angles to reduce the computational effort.

It is important to note that due to the forced cylindrical and up-down symmetry at Step 5, the pair-excluded volume can eventually be represented by a series in $\sin(\gamma)$. For reasons discussed previously, such a representation will be helpful for solving the Onsager Helmholtz energy functional [18, 19, 117].

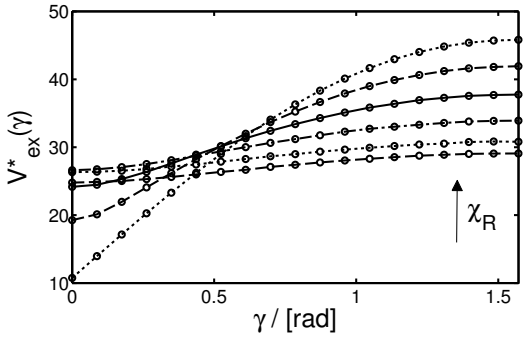

Figure 2.1: The orientation dependence of the dimensionless excluded volume of a pure rod-coil fluid of m=12 and m_{R} = 2,4,6,8,10,12. Symbols are MC data; lines are a guide for the eye.

2.5 Correlation for the excluded volume

2.5.1. Pure components

The natural starting point to find a suitable functional form for the pair-excluded volume of rod-coil molecules is the work of Williamson and Jackson [118]. Based on the work of Kihara [119] on the excluded volume of hard homo-segmented tangent dimers, Williamson and Jackson derived an exact expression for the dimensionless excluded volume of linear, homo-segmented tangent hard-sphere chains of arbitrary chain length m. Since the analytical solution of this expression is rather involved, a linear function in $\sin(\gamma)$ was fitted to the numerical results to obtain

$$V^*_{\mathrm{ex}}(\gamma) = \frac{V_{\mathrm{ex}}(\gamma)}{V_m} = \frac{11m-3}{m} + 3.5339\frac{(m-1)^2}{m}\sin(\gamma) \tag{2.12}$$

Here, V_m is the molecular volume of a chain of m tangent hard spheres. It is important to note that the first term, *i.e.* the excluded volume for the parallel orientation, and the factor $(m-1)^2/m$ of the second term are exact. Only the factor $3.5339\sin(\gamma)$ results from the fitting. This expression is very accurate and when used in Eq. (2.9) to calculate the (isotropic) second virial coefficient of hard linear tangent-sphere chains of length ranging from 2 to 10, one finds a near exact agreement (deviation at worst 0.02%) with MC data [118, 120].

To extend Eq. (2.12) to rod-coil molecules, it is instructive to examine the behaviour of the excluded volume as a function of the rigidity parameter χ_{R}. As an example, we show the excluded volume of a set of rod-coils with $m = 12$ and $m_{\mathrm{R}} = 2, 4, 6, 8, 10, 12$ in Fig. 2.1. In this figure, the symbols represent MC data and the lines are a guide for the eye. In the limit of completely linear molecules, *i.e.* $\chi_R = 1$, the excluded volume can perfectly be represented by a function of $\sin(\gamma)$. However, when the rigidity is decreased, the excluded volume requires a higher order term, such as a $\sin^2(\gamma)$-term, suggesting the following general functional form for the excluded volume of rod-coils

$$V^*_{\mathrm{ex}}(\gamma) = C_1(m,\chi_{\mathrm{R}}) + C_2(m,\chi_{\mathrm{R}})\sin(\gamma) + C_3(m,\chi_{\mathrm{R}})\sin^2(\gamma) \tag{2.13}$$

Independent fits of Eq. (2.13) to the excluded volume of different rod-coils (not included for brevity) suggested a linear dependence of the C_1, C_2 and C_3 parameters

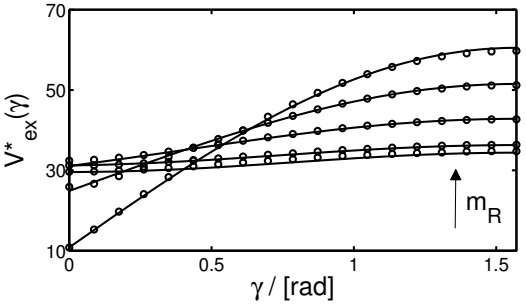

Figure 2.2: Excluded volume of a pure rod-coil fluid with m=16 and m_{R}=2,4,8,12,16. Comparison between Eqs. (2.13)-(2.19) (lines) and MC data (symbols) not included in the regression.

on the chain length m and a χ_R-dependence that can be well captured by a power law. We find the best representation of our pure component two-chain MC data using the following functional forms for C_1, C_2 and C_3

$$C_1(m,\chi_{\mathrm{R}}) = \frac{11m-3}{m} + \frac{(m-1)^2}{m}\sum_{k=1}^{3} a_k(1-\chi_{\mathrm{R}})^k \tag{2.14}$$

$$C_2(m,\chi_{\mathrm{R}}) = 3.5339\frac{(m-1)^2}{m}\chi_{\mathrm{R}}^2 \tag{2.15}$$

$$C_3(m,\chi_{\mathrm{R}}) = \frac{(m-1)^2}{m}\sum_{k=1}^{2} b_k(1-\chi_{\mathrm{R}})^k \tag{2.16}$$

where we have introduced an additional m-dependence in the a_2, a_3 and b_2 parameters as

$$a_2 = a_{21} + \frac{a_{22}}{m} \tag{2.17}$$

$$a_3 = a_{31} + \frac{a_{32}}{m} \tag{2.18}$$

$$b_2 = b_{21} + \frac{b_{22}}{m} \tag{2.19}$$

Here a_1, a_{21}, a_{22}, a_{31}, a_{32}, b_1, b_{21} and b_{22} are adjusted constants. Note that for the case of linear chains (which by definition also includes hard spheres and dimers) Eqs. (2.13)-(2.19) simply reduce to the linear chain limit from Eq. (2.12). The linear dependence on m is introduced by the factor $(m-1)^2/m$; this is based on analogy to Eq. (2.12) and, as shown in the next section, it allows for a simple extension to mixtures.

A total of 8 dimensionless adjustable constants were determined by minimizing deviations of Eqs. (2.13)-(2.19) to simulation data of the following rod-coils: 3-2, 4-(2, 3), 5-(2,3,4), 6-(2,3,4,5), 7-(2,3,4,5,6), 8-(2,3,4,5,6,7), 12-(2,3,4,6,8,10), 18-(2,3,4,6,8,10,12,14,16), 24-(2,4,8,15,22) and 30-(2,4,10,15,20,25). The regression gives an excellent result with an average relative error per data point of approximately 1.5%. The values of the 8 adjustable constants a_1-b_{22} are shown in Table 2.1.

To test the adequacy of the correlation for molecule types not included in the regression, we show the excluded volume of a rod-coil of respectively 16 segments

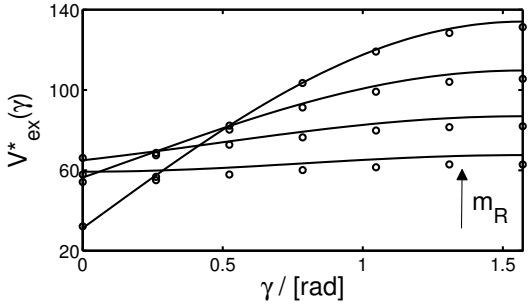

Figure 2.3: Excluded volume of a pure rod-coil fluid with m=40 and m_{R}=2,15,25,35. Comparison between Eqs. (2.13)-(2.19) (lines) and MC data (symbols) not included in the regression.

Table 2.1: The 8 model constants obtained by minimizing deviations of Eqs. (2.13)-(2.19) to MC data of the excluded volume of pure rod-coil fluids.

i	a_1	a_{2i}	a_{3i}	b_1	b_{2i}
1	4.63	−4.71	1.31	0.305	−0.171
2		7.84	−6.18		3.32

and 40 segments, for different degrees of flexibility (as defined by Eq. (2.1)), in Figs. 2.2 and 2.3. The symbols are MC data and the lines are calculated using Eqs. (2.13)-(2.19). As can be observed, the correlation can well be extrapolated to chain lengths not included in the fitting.

2.5.2. Mixtures

To extend the above approach to mixtures, *i.e.* two rod-coils of different chain length and rigidity, we start by considering the limit of two completely linear chains of different chain length m_1 and m_2. For this case, we show in Appendix A that one can reformulate Eq. (2.12) as

$$V^*_{\mathrm{ex}}(\gamma) = \frac{11\bar{m}_{12} - 3}{\bar{m}_{12}} + 3.5339\frac{(m_1 - 1)(m_2 - 1)}{\bar{m}_{12}}\sin(\gamma) \tag{2.20}$$

where we have introduced an average chain length $\bar{m}_{12}$ defined as

$$\bar{m}_{12} = \frac{m_1 + m_2}{2} \tag{2.21}$$

Here, the excluded volume is made dimensionless by dividing through $V_{\bar{m}_{12}}$, *i.e.* the molecular volume of a chain of $\bar{m}_{12}$ tangent hard spheres. It is important to note that no additional approximations were introduced to extend Eq. (2.12) to Eq. (2.20). Therefore, Eq. (2.12) can be considered as a special case of this general result for mixtures.

As for pure components, the excluded volume of a mixture of two rod-coils can be well represented by a second order series in $\sin(\gamma)$ and we find an excellent agreement

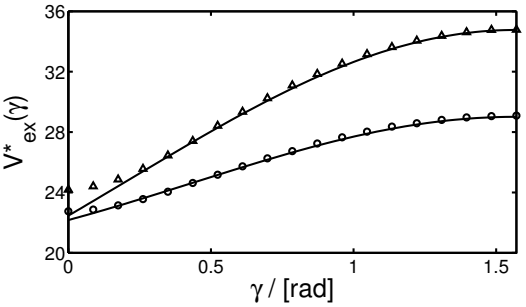

Figure 2.4: Excluded volume for a mixture of an 18-10 and 8-6 rod-coil (triangles) as well as for a mixture of a 12-4 and 8-6 rod-coil (circles). Comparison between predictions from Eqs. (2.23)-(2.26) (lines) and MC data (symbols).

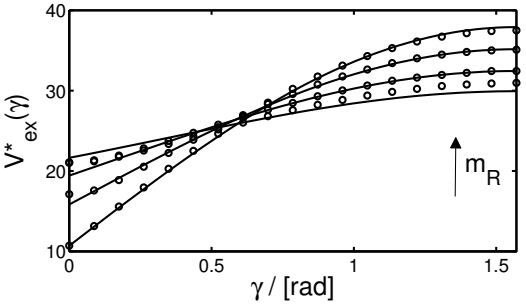

Figure 2.5: Excluded volume for a mixture of a linear chain of 12 segments and a rod-coil of $m = 8$ and $m_{\mathrm{R}} = 2,4,6,8$. Comparison between predictions from Eqs. (2.23)-(2.26) (lines) and MC data (symbols).

with MC data by introducing a combining rule for the rigidity parameter as

$$\bar{\chi}_{\mathrm{R},12} = \frac{\chi_{\mathrm{R},1} + \chi_{\mathrm{R},2}}{2} \tag{2.22}$$

In analogy to our extension of Eq. (2.12) to mixtures (Eq. (2.20)), we now define the excluded volume of the rod-coil mixture, as

$$V^*_{\mathrm{ex}}(\gamma) = C_1(\bar{m}_{12}, \bar{\chi}_{\mathrm{R},12}) + C_2(\bar{m}_{12}, \bar{\chi}_{\mathrm{R},12}) \sin(\gamma) + C_3(\bar{m}_{12}, \bar{\chi}_{\mathrm{R},12}) \sin^2(\gamma) \tag{2.23}$$

where

$$C_1(\bar{m}_{12}, \bar{\chi}_{\mathrm{R},12}) = \frac{11\bar{m}_{12} - 3}{\bar{m}_{12}} + \frac{(m_1 - 1)(m_2 - 1)}{\bar{m}_{12}} \sum_{k=1}^{3} a_k (1 - \bar{\chi}_{\mathrm{R},12})^k \tag{2.24}$$

$$C_2(\bar{m}_{12}, \bar{\chi}_{\mathrm{R},12}) = 3.5339 \frac{(m_1 - 1)(m_2 - 1)}{\bar{m}_{12}} \bar{\chi}^2_{\mathrm{R},12} \tag{2.25}$$

$$C_3(\bar{m}_{12}, \bar{\chi}_{\mathrm{R},12}) = \frac{(m_1 - 1)(m_2 - 1)}{\bar{m}_{12}} \sum_{k=1}^{2} b_k (1 - \bar{\chi}_{\mathrm{R},12})^k \tag{2.26}$$

For the case of a pair of linear chains of different chain length Eqs. (2.23)-(2.26) reduce to the quasi-exact linear chain limit of Eq. (2.20). For the case of two rod-coils of the same chain length and rigidity, one simply obtains the pure component result from Eqs. (2.13)-(2.16).

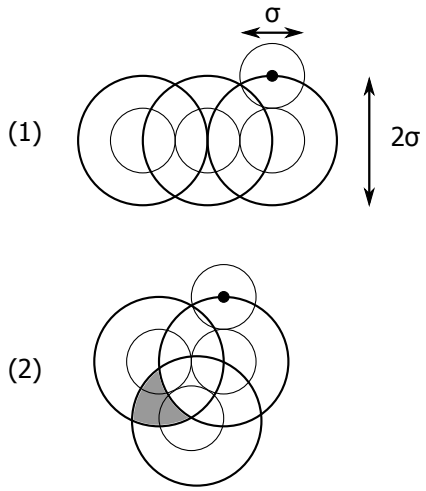

Figure 2.6: The excluded volume (large spheres of diameter 2σ) of (1) a hard sphere and a linear trimer and (2) a hard sphere and a fully flexible trimer. For case (2), the first and last segment of the excluded volume have an additional overlap (marked gray) resulting in a smaller excluded volume than for case (1).

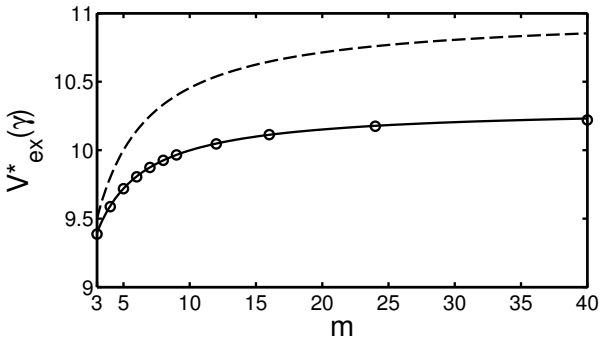

Figure 2.7: The excluded volume of a hard sphere and a fully flexible chain of m segments. The dashed line is the result from Eqs. (2.23)-(2.26) without the correction from Eq. (2.29); the solid line is the correlation from Eqs. (2.23)-(2.26) with the correction from Eq. (2.29) included. The symbols represent MC data.

In Fig. 2.4 we compare predictions of Eqs. (2.23)-(2.26) (lines) with MC data (symbols) for a mixture of an 18-10 and 8-6 rod-coil and a mixture of a 12-4 and 8-6 rod-coil. The overall agreement is very good except for a small underestimation of the excluded volume at small angles γ. Since the 8 constants a_1-b_{22} (see Table 2.1) were fitted to excluded volume data for identical chains only, it is expected that predictions based on Eqs. (2.23)-(2.26) become less accurate when the two molecules become less similar. A more stringent test is therefore the case of a linear chain and a fully flexible chain. In Fig. 2.5 we show the excluded volume of a linear chain of 12 segments and a rod-coil of 8 segments with variable degree of flexibility (as defined by Eq. (2.22)). Indeed we see that predictions become less accurate when the flexibility of the rod-coil is increased (and thus the two molecules become less similar), however even for the case of a linear chain and a fully flexible chain the overall agreement between MC data and predictions is very satisfying.

A clear limitation of Eqs. (2.23)-(2.26) is the case of a hard sphere and a rod-coil. The functional form of $C_1(\bar{m}_{12}, \bar{\chi}_{\mathrm{R},12})$ is such that for this case the second term equals zero and thus the calculated excluded volume is the same as for a hard sphere and a linear chain. In this, any next-nearest (and higher order) neighbour effects

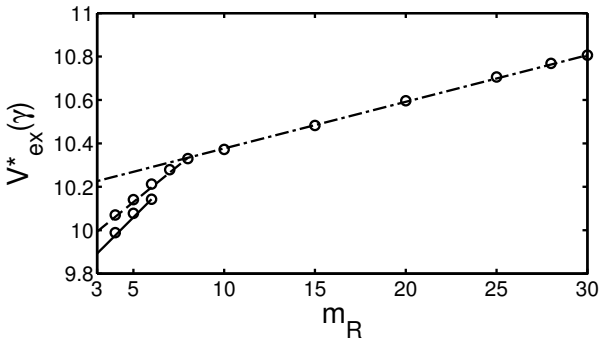

Figure 2.8: The excluded volume of a hard sphere and respectively a 6-m_{R} rod-coil (solid line), an 8-m_{R} rod-coil (dashed line) and a 30-m_{R} rod-coil (dash-dotted line). Comparison between the correlation from Eqs. (2.23)-(2.26) with the correction from Eq. (2.29) included (lines) and MC data (symbols).

are neglected (as illustrated in Fig. 2.6), leading to a systematic overestimation of the excluded volume (marked gray in Fig. 2.6). This limiting case is relevant, for example for mixtures of liquid crystals with small solutes, and therefore we add a scaling $1 - D(\bar{m}_{12}, \bar{\chi}_{\mathrm{R},12})$ to the first term of the C_1 parameter from Eq. (2.24) to correct for this overestimation as

$$C_1(\bar{m}_{12}, \bar{\chi}_{\mathrm{R},12}) = \left(\frac{11\bar{m}_{12} - 3}{\bar{m}_{12}}\right)[1 - D(\bar{m}_{12}, \bar{\chi}_{\mathrm{R},12})] + \tag{2.27}$$

$$\frac{(m_1 - 1)(m_2 - 1)}{\bar{m}_{12}} \sum_{k=1}^{3} a_k (1 - \bar{\chi}_{\mathrm{R},12})^k \tag{2.28}$$

In general, each flexible bond-angle of the chain molecule will result in an overlap volume (similar to that in Fig. 2.6) that needs to be corrected for. The overlap volume for the first bond-angle in the chain only contains next-nearest neighbour effects, the second will additionally contain next-next-nearest neighbour effects, and so on. Because of this, the flexible bond angles at the beginning of a chain will result in a somewhat smaller overlap volume than those further in the chains backbone and, consequentially, require a smaller correction. For a very long chain, this effect averages out and all overlap volumes can be considered as identical. For this case, the correction to the excluded volume $V_{\mathrm{corr}} = -(11\bar{m}_{12} - 3)D(\bar{m}_{12}, \bar{\chi}_{\mathrm{R},12})$ should scale linearly with the number of flexible bond angles, suggesting a functional form as $D(\bar{m}_{12}, \bar{\chi}_{\mathrm{R},12}) = d_1(1 - \bar{\chi}_{\mathrm{R},12})$. To obtain a smaller correction for shorter chain lengths, a hyperbolic term in the chain length $\bar{m}_{12}$ is included as

$$D(\bar{m}_{12}, \bar{\chi}_{\mathrm{R},12}) = [\delta_{1m_1} - \delta_{1m_2}]^2 \left(d_1 - \frac{d_2}{\bar{m}_{12}}\right)(1 - \bar{\chi}_{\mathrm{R},12}) \tag{2.29}$$

The term $[\delta_{1m_1} - \delta_{1m_2}]^2$, with δ being a Kronecker delta, is a correction factor for the case of a hard sphere and a partially flexible (rod-coil) chain fluid. For any other case, it reduces to zero. The d_1 and d_2 parameters were fitted to MC data of the excluded volume of several hard-sphere/rod-coil mixtures; the values are respectively d_1=0.125 and d_2=0.206. As shown in Figs. 2.7 and 2.8 the scaling is excellent and both the dependence of D on $\bar{m}_{12}$ and on $\bar{\chi}_{\mathrm{R},12}$ is very well correlated for a wide

range of chain lengths (at least up to $\bar{m}_{12} = 20.5$) and rigidities. It is important to note that the functional form of the $C_2(\bar{m}_{12}, \bar{\chi}_{\mathrm{R},12})$ and $C_3(\bar{m}_{12}, \bar{\chi}_{\mathrm{R},12})$ parameters from Eqs. (2.25) and (2.26) remains unchanged.

2.6 Conclusion

We developed an analytical approximation for the orientation-dependent excluded volume of two rod-coil molecules. The expression has a total of 8 adjustable constants that were regressed to a wide range of pure-component excluded-volume data (with chain lengths up to 30 segments) obtained from MC simulations of two chain molecules. We find an excellent representation of the simulation data with an average relative deviation of approximately 1.5% per data point. The correlation accurately covers the effects of intramolecular flexibility and can be extrapolated to (larger) chain lengths not included in the regression with reasonable accuracy. An extension to mixtures of different chains of equally-sized segments is possible by introducing combining rules for the chain length and rigidity parameter. Both for pure components and mixtures, the correlation reduces to an exact expression in the limit of linear chains.

3

An equation of state for the isotropic phase of linear, partially flexible and fully flexible tangent hard-sphere chain fluids

A new equation of state (EoS) is developed that accurately describes the isotropic phase behaviour of linear, partially flexible and fully flexible tangent hard-sphere chain fluids and their mixtures. The EoS is based on the EoS of Liu and Hu [H. Liu and Y. Hu, Fluid Phase Equilibr. ***122****, 75 (1996)] for fully flexible chain fluids. The effect of molecular flexibility is described by a pure-component parameter that is introduced in the theory at the level of the cavity correlation function of next-to-nearest neighbour segments in a chain molecule. The EoS contains a total of three adjustable model constants. The extension to partially flexible- and linear chain fluids is based on a refitting of the first model constant to numerical data of the second virial coefficient of partially flexible and linear tangent hard-sphere chain fluids. The numerical data was obtained from the analytical approximation for the pair-excluded volume that was developed in Chapter 2. The other two parameters were adjusted to MC data for the pressure of linear tangent hard-sphere chain fluids. For both, pure component systems and mixtures of chains of variable flexibility, the pressure and second virial coefficient obtained from the EoS are in excellent agreement with the results from MC simulations. A significant improvement to TPT1, TPT2, generalized Flory-dimer theory (GFD) and Scaled Particle Theory (SPT) is observed.*

Parts of this chapter have been published as:
T. van Westen, B. Oyarzún, T.J.H. Vlugt and J. Gross *Mol. Phys.* 112 (2014) 919-928 [121].

3.1 Introduction

In the past three decades, there has been considerable effort to develop equations of state for hard-chain fluids [59, 60, 122–125]. Predominantly, this is inspired by the successes of molecular perturbation theory [54, 55, 126, 127]. In such an approach, an accurate description of the thermodynamic properties of a hard, purely repulsive reference fluid can be considered as a prerequisite for developing a reliable fluid theory for describing physical properties of real (polymeric) fluids. Using the reference fluid as a basis, the effect of attractive intermolecular interactions can be added as a perturbation. Whereas the fully flexible hard-chain fluid has served as a reference for the development of some successful equations of state for isotropic fluids (*e.g.* the SAFT family of equations of state [63, 65, 72]), it is well-known that the description of more complex fluids, like liquid crystals, requires a molecular model that includes some rigidity in the chain's backbone [89–93].

Any theoretical treatment aimed at a description of the liquid crystalline phase transition critically relies on an accurate description of the properties of the isotropic phase. Therefore, in the present chapter, we develop a new equation of state (EoS) that is applicable to the isotropic phase of mixtures of both linear, partially flexible and fully flexible tangent hard-sphere chain fluids. Inspired by the typical structure of real (thermotropic) liquid crystal molecules [89], the 'partial' flexibility is introduced by arranging one part of the chain in a rigid, linear conformation while maintaining the other part fully flexible. Following the work of Liu and Hu on fully flexible chains [125, 128], the new EoS is derived by approximating the cavity correlation function (CCF) of a chain fluid by a product of nearest- and next-to-nearest neighbour contributions. We thereby extend their approach to linear and partially flexible chains by reformulating the next-to-nearest neighbour CCF in terms of the dimensionless rigidity parameter from Eq. (2.1). For the fully flexible case, this parameter equals zero and the original EoS of Liu and Hu is retained.

This chapter is organized as follows. In Section 3.2 we list the details of the MC simulations that were performed. The equation of state is derived in Section 3.3. In Section 3.4, theoretical results for the pressure and second virial coefficient of both pure component systems and mixtures of chains of variable degree of flexibility are compared to the results from MC simulations obtained in this work and from literature.

3.2 Simulation details

Both for the development and testing of the EoS presented in this chapter, we calculated the isotropic fluid behaviour of tangent hard-sphere chain fluids from MC simulations in the isobaric-isothermal NPT ensemble [116]. The different MC moves used in the simulations are translation, rotation, volume change and (for partially flexible molecules) configurational-bias regrowth moves [116, 129, 130] with relative probabilities of 41.5% (49% for linear chains), 41.5% (49% for linear chains), 2% and 15% (0% for linear chains), respectively. A rectangular simulation box with independently varying sides was used. Periodic boundary conditions were applied. The maximum translational displacement, rotational displacement and volume expan-

sion/contraction were adjusted to obtain approximately 20% acceptance. For the simulation of pure component systems we typically used a number of 350 molecules. For the equimolar binary mixtures, we used 400 molecules per molecule type in the system. For the other mixtures, we used 360 chain molecules and 40 hard spheres. A typical simulation run consisted of at least 10^6 MC cycles for equilibration and 10^6 MC cycles for production. The number of MC moves per cycle was set to the total number of molecules in the system. Statistical errors in the calculated packing fractions were in the range of 1-2%.

3.3 Equation of state

3.3.1. Fully flexible tangent hard-sphere chain fluids

The equation of state developed in this chapter is based on the equation of state of Liu and Hu for fully flexible tangent hard-sphere chain fluids [125, 128]. In this section, we shortly review their work and related work that is relevant to our discussion.

Based on a sticky-point model for chemical association, Zhou and Stell [124] derived an equation of state for a system of N chain molecules comprising m spherical segments

$$Z = \frac{PV}{NkT} = 1 + mZ^{\mathrm{hs}} - \eta \frac{\partial \ln y^{(m)}}{\partial \eta} \tag{3.1}$$

Here, $\eta = (\pi/6)\rho m \sigma^3$ is the packing fraction of the system, $\rho = N/V$ is the total number density of chain molecules, Z^{hs} is the hard-sphere contribution to the compressibility factor (which is a residual property) and $y^{(m)}$ is the m-particle cavity correlation function (CCF) of the hard-sphere reference system, evaluated at the positions which yield the configuration of the chain fluid. The CCF is defined as the m-particle distribution function divided by the m-particle Boltzmann factor as $y^{(m)} = g^{(m)} \exp[u^{(m)}/kT]$, where $u^{(m)}$ is the total intermolecular potential energy of the assembly of m hard spheres [54]. Since the above equation involves properties of the hard-sphere fluid only, it can be straightforwardly generalized to a mixture of $i = 1, \ldots, N_c$ components as

$$Z = \frac{PV}{NkT} = 1 + \sum_{i=1}^{N_c} x_i \left[m_i Z^{\mathrm{hs}} - \eta \frac{\partial \ln y_{(i)}^{(m_i)}}{\partial \eta} \right] \tag{3.2}$$

The packing fraction of the mixture is defined as $\eta = (\pi/6)\rho \sum_{i=1}^{N_c} x_i m_i \sigma_i^3$, where $x_i = N_i/N$ is the mole fraction of component i. Since we will only evaluate mixtures of chains with equally-sized segments, the hard-sphere contribution can be accurately obtained from the Carnahan-Starling EoS [131]

$$Z^{\mathrm{hs}} = \frac{4\eta - 2\eta^2}{(1-\eta)^3} \tag{3.3}$$

Different approximations have been developed to calculate the m-particle CCF [124, 125, 128]. We use the approximation of Liu and Hu [125, 128], and assume correla-

tions between nearest- and next-to-nearest neighbour segments only, leading to

$$y_{(i)}^{(m_i)} \approx \prod_{j=1}^{m_i-1} y_{(i),j,j+1}^{(2)} \prod_{j=1}^{m_i-2} y_{(i),j,j+2}^{(2)} \tag{3.4}$$

Here, $y_{(i),j,j+1}^{(2)}$ and $y_{(i),j,j+2}^{(2)}$ are the pair-CCF for the nearest- $(j, j+1)$ and next-to-nearest neighbour pairs $(j, j+2)$ in a chain molecule of component i, respectively. Assuming all pairs can be considered as identical (neglecting end effects), substitution of Eq. (3.4) in Eq. (3.2) results in

$$Z = 1 + \sum_{i=1}^{N_c} x_i \left[m_i Z^{\text{hs}} - (m_i - 1)\eta \frac{\partial \ln y_{(i),j,j+1}^{(2)}}{\partial \eta} - (m_i - 2)\eta \frac{\partial \ln y_{(i),j,j+2}^{(2)}}{\partial \eta} \right] \tag{3.5}$$

The nearest-neighbour CCF is accurately obtained from the Tildesley-Street equation for hard dumbbells as [132]

$$\ln y_{(i),j,j+1} = \frac{(3 + a_{20})\eta - (1 + b_{20})}{2(1-\eta)} + \frac{1 + b_{20}}{2(1-\eta)^2} - (c_{20} + 1)\ln(1-\eta) \tag{3.6}$$

Here, $a_{20} = -a_2 + b_2 - 3c_2$; $b_{20} = -a_2 - b_2 + c_2$; $c_{20} = c_2$ and $a_2 = 0.45696$; $b_2 = 2.10386$; $c_2 = 1.75503$. To obtain an expression for the next-to-nearest-neighbour CCF, Liu and Hu assumed a similar functional form as in the equation above

$$\ln y_{(i),j,j+2} = \frac{m_i - 1}{m_i} \left[\frac{a_{30}\eta - b_{30}}{2(1-\eta)} + \frac{b_{30}}{2(1-\eta)^2} - c_{30}\ln(1-\eta) \right] \tag{3.7}$$

where the parameters a_{30}, b_{30} and c_{30} were obtained by fitting molecular simulation data [133, 134] for the compressibility factor of linear tangent trimers. The parameters are given by $a_{30} = -a_3 + b_3 - 3c_3$; $b_{30} = -a_3 - b_3 + c_3$; $c_{30} = c_3$ and $a_3 = -0.74745$; $b_3 = 3.49695$; $c_3 = 4.83207$. By combining Eqs. (3.5)-(3.7), the compressibility factor can be written in the following compact form

$$Z = \frac{1 + a\eta + b\eta^2 - c\eta^3}{(1-\eta)^3} \tag{3.8}$$

where the a, b and c parameters are defined as

$$a = \sum_i^{N_C} x_i m_i \left[1 + \frac{m_i - 1}{m_i} a_2 + \frac{m_i - 1}{m_i} \frac{m_i - 2}{m_i} a_3 \right] \tag{3.9}$$

$$b = \sum_i^{N_C} x_i m_i \left[1 + \frac{m_i - 1}{m_i} b_2 + \frac{m_i - 1}{m_i} \frac{m_i - 2}{m_i} b_3 \right] \tag{3.10}$$

$$c = \sum_i^{N_C} x_i m_i \left[1 + \frac{m_i - 1}{m_i} c_2 + \frac{m_i - 1}{m_i} \frac{m_i - 2}{m_i} c_3 \right] \tag{3.11}$$

The resulting EoS provides an excellent description of the phase behaviour of fully flexible tangent hard-sphere chain fluids and their mixtures [125, 128]. In the remainder of this chapter it is referred to as the LH EoS. Compared to other equations of state, such as TPT1, TPT2 and GFD, the LH EoS leads to a superior description of both the compressibility factor and second virial coefficient.

3.3.2. Extension to linear and partially flexible chain fluids

In Eqs. (3.9)-(3.11), the a_3-, b_3- and c_3-parameters govern the next-to-nearest neighbour correlations in a chain. Therefore, to extend the LH EoS to describe chain molecules of different flexibility constraints, the effect of molecular rigidity should be reflected in these parameters. We choose to do this in terms of the rigidity parameter χ_{R} that was defined in Eq. (2.1) from Chapter 2. The a_3-parameter was fitted to the reduced isotropic second virial coefficient of pure-component tangent hard-sphere chain fluids of length $m = 1$ to 120, using Eq. (3.9) and

$$B_2^* = \frac{B_2}{V_m} = (3 + a) \tag{3.12}$$

Here, $V_m = (\pi/6)m\sigma^3$ is the molecular volume of a chain of m segments of diameter σ (please note that for the the pure components considered here we have dropped the subscript i for m and σ). The data for the second virial coefficient that was used in the parameter regression was obtained from the analytical approximation for the pair-excluded volume that was developed in the previous chapter. In terms of the second virial coefficient, this correlation can be written as

$$B_2^* = \frac{C_1(m, \chi_{\mathrm{R}})}{2} + \frac{\pi C_2(m, \chi_{\mathrm{R}})}{8} + \frac{C_3(m, \chi_{\mathrm{R}})}{3} \tag{3.13}$$

For the functional form of the coefficients $C_1(m, \chi_{\mathrm{R}})$, $C_2(m, \chi_{\mathrm{R}})$, and $C_3(m, \chi_{\mathrm{R}})$ the reader is referred to Eqs. (2.14)-(2.16). The model parameter a_3 was individually optimized for $\chi_{\mathrm{R}} = \{0.0\ 0.1\ 0.2\ 0.3 \ldots 1.0\}$.

As could be expected from the functional form of the coefficients of Eq. (3.13), the χ_{R}-dependence of a_3 is captured accurately by the following polynomial

$$a_3 = x(1) + x(2)\chi_R + x(3)\chi_R^2 + x(4)\chi_R^3 \tag{3.14}$$

Here, $\boldsymbol{x} = (-0.74745,\ 0.29915,\ 1.08727,\ -0.70898)$. The model constant $x(1)$ was forced to a value of -0.74745 to recover the original result of Liu and Hu for the fully flexible chain limit at $\chi_{\mathrm{R}} = 0$. As shown in Fig. 3.1, the second virial coefficients calculated from Eqs. (3.9), (3.12) and (3.14) are in excellent agreement with those obtained from Eq. (3.13) and MC simulations [135]. It is important to note that for rigid, linear chains, *i.e.* $\chi_{\mathrm{R}} = 1$, the expression for the second virial coefficient from Eq. (3.13) reduces to the quasi-exact result of Williamson and Jackson [118].

The b_3- and c_3-parameters become important for interactions above the pair-level. Their dependence on χ_{R} is difficult to know *a priori*. In this study, we assume linear relations between the fully flexible ($b_3 = 3.49695$, $c_3 = 4.83207$ [128]) and completely rigid chain limit. The b_3- and c_3-parameters for the rigid chain limit were

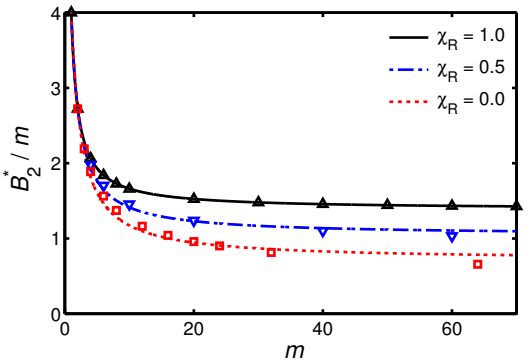

Figure 3.1: The variation of the reduced second virial coefficient $B_2^* = B_2/V_m$ with chain-length m for different values of the rigidity parameter χ_R. The lines are results from the equation of state that was developed in this chapter. The upward triangles ($\chi_R = 1.0$) are the quasi-exact results from Eq. (3.13). The downward triangles ($\chi_R = 0.5$) and squares ($\chi_R = 0.0$) are MC data obtained by us (using a MC integration method similar to that from Chapter 2) and from Ref. [135], respectively. Standard deviations of the MC data fall within the symbol size.

obtained by fitting MC data for the pressure of linear tangent hard-sphere chains of length $m = 3$ to 15 [133, 134, 136]. For completeness, all MC data used in the regression is presented in tabular form in the supplementary material of Ref. [121]. For the values of $b_3 = -0.317719$ and $c_3 = 3.48016$ we found the best fit, with an average relative deviation per data-point of 2.2% (compared to 6.7% for the original LH EoS). Accordingly, the b_3 and c_3 parameters can be written as

$$b_3 = 3.49695 - 3.81467\chi_R \tag{3.15}$$

$$c_3 = 4.83207 - 1.35191\chi_R \tag{3.16}$$

Although the assumption of linearity is *ad hoc*, we show in Fig. 3.2 that it sufficiently accounts for the effect of molecular rigidity on the packing fraction of a chain fluid at fixed pressure. An interesting result that can be extracted from the MC data is the inversion of the relationship between the pressure and the rigidity parameter at increased densities, *i.e.* for low densities the pressure of a rigid, linear chain fluid ($\chi_R = 1$) is higher than that of a fully flexible chain fluid (as can be expected from the pair-excluded volume/second virial coefficient) and for high densities the pressure of a rigid, linear chain fluid is lower than that of a fully flexible chain fluid. Apparently, at high density, linear chains pack better than their fully flexible counterparts. The nature of this effect must be due to complex higher-body interactions between the molecules in the fluid. We note that Phan *et al.* [137] already predicted this effect using a slightly modified version of the TPT2 equation of state of Wertheim [60]. However, they suspected it was an artefact of the theory and not intrinsic to the system, which we hereby clarify. The TPT2 of Phan *et al.* also lends itself for an extension to partially flexible chain fluids (see Appendix B for details). Results for this TPT2-implementation are also included in Fig. 3.2. Although these results do not show any inversion of the rigidity-pressure relationship, at higher pressure an inversion does occur (not included for brevity).

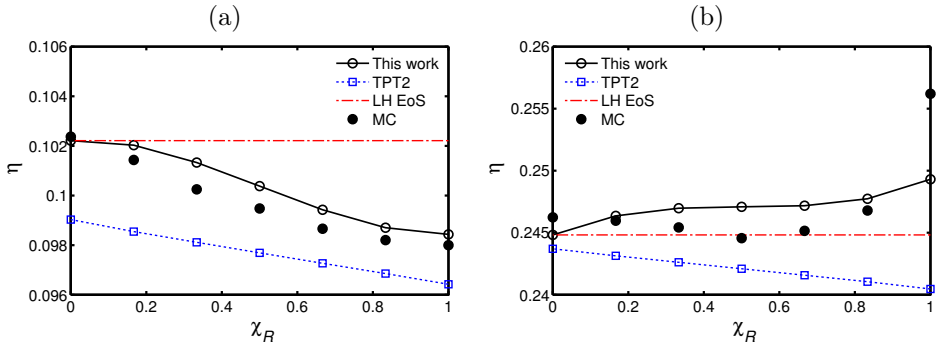

Figure 3.2: The effect of molecular rigidity on the packing fraction of a system of 8-m_{R} chain molecules at a dimensionless pressure (a) $P^* = PV_m/kT = 0.3$ and (b) $P^* = PV_m/kT = 2.6$, respectively. Closed symbols are results obtained from NPT MC simulations. Open symbols are results obtained from the equation of state developed in this chapter (circle) and TPT2 (square). The lines connecting these symbols are a guide for the eye. Results obtained from the original LH EoS are also included (dash-dotted line).

3.4 Results

3.4.1. Pure components

In Figs. 3.3 and 3.4 we compare predictions from the EoS developed in this chapter to the results from NPT MC simulations for the dimensionless pressure of linear and partially flexible tangent hard-sphere chain fluids [136], respectively. For comparison, the pressure as obtained from the original LH EoS is also included. For all systems considered, the new EoS shows a clear improvement in predicting the MC data.

A more thorough assessment of the EoS is presented in Tables 3.1 and 3.2. Here we show the percentage average absolute deviation (AAD) of the EoS with respect to NPT MC data [133, 134, 136] of the dimensionless pressure for a range of different linear and partially flexible tangent hard-sphere chain fluids, respectively. All MC data used for the comparison is presented in tabular form in the supplementary material of Ref. [121]. The results are compared to those obtained from TPT1 [63], TPT2 [137], generalized Flory-dimer theory (GFD) [123], the SPT of Jaffer *et al.* [104] and the original LH EoS [128]. The model inputs for SPT (second virial coefficient) and GFD (exclusion volume, *i.e.* pair-excluded volume of a hard-sphere and chain molecule) were accurately obtained from Eq. (3.13) and the correlation for the pair-excluded volume from Chapter 2, respectively. The application of TPT2 to partially flexible chain fluids is based on its recursive form as was developed by Phan *et al.* [137]. This EoS is summarized in Appendix B. In summary, TPT2, GFD theory and SPT are applied explicitly accounting for the partial flexibility of the molecular model used in this study.

Both for linear (AAD = 2.49%) and partially flexible (AAD = 1.99%) chain fluids, the EoS developed in this chapter provides the most reliable description of the MC data. Obviously, the description of the trimer system (and to some extent the 4-mer system) is somewhat less accurate since through the fitting to chains

Table 3.1: The percentage average absolute deviation (AAD) of the dimensionless pressure of linear m-mers as predicted from TPT1, TPT2, SPT, GFD, LH and the equation of state developed in this chapter with respect to MC data [133, 134, 136, 138]. The numerical (MC) data used to calculate the AAD is listed in the supplementary material of Ref. [121].

			AAD / [%]					
m	η-range	# data points	TPT1	TPT2	SPT	GFD	LH	This work
3	0.05-0.45	12	0.76	1.29	2.48	0.81	1.28	3.17
4	0.10-0.43	30	5.14	2.85	2.77	5.25	3.87	3.28
5	0.10-0.35	16	6.02	5.32	2.23	6.19	4.22	2.08
6	0.14-0.32	24	8.80	8.48	3.85	9.00	6.26	2.04
7	0.18-0.29	30	10.98	11.20	4.67	11.22	6.92	2.52
8	0.13-0.26	27	9.29	10.07	3.94	9.40	6.05	2.47
9	0.15-0.23	30	12.48	13.46	5.22	12.65	6.50	3.48
10	0.12-0.21	19	12.11	13.29	4.79	12.21	5.18	3.50
11	0.07-0.19	35	10.39	11.62	3.79	10.33	4.50	2.97
12	0.13-0.18	39	9.89	11.23	2.76	9.79	2.95	2.38
13	0.11-0.17	36	9.36	10.69	2.56	9.18	3.57	2.33
14	0.07-0.16	36	8.27	9.54	1.68	8.00	5.38	1.70
15	0.09-0.15	39	8.95	10.26	1.78	8.65	5.43	1.98
20	0.04-0.11	19	6.21	7.02	1.11	5.51	13.06	1.03
		AAD / [%]	8.47	9.02	3.12	8.44	5.37	2.49

Table 3.2: The percentage average absolute deviation (AAD) of the dimensionless pressure of partially flexible m-m_{R} chains as predicted from TPT1, TPT2, SPT, GFD, LH and the equation of state developed in this chapter with respect to MC data [136]. The numerical (MC) data used to calculate the AAD is listed in the supplementary material of Ref. [121].

				AAD / [%]					
m-m_{R}	χ_{R}	η-range	# data points	TPT1	TPT2	SPT	GFD	LH	This work
7-6	0.80	0.29-0.37	11	15.08	12.14	5.66	14.55	11.97	3.83
8-7	0.83	0.17-0.32	18	10.62	9.60	3.22	10.25	6.98	1.93
8-6	0.67	0.17-0.37	16	8.50	6.32	5.27	7.43	5.27	2.20
10-8	0.75	0.16-0.28	11	9.06	8.27	3.95	8.24	4.57	1.15
10-6	0.50	0.16-0.35	10	6.09	4.09	13.06	4.22	1.92	3.13
14-13	0.92	0.09-0.17	9	7.72	8.35	2.10	7.14	5.27	1.64
14-12	0.83	0.14-0.19	4	9.09	9.28	2.54	8.30	2.33	1.46
14-10	0.67	0.14-0.25	12	11.12	10.08	6.32	9.68	4.58	1.81
15-14	0.92	0.07-0.16	10	7.52	8.10	1.69	6.88	6.69	1.50
15-13	0.85	0.07-0.18	13	7.97	8.05	2.80	7.06	5.57	1.33
15-12	0.77	0.14-0.21	12	10.27	10.01	3.71	9.18	3.00	1.90
			AAD / [%]	9.37	8.57	4.58	8.45	5.28	1.99

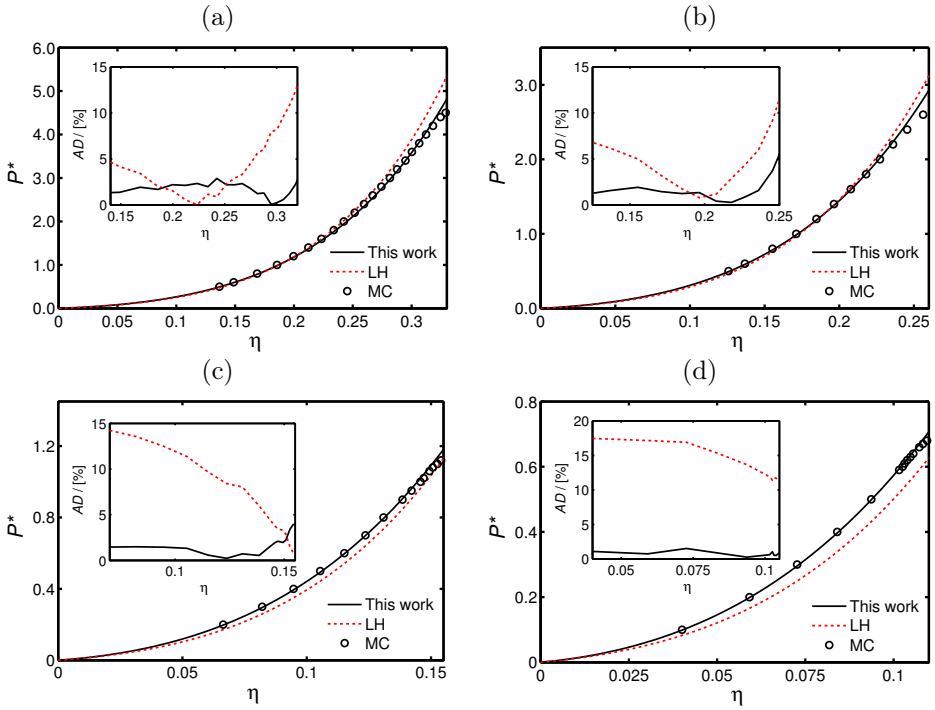

Figure 3.3: The dimensionless pressure $P^* = PV_m/kT$ vs packing fraction η for a system of (a) linear 6-mers, (b) linear 8-mers, (c) linear 14-mers and (d) linear 20-mers. The solid line corresponds to the equation of state developed in this chapter, the dotted line to the original EoS of Liu and Hu [128] and the symbols to MC data obtained by us (linear 6-mer) and from Ref. [136]. The figures in the insets show the percentage absolute deviation (AD) of the equations of state with respect to the MC data.

with segment numbers greater than 3 we effectively included the effect of correlations between segments separated for more than two bonds in the a_3-, b_3- and c_3-parameters of the next-to-nearest neighbour CCF (Eq. 3.7), whereas the LH model was parametrized to trimer fluids. For systems of dimers and hard spheres, the EoS in this chapter reduces to the Tildesley-Street and Carnahan-Starling equation, respectively. Thereby, an accurate description of these systems is maintained.

3.4.2. Mixtures

In Fig. 3.5, we compare predictions from the EoS developed in this chapter to the results from *NPT* MC simulations for the dimensionless pressure of several mixtures of linear and fully flexible tangent hard-sphere chain fluids. For comparison, the pressure as obtained from the original LH EoS is also included. For all systems considered, the new EoS shows an improvement in predicting the MC data. A more extensive comparison to the results obtained from TPT1, GFD, SPT and the LH EoS is presented in Table 3.3. To describe a mixture with GFD, we used the one-fluid theory as was derived in Section II D of Ref. [139]. Accordingly,

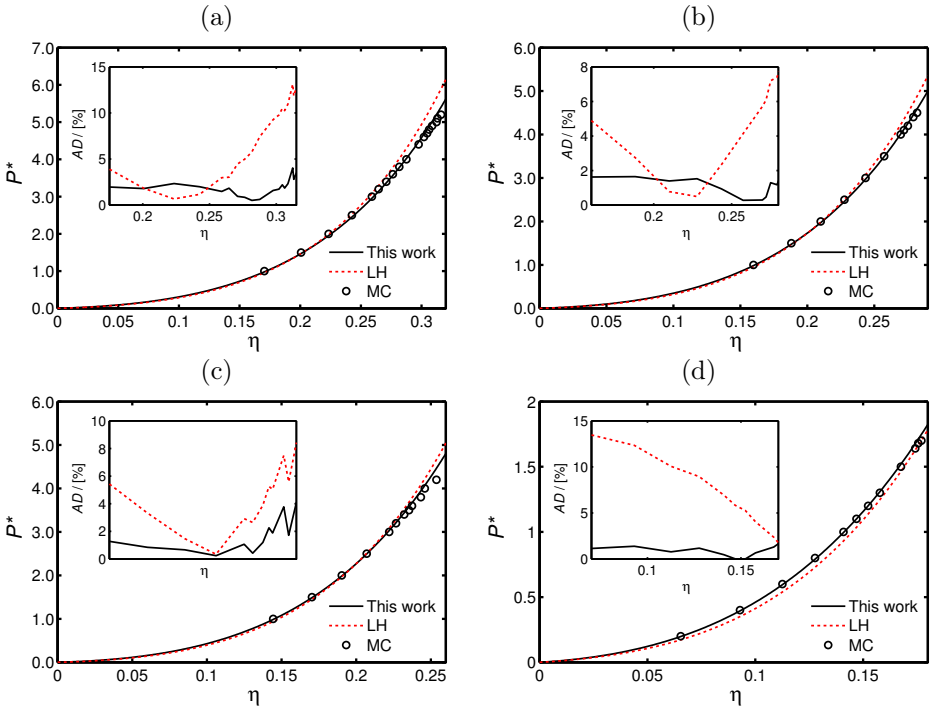

Figure 3.4: The dimensionless pressure $P^* = PV_m/kT$ vs packing fraction η for a system of partially flexible (a) 8-7 chains, (b) 10-8 chains, (c) 14-10 chains and (d) 15-13 chains. The solid line corresponds to the equation of state developed in this chapter, the dotted line to the original EoS of Liu and Hu [128] and the symbols to MC data of Oyarzún *et al.* [136]. The figures in the insets show the percentage absolute deviation (AD) of the equations of state with respect to the MC data.

the exclusion volume of the mixture was calculated using the average chain-length of the mixture $\tilde{m} = \sum_i x_i m_i$. For SPT, we used the SPT of Jaffer *et al.* [104], where the second virial coefficient of the mixture was obtained from the mixture version of Eq. (3.13) (see Chapter 2 for details). To extend the treatment of Jaffer to mixtures, we calculated the required molecular volume and -surface area by a simple mole fraction weighted sum over the respective pure-component quantities. For all systems considered, the EoS developed in this chapter leads to the most accurate prediction of the MC data.

Let us now shift our analysis to the second virial coefficient. From statistical mechanics (graph/cluster theory [45]) we know that, under the assumption of pairwise-additive interactions, the second virial coefficient of a mixture is defined as a mole-fraction-weighted sum of the second virial coefficients of the individual pair interactions over all possible pair interactions, according to

$$\bar{B}_2 = \sum_i^{N_C} \sum_j^{N_C} x_i x_j B_{2,ij} \tag{3.17}$$

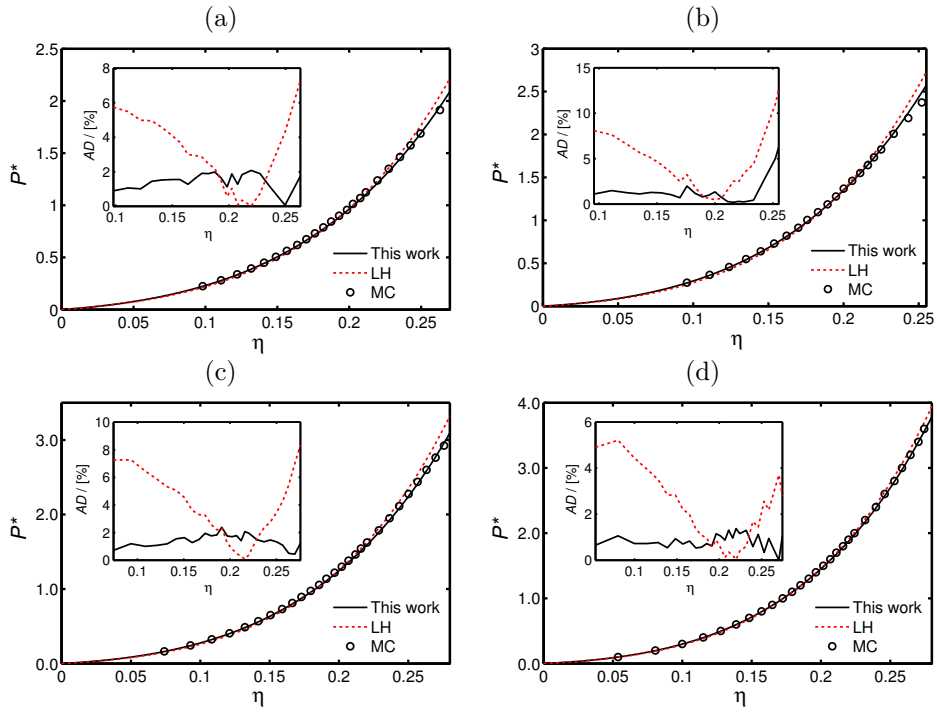

Figure 3.5: The dimensionless pressure $P^* = PV_m/kT$ vs packing fraction η for a binary mixture of (a) linear 8-mers and hard spheres at $x_{\mathrm{hs}} = 0.5$, (b) linear 8-mers and hard spheres at $x_{\mathrm{hs}} = 0.1$, (c) equimolar linear 8-mers and linear 5-mers and (d) equimolar linear 8-mers and fully flexible 8-mers. The solid line corresponds to the equation of state developed in this chapter, the dotted line to the original EoS of Liu and Hu [128] and the symbols to MC data obtained in this study. The figures in the insets show the percentage absolute deviation (AD) of the equations of state with respect to the MC data.

Table 3.3: The percentage average absolute deviation (AAD) of the dimensionless pressure of some mixtures of tangent hard-sphere chains of variable degree of flexibility as predicted from TPT1, SPT, GFD, LH and the equation of state developed in this chapter with respect to MC data. The numerical (MC) data used to calculate the AAD is listed in the supplementary material of Ref. [121]. Approximately 25 data points per system were included.

				AAD / [%]				
m_1-$m_{R,1}$	m_2-$m_{R,2}$	x_1	η-range	TPT1	SPT	GFD	LH	This work
8-8	1-1	0.50	0.10-0.26	3.94	17.42	3.96	2.96	1.44
8-8	1-1	0.90	0.10-0.26	7.07	4.69	7.10	4.60	1.60
8-8	5-5	0.50	0.07-0.28	6.29	2.88	6.36	4.44	1.82
8-6	1-1	0.50	0.06-0.26	2.88	20.14	2.58	2.48	1.89
8-6	1-1	0.90	0.10-0.27	4.30	11.22	3.42	2.45	2.15
8-6	5-5	0.50	0.07-0.27	3.57	6.27	3.14	2.62	2.17
8-2	8-8	0.50	0.05-0.27	6.46	8.88	4.80	2.01	0.82
			AAD / [%]	4.93	10.21	4.48	3.08	1.70

Table 3.4: Comparison of the second virial coefficient of some mixtures of tangent hard-sphere chain fluids as obtained from TPT1, the mixture version of Eq. (3.13) [88]/SPT, GFD, the LH EoS, the EoS obtained in this chapter and MC (MC) simulations. The MC data was obtained using a MC integration method similar to that from Ref. [88]. Standard deviations of the MC data are less than 1%.

			$\bar{B}_2$					
m_1-$m_{R,1}$	m_2-$m_{R,2}$	x_1	TPT1	SPT	GFD	LH	This work	MC
20-11	30-30	0.4	565.0	500.5	544.6	315.5	496.2	496.0
20-11	30-30	0.8	408.9	333.3	390.5	234.1	328.8	329.6
20-11	2-2	0.4	78.5	64.6	76.2	52.2	63.2	64.0
20-11	2-2	0.8	232.7	180.9	222.8	139.2	178.3	179.7

For the EoS developed in this chapter, the second virial coefficient of the individual pair interactions can be obtained as

$$B_{2,ij} = (\pi/6)\sigma^3 m_i m_j \left[1 + \frac{m_j - 1}{m_j} a_2 + \frac{m_j - 1}{m_j}\frac{m_j - 2}{m_j} a_3\right] \tag{3.18}$$

Apparently, the equation of state predicts asymmetric cross-virial coefficients, *i.e.* $B_{2,ij} \neq B_{2,ji}$. Although this predicted asymmetry is fundamentally wrong, it is a common artefact of theories of this type (it can be shown that TPT1 and TPT2 suffer from the same problem). As shown by the results for $\bar{B}_2$ in Table 3.4, the errors in the individual cross-virial coefficients (due to the fact that $B_{2,ij} \neq B_{2,ji}$) cancel to large extend when used in Eq. (3.17). For all systems considered in Table 3.4, the EoS compares accurately (to within 1.4%) to the MC data and shows much better results than those obtained from TPT1 and GFD. For second virial coefficients, the results obtained from SPT are of similar quality. The reason is that for SPT we could directly use the second virial coefficient obtained from the mixture version of Eq. (3.13) as an input. As shown in the previous chapter of this thesis, the mixture version of Eq. (3.13) is very accurate, therefore this result is not surprising.

3.5 Conclusion

We developed an extension of the EoS of Liu and Hu [128] to linear- and partially flexible tangent hard-sphere chain fluids. The partial flexibility is introduced by the rod-coil model as defined in Sec. 2.2. The effect of flexibility on the phase behaviour is described by the pure-component 'rigidity' parameter from Eq. (2.1), which is introduced in the theory at the level of the cavity correlation function. For both, pure component systems and mixtures of chains of variable degree of flexibility, theoretical predictions for the pressure and second virial coefficient were compared to the results from MC simulations obtained by us and from literature. Compared to other theories, *i.e.* TPT1, TPT2, generalized Flory-dimer theory (GFD), scaled particle theory (SPT) and the original EoS of Liu and Hu, the theory developed in this chapter results in a significantly improved description of the MC data.

4

The isotropic-nematic phase transition of tangent hard-sphere chain fluids—Pure components

In this chapter, we extend Onsager's second virial theory to partially flexible (rod-coil) tangent hard-sphere chain fluids. The effect of chain-flexibility on the second virial coefficient is described by the analytical approximation for the orientation-dependent pair-excluded volume from Chapter 2. To approximate the effect of higher virial coefficients we evaluate the Vega-Lago rescaling and Scaled Particle Theory (SPT). The resulting theory allows for an analytical description of the effects of intramolecular flexibility on the isotropic-nematic transition. Based on the Onsager-Trial-Function (OTF) approximation, the theory is reformulated to analytical form in terms of a single variational parameter to describe orientational ordering. By using appropriate expansions in this parameter, the theory is simplified further, resulting in a closed algebraic description of the orientational state of the system. For linear chain fluids, the approximate algebraic form of the Helmholtz energy is shown to lead to results of comparable accuracy as the full numerical theory. We find that the the approximate theory loses its validity for chains of increased flexibility. Theoretical results for the equation of state and nematic order parameter are compared extensively to results from MC simulations. For linear chains, accurate comparison is obtained down to a chain length m of $\sim$9. For rod-coil fluids of reasonable rigidity, a quantitative comparison between theory and MC simulations is obtained. For more flexible chains, however, both the Vega-Lago rescaling and SPT lead to a small underestimation of the location of the phase transition.

Parts of this chapter have been published as:
T. van Westen, B. Oyarzún, T.J.H. Vlugt and J. Gross *J. Chem. Phys.* 139 (2013) 034505 [140].

4.1 Introduction

As already pointed out by Onsager in the early 1940's, a key attribute for the formation of a liquid crystalline phase is anisotropy in the shape of the molecular hard cores [9, 109]. For a system of hard rods, Onsager showed that the orientational ordering transition is completely entropically driven. While at low density the orientational entropy dominates, forcing the molecules in an isotropic (randomly orientated) state, at higher densities there is a compensating configurational entropy/free volume that can be gained by aligning the molecules to minimize the excluded volume. Onsager's formalism can be generalized to many different types of hard anisotropic molecules [18], and, as shown by Bolhuis and Frenkel [94], it becomes exact in the low density limit (*i.e.* for molecules of infinite shape anisotropy). Typical model systems that have been studied in this respect, are hard discs [95, 96], -rods [141], -cut spheres [142, 143], -spherocylinders [94, 144], -ellipsoids [97, 98], -Gaussian overlap particles [145] and hard-sphere chains [92, 93, 103, 136, 146].

As discussed previously in this thesis, most real LC molecules are not completely rigid but possess a certain degree of intramolecular flexibility. As this flexibility is known to have a profound effect of the stability of nematic phases, it is desirable to include its effects into a theoretical description of the isotropic-nematic phase transition. In the present chapter, therefore, we extend Onsager's theory to partially flexible (rod-coil) molecules using the decoupling of the conformational distribution function that was proposed in Chapter 2. The method renders a theory of similar form as that of Fynewever and Yethiraj [103], with the important difference that we obtain the required ensemble average of the pair-excluded volume from an analytical approximation (from Chapter 2) instead of MC simulations of two chain molecules. Consequently, the resulting theory is computationally much more efficient, without compromising its accuracy. A key result of this approach is that the flexibility of a molecule is treated analytically and can be described by the pure-component rigidity parameter from Eq. (2.1). In the spirit of a molecular perturbation theory for liquid crystalline fluids, this result is appealing since intramolecular flexibility can with this approach be treated at the stage of the purely repulsive reference fluid.

Central to the EoS developed in this chapter is the use of the Onsager Trial Function (OTF) to characterize the orientational distribution function (ODF). The use of the OTF is convenient since it allows for an analytical description of the orientational state of the system. Moreover, for the specific case of a system of hard spherocylinders, it was recently shown that the use of the OTF leads to an almost identical description of the nematic ordering compared to the use of a full numerical solution of the ODF [18]. We show this observation also holds for our case.

This chapter is organized as follows. In Section 4.2, Onsager's second virial theory is extended to partially flexible chain molecules. In addition, the Vega-Lago approach and SPT are discussed. Using the OTF approximation, the Helmholtz energy functional is rewritten to analytical form, involving a closed description of the orientational state of the system. In Section 4.3, theoretical predictions for the equation of state and nematic order parameter are extensively compared to MC simulations. We summarize our findings in Section 4.4.

4.2 Theory

Let us define the configuration $\tilde{\boldsymbol{r}}$ of a molecule by the position vector $\boldsymbol{r}$ of its center of mass together with the molecule's conformation $\tilde{\boldsymbol{\omega}}$. The latter is defined as the set of all bond- and torsion angles $\boldsymbol{\omega}'$ of the molecule and the orientation $\boldsymbol{\omega}$ of the overall molecular axis with respect to some fixed reference frame. Analogous to the definition from Chapter 2, the molecular axis is defined as the axis around which the molecule has the smallest moment of inertia. The probability density, or single-molecule density [54], to find any molecule in a configuration $\tilde{\boldsymbol{r}}$ is denoted by $\rho(\tilde{\boldsymbol{r}})$, which is normalized as

$$\int \rho(\tilde{\boldsymbol{r}}) d\tilde{\boldsymbol{r}} = N \tag{4.1}$$

Here, N is the number of molecules.

4.2.1. Ideal part of the Helmholtz energy

According to the general graphical and functional formalism developed by Chandler and Pratt [147, 148], the ideal part of the Helmholtz energy of an inhomogeneous canonical system of N nonrigid chain molecules can be written as a functional of $\rho(\tilde{\boldsymbol{r}})$:

$$\beta A^{\mathrm{id}}[\rho(\tilde{\boldsymbol{r}})] = \int_V \rho(\tilde{\boldsymbol{r}}) \left[\ln\left(\rho(\tilde{\boldsymbol{r}})\Lambda^3\right) - 1 + \beta\Phi_{\mathrm{intra}}(\tilde{\boldsymbol{r}})\right] d\tilde{\boldsymbol{r}} \tag{4.2}$$

Here, $\beta^{-1} = kT$ is the product of the Boltzmann constant k and the absolute temperature T, Λ is the thermal De Broglie wavelength and $\Phi_{\mathrm{intra}}(\tilde{\boldsymbol{r}})$ is the total intramolecular potential energy, containing all bonding and flexibility constraints. For the molecular model considered here, the bond length is fixed; therefore the functional dependence of Φ_{intra} can be reduced to $\boldsymbol{\omega}'$. Furthermore, since we are concerned with describing nematic phases, the single-molecule density can be factorized into a uniform number density $\rho = N/V$ and a conformational distribution function $f(\tilde{\boldsymbol{\omega}})$ as $\rho(\tilde{\boldsymbol{r}}) = \rho f(\tilde{\boldsymbol{\omega}})$. Consequently, all positional dependence of Eq. (4.2) can be averaged out and the ideal part of the Helmholtz energy becomes

$$\frac{\beta A^{\mathrm{id}}[f(\tilde{\boldsymbol{\omega}})]}{N} = \ln\left(\rho\Lambda^3\right) - 1 + \int f(\tilde{\boldsymbol{\omega}}) \left[\ln\left(f(\tilde{\boldsymbol{\omega}})\right) + \beta\Phi_{\mathrm{intra}}(\boldsymbol{\omega}')\right] d\tilde{\boldsymbol{\omega}} \tag{4.3}$$

Since a theory formulated in terms of the conformational distribution function of a chain molecule in a condensed fluid is of considerable complexity, some approximations are required to transform this result into a practical functional for nematic fluids. In this, we follow the same approach as in Chapter 2 and assume a molecule's internal conformational- ($\boldsymbol{\omega}'$) and orientational ($\boldsymbol{\omega}$) degrees of freedom can be decoupled

$$f(\tilde{\boldsymbol{\omega}}) \approx f(\boldsymbol{\omega}')f(\boldsymbol{\omega}) \tag{4.4}$$

We note that this assumption is not in accordance with the increase of the end-to-end length of a molecule that is generally observed in molecular simulation studies of the isotropic-nematic phase transition [92, 99, 136]. However, it is analogous to that underlying many accurate theories for isotropic fluids (*e.g.* SAFT [63], PC-SAFT [72]) where a similar increase in the end-to-end length for vapour-liquid phase

transitions [112] is neglected. Substituting Eq. (4.4) in Eq. (4.3), all $\boldsymbol{\omega}'$-dependence can be averaged out to two temperature dependent terms. By generalizing the definition of the De Broglie wavelength (denoted by Λ'), these temperature dependent terms can be considered in the isotropic part of the ideal Helmholtz energy. Accordingly, the ideal Helmholtz energy contribution of a nematic fluid of nonrigid tangent hard-sphere chain molecules can be put in a simple Onsager-like form, as

$$\frac{\beta A^{\mathrm{id}}[f(\boldsymbol{\omega})]}{N} = \ln\left(\frac{\rho\Lambda'^3}{\Omega}\right) - 1 + \int f(\boldsymbol{\omega}) \ln\left(\Omega f(\boldsymbol{\omega})\right) d\boldsymbol{\omega} \tag{4.5}$$

where $\Omega = \int d\boldsymbol{\omega} = 4\pi$ is the usual normalization constant. The isotropic- and anisotropic contribution to the ideal Helmholtz energy are given by, respectively

$$\frac{\beta A^{\mathrm{id}}_{\mathrm{iso}}}{N} = \ln\left(\frac{\rho\Lambda'^3}{\Omega}\right) - 1 \tag{4.6}$$

$$\frac{\beta A^{\mathrm{id}}_{\mathrm{aniso}}[f(\boldsymbol{\omega})]}{N} = \int f(\boldsymbol{\omega}) \ln\left(\Omega f(\boldsymbol{\omega})\right) d\boldsymbol{\omega} \tag{4.7}$$

For an isotropic distribution of molecular orientations, $f_{\mathrm{iso}}(\boldsymbol{\omega}) = 1/\Omega$, and thus the anisotropic part is zero. For partial orientational order, the anisotropic contribution becomes larger than zero, corresponding to a decrease in orientational entropy.

4.2.2. Residual part of the Helmholtz energy

To describe the residual Helmholtz energy, let us write a virial expansion in the homogeneous number density ρ

$$\frac{A^{\mathrm{res}}[f(\tilde{\boldsymbol{\omega}})]}{NkT} = B_2[f(\tilde{\boldsymbol{\omega}})]\rho + \frac{1}{2}B_3[f(\tilde{\boldsymbol{\omega}})]\rho^2 + \ldots \tag{4.8}$$

Analogous to Chapter 2, we treat the second virial coefficient of a non-rigid chain molecule based on the decoupling from Eq. (4.4). As a result, the second virial coefficient can be calculated from Eq. (2.9), which is repeated here for clarity

$$B_2[f(\boldsymbol{\omega}] = \frac{1}{2}\iint \langle V_{\mathrm{ex}}(\tilde{\boldsymbol{\omega}}_1, \tilde{\boldsymbol{\omega}}_2)\rangle_{\boldsymbol{\omega}'_1,\boldsymbol{\omega}'_2} f(\boldsymbol{\omega}_1) f(\boldsymbol{\omega}_2) d\boldsymbol{\omega}_1 d\boldsymbol{\omega}_2 \tag{4.9}$$

In Chapter 2, we obtained the resulting ensemble average $\langle \ldots \rangle$ of the pair-excluded volume from MC simulations of two chain molecules. Due to the averaging, the ensemble average maintains a dependence on the angle γ between the molecular axes only

$$\langle V_{\mathrm{ex}}(\tilde{\boldsymbol{\omega}}_1, \tilde{\boldsymbol{\omega}}_2)\rangle_{\boldsymbol{\omega}'_1,\boldsymbol{\omega}'_2} = V_{\mathrm{ex}}(\gamma) \tag{4.10}$$

In Chapter 2, $V_{\mathrm{ex}}(\gamma)$ was calculated for a wide range of different rod-coil molecules. The following analytical approximation was developed by correlating the MC simulation results:

$$V^*_{\mathrm{ex}}(\gamma) = \frac{V_{\mathrm{ex}}(\gamma)}{V_m} = C_1(m, \chi_{\mathrm{R}}) + C_2(m, \chi_{\mathrm{R}}) \sin(\gamma) + C_3(m, \chi_{\mathrm{R}}) \sin^2(\gamma) \tag{4.11}$$

Here, $V_m = (\pi/6)m\sigma^3$ is the molecular volume of a chain of m tangent hard spheres of diameter σ. For the functional form of the coefficients C_1, C_2 and C_3, the reader is referred to Chapter 2.

To describe the higher order terms in the virial expansion from Eq. (4.8), two different approximate methods are evaluated; namely, the Vega-Lago rescaling [52], and Scaled Particle Theory (SPT) [16, 53, 149–153]. The approach of Vega and Lago is based on a clever rescaling of the higher virial coefficients to those of the isotropic fluid of the system being described, with

$$B_n[f(\tilde{\boldsymbol{\omega}})] \approx B_{n,\mathrm{iso}} \frac{B_2[f(\tilde{\boldsymbol{\omega}})]}{B_{2,\mathrm{iso}}} \tag{4.12}$$

Although the rescaling of virial coefficients might seem *ad hoc* in nature, it has a sound statistical mechanical basis in the form of the decoupling approximation [49–51, 144], which is briefly discussed in Appendix C. Resumming the virial expansion from Eq. (4.8), and using Eq. (4.9) to approximate the second virial coefficient, one obtains the following results for the residual Helmholtz energy and compressibility factor $Z = PV/NkT$, respectively

$$\frac{\beta A^{\mathrm{res}}[f(\boldsymbol{\omega})]}{N} = \frac{\beta A^{\mathrm{res}}_{\mathrm{iso}}}{N} \frac{B_2[f(\boldsymbol{\omega})]}{B_{2,\mathrm{iso}}} \tag{4.13}$$

$$Z = 1 + Z^{\mathrm{res}}_{\mathrm{iso}} \frac{B_2[f(\boldsymbol{\omega})]}{B_{2,\mathrm{iso}}} \tag{4.14}$$

The second virial coefficient of the isotropic fluid is obtained by substituting $f_{\mathrm{iso}}(\boldsymbol{\omega}) = 1/4\pi$ in Eqs. (4.9)-(4.11):

$$B_{2,\mathrm{iso}} = V_{\mathrm{m}} \left[\frac{C_1(m, \chi_{\mathrm{R}})}{2} + \pi \frac{C_2(m, \chi_{\mathrm{R}})}{8} + \frac{C_3(m, \chi_{\mathrm{R}})}{3} \right] \tag{4.15}$$

Clearly, a major advantage of using the rescaling is that the conformation dependence of the complete virial expansion is approximately considered in the second virial coefficient. Since we describe the second virial coefficient using Eqs. (4.9)-(4.11), the resulting expressions retain a functional dependence on the orientational distribution function only. An Onsager-like theory for non-rigid chain molecules is thereby obtained.

Furthermore, the rescaling allows for the use of an accurate EoS for the description of the isotropic fluid. For this purpose we evaluate both the LH EoS [128] and the LHrc EoS. In Chapter 3 we have shown that, compared to the LH EoS, the LHrc EoS leads to a more reliable description of the isotropic EoS of linear and partially flexible (rod-coil) tangent hard-sphere chain fluids. It is interesting to evaluate to what extend these improved results for the isotropic fluid are reflected in the predicted isotropic-nematic phase equilibrium. In the remainder of this chapter, Eqs. (4.5), (4.9)-(4.11) and (4.13)-(4.15) will be referred to as the Onsager Vega-Lago (OVL) theory.

In contrast to the OVL theory, SPT cannot be derived directly from the virial expansion. However, SPT shows the same features in that the higher virial terms

are approximated by a non-linear dependence on density whereas the second virial coefficient is treated explicitly. By combining the work of Cotter [16, 149, 150] and Boublík [53, 151–153], Jaffer *et al.* [104] proposed a SPT that is directly applicable to describe both the isotropic and nematic phase of tangent hard-sphere chain fluids. The residual Helmholtz energy and compressibility factor obtained from this SPT are given by, respectively

$$\frac{\beta A^{\mathrm{res}}}{N} = (\psi - 1)\ln(1-\eta) + \frac{3a\eta}{1-\eta} + \frac{\psi\eta}{(1-\eta)^2} \tag{4.16}$$

$$Z = \frac{1}{1-\eta} + \frac{3a\eta}{(1-\eta)^2} + \frac{3\psi\eta^2}{(1-\eta)^3} - \frac{\psi\eta^3}{(1-\eta)^3} \tag{4.17}$$

Here, $\eta = \rho V_{\mathrm{m}}$ is the packing fraction of the system. Using the definition of the reduced second virial coefficient $B_2^* = B_2/V_m = \partial Z/\partial\eta|_{\eta=0}$, the non-sphericity parameter a can be written as

$$a = \frac{B_2^* - 1}{3} \tag{4.18}$$

Since the non-sphericity parameter is expressed explicitly in the reduced second virial coefficient, the SPT can be directly applied to nematic fluids through the use of Eqs. (4.9)-(4.11). Please note that in related work, the non-sphericity parameter is usually referred to as α. Since this symbol will be used as the variational parameter for the Onsager Trial function (see next section) we have used the symbol a instead. The reduced second virial coefficient in the isotropic phase can be calculated from Eq. (4.15). The ψ-parameter in Eq. (4.16) is given by [104]

$$\psi = \frac{\sigma S_m}{9V_m}\left[3a - \left(\frac{\sigma S_m}{4V_m}\right)\left(1 - \frac{m-1}{4}\right)\right] \tag{4.19}$$

Here, $S_m = \pi m\sigma^2$ is the surface area of a chain molecule. Eqs. (4.5), (4.9)-(4.11), (4.15) and (4.16)-(4.19) will be referred to as SPT.

4.2.3. Solving the phase equilibrium

In principle, phase equilibrium is attained when two phases are in thermal, mechanical and material equilibrium. The conditions for this are equality of temperature (T), pressure (P) and chemical potential (μ), respectively. For the hard, purely repulsive molecules considered here, however, temperature is an irrelevant parameter. Consequently, for these systems the phase equilibrium can be solved by equating the pressure P and chemical potential μ of both phases

$$P^{\mathrm{iso}}(\rho_{\mathrm{iso}}) = P^{\mathrm{nem}}[f_{\mathrm{eq}}(\boldsymbol{\omega}); \rho_{\mathrm{nem}}] \tag{4.20}$$

$$\mu^{\mathrm{iso}}(\rho_{\mathrm{iso}}) = \mu^{\mathrm{nem}}[f_{\mathrm{eq}}(\boldsymbol{\omega}); \rho_{\mathrm{nem}}] \tag{4.21}$$

The equilibrium orientational distribution function $f_{\mathrm{eq}}(\boldsymbol{\omega})$ minimizes the total Helmholtz energy $A = A^{\mathrm{id}} + A^{\mathrm{res}}$ and can be obtained by solving the following variational equation

$$\left(\frac{\delta A[f(\boldsymbol{\omega})]}{\delta f(\boldsymbol{\omega})}\right)_{NVT, f(\boldsymbol{\omega}) = f_{\mathrm{eq}}(\boldsymbol{\omega})} = 0 \tag{4.22}$$

Subsequently, the pressure and chemical potential can be obtained from

$$P = -\left(\frac{\partial A[f_{\mathrm{eq}}(\boldsymbol{\omega})]}{\partial V}\right)_{NT} \tag{4.23}$$

$$\mu = \left(\frac{\partial A[f_{\mathrm{eq}}(\boldsymbol{\omega})]}{\partial N}\right)_{VT} \tag{4.24}$$

Although, in principle, Eq. (4.22) can be solved numerically [154–159], a well chosen trial function can make the solution more tractable without losing too much of the numerical accuracy [18]. In this chapter, we use the hyperbolic trial function as originally proposed by Onsager [9] (referred to as OTF) and consider the degree of orientational order in a single parameter α:

$$f(\boldsymbol{\omega}) \approx f_{\mathrm{OTF}}(\theta) = \frac{\alpha \cosh[\alpha \cos(\theta)]}{4\pi \sinh(\alpha)} \tag{4.25}$$

Here, θ is the polar angle of a molecule's axis with respect to the nematic director (mean direction of all molecules). For an isotropic phase $f_{\mathrm{OTF}} = 1/4\pi$ and thus $\alpha = 0$. For higher values of α, the OTF becomes sharply peaked at the parallel orientations $\theta = 0$ and $\theta = \pi$, thereby modelling a nematic phase. As we will show in detail in the following section, the use of the OTF allows the orientation-dependent terms of the Helmholtz energy to be expressed as a function solely of α. Accordingly, the variational problem from Eq. (4.22) can be transformed to a simpler one-dimensional parameter optimization of the equilibrium degree of orientational order α_{eq}, as

$$\left(\frac{\partial A(\alpha)}{\partial \alpha}\right)_{NVT,\alpha=\alpha_{\mathrm{eq}}} = 0 \tag{4.26}$$

A modified Newton method was used to solve this equation. The resulting $\alpha = \alpha_{\mathrm{eq}}$ determines the orientational distribution function $f(\boldsymbol{\omega})$ according to Eq. (4.25). Once $\alpha = \alpha_{\mathrm{eq}}$ is calculated, the nematic order parameter S_2 can be obtained from

$$S_2 = \frac{1}{2}\left\langle 3\cos^2(\theta) - 1\right\rangle_{\boldsymbol{\omega}} \tag{4.27}$$

$$= 1 - \frac{3\coth(\alpha)}{\alpha} + \frac{3}{\alpha^2} \tag{4.28}$$

The nematic order parameter varies between zero and unity for the isotropic and perfect nematic phase, respectively. It is therefore a convenient measure of the degree of orientational order in a system.

4.2.4. The Helmholtz energy functional in terms of the Onsager Trial Function

In this section, the orientation-dependent parts of the Helmholtz energy functional (Eqs. (4.7), (4.9)-(4.11), and (4.13)) are expressed in terms of the OTF (Eq. (4.25)). Exact, analytical results in terms of the variational parameter α are presented. For

a detailed derivation of the expressions, the reader is referred to the work of Franco-Melgar *et al.* [18].

In the OTF approximation, the ideal contribution to the Helmholtz energy (Eq. (4.7)) is obtained from the following expression

$$\frac{\beta A^{\mathrm{id}}_{\mathrm{aniso}}}{N} = \ln[\alpha \coth(\alpha)] - 1 + \frac{\arctan(\sinh(\alpha))}{\sinh(\alpha)} \tag{4.29}$$

The orientation-dependence of the residual contribution to the Helmholtz energy is covered by the second virial coefficient (Eqs. (4.9)-(4.11)). For a nematic fluid, this can be written as the following orientational average

$$B_2[f(\boldsymbol{\omega})] = \frac{1}{2} V_m \left[C_1 + C_2 \left\langle \sin(\gamma) \right\rangle_{\boldsymbol{\omega}_1,\boldsymbol{\omega}_2} + \; C_3 \left\langle \sin^2(\gamma) \right\rangle_{\boldsymbol{\omega}_1,\boldsymbol{\omega}_2} \right] \tag{4.30}$$

Note that for an isotropic distribution of molecular orientations, this reduces to Eq. (4.15). If using the OTF to calculate the orientational averages, one obtains the following results

$$\left\langle \sin(\gamma) \right\rangle_{\boldsymbol{\omega}_1,\boldsymbol{\omega}_2} = \frac{\pi I_2(2\alpha)}{2\sinh^2(\alpha)} \tag{4.31}$$

$$\begin{aligned} \left\langle \sin^2(\gamma) \right\rangle_{\boldsymbol{\omega}_1,\boldsymbol{\omega}_2} = \frac{1}{\sinh^2(\alpha)} \Bigg\{ & \sinh(2\alpha) \left[\frac{2}{\alpha} + \frac{6}{\alpha^3} \right] + \\ & - \cosh(2\alpha) \left[\frac{5}{\alpha^2} + \frac{3}{\alpha^4} \right] - \frac{1}{\alpha^2} + \frac{3}{\alpha^4} \Bigg\} \end{aligned} \tag{4.32}$$

Here, $I_2(2\alpha)$ is a modified Bessel function of second order, which is defined by the following general integral representation

$$I_{2j}(2\alpha) = \frac{1}{\pi} \int_{u=0}^{\pi} \exp(2\alpha \cos u) \cos(2ju) du \tag{4.33}$$

The Bessel function is solved by numerical integration. To obtain the equilibrium degree of orientational ordering α_{eq} from Eq. (4.26), the following derivatives are required:

$$\left(\frac{\partial \left[\beta A^{\mathrm{id}}_{\mathrm{aniso}} / N \right]}{\partial \alpha} \right)_{NVT} = \frac{1}{\alpha} + \frac{\arctan[\sinh(\alpha)] \cosh(\alpha)}{\sinh^2(\alpha)} \tag{4.34}$$

$$\begin{aligned} \left(\frac{\partial \left\langle \sin(\gamma) \right\rangle_{\boldsymbol{\omega}_1,\boldsymbol{\omega}_2}}{\partial \alpha} \right)_{NVT} = \frac{\pi}{\sinh^2(\alpha)} \Bigg\{ & I_2(2\alpha) \left[\frac{\alpha^2 + 3}{3\alpha} - \coth(\alpha) \right] \\ & - \frac{\alpha}{3} I_4(2\alpha) \Bigg\} \end{aligned} \tag{4.35}$$

$$\left(\frac{\partial\left\langle\sin^2(\gamma)\right\rangle_{\boldsymbol{\omega}_1,\boldsymbol{\omega}_2}}{\partial\alpha}\right)_{NVT} = \frac{2}{\sinh^2(\alpha)}\left\{\cosh(2\alpha)\left(\frac{2}{\alpha}+\frac{11}{\alpha^3}+\frac{6}{\alpha^5}\right)\right.$$
$$-\sinh(2\alpha)\left(\frac{6}{\alpha^2}+\frac{12}{\alpha^4}\right)+\frac{1}{\alpha^3}-\frac{6}{\alpha^5}$$
$$-\coth(\alpha)\left[\sinh(2\alpha)\left(\frac{2}{\alpha}+\frac{6}{\alpha^3}\right)\right.$$
$$\left.\left.-\cosh(2\alpha)\left(\frac{5}{\alpha^2}+\frac{3}{\alpha^4}\right)-\frac{1}{\alpha^2}+\frac{3}{\alpha^4}\right]\right\} \tag{4.36}$$

4.2.5. Approximate algebraic OVL theory for the nematic state of rod-coil fluids

Inspired by the work of Franco-Melgar *et al.* [18], we now proceed by developing an approximate, algebraic form of the OVL theory, involving a closed description of the variational parameter α. The assumption underlying the approximate results derived in this section is that for typical nematic phases $\alpha >> 1$. Under this assumption, the ideal contribution to the Helmholtz energy (Eq. (4.29)) can to a very good approximation be written as [18]

$$\frac{\beta A^{\text{id}}_{\text{aniso}}}{N} \approx \ln(\alpha) - 1 \tag{4.37}$$

To approximate the orientational average of the $\sin(\gamma)$-kernel from Eq. (4.31), we can write the modified Bessel function in terms of a truncated asymptotic expansion [18]

$$I_2(2\alpha) = \frac{\exp(2\alpha)}{2(\pi\alpha)^{1/2}}\left\{1-\frac{15}{16\alpha}+\frac{105}{512\alpha^2}+\frac{315}{8192\alpha^3}+\ldots\right\}$$
$$\approx \frac{\exp(2\alpha)}{2(\pi\alpha)^{1/2}}\left\{1-\frac{15}{16\alpha}+\mathcal{O}\left(\alpha^{-2}\right)\right\} \tag{4.38}$$

Substitution of this result in Eq. (4.31), and using the fact that $\exp(2\alpha)/\sinh(2\alpha) \approx 2$, gives the following approximate result

$$\left\langle\sin(\gamma)\right\rangle_{\boldsymbol{\omega}_1,\boldsymbol{\omega}_2} \approx \left(\frac{\pi}{\alpha}\right)^{1/2}\left\{1-\frac{15}{16\alpha}+\mathcal{O}(\alpha^{-2})\right\} \tag{4.39}$$

To approximate the orientational average of the $\sin^2(\gamma)$-kernel, let us first use the hyperbolic properties $\sinh(x+y) = \sinh(x)\cosh(y) + \cosh(x)\sinh(y)$ and $\cosh(x+y) = \cosh(x)\cosh(y) + \sinh(x)\sinh(y)$ to rewrite the hyperbolic terms of Eq. (4.32) as

$$\frac{\sinh(2\alpha)}{\sinh^2(\alpha)} = 2\coth(\alpha)$$
$$\frac{\cosh(2\alpha)}{\sinh^2(\alpha)} = \coth^2(\alpha)+1 \tag{4.40}$$

For any reasonable value of α, the coth(...)-terms can be reduced to unity; therefore, Eq. (4.32) can be simplified to the following approximate result

$$\begin{aligned}\left\langle \sin^2(\gamma)\right\rangle_{\boldsymbol{\omega}_1,\boldsymbol{\omega}_2} &\approx \frac{4}{\alpha} - \frac{10}{\alpha^2} + \frac{12}{\alpha^3} - \frac{6}{\alpha^4} \\ &\approx \frac{4}{\alpha} + \mathcal{O}(\alpha^{-2})\end{aligned} \tag{4.41}$$

Substitution of these results in Eqs. (4.7), (4.13) and (4.30) leads to the following approximate expression for the OVL Helmholtz energy of nematic rod-coil fluids

$$\frac{\beta A}{N} \approx \frac{\beta A^{\text{id}}_{\text{iso}}}{N} + \ln(\alpha) - 1 + G(\eta)\left[C_1 + C_2\left(\frac{\pi}{\alpha}\right)^{1/2}\left\{1 - \frac{15}{16\alpha}\right\} + C_3\frac{4}{\alpha}\right] \tag{4.42}$$

Here we have introduced the shorthand notation for the density-dependent scaling factor $G(\eta) = \beta A^{\text{res}}_{\text{iso}}/2NB^*_{2,\text{iso}}$ with $B^*_{2,\text{iso}} = B_{2,\text{iso}}/V_m$. To find the equilibrium degree of orientational ordering based on this approximate expression for the Helmholtz energy, one has to solve the following equation

$$\left(\frac{\partial \beta A/N}{\partial \alpha}\right)_{NVT} = \frac{1}{\alpha} + G(\eta)\left[C_2\sqrt{\pi}\left(\frac{45}{32\alpha^{5/2}} - \frac{1}{2\alpha^{3/2}}\right) - C_3\frac{4}{\alpha^2}\right] = 0 \tag{4.43}$$

By making the substitution $x = \alpha^{1/2}$, this can be recast to the form of a cubic, according to

$$\frac{1}{x^5}\left(a_0 + a_1 x + a_2 x^2 + x^3\right) = 0 \tag{4.44}$$

where we have introduced the following orientation-independent terms

$$\begin{aligned} a_0 &= \frac{45}{32}G(\eta)C_2\sqrt{\pi} \\ a_1 &= -4G(\eta)C_3 \\ a_0 &= -\frac{1}{2}G(\eta)C_2\sqrt{\pi} \end{aligned} \tag{4.45}$$

Using the general solution of a cubic as derived by Nickalls [160], we find the following result for the equilibrium degree of orientational ordering α_{eq}

$$\begin{aligned}\alpha_{\text{eq}} = \frac{1}{9}\Bigg\{ & a_2 - 2\sqrt{a_2^2 - 3a_1} \\ & \cos\left(\frac{2j\pi}{3} + \frac{1}{3}\arccos\frac{-27[a_0 - \frac{1}{3}a_1a_2 + \frac{2}{27}a_2^3]}{2[a_2^2 - 3a_1]^{3/2}}\right)\Bigg\}^2\end{aligned} \tag{4.46}$$

where $j = 0, 1, 2$ denotes each root. We found that α_{eq} corresponds to the largest root ($j = 0$) of this expression.

With this result an algebraic OVL theory for the nematic state of rod-coil fluids is obtained. Due to the closed description of α, the resulting EoS is of similar complexity as conventional equations of state for isotropic fluids.

4.3 Results

In this section, theoretical results for the pressure, the nematic order parameter, the density difference at the I-N transition, and the phase diagram are compared to the results from isobaric-isothermal *NPT* MC simulations from Oyarzun *et al.* [136]. The effect of the chain length (m) and the rigidity parameter (χ_{R}) on the I-N phase behaviour is systematically investigated.

4.3.1. Linear m-mers

First we assess the accuracy of the OVL theory in predicting the isotropic-nematic phase equilibrium of linear chains. In Fig. 4.1, the equation of state of a system of linear 7-, 11-, 15- and 20-mers as obtained from the OVL-LH theory and the OVL-LHrc theory is compared to MC simulations. The results show a large sensitivity of the OVL theory towards the EoS that is used for the isotropic phase. It is rewarding to see that the relatively small improvement in the description of the isotropic phase obtained from using the LHrc EoS results in a considerably more accurate description of the isotropic-nematic phase equilibrium.

For the 7-mer system, some deviation between OVL-LHrc theory and simulations is observed, pointing at limitations in the use of the rescaling of virial coefficients from Eq. (4.12). For smaller chain lengths, the phase equilibrium is shifted to higher packing fractions; therefore more error is introduced due to the approximate treatment of the higher virial coefficients in Eq. (4.12). The observation that, for this system, the OVL-LH theory results in a better prediction of the phase transition pressure and nematic branch, is most likely caused by a fortuitous cancellation of errors from the approximate rescaling of virial coefficients and the inaccurate description of the isotropic EoS in Eq. (4.14). In fact, given that at equilibrium the chemical potentials of both phases are equal, we can write the following for the phase transition pressure

$$P_{\mathrm{trans}} = -\frac{a_{\mathrm{nem}} - a_{\mathrm{iso}}}{v_{\mathrm{nem}} - v_{\mathrm{iso}}} \tag{4.47}$$

Here, a and v are the molar Helmholtz energy and volume, respectively. Accordingly, the observation that P_{trans} is predicted correctly while the difference in coexistence packing fractions (and thus molar volumes) is overestimated, can only be due to an overestimation of the isotropic-nematic Helmholtz energy difference. Consistently, the nematic order parameter obtained from the OVL-LH theory for this system (See Fig. 4.2 (a)) is also overestimated.

In Fig. 4.2, we compare nematic order parameters for the same systems as in Fig. 4.1. For the OVL-LHrc theory, the results show consistency with those obtained for the equation of state in Fig. 4.1. For the linear 11-, 15- and 20-mer systems, the theory is in excellent agreement with the MC data.

As indicated by the results from Fig. 4.3, where we compare predictions based on the OTF and a full numerical solution of the orientational distribution function, the small overestimation of the order parameter close to the phase equilibrium is most probably an artefact of the use of the OTF. For the OVL-LH theory, the seemingly accurate comparison with MC data for the order parameter of the linear

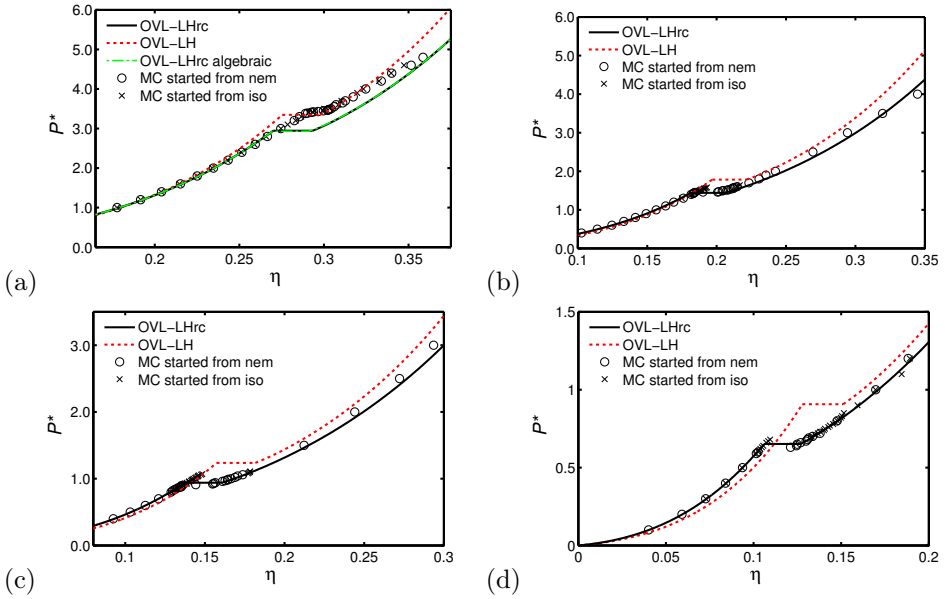

Figure 4.1: The equation of state of a system of (a) linear 7-mers, (b) linear 11-mers, (c) linear 15-mers and (d) linear 20-mers, as obtained from the OVL theory, using the LHrc (solid line) and LH (dotted line) EoS as input. The dash-dotted line was calculated using the approximate, algebraic form of the Helmholtz energy from Eqs. (4.42) and (4.46). Symbols correspond to MC simulations [136].

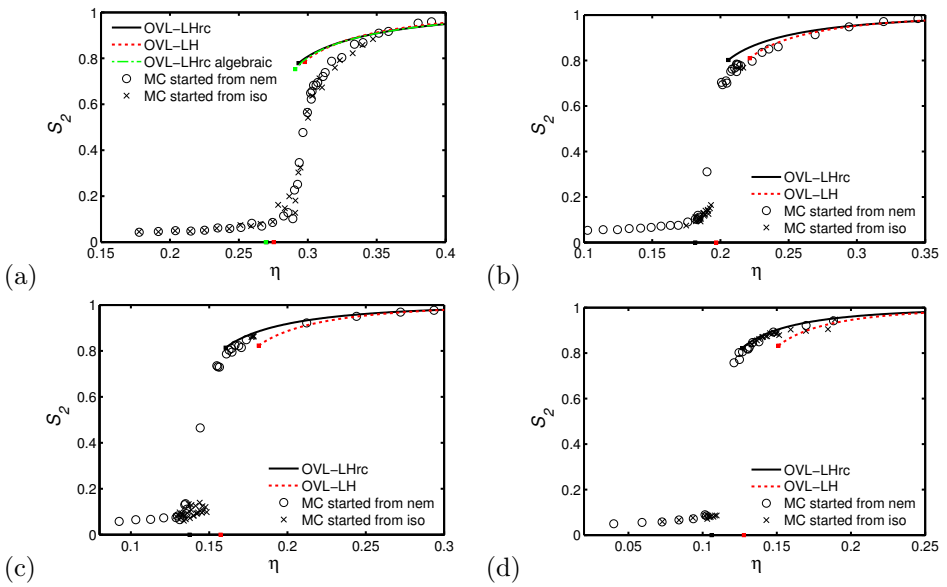

Figure 4.2: The nematic order parameter S_2 of a system of (a) linear 7-mers, (b) linear 11-mers, (c) linear 15-mers and (d) linear 20-mers. Lines and symbols as in Fig. 4.1.

Table 4.1: Comparison of theoretical results for the I-N transition of linear m-mers as obtained from the full numerical solution of the OVL-LHrc theory from Sec. 4.2.4 (denoted as NUM) and the approximate algebraic form of the OVL-LHrc theory from Sec. 4.2.5 (denoted as ALG). We show results for the dimensionless pressure $P^* = PV_m/kT$, the coexistence packing fractions η_{I} and η_{N}, the packing fraction difference at the I-N transition $\Delta\eta$, and the value of the variational parameter of the OTF α and the nematic order parameter S_2 at the phase transition.

m	EoS	$P^* = PV_m/kT$	η_{I}	η_{N}	$\Delta\eta$	α	S_2
3	ALG	-	-	-	-	-	-
	NUM	20.9669	0.5412	0.5509	0.0097	9.2045	0.7095
4	ALG	-	-	-	-	-	-
	NUM	9.3619	0.4328	0.4484	0.0156	10.3390	0.7379
5	ALG	5.5727	0.3592	0.3771	0.0179	9.0227	0.7044
	NUM	5.6151	0.3601	0.3795	0.0195	11.2167	0.7564
6	ALG	3.8748	0.3078	0.3269	0.0190	9.8102	0.7254
	NUM	3.8973	0.3084	0.3303	0.0219	11.9224	0.7695
7	ALG	2.9306	0.2696	0.2909	0.0213	11.0463	0.7530
	NUM	2.9443	0.2700	0.2933	0.0233	12.5054	0.7793
10	ALG	1.6513	0.1972	0.2205	0.0233	12.8023	0.7840
	NUM	1.6567	0.1975	0.2220	0.0245	13.7806	0.7981
15	ALG	0.9372	0.1374	0.1596	0.0222	14.2726	0.8045
	NUM	0.9395	0.1376	0.1605	0.0230	15.0515	0.8139
20	ALG	0.6504	0.1059	0.1260	0.0201	15.1050	0.8145
	NUM	0.6517	0.1060	0.1268	0.0208	15.8092	0.8222

11-mer system (Fig. 4.2 (b)) is merely an effect of the overestimation of the nematic coexistence packing fraction.

To evaluate the accuracy of the approximate algebraic form of the OVL theory from Section 4.2.5, we compare results to those obtained from its full numerical solution in Figs. 4.1 (a), 4.2 (a), and Table 4.1. Consistent with the findings of Franco-Melgar *et al.* for hard spherocylinders [18], we find that for linear chain fluids the algebraic form of the OVL theory is of comparable accuracy as the full numerical theory. Differences start to arise for chain lengths 3 and 4, for which the algebraic OVL theory shows no stable nematic phase.

It is important to note that in molecular simulation studies of linear tangent hard-sphere chain fluids [138], no nematic phase is observed for chain lengths smaller than 5. The reason is that for such short chains the isotropic-nematic phase equilibrium is shifted to packing fractions beyond the isotropic-solid phase equilibrium. The isotropic-nematic coexistence packing fractions obtained from the theory are in accordance with these results. For example, for a linear 3- and 4-mer, the OVL-LHrc theory predicts isotropic-nematic coexistence packing fractions of $\eta_{\mathrm{iso}} = 0.541$ and $\eta_{\mathrm{nem}} = 0.551$, and $\eta_{\mathrm{iso}} = 0.433$ and $\eta_{\mathrm{nem}} = 0.448$, respectively. These values are larger than the isotropic-solid coexistence packing fractions obtained from molecular simulations [138], *i.e.* $\eta_{\mathrm{iso}} \geq 0.430$ and $\eta_{\mathrm{solid}} \leq 0.529$ for a linear 3-mer, and $\eta_{\mathrm{iso}} = 0.43$ and $\eta_{\mathrm{solid}} = 0.51$ for a linear 4-mer. Since the theory presented in this chapter does not include a description of the solid phase, no direct comparison between theory and molecular simulations can be made for the isotropic-solid coexistence packing fractions.

In Figs. 4.4 and 4.5, we show the results obtained from SPT (dotted lines) for the same systems as in Figs. 4.1 and 4.2. The results obtained from the OVL-LHrc

theory (solid lines) are also included for comparison. The predicted equation of state and nematic order parameter obtained from both theories are very similar. As indicated by the results for the linear 7-mer system, SPT suffers from the same shortcomings as the OVL theory and results in a less accurate description of the phase transition for smaller chain lengths. A comparison of results obtained from SPT and the OVL-LHrc theory to the MC simulations of Oyarzun *et al.* [136] (not included for brevity) showed that both theories are accurate down to a chain length of 9, resulting in an underestimation of the coexistence pressure, isotropic packing fraction and nematic packing fraction of less than 7%, 5% and 1%, respectively.

In Figs. 4.6 (a) and (b), we show a plot of the relative density difference $\Delta\eta/\eta_{\text{iso}}$ and the density difference $\Delta\eta$ at the I-N transition versus chain length m. We include results obtained from the OVL-LHrc theory, SPT and MC simulations. As is common with theories of this type, both OVL-LHrc and SPT result in an overestimation of the density difference for small chain lengths. For larger chain lengths, however, theoretical results are in excellent agreement with MC simulations. For very large chain lengths, the coexistence densities obtained from SPT and OVL-LHrc converge to the same constant values (corresponding to the Onsager limit) and a constant relative density difference of approximately 34% is obtained.

As shown in Fig. 4.6 (b), both theory and simulations predict a maximum of the isotropic-nematic density difference for a certain chain length m. For the potential application of LCs as solvents in gas-absorption processes, this maximum is interesting, since a larger density difference at the phase transition corresponds to a larger solubility difference of small solutes. Since in absorption processes this solubility difference is to be maximized, these results suggest the existence of a LC solvent of optimal molecular length.

To finalize this part, we should stress that both, the density difference- and nematic order parameter at the I-N transition (see Table 4.1) as obtained here are significantly larger than those found experimentally for typical thermotropic mesogens ($\Delta\eta/\eta_{\text{iso}} \sim 0.5\%$, $S_{2,\text{coex}} \sim 0.5$) [3, 161]. Certainly, the choice for a purely repulsive molecular model does not put us in the position to make a true comparison to such systems; however, even when coupled to a suitable framework for describing the attractive interactions between mesogens, Onsager-type theories based on a rigid molecular model generally result in an overestimation of these properties [3, 15]. Clearly, a rigid molecular model is not a good representation of real LCs, since chain-conformational changes are expected to have a large effect on the phase behaviour. In the next section, we show that the incorporation of molecular flexibility in the molecular model leads to more realistic values of phase transition properties.

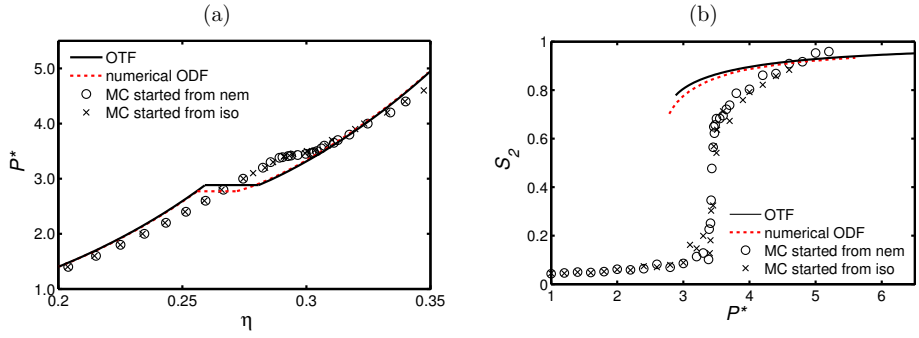

Figure 4.3: The equation of state and nematic order parameter of a system of linear 7-mers as obtained from OVL-TPT1 based on the OTF (solid line) and a full numerical solution of the orientational distribution function [146] (dotted line) compared to MC simulations [136] (symbols). The MC simulations were started either from an isotropic or a nematic initial configuration.

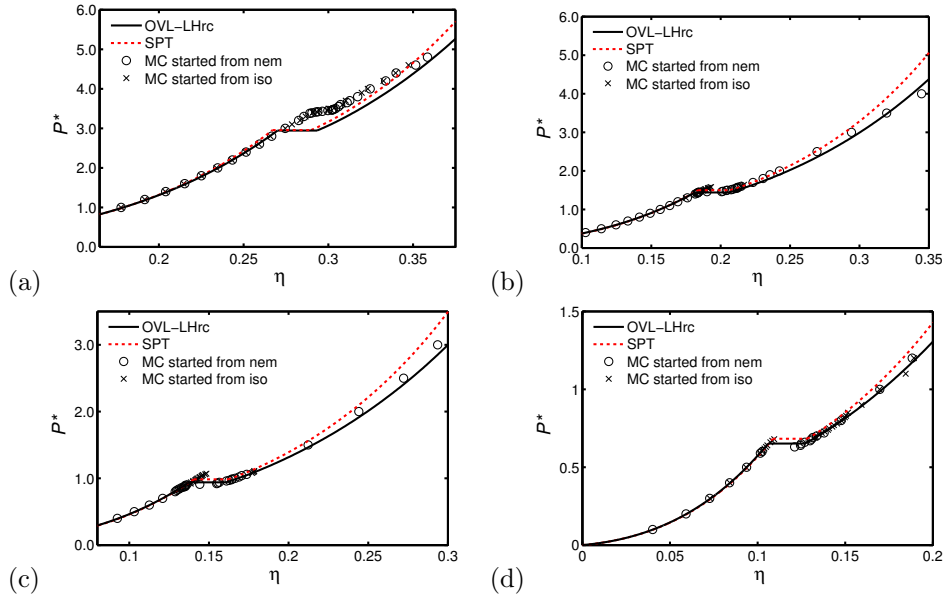

Figure 4.4: The equation of state of a system of (a) linear 7-mers, (b) linear 11-mers, (c) linear 15-mers and (d) linear 20-mers, as predicted from OVL-LHrc (solid line) and SPT (dotted line) compared to MC simulations [136] (symbols). The MC simulations were started either from an isotropic or a nematic initial configuration.

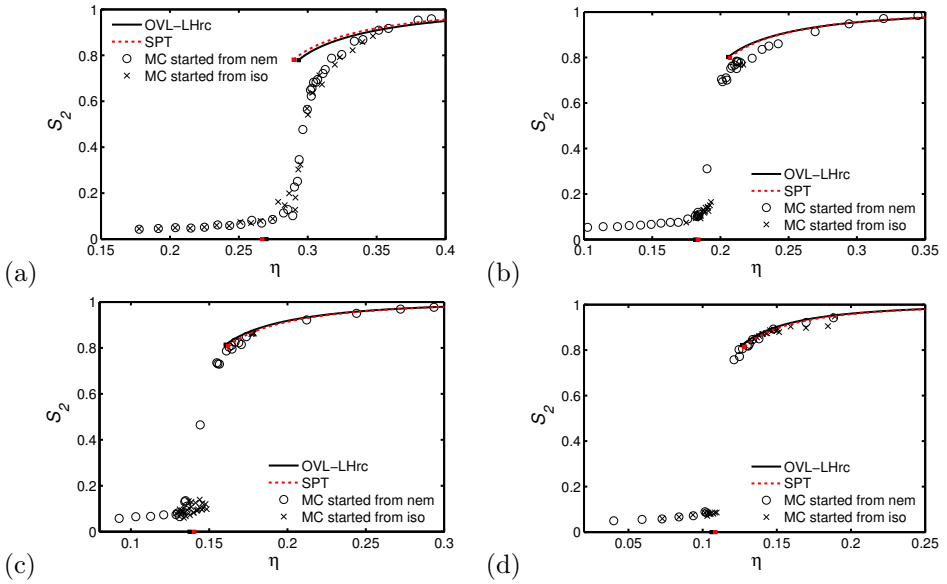

Figure 4.5: The nematic order parameter S_2 of a system of (a) linear 7-mers, (b) linear 11-mers, (c) linear 15-mers and (d) linear 20-mers, as predicted from OVL-LHrc (solid line) and SPT (dotted line) compared to MC simulations [136] (symbols). The MC simulations were started either from an isotropic or a nematic initial configuration.

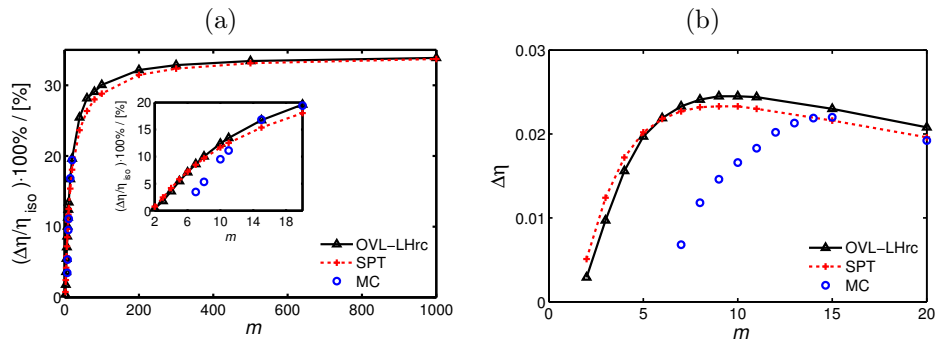

Figure 4.6: The chain-length-dependence of the density difference $\Delta\eta$ at the isotropic-nematic phase transition. Comparison between predictions obtained from OVL-LHrc (triangles), SPT (plus signs) and MC simulations [136] (circles). The lines are a guide for the eye. The solid line corresponds to OVL-LHrc; the dotted line corresponds to SPT.

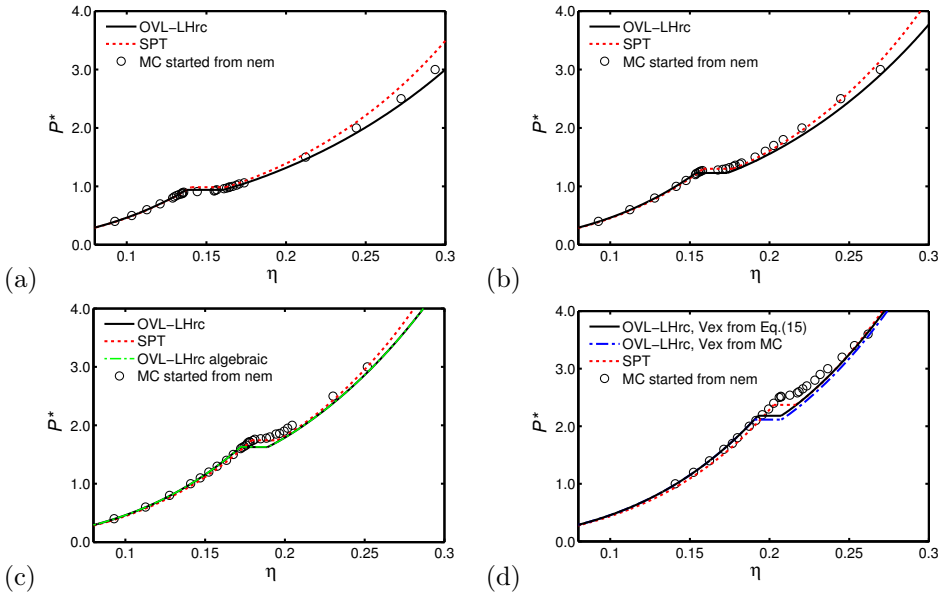

Figure 4.7: The equation of state of a system of (a) linear 15-mers, (b) 15-14 rod-coils, (c) 15-13 rod-coils and (d) 15-12 rod-coils, as predicted from the OVL-LHrc theory (solid line), the approximate algebraic form of the OVL theory from Eqs. (4.42) and (4.46) (green dash-dotted line) and SPT (dotted line), compared to MC simulations [136] (symbols). To check the effect of using the correlation from Eq. (4.11) for the pair-excluded volume, the pair-excluded volume of the 15-12 rod-coil was calculated from MC simulations (using the method from Chapter 2). A third order series in $\sin(\gamma)$ essentially gave a perfect fit. The results obtained from OVL-LHrc based on this fit are included (blue dash-dotted line) in (d). It is rewarding to see that both approaches practically yield the same results.

4.3.2. Rod-coil fluids

Given the results obtained in the previous section for linear m-mers, only SPT and the OVL-LHrc theory are evaluated further for the description of rod-coil fluids. The equation of state and nematic order parameter obtained from these theories are compared to MC simulations in Figs. 4.7 and 4.8, respectively. The test systems included are (a) a linear 15-mer, (b) a 15-14 rod-coil, (c) a 15-13 rod-coil, and (d) a 15-12 rod-coil. For all systems shown, the overall agreement of SPT and the OVL-LHrc theory with MC simulations is satisfactory. Moreover, for the 15-13 rod-coil we show that the approximate algebraic form of the OVL-LHrc theory is of comparable accuracy as its full numerical solution. The general trends with molecular rigidity are well captured. It can be clearly observed that for less rigid chains, the phase transition is shifted to higher packing fractions. The reason is that the shape of such molecules is less anisotropic. Accordingly, the difference of the orientational average of the pair-excluded volume between an isotropic and nematic distribution of molecular orientations (as obtained from Eq. (4.11)) is smaller, resulting in a smaller driving force for the phase transition.

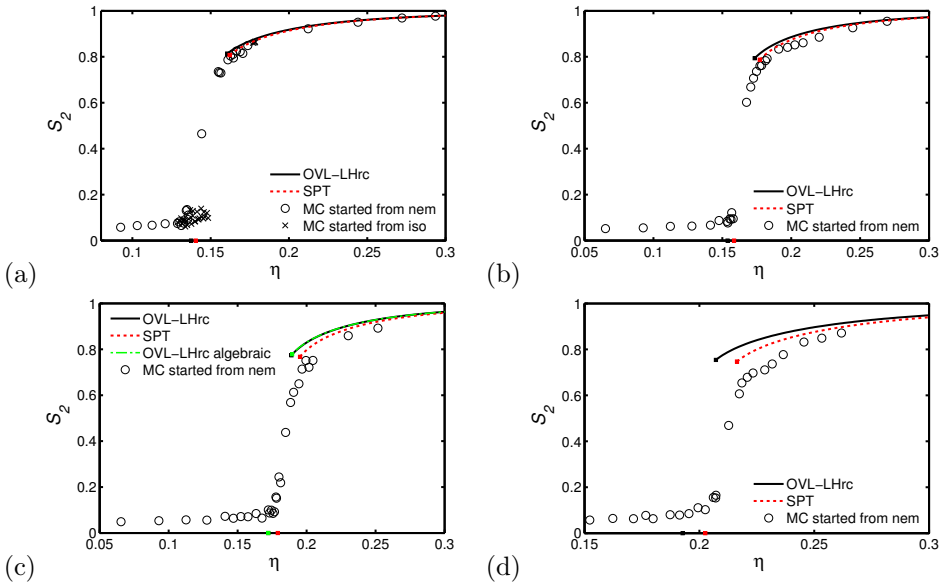

Figure 4.8: The nematic order parameter S_2 of a system of (a) linear 15-mers, (b) 15-14 rod-coils, (c) 15-13 rod-coils and (d) 15-12 rod-coils. Lines and symbols as in Fig. 4.7.

As can be observed in Figs. 4.7 and 4.8, both SPT and the OVL-LHrc theory result in a small underestimation of the location (pressure and coexistence densities) of the phase transition for more flexible chains. Part of the reason is that, due to the increased flexibility of the molecules, the phase transition is shifted to higher packing fraction and thus errors introduced by the approximate treatment of the higher virial coefficients become apparent. As shown previously for linear m-mers, inaccuracies of this kind result in an underestimation of the location of the phase transition. Compared to linear chains, however, the underestimation seems to be more severe. This could be due to several reasons. The first, and most probable reason is that the approximate description of the higher virial coefficients becomes less accurate for chains of increased flexibility. Second, it could be due to the introduction of small inaccuracies through the use of the correlation for the pair-excluded volume from Eq. (4.11). To test this hypothesis, we calculated the orientation-dependent pair-excluded volume of a 15-12 rod-coil using the MC method from Chapter 2. A third order series in $\sin(\gamma)$ (*i.e.* $V_{\rm ex}(\gamma) = \sum_{i=1}^{4} C_i \sin^{i-1}(\gamma)$, with $C_1 = 22.5871$, $C_2 = 17.1903$, $C_3 = 26.4334$ and $C_4 = -16.3469$) gave a nearly perfect fit. Calculations of the OVL-LHrc theory based on this fit are included (dash-dotted line) in Fig. 4.7 (d). It is reassuring to see that the difference with the results obtained from using Eq. (4.11) is very small. Moreover, the use of the fit leads to a slightly lower—not higher—prediction of the location of phase transition. Finally, the reason could be the decoupling of the conformational distribution function in Eq. (4.4). First of all, the decoupling is in contradiction to the increase in end-to-end length at the isotropic-nematic phase transition. Given the MC simulation results of Oyarzun *et*

al. [136] (*i.e.* increase end-to-end-length $< 2\%$), however, it is unlikely this effect is significant here. Furthermore, the increase in end-to-end length has two opposite effects on the driving force of the phase transition (a negative effect due to a decrease in chain-conformational entropy and a positive effect due to an increase in shape anisotropy of the molecules) which may just as well cancel each other out. The second implication of the decoupling is of more fundamental nature. Essentially, the decoupling comes down to modeling a (partially) flexible molecular model by a cylindrically symmetric, rigid molecular model, the pair-excluded volume interaction of which can be described by Eq. (4.10). It seems plausible that due to the averaging, part of the destabilizing effect of molecular flexibility on the isotropic-nematic phase transition is lost. Having that said, it seems reasonable to assume these effects are minor for the relatively stiff chains shown in Figs. 4.7 and 4.8. In conclusion, we expect the approximate treatment of the higher virial coefficients to cause the deviations of theory to simulations in Figs. 4.7 and 4.8.

Let us now turn our attention to the effect of molecular flexibility on the phase transition properties. In Fig. 4.9 we show the relative density difference $\Delta\eta/\eta_{\text{iso}}$ and the total density difference $\Delta\eta$ at the I-N phase transition of a 15-m_{R} rod-coil fluid as function of the rigidity parameter χ_{R}. As for linear chain fluids, both SPT and the OVL-LHrc theory result in an overestimation of the density difference as obtained from MC simulations. Qualitative agreement is obtained, in that both theory and simulation predict a decrease of the relative- and total density difference for chains of increased flexibility. In contrary to the maximum of the total density difference with chain length m (as was found for linear chains in Fig. 4.6 (b)), no maximum with χ_{R} is obtained. Consistent with the results from Figs. 4.7-4.8, the approximate algebraic form of the OVL-LHrc theory leads to comparable results as obtained from its numerical solution, provided the chains are relatively stiff. For more flexible chains ($\chi_{\text{R}} < 0.8$), the algebraic theory starts to overestimate the numerical results. As shown in Fig. 4.10, the nematic order parameter (and thus α) at I-N coexistence decreases with increased flexibility of the chains. Since the approximate algebraic theory was derived based on a truncated asymptotic expansion in α (Eq. (4.38)), it loses its validity for these smaller values of α (and χ_{R}). As shown in Fig. 4.10, the approximation quickly deteriorates for flexibilities of $\chi_{\text{R}} < 0.8$.

It is interesting to see that, for $\chi_{\text{R}} < 0.3$, the density difference as obtained from the full numerical OVL theory and SPT approaches the values typically found for real thermotropic nematogens ($\sim 0.5\%$). We should stress that when using a rigid molecular model, these results are simply unattainable (see Section 4.3.1). Moreover, when describing a flexible molecular model with a Khoklov-Semenov-type theory (where molecular flexibility is incorporated in the ideal contribution instead of the residual contribution to the Helmholtz energy) [100–102, 162, 163], larger density differences ($\sim 2\%$) are obtained. These results suggest that in order to arrive at a quantitative description of phase transition properties such as the density difference at the I-N transition, the effect of molecular flexibility should be incorporated in the (density-dependent) residual contribution to the Helmholtz energy, as is done in the theory derived in this chapter.

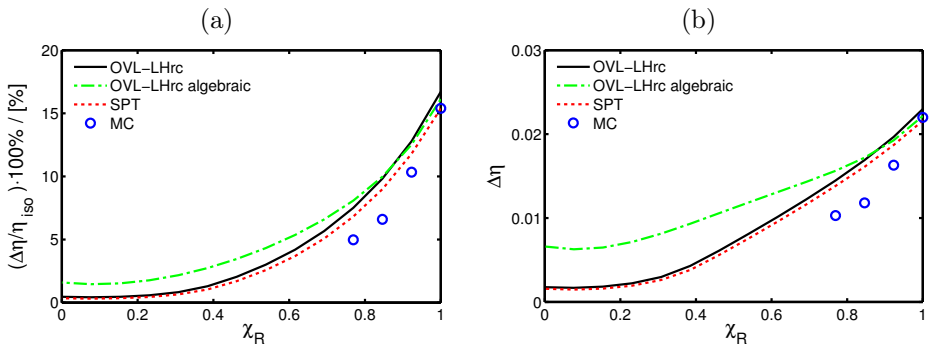

Figure 4.9: The variation of the density difference $\Delta\eta$ at the isotropic-nematic phase transition with the rigidity parameter χ_{R} of a 15-m_{R} rod-coil fluid. Comparison between predictions obtained from the OVL-LHrc theory (solid line), the approximate algebraic form of the OVL-LHrc theory (dash-dotted line) and SPT (dotted line) to MC simulations [136] (symbols).

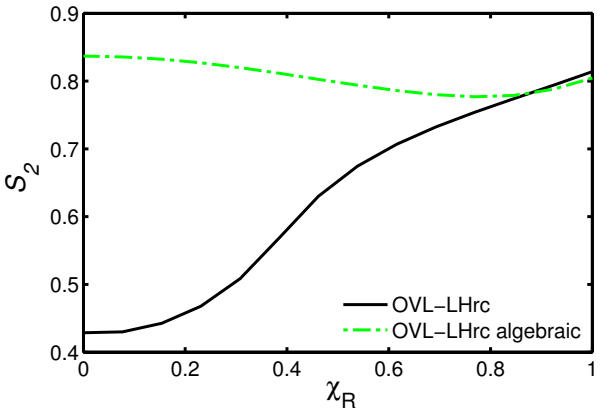

Figure 4.10: The variation of the isotropic-nematic coexistence value of the nematic order parameter S_2 with the rigidity parameter χ_{R} of a 15-m_{R} rod-coil fluid. Comparison between predictions obtained from OVL-LHrc theory (solid line) and the approximate algebraic form of the OVL-LHrc theory (dash-dotted line).

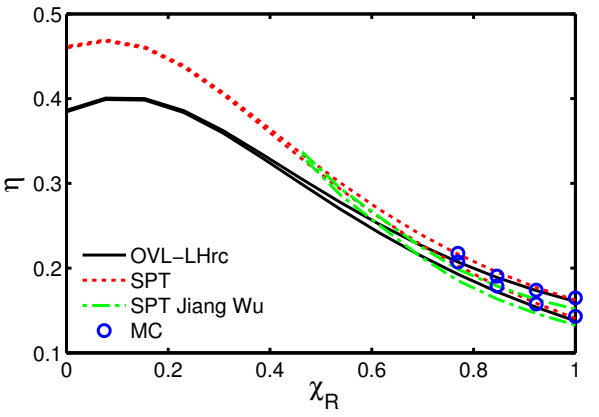

Figure 4.11: The phase diagram of a 15-m_{R} rod-coil fluid. Comparison between predictions obtained from OVL-LHrc (solid line), SPT (dotted lines), and the SPT of Jiang and Wu [108] to MC simulations (symbols).

In Fig. 4.11, we compare the phase diagram (in an η-χ_R representation) of a 15-m_R rod-coil fluid as obtained from SPT and OVL-LHrc theory to MC simulations. Satisfactory agreement is obtained. Both SPT and the OVL-LHrc theory correctly capture the general trends with respect to the rigidity parameter. An interesting point is the fact that we find I-N coexistence for the full range of the rigidity parameter. In a comparable study of Jiang and Wu, who studied the same test system using the SPT of Jaffer *et al.* [108] with a full numerical solution of the ODF, no stable nematic phase was reported for $\chi_R \leq 0.46$. Their results are also included in Fig. 4.11. We should stress that the only significant difference between the approach of Jiang and Wu and the SPT employed in this work is the use of the OTF. One might argue that if a solution is found based on the OTF, a numerical solution for the ODF is bound to find a solution as well. Therefore the results of Jiang and Wu raise some questions. The fact that Jiang and Wu relate their theoretical lower limit of the rigidity parameter that supports a nematic phase to that of a certain real rod-coil polymer system, does not support their case.

From a theoretical point of view, the fact that we find I-N coexistence over the whole range of the rigidity parameter, raises some questions about the possibilities for extending the theory developed as such to describe the global (isotropic, nematic, smectic, solid) fluid phase behaviour of rod-coil chains of arbitrary flexibility. As we have shown in a recent MC simulation study [136], rod-coil fluids of intermediate flexibility (for example 14-10, 10-8 or 8-6 rod-coils) experience a direct transition from the isotropic to a smectic phase. Although not reported in that paper, we found this also holds true for a 15-10 rod-coil fluid. Given these results, it can be expected that for intermediate values of the rigidity parameter, the theoretical results found for the nematic phase of the 15-m_R system are metastable with respect to a smectic phase. Although it is possible to extent Onsager-like theories to describe smectic phases [164], this is regarded beyond the scope of this work. Also, no test for metastability is performed since the results from Ref. [136] are inconclusive on the exact location of the isotropic-smectic transition. For a value of the rigidity parameter equal (and probably close) to zero, no liquid crystalline phase can be formed. Instead, the isotropic phase will experience a direct transition to a solid phase [165]. Since the theory developed in this work does not include a description of the solid phase, this behaviour is not covered. However, we can test for metastability. Recently, Alavi and Feyzi [165] used Monte Carlo simulations to calculate the isotropic-solid coexistence packing fractions of fully flexible m-mers. For the 15-mer system, they found $\eta_{iso} = 0.55$ and $\eta_{solid} = 0.62$. For the theories to be consistent with these results, the predicted isotropic-nematic coexistence packing fractions for $\chi_R = 0$ shown in Fig. 4.9 should be larger. Unfortunately, this is not the case. In fact, it can be shown (not included for brevity) that the isotropic-nematic coexistence obtained from SPT and the OVL-LHrc theory is inconsistent with the isotropic-solid coexistence from Ref. [165] for chain lengths down to 7 and 6, respectively.

From a practical point of view, it is important to note that even if the theory developed here is extended to incorporate (anisotropic) attractive interactions between LC molecules (part B of this thesis), the upper limit for a nematic coexistence

packing fraction as found for $\chi_R = 0$ can only decrease in value. Depending on (1) the nematic coexistence packing fraction of a real LC, and (2) the value of the chain length m, this may lead to the prediction of IN coexistence, where a phase transition does in fact not appear.

4.4 Conclusion

An extension of Onsager's second virial theory is developed that analytically accounts for the effect of intramolecular flexibility on the isotropic-nematic phase behaviour. The effect of chain flexibility on the second virial coefficient is described using the analytical approximation for the orientation-dependent pair-excluded volume from Chapter 2. To approximate higher order virial coefficients, both the Vega-Lago rescaling and Scaled Particle Theory (SPT) were evaluated.

Theoretical results for the equation of state and nematic order parameter were extensively tested against the results from MC simulations. For all systems considered, the results from the Vega-Lago rescaling and SPT are of similar accuracy. For linear chains, we found that both theories compare accurately to the MC data for chain lengths down to 9. For shorter chains, the isotropic-nematic transition is shifted to such high density that errors introduced by the approximation of the higher virial coefficients become apparent and, consequently, the pressure and density difference at the phase transition are under- and overestimated, respectively. It is important to note that the results for the Vega-Lago approach were obtained using an improved description of the isotropic EoS that was developed in Chapter 3. This new EoS explicitly treats the effect of intramolecular flexibility. When using an isotropic EoS for fully flexible chain fluids instead, the Vega-Lago approach was less successful. Although for many purposes the isotropic phase behaviour of linear and fully flexible chains can be assumed to be identical [53, 166], the results obtained in this chapter show that there are differences that need to be captured to arrive at a satisfactory description of the isotropic-nematic phase equilibrium.

For rod-coil fluids, a near-quantitative agreement between theory and simulation data is obtained. The theoretical results correctly capture the general trends of the phase behaviour with respect to the rigidity of the molecules. With increased rigidity, the shape anisotropy of the molecules is increased, resulting in a shift of the isotropic-nematic phase equilibrium to lower density. In addition, the (relative) density difference at the phase transition grows for increasingly rigid chains. Our results suggest that the approximate description of the higher virial coefficients that results from the Vega-Lago rescaling and SPT becomes less accurate for chains of increased flexibility.

Based on the Onsager Trial Function approximation, an approximate fully algebraic OVL theory for the description of the isotropic-nematic transition of rod-coil fluids was derived. In this algebraic theory, a closed description of the variational parameter of the OTF (and thus the nematic order parameter) as a function of density and molecular architecture (chain length m and rigidity parameter χ_R) is obtained. Although for linear m-mers, the results of the approximate theory are almost indistinguishable form the full numerical solution of the OVL theory, for partially flexible chain fluids we found the accuracy of the approximate theory to

decrease fast with increased flexibility of the chains.

One important conclusion we can draw from the results shown in this chapter is that the incorporation of flexibility into a molecular model for LCs is essential if one requires a quantitative description of certain phase transition properties of real thermotropic nematogens. While for this class of LCs the choice for a rigid molecular model is known to lead to a significant overestimation of for example the density difference and nematic order parameter at the isotropic-nematic transition, our results show that by making the molecules partially flexible much more realistic values for these properties can be obtained.

With regard to the application of LCs as solvents in gas-absorption processes, the results in this chapter suggest that in order to maximize the density difference—and thus the solubility difference of small solutes—across the I-N transition, the molecules of the LC solvent should preferably be linear and rigid. Moreover, our results suggest the existence of an optimal chain length for linear LC solvents of somewhere between 10 and 15 segments.

5

The isotropic-nematic and nematic-nematic phase transition of tangent hard-sphere chain fluids—Mixtures

In this chapter we develop an analytical EoS to describe the isotropic- (I) and nematic (N) phase behaviour of linear- and partially flexible tangent hard-sphere chain fluids and their mixtures. The EoS is an extension of the EoS for pure-component systems that was presented in Chapter 4. Higher virial coefficients are calculated using a Vega-Lago rescaling procedure, which is hereby generalized to mixtures. The EoS is used to study (1) the effect of length bidispersity on the I-N and N-N phase behaviour of binary mixtures of linear tangent hard-sphere chain fluids, (2) the effect of partial molecular flexibility on the binary phase diagram and (3) the solubility of hard-sphere solutes in I- and N tangent hard-sphere chain fluids. By changing the length bidispersity, two types of phase diagrams were found. The first type is characterized by an I-N region at low pressure and a N-N demixed region at higher pressure that starts from an I-N-N triphase equilibrium. For the second type, the N-N region starts from a lower critical point at a pressure above the I-N region. The results for the I-N region are in excellent agreement with the results from molecular simulations. It is shown that the N-N demixing is driven both by orientational and configurational/excluded volume entropy. By making the chains partially flexible, it is shown that the driving force resulting from the configurational entropy is reduced (due to a less anisotropic pair-excluded volume), resulting in a shift of the N-N demixed region to higher pressure. Compared to linear chains, no topological differences in the phase diagram were found. We show that the solubility of hard-sphere solutes (as measured by the Henry's law constant) decreases across the I-N phase transition. Furthermore, it is shown that by using a LC mixture as the solvent, the solubility difference can be maximized by tuning the composition.

Parts of this chapter have been published as:
T. van Westen, T.J.H. Vlugt and J. Gross *J. Chem. Phys.* 140 (2014) 034504 [33].

5.1 Introduction

Mixtures of liquid crystals (LCs) with other LCs, polymers or non-LC additives are commonly employed to tailor the properties of liquid crystalline materials for specific tasks [3, 167]. Some examples are the addition of chiral dopants to achiral LCs to induce supra-molecular chirality for LC displays [3, 168, 169], the mixing of LCs to enhance the range of stability of a nematic phase [167], the mixing of LCs and polymers for improved polymer processing [170] and the addition of LCs to membranes for improved transport properties [170]. From a more fundamental point of view, mixtures of LCs are interesting since mixing LCs of different molecular architecture is known to produce very different phase behaviour compared to the pure components [3, 171, 172].

The theoretical description of LCs dates back to the work of Onsager [9, 109]. In this seminal work, the isotropic-nematic (I-N) phase transition was explained as a consequence of a competition between an orientational entropy, favouring the I (isotropic, disordered) state, and a configurational entropy, favouring the N (nematic, orientationally ordered) state. Although Onsager performed calculations for pure components only, he argued that for mixtures of LCs of different length, the longer molecules would preferentially partition in the N phase, leading to a fractionation of components between the coexisting phases (fractionation effect). Since then, different experimental studies have confirmed this hypothesis [173–175]. The first theoretical confirmation is due to Flory and Abe [176], who studied a binary mixture of rod-like polymers in the lattice approximation. Later, Lekkerkerker *et al.* extended Onsager's formalism to mixtures and confirmed his predictions from a continuum fluid approach [157]. From that point, numerous theoretical [177–185] and some molecular simulation [180, 186–188] studies have been performed on the subject, showing interesting phase behaviour such as the fractionation effect [177, 179–186], demixing (N-N [178, 182, 183, 185, 187–189], I-I [179, 182, 190] and smectic-smectic [181, 183]), re-entrant phenomena [177–179, 182, 185] and density inversion [189] (isotropic phase denser than LC phase). Many of these phenomena have also been observed experimentally [175, 191–193].

In the present chapter, we study the I-N phase behaviour and N-N demixing behaviour of binary mixtures of tangent hard-sphere chain fluids within a Vega-Lago rescaled Onsager theory [52]. We herewith extend our analysis on pure component systems from Chapter 4. Due to the combined use of the analytical approximation for the pair-excluded volume from Chapter 2 and the Onsager Trial Function (OTF) for the orientational distribution function, an analytical EoS is obtained (Sec 5.2). An algebraic form of the EoS (as presented in the previous chapter), however, could not be derived. In particular, the analytical EoS is used to study the effect of changing the length ratio of two linear chains in a binary mixture (length bidispersity) on the I-N and N-N phase behaviour (Sec 5.3.1). Furthermore, we investigate the effect of making one component of the binary mixture partially flexible (Sec 5.3.2). Finally, the solubility of hard spheres in linear and partially flexible tangent hard-sphere chain solvents is studied (Sec 5.3.3). For a thorough assessment of the EoS, we provide an extensive comparison to recent MC data for the binary phase diagram and Henry coefficient of hard-sphere solutes in various (binary) systems of linear and

partially flexible tangent hard-sphere chain fluids.

5.2 Theory

In the previous chapter, an Onsager-like Helmholtz energy functional was derived to describe the isotropic-nematic ordering transition in pure component systems of tangent hard-sphere chain molecules. The resulting Helmholtz energy functional could be expressed in terms of an orientational distribution function only, leading to a unified description of linear and partially flexible (rod-coil) tangent hard-sphere chain fluids. In this chapter, the developed formalism is extended to mixtures (Sec 5.2.1). To avoid repetition, only the main points needed for the extension are discussed. In Sec 5.2.2, details on the solution of the phase equilibrium are provided. Furthermore, in Sec 5.2.3 we use the Onsager Trial Function (OTF) approximation [9, 18] to derive analytical results for the Helmholtz energy of the nematic fluid mixture in terms of the variational parameters of the OTF.

5.2.1. Helmholtz energy functional

For a canonical, multicomponent mixture (of N_C components) of tangent hard-sphere chain molecules, the total reduced Helmholtz energy density can be written as the sum of an ideal and residual contribution, according to

$$a[f(\boldsymbol{\omega})] = \frac{\beta A[f(\boldsymbol{\omega})]}{V} = a^{\mathrm{id}}[f(\boldsymbol{\omega})] + a^{\mathrm{res}}[f(\boldsymbol{\omega})] \tag{5.1}$$

Here, $\beta^{-1} = kT$ is the product of Boltzmann's constant k with the absolute temperature T, V is the volume of the system, and the vector $\boldsymbol{\omega}$ is the orientation of a molecule's axis with respect to the director (average direction of all molecules in a phase). The probability density to find any molecule of a component i in an orientation $\boldsymbol{\omega}$ is defined by the orientational distribution function (ODF) $f_i(\boldsymbol{\omega})$, which is normalized as $\int f_i(\boldsymbol{\omega})\mathrm{d}\boldsymbol{\omega} = 1$. We use the shorthand notation $f(\boldsymbol{\omega})$ to denote the ODFs $f_1(\boldsymbol{\omega}), f_2(\boldsymbol{\omega}), \ldots, f_{N_C}(\boldsymbol{\omega})$ of all N_C components in the mixture.

The ideal contribution can be written as the sum of an isotropic part and an anisotropic part (related to the orientational entropy) as

$$a^{\mathrm{id}}\left[f(\boldsymbol{\omega})\right] = a^{\mathrm{id}}_{\mathrm{iso}} + a^{\mathrm{id}}_{\mathrm{aniso}}\left[f(\boldsymbol{\omega})\right] \tag{5.2}$$

where

$$a^{\mathrm{id}}_{\mathrm{iso}} = \sum_i^{N_C} \rho_i \left[\ln\left(\frac{\rho_i \Lambda_i'^3}{\Omega}\right) - 1\right] \tag{5.3}$$

$$a^{\mathrm{id}}_{\mathrm{aniso}}\left[f(\boldsymbol{\omega})\right] = \sum_i^{N_C} \rho_i \int f_i(\boldsymbol{\omega}) \ln\left[\Omega f_i(\boldsymbol{\omega})\right] \mathrm{d}\boldsymbol{\omega} \tag{5.4}$$

Here, $\rho_i = N_i/V$ is the number density of molecules of component i, $\Lambda_i'^3$ is a generalized De Broglie volume (which for partially flexible molecules incorporates a contribution due to the internal conformational degrees of freedom of a molecule

cf. Chapter 4) and the factor $\Omega = \int \mathrm{d}\boldsymbol{\omega} = 4\pi$ is a normalization constant which ensures that the anisotropic part vanishes for an isotropic distribution of molecular orientations (since $f_{i,\mathrm{iso}}(\boldsymbol{\omega}) = 1/\Omega = 1/4\pi$).

Analogous to our treatment of pure-component systems(Chapter 4), the Vega-Lago rescaling [52] is used to describe the residual contribution to the Helmholtz energy. In this approach, the higher virial coefficients of the nematic fluid are approximated by a mapping onto those of an isotropic fluid using a scaling of second virial coefficients. Upon introducing a second virial coefficient of the mixture $\bar{B}_2$, the Vega-Lago approach can be generalized to mixtures as

$$a^{\mathrm{res}}[f(\boldsymbol{\omega})] = a^{\mathrm{res}}_{\mathrm{iso}} \frac{\bar{B}_2[f(\boldsymbol{\omega})]}{\bar{B}_{2,\mathrm{iso}}} \tag{5.5}$$

Differentiation with respect to density results in the compressibility factor $Z = \beta P/\rho$, according to

$$Z = 1 + Z^{\mathrm{res}}_{\mathrm{iso}} \frac{\bar{B}_2[f(\boldsymbol{\omega})]}{\bar{B}_{2,\mathrm{iso}}} \tag{5.6}$$

5

For a more rigorous derivation of the above equations, the reader is referred to Appendix D. The residual Helmholtz energy and compressibility factor of the isotropic fluid are obtained from the LHrc EoS (Chapter 4). The second virial coefficient of the mixture is calculated from a mole-fraction-weighted sum over the second virial coefficients of all possible pair interactions ij [45, 48]

$$\bar{B}_2[f(\boldsymbol{\omega})] = \sum_i^{N_C} \sum_j^{N_C} x_i x_j B_{2,ij}[f_i(\boldsymbol{\omega}), f_j(\boldsymbol{\omega}] \tag{5.7}$$

The second virial coefficient of the pair interaction ij is calculated from the following ensemble average

$$B_{2,ij}[f_i(\boldsymbol{\omega}), f_j(\boldsymbol{\omega})] = \frac{1}{2} \left\langle V_{\mathrm{ex},ij}(\gamma) \right\rangle_{\boldsymbol{\omega}_1,\boldsymbol{\omega}_2} \tag{5.8}$$

For both linear and partially flexible chain molecules, the orientation-dependent pair-excluded volume $V_{\mathrm{ex},ij}(\gamma)$ is obtained from the analytical approximation that was developed in Chapter 2

$$\begin{aligned} V^*_{\mathrm{ex},ij}(\gamma) = \frac{V_{\mathrm{ex},ij}(\gamma)}{V_{\bar{m}_{ij}}} = C_{1,ij}(\bar{m}_{ij}, \bar{\chi}_{\mathrm{R},ij}) + C_{2,ij}(\bar{m}_{ij}, \bar{\chi}_{\mathrm{R},ij}) \sin(\gamma) \\ + C_{3,ij}(\bar{m}_{ij}, \bar{\chi}_{\mathrm{R},ij}) \sin^2(\gamma) \end{aligned} \tag{5.9}$$

where

$$\bar{m}_{ij} = \frac{m_i + m_j}{2} \tag{5.10}$$

$$\bar{\chi}_{\mathrm{R},ij} = \frac{\chi_{\mathrm{R},i} + \chi_{\mathrm{R},j}}{2} \tag{5.11}$$

The isotropic second virial coefficient of the pair interaction ij follows from

$$B_{2,\mathrm{iso},ij} = V_{\bar{m}_{ij}} \left[\frac{C_{1,ij}(\bar{m}_{ij}, \bar{\chi}_{\mathrm{R}ij})}{2} + \frac{\pi C_{2,ij}(\bar{m}_{ij}, \bar{\chi}_{\mathrm{R}ij})}{8} + \frac{C_{3,ij}(\bar{m}_{ij}, \bar{\chi}_{\mathrm{R},ij})}{3} \right] \tag{5.12}$$

Eqs. (5.1)-(5.12) completely define our extension of the Onsager-Vega-Lago theory to mixtures of linear and/or (partially) flexible tangent hard-sphere chain fluids.

5.2.2. Solving the phase equilibrium

For the hard, purely repulsive molecules considered in this chapter, the determination of phase equilibrium between two phases A and B follows from the equality of pressure (P) and chemical potential of each component i (μ_i) in the coexisting phases

$$P^{\mathrm{A}} = P^{\mathrm{B}} \tag{5.13}$$

$$\mu_i^{\mathrm{A}} = \mu_i^{\mathrm{B}} \qquad \text{for} \quad i = 1, 2, \ldots, N_C \tag{5.14}$$

In terms of the Helmholtz-energy density $a = \beta A/V$, these can be obtained as

$$\beta P = -a + \sum_i^{N_C} \rho_i \left(\frac{\partial a[f_{\mathrm{eq}}(\boldsymbol{\omega})]}{\partial \rho_i} \right)_{T \rho_{j \neq i}} \tag{5.15}$$

$$\beta \mu_i = \left(\frac{\partial a[f_{\mathrm{eq}}(\boldsymbol{\omega})]}{\partial \rho_i} \right)_{T \rho_{j \neq i}} \tag{5.16}$$

To calculate these quantities for a nematic phase, one first has to solve for the equilibrium ODFs which minimize the total Helmholtz energy. Analogous to Chapter 4, we choose the Onsager Trial Function (OTF) approach and assume the ODF of a component i can be approximated as [9]

$$f_i(\boldsymbol{\omega}) \approx f_{\mathrm{OTF},i}(\theta) = \frac{\alpha_i \cosh[\alpha_i \cos(\theta)]}{4\pi \sinh(\alpha_i)} \tag{5.17}$$

Here, α_i is a variational parameter defining the degree of orientational order of a component i. θ is the polar angle of a molecule's axis with respect to the nematic director. Due to the use of the OTF, the functional minimization can be reduced to a simpler parameter minimization, and the equilibrium orientational state of the system is obtained by simultaneously solving the following set of non-linear equations for $i = 1, 2, \ldots, N_C$

$$\left(\frac{\partial a(\boldsymbol{\alpha})}{\partial \alpha_i} \right)_{T \rho, \boldsymbol{\alpha} = \boldsymbol{\alpha}_{eq}} = 0 \tag{5.18}$$

Here, $\boldsymbol{\alpha}$ is a vector containing the α_i of all N_C components in the mixture. A modified Newton-Raphson method [194] was used to solve this problem. The resulting $\boldsymbol{\alpha}_{\mathrm{eq}}$ determine the equilibrium ODFs according to Eq. (5.17). Accordingly, the (partial) nematic order parameter of a component i can be calculated from [9]

$$S_{2,i} = 1 - \frac{3 \coth(\alpha_i)}{\alpha_i} + \frac{3}{\alpha_i^2} \tag{5.19}$$

We choose to calculate the total nematic order parameter of the mixture as a simple mole-fraction-weighted sum of the partial nematic order parameters, according to

$$S_2 = \sum_i^{N_C} x_i S_{2,i} \tag{5.20}$$

Both the partial- and total nematic order parameters vary conveniently between zero and unity for an isotropic and perfectly ordered nematic phase, respectively.

5.2.3. Approximate analytical form of the Helmholtz energy in terms of the Onsager Trial Function

In this section, the Onsager-Vega-Lago Helmholtz energy functional as derived in Section 5.2.1 (Eqs. (5.1)-(5.5)) is evaluated in terms of the OTF (Eq. (5.17)). We show that for an excluded volume interaction given by Eq. (5.9), analytical results in terms of the variational parameters of the OTF can be obtained. By using appropriate expansions in these parameters, the theoretical approach is very much simplified. An algebraic theory with a closed description of the orientational ordering (cf. Chapter 4), however, is not obtained.

Let us first be concerned with the ideal contribution to the Helmholtz energy. Substituting the OTF in Eq. (5.4), followed by the substitution $u = \cos(\theta)$ and integration by parts leads to the following analytical result

$$a^{\mathrm{id}}_{\mathrm{aniso}} = \sum_i^{N_C} \rho_i \left\{ \ln[\alpha_i \coth(\alpha_i)] - 1 + \frac{\arctan(\sinh(\alpha_i))}{\sinh(\alpha_i)} \right\} \tag{5.21}$$

For large values of α_i (say $\alpha_i > 800$), the hyperbolic terms in this equation become too large to be naively computed on a regular computer; therefore, for $\alpha_i > 125$, we approximate the above result to within the machine epsilon of a 64-bit double precision (error$< 2^{-53}$) as

$$a^{\mathrm{id}}_{\mathrm{aniso}} = \sum_i^{N_C} \rho_i \left\{ \ln[\alpha_i] - 1 \right\} \tag{5.22}$$

Clearly, the introduced error can be neglected. The derivative of the ideal Helmholtz energy contribution with respect to α_i, which is needed for solving Eq. (5.18), can now be obtained as

$$\left(\frac{\partial a^{\mathrm{id}}}{\partial \alpha_i} \right)_{T\rho,\alpha_{j\neq i}} = \rho_i \left\{ \frac{1}{\alpha_i} + \frac{\arctan[\sinh(\alpha_i)]\cosh(\alpha_i)}{\sinh^2(\alpha_i)} \right\} \tag{5.23}$$

For $\alpha_i > 125$, this is approximated as (error$< 2^{-53}$)

$$\left(\frac{\partial a^{\mathrm{id}}}{\partial \alpha_i} \right)_{T\rho,\alpha_{j\neq i}} = \frac{\rho_i}{\alpha_i} \tag{5.24}$$

Let us now focus on the residual Helmholtz energy contribution (Eq. (5.5)). To evaluate this term, we need to solve the second virial coefficient (Eqs. (5.7)-(5.8))

in terms of the variational parameters of the OTF. Using the excluded volume expression from Eq. (5.9), the second virial coefficient of any two molecules 1 and 2 of type i and j, respectively, can be written as

$$B_{2,ij}[f_i(\boldsymbol{\omega}_1), f_j(\boldsymbol{\omega}_2)] = \frac{1}{2} V_{\tilde{m}_{ij}} \Big[C_{1,ij} + C_{2,ij} \left\langle \sin(\gamma) \right\rangle_{ij,\boldsymbol{\omega}_1,\boldsymbol{\omega}_2} + C_{3,ij} \left\langle \sin^2(\gamma) \right\rangle_{ij,\boldsymbol{\omega}_1,\boldsymbol{\omega}_2} \Big] \tag{5.25}$$

Clearly, the evaluation of the orientational averages of the $\sin(\gamma)$- and $\sin^2(\gamma)$-kernels of the pair-excluded volume is of central importance for the calculation of the second virial coefficient—and thus the residual Helmholtz energy—of the nematic fluid. In terms of the OTF, these averages can be derived as

$$\left\langle \sin(\gamma) \right\rangle_{ij,\boldsymbol{\omega}_1,\boldsymbol{\omega}_2} = \frac{1}{2\sinh(\alpha_i)\sinh(\alpha_j)} \int_{\gamma=0}^{\pi} \cosh\left(\sqrt{\alpha_i^2 + \alpha_j^2 + 2\alpha_i\alpha_j\cos(\gamma)} \right) \cos(\gamma) \mathrm{d}\gamma \tag{5.26}$$

$$\left\langle \sin^2(\gamma) \right\rangle_{ij,\boldsymbol{\omega}_1,\boldsymbol{\omega}_2} = \frac{1}{\sinh(\alpha_i)\sinh(\alpha_j)} \int_{\gamma=0}^{\pi} \cosh\left(\sqrt{\alpha_i^2 + \alpha_j^2 + 2\alpha_i\alpha_j\cos(\gamma)} \right) \cos(\gamma)\sin(\gamma) \mathrm{d}\gamma \tag{5.27}$$

For a detailed analysis on the derivation of these two integrals, the reader is referred to the comprehensive work of Franco-Melgar *et al.* [18, 195]. For brevity, this derivation is here omitted. Although, in principle, both of the above integrals can be evaluated numerically, it is much more attractive to use an analytical—albeit approximate—solution instead. The reason for this is twofold. First, both integrals are calculated inside a double iteration-loop for solving for the equilibrium orientational state of the system (Eq. (5.18)) and phase equilibrium (Eqs. (5.13)-(5.14)), respectively. As a consequence, their computation (and that of the required numerical derivatives) is intensive. Second, for systems with very high orientational order, say $\alpha_i > 800$ (which can happen in the dense nematic phase), these terms become too large to be naively computed on a regular computer. We devote the remainder of this section to obtaining approximate solutions of Eqs. (5.26)-(5.27).

The first integral (Eq. (5.26)) was approximated by Onsager in the Appendix of his paper from 1949 [9]. Since from Onsager's analysis it is difficult to extract for which cases his approximation is justified, we will here go through his derivation in a bit more detail and put some emphasis on the assumptions made. Let us first make the following substitution

$$\alpha_i^2 + \alpha_j^2 + 2\alpha_i\alpha_j\cos(\gamma) = (\alpha_i + \alpha_j - t)^2 \tag{5.28}$$

Using this, we obtain two solutions for the lower and upper boundary of integration, *i.e.* $t_l = 0$ or $t_l = 2(\alpha_i + \alpha_j)$ and $t_u = 2\alpha_i$ or $t_u = 2\alpha_j$, respectively. Although the choice for a specific solution is arbitrary, it is convenient to choose $t_l = 0$ and $t_u = 2\alpha_k$ where k is the index of the component with the lowest degree of

orientational order of the pair ij. For the purely repulsive molecules considered here, this component will always be the less elongated one (see Section 5.3.1). It can be verified that by choosing these boundaries, the range of integration is such that the factor $t-\alpha_i-\alpha_j$ is always smaller than—or equal to—zero; therefore, the hyperbolic terms can be approximated by an exponential as

$$\begin{aligned}\frac{\cosh(\alpha_i+\alpha_j-t)}{2\sinh(\alpha_i)\sinh(\alpha_j)} &= \frac{\exp(\alpha_i+\alpha_j-t)+\exp(t-\alpha_i-\alpha_j)}{4\sinh(\alpha_i)\sinh(\alpha_j)} \\ &\approx \frac{\exp(\alpha_i+\alpha_j)}{4\sinh(\alpha_i)\sinh(\alpha_j)}\exp(-t) \\ &\approx \exp(-t)\end{aligned} \tag{5.29}$$

To complete the transformation of variables, we write

$$\cos(\gamma)\mathrm{d}\gamma = \cos(\gamma)\frac{\mathrm{d}\gamma}{\mathrm{d}t}\mathrm{d}t = \frac{\mathrm{d}\sin(\gamma)}{\mathrm{d}t}\mathrm{d}t \tag{5.30}$$

5

which, combined with Eqs. (5.26) and (5.29), leads to

$$\langle\sin(\gamma)\rangle_{ij,\boldsymbol{\omega}_1,\boldsymbol{\omega}_2} = \int_0^{2\alpha_k}\exp(-t)\frac{\mathrm{d}\sin(\gamma)}{\mathrm{d}t}\mathrm{d}t \tag{5.31}$$

To proceed, we obtain $\sin(\gamma)$ from the trigonometric identity $\sin(\gamma)=\sqrt{1-\cos^2(\gamma)}$, with $\cos(\gamma)$ evaluated from Eq. (5.28) as $\cos(\gamma)=1-t/\alpha_i-t/\alpha_j+t^2/(2\alpha_i\alpha_j)$. After some rearrangements, we obtain

$$\sin(\gamma) = \sqrt{2t\left(\frac{\alpha_i+\alpha_j}{\alpha_i\alpha_j}\right)}\sqrt{1-x} \tag{5.32}$$

where

$$\begin{aligned}x = \frac{3t}{2(\alpha_i+\alpha_j)} &+ \frac{t}{2(\alpha_i+\alpha_i^2/\alpha_j)} + \frac{t}{2(\alpha_j+\alpha_j^2/\alpha_i)} \\ &- \frac{t^2}{2(\alpha_i\alpha_j+\alpha_i^2)} - \frac{t^2}{2(\alpha_i\alpha_j+\alpha_j^2)} + \frac{t^3}{8(\alpha_i\alpha_j^2+\alpha_i^2\alpha_j)}\end{aligned} \tag{5.33}$$

Onsager proceeded by expanding the square root $\sqrt{1-x}$ around $x=0$ (as $1-x/2-x^2/8-x^3/16-\ldots$) and truncating after second order in x. Before we do this, it is instructive to look at the behaviour of x as a function of the relevant parameters, and gain some insight into the accuracy of this expansion. As imposed by the limits of integration of Eq. (5.31), $t=\epsilon\cdot\alpha_k$, where $0\le\epsilon\le 2$. Accordingly, one can rewrite the above equation for x in terms of ϵ and a newly introduced variable $Q=\alpha_i/\alpha_j$, where $i=k$ is chosen as the component with the lowest orientational order (*i.e.* $0\le Q\le 1$). Different diagrams of x versus Q for $\epsilon=0,0.25,0.5,\ldots,2.0$ (Fig. 5.1) show that the expansion is justified as long as ϵ is small. For ϵ close to 2, on the other hand, the value of x tends to unity, leading to a decreased accuracy of the

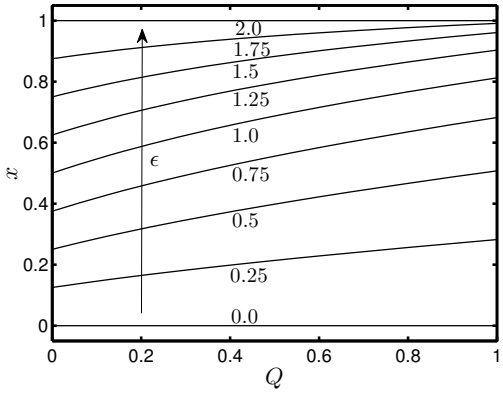

Figure 5.1: The x-parameter from Eq. (5.33) versus the ratio of orientational order $Q = \alpha_1/\alpha_2$ (where $\alpha_2 \geq \alpha_1$) for various values of $t = \epsilon \cdot \alpha_1$, with $\epsilon = 0.0, 0.25, 0.5, \ldots, 2.0$. The expansion $\sqrt{1-x} = 1 - x/2 - x^2/8 - x^3/16 - \ldots$ converges only when $x < 1$.

expansion. For $x = 1$, the expansion is not justified. Consequently, only close to the upper integration boundary of Eq. (5.31) the use of the expansion constitutes a non-negligible degree of approximation to the integrand. Whether this decrease in accuracy will affect the calculated result from Eq. (5.31) depends on the value of α_k. For any reasonable value of α_k (say, 5 or larger) the exponential will be the dominant factor in the integrand; thereby scaling any errors introduced by the expansion of the square root to approximately zero. For smaller values of α_k, which occur for very bidisperse mixtures (see Section 5.3.1), some error in the computed results can be expected. Performing the expansion, taking the derivative to t and truncating after third order in α, leads to the following result

$$\begin{aligned}\frac{\mathrm{d}\sin(\gamma)}{\mathrm{d}t} = \sqrt{\frac{\alpha_i+\alpha_j}{2\alpha_i\alpha_j}}\Bigg\{\frac{1}{\sqrt{t}} - \Bigg[\frac{9\sqrt{t}}{4(\alpha_i+\alpha_j)} + \frac{3\sqrt{t}}{4(\alpha_i+\alpha_i^2/\alpha_j)} + \frac{3\sqrt{t}}{4(\alpha_j+\alpha_j^2/\alpha_i)} \\ - \frac{5t^{3/2}}{4(\alpha_i\alpha_j+\alpha_i^2)} - \frac{5t^{3/2}}{4(\alpha_i\alpha_j+\alpha_j^2)} + \ldots\Bigg] - \frac{1}{32}\Bigg[\frac{45t^{3/2}}{(\alpha_i+\alpha_j)^2} \\ + \frac{5t^{3/2}}{(\alpha_i+\alpha_i^2/\alpha_j)^2} + \frac{5t^{3/2}}{(\alpha_j+\alpha_j^2/\alpha_i)^2} + \frac{10t^{3/2}}{(\alpha_i+\alpha_i^2/\alpha_j)(\alpha_j+\alpha_j^2/\alpha_i)} \\ + \frac{30t^{3/2}}{(\alpha_i+\alpha_j)(\alpha_i+\alpha_i^2/\alpha_j)} + \frac{30t^{3/2}}{(\alpha_i+\alpha_j)(\alpha_j+\alpha_j^2/\alpha_i)} + \ldots\Bigg]\Bigg\}\end{aligned} \tag{5.34}$$

Substitution in Eq. (5.31) leads to a series of integrals of the form $K_n(\alpha_i, \alpha_j)$ $\int_0^{2\alpha_k} \exp(-t)t^{n/2}\mathrm{d}t$ where $n = -1$, 1 or 3, respectively, and $K_n(\alpha_i, \alpha_j)$ is a t-independent factor to be determined from Eq. (5.34). As discussed, for a sufficiently large value of the variational parameter α_k, the exponential forces the value of the integrand to zero close to the upper boundary of integration, allowing for an extension of the range of integration to $t = [0 \quad \infty]$. This extension is particularly useful since now a transformation $t = y^2$ can be used to reduce these integrals to the following

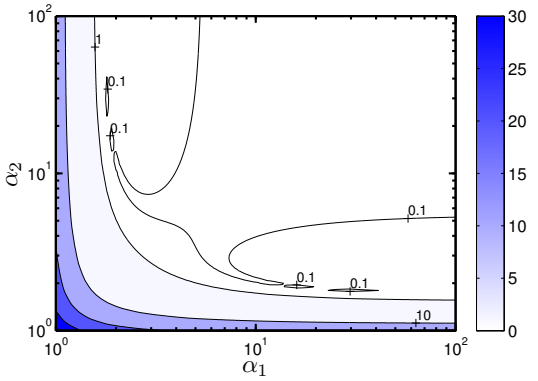

Figure 5.2: The percentage deviation of the analytical approximation for the orientational average of the $\sin(\gamma)$-kernel of the pair-excluded volume from Eq. (5.35) compared to the full numerical solution from Eq. (5.26).

standard Gaussian types: $\int_0^\infty \exp(-y^2)\mathrm{d}y = \sqrt{\pi/4}$, $\int_0^\infty \exp(-y^2)y^2\mathrm{d}y = \sqrt{\pi/16}$ and $\int_0^\infty \exp(-y^2)y^4\mathrm{d}y = (3/8)\sqrt{\pi}$. Now, we obtain Onsager's approximation for the orientational average of the $\sin(\gamma)$-kernel of the pair-excluded volume after rearranging

$$\begin{aligned}\langle \sin(\gamma)\rangle_{ij,\boldsymbol{\omega}_1,\boldsymbol{\omega}_2} = \sqrt{\frac{\pi}{2}\left(\frac{\alpha_i+\alpha_j}{\alpha_i\alpha_j}\right)}\Bigg\{1 - \frac{3}{8}\left[\frac{1}{\alpha_i+\alpha_j} + \frac{1}{\alpha_i} + \frac{1}{\alpha_j} + \ldots\right] \\ + \frac{15}{128}\left[\frac{8}{\alpha_i\alpha_j} - \left(\frac{1}{\alpha_i+\alpha_j} + \frac{1}{\alpha_i} + \frac{1}{\alpha_j}\right)^2 + \ldots\right]\Bigg\}\end{aligned} \tag{5.35}$$

For completeness, the percentage difference of the above analytical result compared to its exact numerical counterpart (Eq. (5.26)) is shown for a grid in α_i and α_j in Fig. 5.2. For the larger part of parameter space, the approximation is remarkably accurate; showing a negligible relative difference ($< 10^{-3}$) for both α-parameters larger than 5. As expected, the approximation breaks down if one of the α-parameters approaches unity; limiting its application to systems of not too extreme bidispersity. For all systems considered in this chapter, however, we will find that the bidispersity is moderate enough to use Eq. (5.35) as an accurate approximation of Eq. (5.26).

To the best of our knowledge, no analytical solution of the second integral (Eq. (5.27)) has thus far been presented in literature. Most probably, the reason is that for typical rigid, hard-core nematogens studied, the orientation dependence of the pair-excluded volume can be captured by a first order term in $\sin(\gamma)$. For the partially flexible molecules studied here, however, the incorporation of a second order term in $\sin(\gamma)$ is required [88]. In many respects, the method followed to evaluate Eq. (5.27) is the same as that layed out by Franco-Melgar *et al.* [18, 195] for the pure-component fluid. We show that, as for the pure-component case, exact analytical results can be obtained.

To proceed, let us start with the transformation of variables $a = \alpha_i^2 + \alpha_j^2$, $b =$

$2\alpha_i\alpha_j$ and $u = \sqrt{a + b\cos(\gamma)}$, which leads to

$$\mathrm{d}\gamma = -\frac{2u\mathrm{d}u}{b\sin(\gamma)} \tag{5.36}$$

$$\cos(\gamma) = \frac{u^2 - a}{b} \tag{5.37}$$

Substitution in Eq. (5.27) results in

$$\left\langle \sin^2(\gamma) \right\rangle_{ij,\boldsymbol{\omega}_1,\boldsymbol{\omega}_2} = \frac{2}{\sinh(\alpha_i)\sinh(\alpha_j)} \left\{ \frac{a}{b^2} \int_{\alpha_i+\alpha_j}^{\alpha_i-\alpha_j} \cosh(u) u \mathrm{d}u \quad + \right. \\ \left. - \frac{1}{b^2} \int_{\alpha_i+\alpha_j}^{\alpha_i-\alpha_j} \cosh(u) u^3 \mathrm{d}u \right\} \tag{5.38}$$

which can be solved straightforwardly by successive integration by parts. After rearranging, we obtain the following exact analytical result

$$\begin{aligned} \left\langle \sin^2(\gamma) \right\rangle_{ij,\boldsymbol{\omega}_1,\boldsymbol{\omega}_2} = \frac{1}{2\sinh(\alpha_i)\sinh(\alpha_j)} \Bigg\{ & \sinh(\alpha_i - \alpha_j) \left(\frac{-2}{\alpha_i} + \frac{2}{\alpha_j} - \frac{6}{\alpha_i\alpha_j^2} + \frac{6}{\alpha_i^2\alpha_j} \right) \\ & - \cosh(\alpha_i - \alpha_j) \left(\frac{6}{\alpha_i\alpha_j} - \frac{6}{\alpha_i^2\alpha_j^2} - \frac{2}{\alpha_i^2} - \frac{2}{\alpha_j^2} \right) \\ & + \sinh(\alpha_i + \alpha_j) \left(\frac{2}{\alpha_i} + \frac{2}{\alpha_j} + \frac{6}{\alpha_i\alpha_j^2} + \frac{6}{\alpha_i^2\alpha_j} \right) \\ & - \cosh(\alpha_i + \alpha_j) \left(\frac{2}{\alpha_i^2} + \frac{2}{\alpha_j^2} + \frac{6}{\alpha_i\alpha_j} + \frac{6}{\alpha_i^2\alpha_j^2} \right) \Bigg\} \end{aligned} \tag{5.39}$$

For $\alpha_i = \alpha_j$ this reduces to the pure-component result obtained by Franco-Melgar *et al.* [18, 195]. Also, using the hyperbolic properties $\cosh(-x) = \cosh(x)$ and $\sinh(-x) = -\sinh(x)$, it can be verified that the above result is symmetric in i and j. As mentioned earlier, the computation of the hyperbolic terms can become problematic for systems of very high orientational order. Is is therefore useful to simplify the above result a little further. Using the hyperbolic properties $\sinh(x+y) = \sinh(x)\cosh(y) + \cosh(x)\sinh(y)$ and $\cosh(x+y) = \cosh(x)\cosh(y) + \sinh(x)\sinh(y)$, we can write

$$\begin{aligned} \frac{\sinh(\alpha_i - \alpha_j)}{\sinh(\alpha_i)\sinh(\alpha_j)} &= \coth(\alpha_j) - \coth(\alpha_i) \\ \frac{\cosh(\alpha_i - \alpha_j)}{\sinh(\alpha_i)\sinh(\alpha_j)} &= \coth(\alpha_i)\coth(\alpha_j) - 1 \\ \frac{\sinh(\alpha_i + \alpha_j)}{\sinh(\alpha_i)\sinh(\alpha_j)} &= \coth(\alpha_j) + \coth(\alpha_i) \\ \frac{\cosh(\alpha_i + \alpha_j)}{\sinh(\alpha_i)\sinh(\alpha_j)} &= \coth(\alpha_i)\coth(\alpha_j) + 1 \end{aligned} \tag{5.40}$$

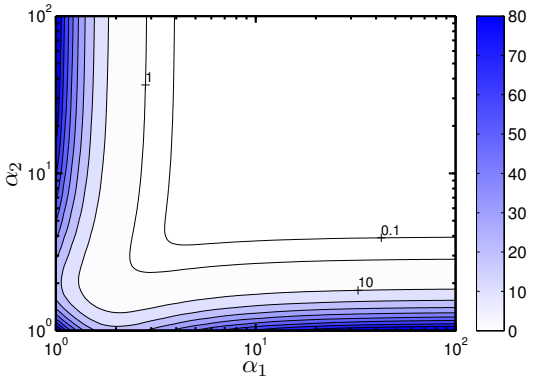

Figure 5.3: The percentage deviation of the analytical approximation for the orientational average of the $\sin^2(\gamma)$-kernel of the pair-excluded volume from Eq. (5.39) compared to the full numerical solution from Eq. (5.27).

For typical nematic mixtures, the values of the α-parameters are larger than 3; therefore, to a very good approximation (error $\sim 10^{-3}$) the coth(...)-terms can be reduced to unity, and Eq. (5.39) can be simplified further to the following algebraic equation

$$\left\langle \sin^2(\gamma) \right\rangle_{ij,\boldsymbol{\omega}_1,\boldsymbol{\omega}_2} = \frac{2}{\alpha_i} + \frac{2}{\alpha_j} - \frac{2}{\alpha_i^2} - \frac{2}{\alpha_j^2} - \frac{6}{\alpha_i\alpha_j} + \frac{6}{\alpha_i\alpha_j^2} + \frac{6}{\alpha_i^2\alpha_j} - \frac{6}{\alpha_i^2\alpha_j^2} \tag{5.41}$$

For all systems considered in the present chapter, Eq. (5.41) is used to approximate the orientational average of the $\sin^2(\gamma)$-kernel from Eq. (5.27). As shown in Fig. 5.3, the approximation is excellent, showing negligible error for a large and relevant part of parameter space. Similar to the approximation of the $\sin(\gamma)$-kernel (Fig. 5.2), the approximation of the $\sin^2(\gamma)$-kernel breaks down if the α-parameter of one (or both) of the components approaches unity.

To solve Eq. (5.18) for the equilibrium orientational state of the system, we also need the derivatives of Eqs. (5.35) and (5.41) to α_i. For configurations between molecules of different type, *i.e.* $i \neq j$, these can be derived as, respectively

$$\begin{aligned}\left(\frac{\partial \left\langle \sin(\gamma) \right\rangle_{ij,\boldsymbol{\omega}_1,\boldsymbol{\omega}_2}}{\partial \alpha_i}\right)_{\alpha_j} = &-\sqrt{\frac{\pi\alpha_j}{8\alpha_i^4 + 8\alpha_j\alpha_i^3}} \left\{ 1 - \frac{3}{8}\left[\frac{1}{\alpha_i+\alpha_j} + \frac{1}{\alpha_i} + \frac{1}{\alpha_j}\right] \right. \\ &\left. + \frac{15}{128}\left[\frac{8}{\alpha_i\alpha_j} - \left(\frac{1}{\alpha_i+\alpha_j} + \frac{1}{\alpha_i} + \frac{1}{\alpha_j}\right)^2\right]\right\} \\ &+ \sqrt{\frac{\pi}{2}\left(\frac{\alpha_i+\alpha_j}{\alpha_i\alpha_j}\right)} \left\{ \frac{3}{8}\left[\frac{1}{(\alpha_i+\alpha_j)^2} + \frac{1}{\alpha_i^2}\right] \right. \\ &+ \frac{15}{128}\left[\frac{-8}{\alpha_i^2\alpha_j} + 2\left(\frac{1}{\alpha_i+\alpha_j} + \frac{1}{\alpha_i} + \frac{1}{\alpha_j}\right)\right. \\ &\left.\left.\left(\frac{1}{(\alpha_i+\alpha_j)^2} + \frac{1}{\alpha_i^2}\right)\right]\right\}\end{aligned} \tag{5.42}$$

$$\left(\frac{\partial \left\langle \sin^2(\gamma) \right\rangle_{ij,\boldsymbol{\omega}_1,\boldsymbol{\omega}_2}}{\partial \alpha_i}\right)_{\alpha_j} = -\frac{2}{\alpha_i^2} - \frac{4}{\alpha_i^3} + \frac{6}{\alpha_i^2\alpha_j} - \frac{6}{\alpha_i^2\alpha_j^2} - \frac{12}{\alpha_i^3\alpha_j} + \frac{12}{\alpha_i^3\alpha_j^2} \tag{5.43}$$

For configurations between molecules of the same type, *i.e.* $i = j$, we obtain

$$\frac{\mathrm{d}\left\langle \sin(\gamma)\right\rangle_{ii,\boldsymbol{\omega}_1,\boldsymbol{\omega}_2}}{\mathrm{d}\alpha_i} = \sqrt{\pi}\left\{\frac{45}{32\alpha_i^{5/2}} - \frac{1}{2\alpha_i^{3/2}} - \frac{525}{1024\alpha_i^{7/2}}\right\} \tag{5.44}$$

$$\frac{\mathrm{d}\left\langle \sin^2(\gamma)\right\rangle_{ii,\boldsymbol{\omega}_1,\boldsymbol{\omega}_2}}{\mathrm{d}\alpha_i} = -\frac{4}{\alpha_i^2} + \frac{20}{\alpha_i^3} - \frac{36}{\alpha_i^4} + \frac{24}{\alpha_i^5} \tag{5.45}$$

In summary, we have derived analytical results for the orientation-dependent parts of the ideal- (Eqs. (5.21)-(5.22)) and residual (Eqs. (5.35) and (5.41)) Helmholtz energy contribution in terms of the variational parameters of the OTF. Also the derivatives of these contributions to the variational parameters have been obtained (Eqs. (5.23)-(5.24) and (5.42)-(5.45)). In the following section, these approximate results are used in the Onsager-Vega-Lago (OVL) theory that was laid out in Section 5.2.1. An analytical EoS for the isotropic and nematic phase of tangent hard-sphere chain fluid mixtures is thereby obtained. This EoS will be referred to as truncated OVL theory. When the exact (numerical) solutions of the orientational parts of the residual Helmholtz energy are used instead (Eqs. (5.26) and (5.39)), it will simply be referred to as OVL theory. It is shown later that both theories result in essentially identical results for the phase diagram of binary tangent hard-sphere chain fluid mixtures.

5.3 Results and Discussion

5.3.1. The effect of length bidispersity on the I-N and N-N phase behaviour

In this section, we analyse the effect of length bidispersity on the isotropic-nematic and nematic-nematic phase behaviour of binary mixtures of linear tangent hard-sphere chain fluids. The effect of length bidispersity on the degree of orientational ordering of the system is also studied. Since the analysis is purely theoretical, it is of value to test the theory to results from molecular simulations first. Until recently, the only available simulation data on I-N equilibria of binary hard-sphere chain systems was that Escobedo and De Pablo [186], who used an expanded Gibbs-ensemble MC method to simulate the I-N pressure-composition envelope of a mixture of linear 8-mers and linear 16-mers. In a recent work of Oyarzun *et al.* [34], the simulated database on these systems was much expanded. In Fig. 5.4, we compare simulation results for a binary mixture of linear 8-mers and 16-mers to those obtained from the truncated OVL theory developed in the previous section. Results from the OVL theory are also included for comparison. The theoretical results are in excellent agreement to simulation data. The results obtained from both theories are virtually indistinguishable, showing the accuracy of the truncated form of the OVL theory. Both theory and simulations show (equally) strong fractionation of the two components between the two phases, with the more anisotropic 16-mer fluid preferentially partitioned in the nematic phase.

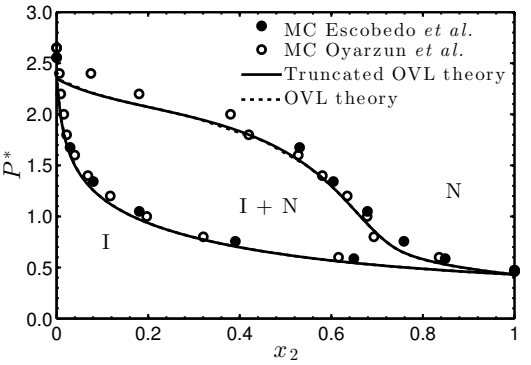

Figure 5.4: A comparison between the dimensionless pressure $P^* = \beta P V_{m=8}$ of a binary mixture of linear 8-mers and linear 16-mers as obtained from the truncated OVL theory (solid line), the full numerical solution of the OVL theory (dotted line), and MC simulations of Escobedo and de Pablo [186] (closed symbols) and Oyarzun *et al.* [34]. Here, x_2 is the mole fraction of 16-mers, $V_{m=8} = (\pi/6)m\sigma^3$ is the molecular volume of the linear 8-mer molecules. The results obtained from the full numerical solution of the OVL theory are almost indistinguishable from those obtained from the truncated variant. For comparison to the MC simulations, the focus of this figure is on the isotropic-nematic (I-N) coexistence; therefore, the nematic-nematic coexistence exhibited at higher pressure is not shown.

5

We view the favourable comparison between theory and simulation as a strong indicator that the developed theory accurately captures the phase behaviour of bidisperse mixtures, which encourages a further analysis of phase equilibria. We define a bidispersity ratio $q = m_1/m_2$, and vary q systematically by changing the length of component 2 (where $m_2 > m_1$). The length of component 1 is fixed at $m_1 = 8$. Using this procedure we were able to locate two types of phase diagrams, shown in Fig. 5.5 for four different systems of decreasing bidispersity ratio. For a bidispersity ratio close to unity, we find I-N coexistence at low pressure and a N-N demixed region with a lower critical point at higher pressure (Fig. 5.5 (a)-(b)). With decreasing bidispersity ratio, the N-N critical point is shifted to lower pressure until, for $m_2 = 19$, the N-N region starts to overlap with the I-N region, resulting in a triphase I-N-N equilibrium at $P^* = PV_{m=8}/kT = 2.234$, $x_{2,\mathrm{I}} = 0.000631$, $x_{2,\mathrm{N}^-} = 0.111$ and $x_{2,\mathrm{N}^+} = 0.428$ (Fig. 5.5 (c)). Here, we have introduced the notation N^- and N^+ for the coexisting nematic phases lean and rich in the longer component, respectively. If the bidispersity ratio is decreased further, an I$\rightarrow$ N$\rightarrow$ I$\rightarrow$ N re-entrant phenomenon [177–179, 182, 185] is observed upon increasing the pressure in some parts of the phase diagram (Fig. 5.5 (d)). For completeness, the phase diagrams from Fig. 5.5 are shown in a $\eta - x$ representation in Fig. 5.6.

It is important to note that we have tried to probe parameter space more rigorously by using different molecule types for the reference component 1, using more extreme bidispersity ratio's (down to 0.0001) and considering non-integer values of the chain length. Nonetheless, we did not find any other types of phase diagrams than those shown in Fig. 5.5, suggesting that (considering only I and N phases) this is the complete picture for binary mixtures of linear tangent hard-sphere chain fluids of equally-sized segments. In a study of Varga *et al.* [182], it was found that systems of hard rods of equal length but different diameter can also exhibit regions of N-N coexistence bounded by an upper critical point and regions of I-I coexistence. Given the similarity to the molecular model studied here, it seems reasonable to suggest

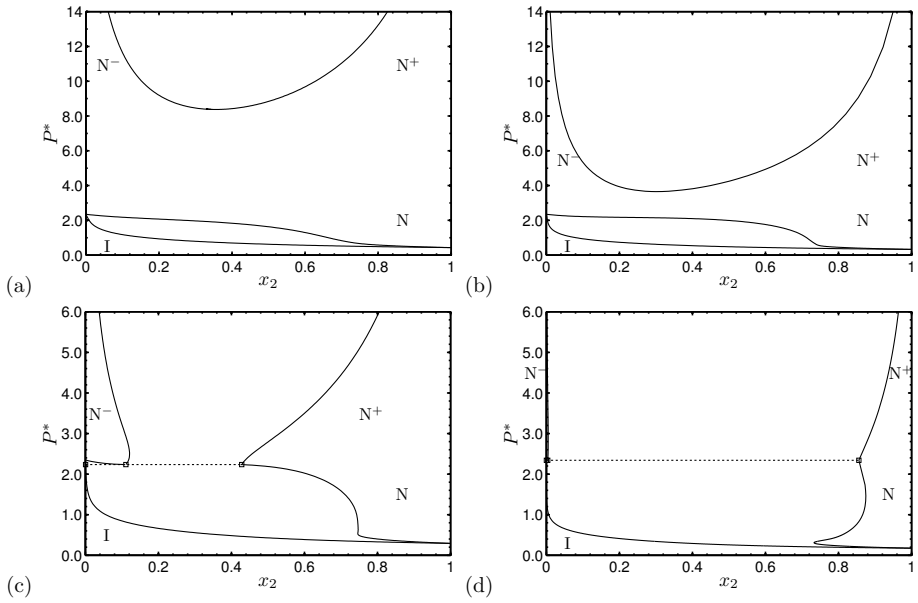

Figure 5.5: The dimensionless pressure $P^* = \beta P V_{m=8}$ of a binary mixture of linear 8-mers and (a) linear 16-mers, (b) linear 18-mers, (c) linear 19-mers, and (d) linear 24-mers, as obtained from the truncated OVL theory. Here, x_2 is the mole fraction of the long component in the mixture, $V_{m=8} = (\pi/6)m\sigma^3$ is the molecular volume of the linear 8-mer molecules. With increasing pressure, coexistence between an isotropic (I) and nematic (N) phase- and two nematic phases lean (N^-) and rich (N^+) in the long component is observed, respectively. The I-N^--N^+ threephase equilibrium is denoted by the dotted line.

these types of phase behaviour will also be observed for binary mixtures of tangent hard-sphere chain fluids of non-equally-sized segments.

Since the results for the N-N region have not been tested by comparing to MC simulations, let us elaborate on the accuracy of the theoretical results. As discussed in Section 5.2.3, the approximations related to truncating the OVL theory become more reliable for large values of the variational parameters (see Figs. 5.2 and 5.3). Therefore, any errors introduced by using these approximations within the framework of the OVL theory can be neglected in the highly ordered N-N region. The OVL framework itself (see Section 5.2.1), however, is expected to become less accurate at this part of the phase diagram. The OVL description of nematic phases relies on approximating higher virial coefficients; therefore, provided an accurate description of the isotropic phase, the N-N equilibrium will be inevitably less accurately described than the I-N equilibrium. Also, compared to the I-N region, the N-N region is located at relatively higher pressure/density; therefore, any errors introduced by the approximation of higher virial coefficients will become more pronounced. To what extent these errors influence the theoretical results is unclear at this point. For an assessment on this, a systematic MC study on the N-N behaviour would be desirable. The high densities of the coexisting nematic phases, however, makes such a study non-trivial.

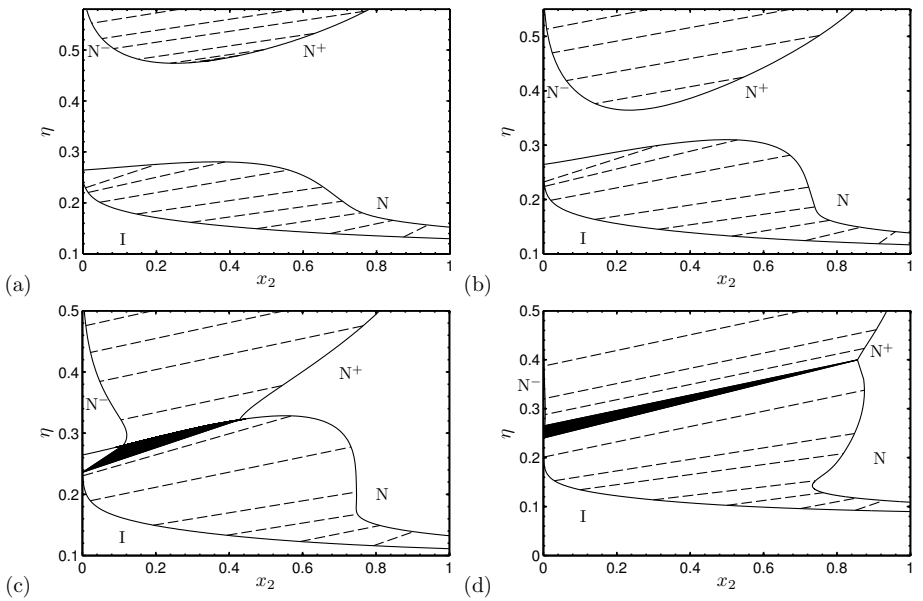

Figure 5.6: The packing fraction $\eta = \rho(\pi/6)\sum_i x_i m_i \sigma^3$ in the coexisting isotropic and nematic phase of a binary mixture of linear 8-mers and (a) linear 16-mers, (b) linear 18-mers, (c) linear 19-mers, and (d) linear 24-mers, as obtained from the truncated OVL theory. Here, x_2 is the mole fraction of the long component in the mixture, $V_{m=8} = (\pi/6)m\sigma^3$ is the molecular volume of the linear 8-mer molecules. The I-N$^-$-N$^+$ threephase equilibrium is denoted by the black shaded region.

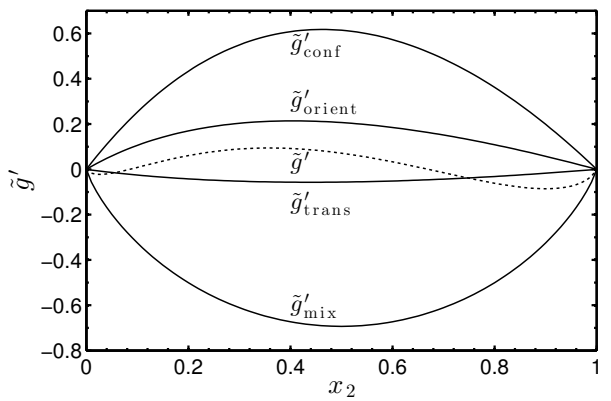

Figure 5.7: The total modified Gibbs energy (dotted line) from Eq. (5.46) for a nematic phase of linear 8-mers and linear 18-mers at a pressure $P^* = \beta P V_{m=8} = 10.3494$. Here, x_2 is the mole fraction of linear 18-mers, $V_{m=8} = (\pi/6)m\sigma^3$ is the molecular volume of the linear 8-mer molecules. Results are obtained from the truncated OVL theory. The solid lines correspond to the individual contributions to the Gibbs energy, arising from, translational- ($\tilde{g}'_{\rm trans}$), orientational- ($\tilde{g}'_{\rm orient}$), mixing- ($\tilde{g}'_{\rm mix}$), and configurational/excluded volume entropy ($\tilde{g}'_{\rm conf}$), respectively.

In contrast to the I-N transition, which was explained by Onsager as the result of a competition between orientational and configurational/excluded volume entropy, the nature of the N-N demixing transition has been a point of debate for some time. What can be extracted from the available literature on this point is that, depending on the molecular architecture of the components in the mixture, both orientational- and configurational/excluded volume entropy can give rise to a N-N demixing transition [178, 182, 189]. To obtain insight into the driving force behind the N-N demixing transition of the tangent hard-sphere chain fluids studied here, we analyse the behaviour of the total Gibbs energy and its individual (entropic) contributions with varying composition of the system. The total dimensionless Gibbs energy $\tilde{g} = \beta G/N$ is obtained from the Helmholtz energy using the thermodynamic relation

$$\tilde{g} = \frac{\beta A}{N} + Z \tag{5.46}$$

Here, $Z = \beta P/\rho$ is the compressibility factor of the system. One should note that in calculating the total Helmholtz energy, the density-independent factor Λ_i^3/Ω from Eq. (5.3) has not been considered since it is of no importance for the location of the phase equilibrium. Accordingly, the individual contributions to $\tilde{g}$ arising from, respectively, translational-, mixing-, orientational- and configurational/excluded volume entropy, are obtained from Eqs. (5.3)-(5.4) as

$$\tilde{g}_{\text{trans}} = \ln \rho \tag{5.47}$$

$$\tilde{g}_{\text{mix}} = \sum_i x_i \ln x_i \tag{5.48}$$

$$\tilde{g}_{\text{orient}} = \sum_i x_i \left(\ln \alpha_i - 1\right) \tag{5.49}$$

$$\tilde{g}_{\text{conf}} = \frac{\beta A^{\text{res}}}{N} + Z^{\text{res}} \tag{5.50}$$

The total Gibbs energy from Eq. (5.46) is then retained from the sum $\tilde{g} = \tilde{g}_{\text{trans}} + \tilde{g}_{\text{mix}} + \tilde{g}_{\text{orient}} + \tilde{g}_{\text{conf}}$. Since for purely repulsive molecules the N-N demixing transition does not occur in pure component systems, it is sufficient for our analysis to consider a modified Gibbs energy, according to

$$\tilde{g}^{'} = \tilde{g} - \sum_i x_i \tilde{g}_i^0 \tag{5.51}$$

$$\tilde{g}^{'}_{\text{trans}} = \tilde{g}_{\text{trans}} - \sum_i x_i \tilde{g}_{i,\text{trans}}^0 \tag{5.52}$$

$$\ldots \quad \text{etc.}$$

This procedure allows for a meaningful graphical representation of the demixing transition in a $\tilde{g}$-x diagram, because the dominant linear contributions from Eqs. (5.47)-(5.50) are subtracted. Subtracting the linear contributions does not alter the location of the phase transition as obtained from a common tangent-line construction [196]. In Fig. 5.7, we show a plot of the modified Gibbs energy and its

individual contributions versus the composition of a binary mixture of linear 8-mers and 18-mers at a pressure $P^* = \beta P V_{m=8} = 10.3494$. The results clearly show that both the translational and mixing entropy favour the (single phase) mixed state. The contributions arising from orientational- and configurational/excluded volume entropy favour a demixing transition to two nematic phases. In this respect, these results are comparable to those obtained by Varga *et al.* [182], who found that, for systems of thin and thick hard rods, both orientational- and configurational entropy favour N-N demixing. The results are different than those obtained by Wensink *et al.* [189], who found that, for systems of thin and thick hard platelets, the N-N demixing transition is driven by configurational entropy only.

Let us now shift focus to the orientational order parameters. As shown in some previous studies [157, 177, 185], the degree of orientational order of the components in a nematic binary mixture is very sensitive to composition. In Fig. 5.8 we show this behaviour is also observed for the tangent hard-sphere chain model. Three binary mixtures are considered. For all three mixtures, the first component is a linear 8-mer. The second component is varied between a linear 10-mer (Fig. 5.8 (a)), 14-mer (Fig. 5.8 (b)) or 16-mer (Fig. 5.8 (c)), respectively. It can be observed that over the whole composition range, the degree of orientational ordering of the long component is significantly larger than that of the short component. The reason is that at a certain density of the system, the shorter molecules have more freedom to rotate their axes away from the nematic director than the longer molecules. For systems of purely repulsive molecules, this behaviour is general. It can also be observed that the orientational order parameter has a maximum with composition. With decreasing bidispersity ratio $q = m_1/m_2$, the maximum becomes more pronounced and takes place at larger values of the mole fraction of the long component. These observations can be explained from a competition between two effects: (1) a decrease of the I-N coexistence pressure with increasing mole fraction of the long component (resulting in a decrease in density—and thus orientational order—of the nematic phase), and (2) induction of orientational order by adding a long component to a short component. In principle, when a long component is added to a nematic phase rich in a short component, the I-N coexistence pressure is much higher than it would be for the pure long component. Consequently, the degree of orientational order of the long component in the mixture is much higher than the typical coexistence value (*i.e.* $S_2 \sim 0.8$) found for the pure component system. As a result, the degree of orientational order of the short component is also increased (which we hereby refer to as 'induction'). Note that this second effect is enhanced by the fractionation of the longer and shorter molecules between the phases.

The maximum in the nematic order parameter has an interesting implication. As shown in Fig. 5.9, it results in a maximum difference in density between the coexisting isotropic and nematic phase. As shown in a previous MC simulation study [136], this density difference is a key factor determining a step-wise decrease in solubility of small gases across the I-N phase transition. In the light of applying LC solvents for gas absorption processes [23, 24], this observation is interesting, since it means that, as for many applications of LCs, the properties of a LC solvent can be optimized by using a LC mixture of specific composition. Below, in Section 5.3.3

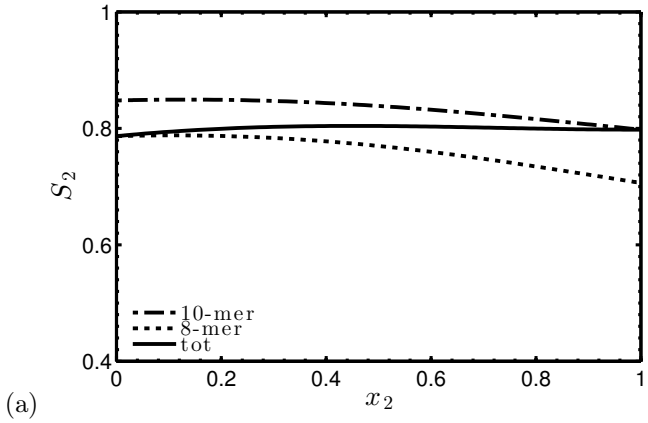

(a)

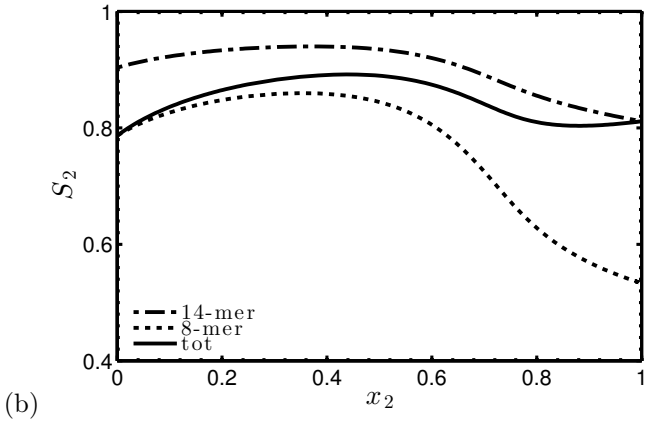

(b)

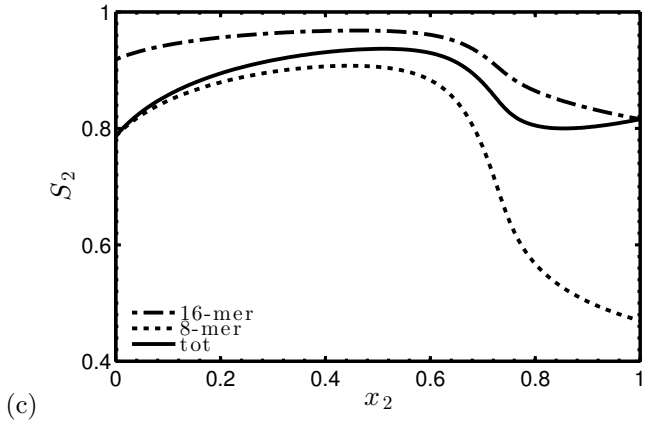

(c)

Figure 5.8: The I-N coexistence values of the total- and partial nematic order parameters S_2 (Eq. (5.20)) and $S_{2,i}$ (Eq. (5.19)), respectively, of a binary mixture of linear 8-mers and (a) linear 10-mers, (b) linear 14-mers, and (c) linear 16-mers, as obtained from the truncated OVL theory. Here, x_2 is the mole fraction of the long component in the nematic mixture.

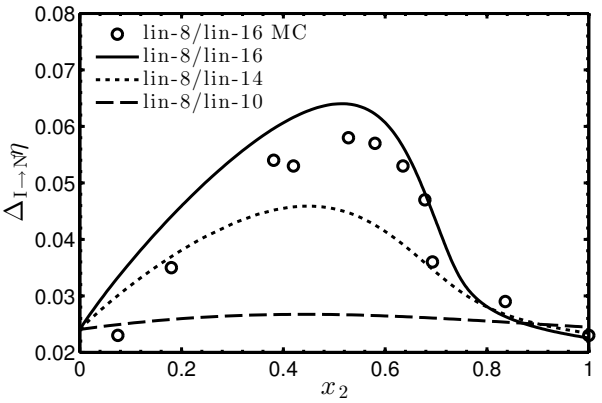

Figure 5.9: The difference of the packing fraction $\eta = \rho(\pi/6)\sum_i x_i m_i \sigma^3$ in the coexisting isotropic and nematic phase for the same binary mixtures as those shown in Fig. 5.8. Comparison between theoretical results as obtained from the truncated OVL theory (lines) and MC simulations of Oyarzun *et al.* [34]. x_2 is the mole fraction of the long component in the nematic phase mixture.

we further elaborate on this point, but for now, we investigate the effect of partial molecular flexibility on the phase diagram.

5

5.3.2. The effect of partial molecular flexibility on the I-N and N-N phase behaviour

Let us define the binary mixture of linear 8-mers and linear 19-mers (Fig. 5.5 (c)) as a reference. To study the effect of partial molecular flexibility, we gradually make the 19-mer more flexible by means of the rod-coil model; considering a number of 1 or 2 segments in the flexible tail, respectively. The rod-coils considered are thus the 19-18 and 19-17. Theoretical results for the phase diagrams are compared to MC simulation results of Oyarzun *et al.* [34] in Fig. 5.10. As for linear chain fluids, the comparison between theory and simulations is excellent. In addition, the truncated form of the OVL theory proves to be very accurate, leading to essentially identical results as obtained from the full numerical solution of the theory. It can be observed that, when compared to linear systems (Fig. 5.5), an increase in flexibility leads to the same topological changes in the phase diagram as a decrease in chain length of the more elongated component, namely a reduced fractionation of components between the I and N phase, a shift of the N-N critical point to higher pressure, and disappearance of the triphase I-N-N equilibrium. The reason for this similarity is that an increase in flexibility of the second (rod-coil) component reduces the length of its rigid block, and thereby 'effectively' increases the bidispersity ratio $q = m_1/m_2$.

In spite of the topological similarity of the phase diagrams of linear- and rod-coil fluids, there is a pronounced difference in the location of the N-N critical points. For example, the lower N-N critical point of a binary fluid of linear 18-mers and linear 8-mers (Fig. 5.5 (b)) is located at much lower pressure than that of a binary fluid of 19-18 rod-coils and linear 8-mers (Fig. 5.10 (a)), despite the fact that the number of beads in the rigid block is equal for the 18-mer and 19-18 rod-coil. Due to the presence of the flexible tail, the pair-excluded volume of the 19-18 rod-coil fluid is less anisotropic than that of the linear 18-mer fluid [88]. Hence, for the binary fluid

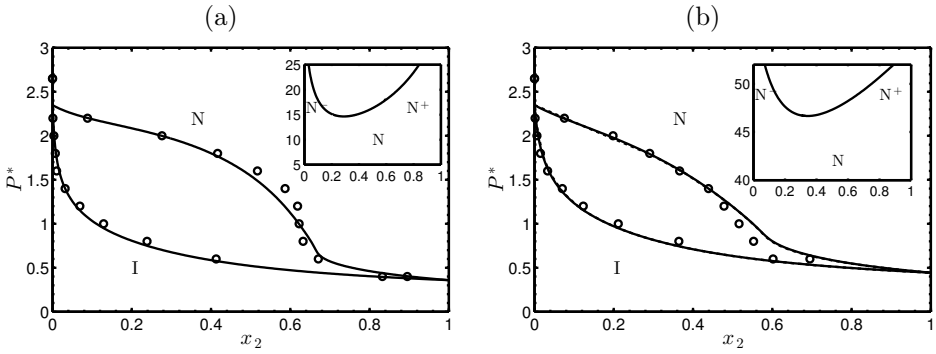

Figure 5.10: The dimensionless pressure $P^* = \beta P V_{m=8}$ of a binary mixture of linear 8-mers and (a) 19-18 rod-coils, and (b) 19-17 rod-coils, as obtained from the truncated OVL theory (solid lines) and MC simulations of Oyarzun *et al.* (symbols) [34]. x_2 is the mole fraction of the rod-coils in the nematic phase, $V_{m=8} = (\pi/6)m\sigma^3$ is the molecular volume of the linear 8-mer molecules. For (b), the results from the numerical solution of the OVL theory are included as well (dotted lines); the results of both theories are essentially indistinguishable. With increasing pressure, coexistence between an isotropic (I) and nematic (N) phase- and two nematic phases lean (N^-) and rich (N^+) in the long component is observed, respectively. The insets show the N^--N^+ demixed region which, due to the partial flexibility of the second component in the mixture, is shifted to very high pressure.

5

of linear 8-mers and 19-18 rod-coils, there is less configurational entropy that can be gained by demixing into two different nematic phases. This is clearly illustrated by comparing the $\tilde{g}$-x diagram from Fig. 5.11 (linear 8-mer/19-18 rod-coil mixture) to that from Fig. 5.7 (linear 8-mer/linear 18-mer mixture). In conclusion, when adding a flexible tail to one of the linear chain molecules of a binary mixture, the driving force for N-N demixing is decreased, leading to a shift of the N-N transition to higher density/pressure.

5.3.3. Solubility of hard-sphere solutes in linear and partially flexible tangent hard-sphere chain solvents

As a measure for the solubility of hard-sphere (hs) solutes in tangent hard-sphere chain solvents, we introduce the Henry's law constant H_k, formally defined by [197]

$$H_k = \lim_{x_k \to 0} \left(\frac{f_k^L}{x_k} \right) \tag{5.53}$$

where k is the hard-sphere component, and x_k and $f_k^L(V, T, \underline{x})$ are the mole fraction and fugacity of this component in the liquid (*i.e.* isotropic or nematic) phase, respectively. In terms of the fugacity coefficient $\phi_k^L = f_k^L/(x_k P) = \exp[\beta \mu_k^{\text{res}}]$, where P is the pressure exerted by the system and $\mu_k^{\text{res}}(V, T, \underline{x})$ is the residual chemical potential of component k, the above definition can be rewritten as

$$H_k = \lim_{x_k \to 0} \left(\phi_k^L P \right) = \lim_{x_k \to 0} \left(\exp[\beta \mu_k^{\text{res}}] P \right) \tag{5.54}$$

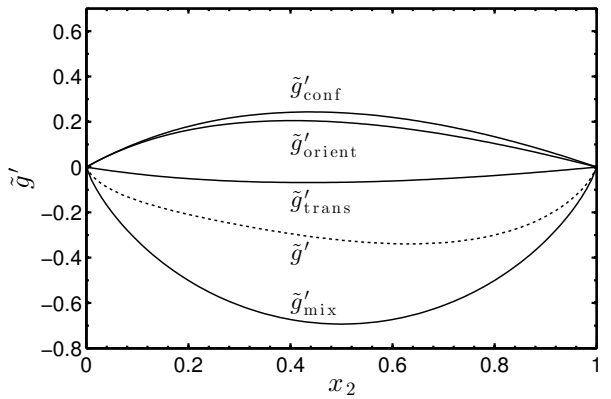

Figure 5.11: The total modified Gibbs energy (dotted line) from Eq. 5.46 versus composition of a nematic phase of linear 8-mers and 19-18 rod-coils at a pressure $P^* = \beta P V_{m=8} = 10.3494$. Here, x_2 is the mole fraction of the 19-18 rod-coils, $V_{m=8} = (\pi/6)m\sigma^3$ is the molecular volume of the linear 8-mer molecules. Results are obtained from the truncated OVL theory. The solid lines correspond to the individual contributions to the Gibbs energy, arising from, translational- ($\tilde{g}'_{\rm trans}$), orientational- ($\tilde{g}'_{\rm orient}$), mixing- ($\tilde{g}'_{\rm mix}$), and configurational/excluded volume entropy ($\tilde{g}'_{\rm conf}$), respectively. Compared to Fig. 5.7, where a similar diagram is shown for a binary fluid of linear 8-mers and linear 18-mers, the configurational contribution to the Gibbs energy is lower, resulting in a smaller driving force for N-N demixing. As a result, the N-N demixing transition is shifted to higher pressure than considered in this Figure.

5

where the residual chemical potential is obtained from

$$\beta\mu_k^{\rm res} = \left(\frac{\partial a^{\rm res}[f_{\rm eq}(\boldsymbol{\omega})]}{\partial \rho_k}\right)_{\rho_{j\neq k}T} \tag{5.55}$$

For convenience, we define a modified Henry's law constant H'_k, according to

$$H'_k = \frac{H_k}{P} = \lim_{x_k\to 0}\left(\exp[\beta\mu_k^{\rm res}]\right) \tag{5.56}$$

The motivation for using this modified Henry's law constant is merely to allow for a better graphical comparison between the Henry's law constants of hard-sphere solutes in different tangent hard-sphere chain solvents.

In Fig. 5.12, we compare the calculated modified Henry's law constant of a hard-sphere solute in a linear 15-mer-, a 15-14 rod-coil-, a 15-13 rod-coil- and a 15-12 rod-coil fluid to MC simulations [136]. For the linear 15-mer solvent, excellent agreement between simulation and theory is obtained. For the partially flexible LC solvents, agreement is satisfactory; deteriorating somewhat with flexibility. For all systems shown, a step-wise increase of the modified Henry's law constant is observed across the I-N transition; corresponding to a step-wise decrease in solubility of the hard-sphere solute.

As shown in a previous MC simulation study [136], this solubility difference is caused primarily by the density difference between the coexisting I and N phase. The orientational ordering was shown to have no—or at most a negligible—effect. In the

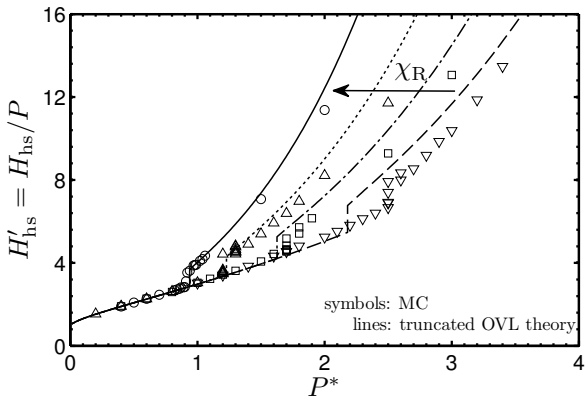

Figure 5.12: Modified Henry's law constant of a hard-sphere (hs) solute in several hard-chain solvents as a function of the dimensionless pressure $P^* = \beta P V_m$, where $V_m = (\pi/6) m \sigma^3$ is the molecular volume of the solvent molecules of chain length m. The hard-chain solvents considered are, (from left to right) in order of decreasing $\chi_{\rm R}$, a linear 15-mer, a 15-14 rod-coil, a 15-13 rod-coil, and a 15-12 rod-coil. Comparison of theoretical results obtained from the truncated OVL theory (lines) and MC simulation data from Ref. [136] (symbols).

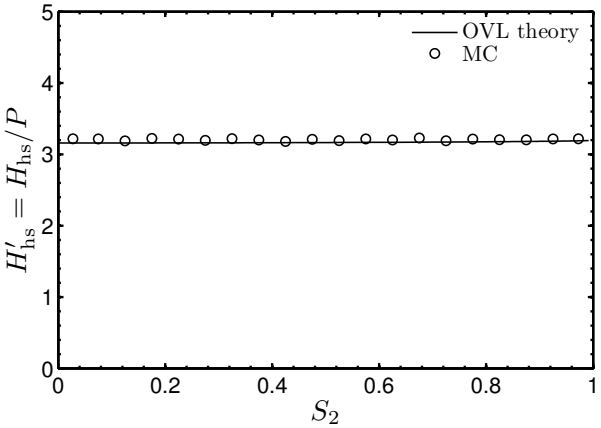

Figure 5.13: Modified Henry's law constant of a hard-sphere (hs) solute in a linear 15-mer solvent with varying orientational order parameter of the system. The density of the system is fixed at $\eta = 0.147$, which is in between the isotropic and nematic coexistence density of the pure solvent. Comparison of theoretical results obtained from the OVL theory (line) and MC simulation data from Ref. [136] (symbols).

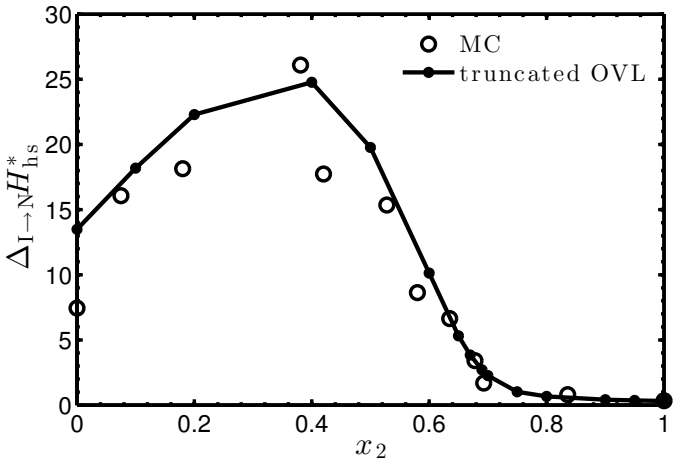

Figure 5.14: The difference of the isotropic- and nematic coexistence value of the dimensionless Henry's law constant $H^* = \beta H V_{m=8}$ of a hard sphere solute in a binary LC solvent of linear 8-mers and linear 16-mers. $V_{m=8} = (\pi/6)m\sigma^3$ is the molecular volume of the linear 8-mer molecules, x_2 is the mole fraction of linear 16-mers in the nematic phase. Theoretical results (filled circles, lines as a guide for the eye) are compared to results from MC simulations as obtained by Oyarzun *et al.* [34] (open circles).

5

simulations, a bias function was used to prescribe orientational order independent of density. The advantage of such a method is, that the effect of ordering on the Henry's law constant can be singled out for a defined density of the system. The theory can equally be applied with a prescribed value of orientational order. In Fig. 5.13 we emphasize this, by considering the modified Henry's law constant of a hard-sphere solute in a linear 15-mer solvent with a varying orientational order parameter S_2 at constant density of the system. Agreement between theory and simulations is excellent. As can be observed, when singled out from density, the orientational ordering has no significant effect on the modified Henry's law constant—and thus the solubility—of the hard-sphere solute.

Given this result, and the observation that for binary LC mixtures the density difference between the coexisting I and N phase shows a maximum with composition (Fig. 5.9), we conclude that the solubility difference of small solutes across the I-N phase transition can be maximized by choosing a binary LC mixture of specific composition as the solvent. To illustrate this, we calculated how the Henry's law constant of a hard-sphere solute changes when a binary LC solvent of linear 8-mers and linear 16-mers changes from the isotropic- to the nematic phase. The results are displayed for varying composition of the LC solvent in Fig. 5.14. A comparison to our recent results obtained from molecular simulations [34] are included as well. Like the density difference, the solubility difference displays a maximum with composition. The composition dependence is remarkably strong, resulting in approximately a factor 2 increase of the solubility difference (compared to the pure solvents) at a mole fraction of the linear 16-mer of $x \approx 0.4$. We performed similar calculations for a mixture of linear 8-mers and 18-mers; for this mixture the increase of the solubility

difference is increased even further to a factor 3 (not shown for brevity).

Whether these results can be extrapolated to mixtures of real LCs depends on several aspects. First, there is the issue of anisotropic attractive intermolecular interactions, such as those arising from dipolar forces. In some studies (see for example Refs. [198]-[199]), it was proposed that such interactions can result in the formation of dimer complexes, wherein the rigid cores of two LCs are aligned. Such a model was used, for example, to explain the occurrence of induced smectic- and re-entrant nematic phase behaviour. Moreover, in two recent experimental studies [200, 201], this proposed dimerization mechanism was used to explain an observed minimum in the nematic order parameter for a certain composition of a binary mixture of dipolar LCs. Clearly, the formation of these complexes should be avoided if one wants to maximize the difference in solubility of small gases across the I-N transition. For such purposes, a maximum in the order parameter is required. For further study, it would be interesting to use molecular simulations to investigate (1) the formation of these dimer complexes, and (2) to what extent they influence the orientational order and solubility of small gases in the mixture. To best of our knowledge, no such study is available in literature.

Second, an important aspect to be considered is the stability of the nematic phase compared to other mesophases. Experiments have shown that in binary mixtures of LCs with a chemically similar core but different length of the (semi-)flexible tail, the smectic phase can become stabilized at the cost of the nematic phase if the length ratio of the tails is increased [171, 172, 202]. Since these results could well be an artefact of increased flexibility of the molecules, it would be interesting to test by experiments/molecular simulations if this stabilization of the smectic phase also occurs when only the length ratio of the rigid cores is increased. The LCs used in such a study should be of nematic type. To best of our knowledge, no such study is available in literature. With regard to applying LC solvents as absorption liquids, the formation of smectic phases at the cost of a nematic phase is probably undesirable, since it could limit the possibility of maximizing the solubility difference across the I-N phase transition.

5.4 Conclusion

In summary, we have developed an analytical EoS to describe the isotropic- and nematic phase behaviour of linear- and partially flexible tangent hard-sphere chain fluids and their mixtures. The EoS is based on a Vega-Lago rescaled Onsager theory in the Onsager Trial Function approximation, and can be considered as an extension of our work on pure component systems from Chapter 4. Due to the use of the approximation for the pair-excluded volume from Chapter 2, analytical results for both the Helmholtz energy and compressibility factor were obtained. The orientational averages of the $\sin(\gamma)$- and $\sin^2(\gamma)$-kernel of the pair-excluded volume were approximated analytically using Onsager's truncated asymptotic expansion [9] and a novel approximation derived by the authors, respectively. The resulting analytical theory can be considered as an important step towards an engineering-oriented EoS for nematic fluid mixtures.

The EoS was extensively tested by comparison to molecular simulation data for

the I-N coexistence of various binary mixtures. The EoS was also compared to simulation data for the Henry's law constants of a hard-sphere solute in different linear and partially flexible tangent hard-sphere chain solvents. Overall agreement of the theory to simulation data is excellent. In particular, the fractionation of the long and short component between the I and N phase is predicted very accurately. For the Henry's law constants, we found that the accuracy of the theoretical results deteriorates somewhat with the flexibility of the hard-chain solvent—a result not that surprising given the results obtained in the previous chapter for pure component systems.

From a theoretical point of view, the EoS developed in this chapter was used to study several phenomena. First, we studied the effect of length bidispersity on the I-N and N-N phase behaviour of binary mixtures of linear m-mers. For a bidispersity ratio $q = m_1/m_2$ (where $m_2 \geq m_1$) close to unity, we found an I-N coexistence region at lower pressure and a N-N demixed region bounded by a lower critical point at higher pressure. With decreasing bidispersity ratio (*i.e.* less-like molecules), the N-N critical point is shifted to lower pressure until the N-N and I-N region start to overlap, resulting in a triphase I-N-N equilibrium. If the bidispersity ratio is decreased even further, a re-entrant I→ N→ I→ N phenomenon can be observed at some parts of the phase diagram. It was shown that the coexistence value of the nematic order parameter of a binary mixture displays a maximum with composition. As a result, the density difference between the coexisting I- and N phase also shows a maximum with composition. With decreasing bidispersity ratio, the maximum becomes more pronounced.

Second, the effect of partial molecular flexibility on the I-N and N-N phase behaviour was studied. Compared to linear chains, no topological difference in the phase diagram was found. However, it was shown that due to a less anisotropic pair-excluded volume, the gain in configurational entropy upon N-N demixing was lower than for comparable linear chain fluids, resulting in a smaller driving force for the N-N transition. As a result the N-N demixing transition was shifted to higher density/pressure.

Finally, the solubility of hard-sphere solutes in the isotropic and nematic phase of linear and partially flexible tangent hard-sphere chain solvents was studied. In accordance with the results of a recent MC simulation study [136], it was shown that the transition from an isotropic to a nematic phase leads to a step-wise decrease in the solubility of the hard-sphere solute. The primary reason for this is a step-wise increase in the density of the system at the phase transition; the orientational ordering alone was shown to have negligible effect. The maximum of the I-N density difference with composition that was found for bidisperse mixtures of linear chain fluids, was utilized to maximize the solubility difference of hard-sphere solutes across the I-N phase transition. These results show that the solubility difference of small gases between a coexisting I- and N phase can be maximized by using a LC mixture of specific composition as the solvent. In the light of applying LCs as solvents for absorption processes [23, 24], these results suggest that the direction of research should be directed towards mixtures of LCs.

part B

Equation of state for mesogens with attractive interactions

6

An equation of state for describing the isotropic phase behaviour of attractive chain fluids

In this chapter, we aim at a theoretical description of the isotropic (vapour and liquid) phase behavior of attractive chain fluids. Special emphasis is placed on the role of molecular flexibility, which is studied by means of a rod-coil model. For this purpose, two new perturbed-chain equations of state are developed for square-well- (SW) and Lennard-Jones (LJ) chain fluids. The equations of state are developed in the framework of a second order Barker Henderson (BH) perturbation theory. The novelty of the approach is based on (1) the use of the hard-chain reference EoS from Chapter 3, (2) the use of recent molecular simulation data for the radial distribution function of hard-chain fluids, and (3) a newly developed effective segment size, which effectively accounts for the soft repulsion between segments of LJ chains. It is shown that the effective segment size needs to be temperature-, density-, and chain-length dependent. To obtain a simplified analytical EoS, the perturbation terms are replaced by polynomials in density (SW and LJ), chain length (SW and LJ) and temperature (only for LJ). It is shown that the equations of state result in a satisfactory comparison to molecular simulation data for vapour-liquid equilibria (VLE) and -isotherms of fully flexible SW- and LJ chain fluids and their mixtures. To evaluate the performance of the equations of state in describing the effects of molecular flexibility on VLE, we present new MC simulation results for the VLE of rigid linear SW- and -LJ chain fluids. For SW chains, the developed EoS results in a good agreement with simulation results. For increased rigidity of the chains, both theory and simulations predict an increase of the VL density difference and a slight increase of the VL critical temperature. For LJ chains, the EoS proves incapable of reproducing part of these trends.

Parts of this chapter have been submitted to:
T. van Westen, T.J.H. Vlugt and J. Gross *J. Chem. Phys.* (2015).

6.1 Introduction

Molecular-based equations of state, where molecules are considered as chains of spherical segments have proven powerful for many practical applications [65, 66]. An important step in the development of such equations of state is obtaining an accurate statistical-mechanical description of certain model fluids. Model fluids that were extensively studied, in this respect, are for example hard-sphere chains [59, 60, 121–125, 203, 204], square-well (SW) chains [68, 71, 205–211], Lennard-Jones (LJ) chains [67, 70, 75, 208, 212–215], and more recently, chains interacting with Mie potentials [69, 70]. The theoretical description of these fluids is largely based on Wertheim's Thermodynamic Perturbation Theory (TPT) [59, 60]. Based on properties of a reference system of *unbonded* monomers (*i.e.* the EoS and cavity correlation function), TPT provides the means to calculate the Helmholtz energy for a fluid in which these monomers are connected to form chains [122, 137]. As an example, applying TPT to a reference fluid of SW monomers leads to an EoS for SW-chain fluids.

A well-known artefact of TPT is that, up to first level of approximation (TPT1), it does not distinguish between chains of different flexibility constraints. While early molecular simulation studies on the subject indeed showed large similarities in the isotropic fluid phase behavior of fully flexible and rigid chains [53], it was shown later these conclusion are valid only for a small range in density and if the chains are sufficiently short (<5 segments) [93]. Among others, it has been shown that there are large differences in the virial coefficients of rigid- and flexible chain fluids [88, 93, 118]. Although, to some extent, these large differences seem to cancel each other in the equation of state of the fluids [53, 93], it has recently been shown that the subtle differences that remain [121] need to be captured to arrive at a reliable description of phase equilibria [140, 216]. In the present work, our focus is on the development of an equation of state that can describe the effects of molecular flexibility on vapor-liquid phase equilibria.

Although TPT can be extended to higher order (such as TPT2), where, in principle, the effect of molecular flexibility can be included to some extent, the extension is cumbersome since it requires the specification of higher order correlation functions of the monomeric reference fluid. For attractive chain fluids, which we aim at in this chapter, these correlation functions are largely unavailable. In addition, if the higher correlation functions of the monomeric reference fluid would be available, such as for the case of hard repulsive chain fluids, the application of TPT2 to describe the effects of molecular flexibility would not likely be very successful (Chapter 3 of this thesis).

A different route to the EoS of attractive chain fluids is to treat the bonding of segments at the stage of the repulsive reference fluid. Attractive interactions between the segments of the chains are then treated as a perturbation to this reference fluid. In the present work, we use such a method to develop a perturbed-chain EoS for the isotropic fluid (vapor and liquid) phase of SW- and LJ chains. The effect of attractive interactions between the segments of the chains is treated within the framework of a second order Barker Henderson (BH) perturbation theory [55, 126]. The merit of using a perturbed-chain approach lies in the fact that we are not limited to TPT for

describing the bonding of segments into chains. Instead, we use the LHrc EoS for this (see Chapter 3). Not only is this EoS considerably more accurate than TPT, it also explicitly accounts for the effects of (partial) intramolecular flexibility, and can thus be used to study the effect of chain flexibility on the vapor-liquid equilibrium (VLE).

Although the concept of applying the BH theory to a hard-chain reference fluid is not strictly new (see for example Refs. [71, 72, 217, 218]), a rigorous evaluation of the method by comparison to molecular simulation data of attractive chain fluids with soft repulsion has not yet been provided in literature. In the present work, we show that naively applying the method to the fluid phase of LJ chains leads to unexpected deviations between simulated and calculated VLE and isotherms. In particular, we show that the conventional Barker-Henderson diameter, which serves to model the soft repulsion between LJ segments, is inadequate when applied to a fluid phase of chain molecules. A new effective diameter, which depends on both temperature, chain length, and density is developed. When applied in the perturbation theory, a major improvement in the prediction of VLE and isotherms is observed. Furthermore, we show that the calculation of VLE is very sensitive to any approximations made for describing the radial distribution function (rdf) of the hard-chain reference fluid. As an example, it is demonstrated that Chiew's PY2 approximation [219] for the hard-chain rdf results in an overestimation of the attractive contribution to the EoS, leading to a significant overestimation of vapor-liquid critical points. We show that inaccuracies of this kind can be overcome by the use of molecular simulation data for the rdf [218, 220, 221] .

This chapter is organized as follows. In the following section, we discuss the molecular model underlying the equations of state. After that we present the details of the MC simulations performed. In Section 6.4, we lay out the perturbation theory and develop the new effective segment size for LJ chain fluids. After that, the equations of state are simplified by developing analytical functions for the first and second order perturbation terms. Finally, the equations of state are extended to mixtures. In Section 6.5, computed VLE, vapor pressure curves and isotherms are compared to molecular simulation results obtained in this work and from literature. Our findings are summarized in Section 6.6.

6.2 Molecular model and intermolecular potentials

As in previous chapters, a molecule is assumed as a homo-segmented chain of m segments. Molecular flexibility is introduced by the rod-coil model laid out in Section 2.2 of this thesis. Both a SW- and LJ 12-6 potential are evaluated to model dispersive intermolecular interactions between the segments of chains. The interaction energy between two segments, both separated by a radial distance r, is thus calculated as

$$u^{\mathrm{SW}}(r) = \begin{cases} \infty & \text{for } r < \sigma \\ -\epsilon & \text{for } \sigma \leq r \leq \lambda\sigma \\ 0 & \text{for } r > \lambda\sigma \end{cases} \tag{6.1}$$

or

$$u^{\mathrm{LJ}}(r) = 4\epsilon \left[\left(\frac{\sigma}{r}\right)^{12} - \left(\frac{\sigma}{r}\right)^{6} \right] \tag{6.2}$$

Here, ϵ and σ are the depth of the potential well and the segment size parameter, respectively. For interactions between chains of different type, these are calculated from the usual Lorentz-Berthelot combining rules, according to [222, 223]

$$\sigma_{ij} = \frac{\sigma_{ii} + \sigma_{jj}}{2} \tag{6.3}$$

$$\epsilon_{ij} = \sqrt{\epsilon_{ii}\epsilon_{jj}} \tag{6.4}$$

where σ_{ii} and ϵ_{ii} are the potential parameters of a chain of type i. For pure component systems, these subscripts will be dropped. For the SW potential, the range of the attractive interactions is set to $\lambda = 1.5$.

6.3 Simulation details

Molecular simulations were conducted as Monte Carlo simulations in the grand-canonical ensemble (GCMC), *i.e.* for a defined chemical potential μ, temperature and volume. We performed simulations for the VLE as well as for pure-component isotherms. The molecule number N is a fluctuating quantity in GCMC simulations. For both types of simulations we divided the N-space into windows of $\Delta N = 10$ and performed an individual GCMC simulation for each window [224, 225]. Any trial move for inserting or deleting molecules beyond the dedicated interval ΔN, is trivially rejected. For an efficient and even sampling of the histogram $p(N)$ within each window, we applied a transition matrix (TM) sampling scheme and applied a TM bias function [226]. For windows of higher molecule numbers, corresponding to liquid-like densities, we applied a configurational-bias scheme [129, 130] for improved statistics of molecule insertions, deletions, and reconfigurations. The volume of the system was set to $V = 2000\sigma^3$. The LJ interactions were calculated for segments belonging to different chains and for segments within the same chain separated by two or more bonds. All interactions were truncated at 4σ. Standard long-ranged tail corrections were applied [116].

GCMC simulations require the definition of chemical potentials. For isotherms we obtained the chemical potentials for each window in N-space from the EoS proposed in this work. The isotherms were then calculated similar to the procedure described by Shen and Errington [225]. Properties along an isotherm, such as pressure and chemical potential, are determined from histogram reweighting techniques in a post-processing step. We determined the equilibrium chemical potential for any defined molecule number $N(\mu, V, T) = \langle N \rangle$, by summing over the probability distribution $\langle N \rangle = \sum_{i=1}^{N_{\max}} p(i) \cdot i$. In doing so, our results much improved for the low density range compared to the procedure in Ref. [225].

Phase equilibria were calculated using a similar approach as for the calculation of isotherms, except that both, the chemical potential μ and the temperature of the windows in N-space were estimated from the EoS described here. The values of μ and T are determined to approximately trace the vapor-liquid phase envelope.

Histogram reweighting then allows the calculation of the actual phase equilibrium properties in a post processing step. The critical point is determined by applying a mixed field scaling approach [227, 228], without performing a finite size scaling extrapolation [229]. Insofar we here report apparent critical points, that carry some system size dependence. For a more detailed description of the simulation procedure we refer to Ref. [230].

6.4 Equation of state

To develop the EoS, we apply a perturbation theory [54]. In doing this, it is assumed that the radial distribution function (rdf) [54] of a fluid is primarily determined by interactions between repulsive molecular cores. Following from this argument, one can write the Helmholtz energy of a system of N molecules at absolute temperature T as a sum of a repulsive reference contribution (A_0) and an attractive perturbation contribution (A^{pert}), according to

$$\frac{A}{VkT} = a = a_0 + a^{\text{pert}} \tag{6.5}$$

Here, k is Boltzmann's constant and $a = A/VkT$ is a reduced Helmholtz energy density.

Different methods have been proposed to split the intermolecular potential into a repulsive and an attractive part [54, 55, 126, 127, 231]. In the present work, we use the method as originally proposed by Barker and Henderson (BH) [55, 126]. We thus obtain

$$u_0(r) = \begin{cases} u(r) & \text{for } r < \sigma \\ 0 & \text{for } r \geq \sigma \end{cases} \tag{6.6}$$

$$u^{\text{pert}}(r) = \begin{cases} 0 & \text{for } r < \sigma \\ u(r) & \text{for } r \geq \sigma \end{cases} \tag{6.7}$$

For LJ fluids, it is common to map the properties of the soft-repulsive reference fluid as defined by Eq. (6.6) to those of a hard-repulsive reference fluid by using an 'effective' temperature-dependent segment diameter $d(T)$. The use of such an effective hard-sphere segment diameter is convenient since the properties of hard repulsive fluids are generally more readily obtained from theoretical methods than those of soft repulsive fluids. In the original BH theory, which was developed for spherical molecules, the effective segment diameter d^{BH} was calculated from the following integral [54, 55]

$$d^{\text{BH}}(T) = \int_0^{\sigma} \left(1 - \exp\left(-\frac{u(r)}{kT}\right)\right) \mathrm{d}r \tag{6.8}$$

In the present work we show that, when applied to chain fluids, the segment size resulting from this equation is too small. As a result, when used in the perturbation theory, computed VLE and isotherms are of poor quality. In Section 6.4.3, we develop a simple expression for the effective segment diameter of chain fluids.

6.4.1. Reference fluid

The EoS of the hard-chain reference fluid is calculated from the sum of an ideal (id), a hard-sphere (hs) and a hard-chain (hc) contribution, according to

$$a_0 = a^{\mathrm{id}} + a^{\mathrm{hs}} + a^{\mathrm{hc}} \tag{6.9}$$

For a canonical, N_C-component mixture, the ideal contribution to the reduced Helmholtz energy density is obtained from

$$a^{\mathrm{id}} = \sum_i^{N_C} \rho_i \left[\ln\left(\rho_i \Lambda_i^3\right) - 1\right] \tag{6.10}$$

where $\rho_i = N_i/V$ is the number density of molecules of component i and Λ_i is a thermal de Broglie wavelength.

Since we will consider both, mixtures of chains with equally- and non-equally sized segments, the hard-sphere contribution is obtained from the expression of Boublík [232] and Mansoori *et al.* [233], according to

$$a^{\mathrm{hs}} = \rho_s \frac{1}{\zeta_0}\left[\left(\frac{\zeta_2^3}{\zeta_3^2} - \zeta_0\right)\ln(1-\zeta_3) + \frac{3\zeta_1\zeta_2}{1-\zeta_3} + \frac{\zeta_2^3}{\zeta_3(1-\zeta_3)^2}\right] \tag{6.11}$$

where $\rho_s = \sum_i m_i\rho_i$ is the total segment density of the system and the quantity $\zeta_n = (\pi/6)\sum_i \rho_i m_i d_{ii}^n$. Please note that $\zeta_3 = \eta$, where η is the packing fraction of the system.

To calculate the hard-chain contribution, the LHrc EoS (Chapter 3) is used. The hard-chain contribution is thus calculated as

$$a^{\mathrm{hc}} = -\sum_i^{N_C} \rho_i(m_i - 1)\ln y_{(i),j,j+1} - \sum_i^{N_C} \rho_i(m_i - 2)\ln y_{(i),j,j+2} \tag{6.12}$$

where the cavity correlation function of the nearest- $(j, j+1)$ and next-to-nearest $(j, j+2)$ neighbouring segments in a chain of type i are calculated as, respectively

$$\begin{aligned}\ln y_{(i),j,j+1} = {} & \frac{(3 - a_2 + b_2 - 3c_2)\eta - (1 - a_2 - b_2 + c_2)}{2(1-\eta)} \\ & + \frac{1 - a_2 - b_2 + c_2}{2(1-\eta)^2} - (c_2 + 1)\ln(1-\eta)\end{aligned} \tag{6.13}$$

$$\begin{aligned}\ln y_{(i),j,j+2} = {} & \frac{m_i - 1}{m_i}\left[\frac{(-a_{3,i} + b_{3,i} - 3c_{3,i})\eta - (-a_{3,i} - b_{3,i} + c_{3,i})}{2(1-\eta)}\right. \\ & \left. + \frac{-a_{3,i} - b_{3,i} + c_{3,i}}{2(1-\eta)^2} - c_{3,i}\ln(1-\eta)\right]\end{aligned} \tag{6.14}$$

with $a_2 = 0.45696;\ b_2 = 2.10386;\ c_2 = 1.75503$ and

$$a_{3,i} = p(1) + p(2)\chi_{\mathrm{R},i} + p(3)\chi_{\mathrm{R},i}^2 + p(4)\chi_{\mathrm{R},i}^3 \tag{6.15}$$

$$b_{3,i} = 3.49695 - 3.81467\chi_{\mathrm{R},i} \tag{6.16}$$

$$c_{3,i} = 4.83207 - 1.35191\chi_{\mathrm{R},i} \tag{6.17}$$

$$\boldsymbol{p} = (-0.74745,\ 0.29915,\ 1.08727,\ -0.70898) \tag{6.18}$$

The rigidity parameter $\chi_{\mathrm{R,i}}$ of a component i was defined in Eq. (2.1).

6.4.2. Contribution due to attractive perturbation

To start, let us assume a pure component system of N chain molecules at a temperature T. In the framework of a second order BH theory, the contribution to the Helmholtz energy due to dispersive intermolecular attractions can then be written as a sum of a first and second order term, according to

$$a^{\text{pert}} = a_1 + a_2 \tag{6.19}$$

Following Barker and Henderson, we treat the first order term exactly, while the second order term is calculated based on the local compressibility approximation [126] (LCA). For simplicity, the density derivatives associated with the LCA are calculated for a constant segment size d. Although this introduces some approximation (since d as developed later in this chapter includes a density dependence), we verified the effect is negligible compared to a 'correct' application of the LCA. For pure-component systems, we obtain

$$a_1 = \frac{2\pi\rho^2}{kT} \sum_{\alpha=1}^{m} \sum_{\beta=1}^{m} \int_{\sigma}^{\infty} u(r) g_{\alpha\beta}^{\text{hc}}(r) r^2 dr \tag{6.20}$$

$$a_2 = -\frac{\pi\rho^2}{(kT)^2} m K_0 \frac{\partial}{\partial\rho} \left(\rho \sum_{\alpha=1}^{m} \sum_{\beta=1}^{m} \int_{\sigma}^{\infty} u^2(r) g_{\alpha\beta}^{\text{hc}}(r) r^2 dr \right)_d \tag{6.21}$$

Here we have introduced the segment-segment radial distribution function (rdf) of the hard-chain reference fluid, $g_{\alpha\beta}^{\text{hc}}(r, m, \chi_{\text{R}}, \eta)$, which is a measure for the probability to find a segment α of chain 1 at a radial distance r from a segment β of chain 2, averaged over the positions of all other segments in the system. In the remainder, only the r-dependence of the rdf will be written explicitly. The isothermal compressibility of the hard-chain reference system $K_0 = kT\,(\partial\rho/\partial P_0)_T$ enters the equation for a_2 due to the use of the LCA. K_0 is obtained from the compressibility factor of the hard-chain reference system $Z_0 = P_0/\rho kT$, as

$$K_0 = \left(Z_0 + \rho \left(\frac{\partial Z_0}{\partial\rho} \right)_d \right)^{-1} \tag{6.22}$$

where Z_0 is calculated using the simplified version of the LHrc EoS from Eq. (3.8). For mixtures of chains with unequally-sized segments, the use of the simplified LHrc EoS to calculate K_0 introduces some approximation since Eq. (3.8) implicitly assumes the Carnahan-Starling equation for the hard-sphere contribution. We verified that the effect of this approximation is negligible.

To proceed, it is convenient to introduce an averaged rdf, according to [219]

$$g^{\text{hc}}(r) = \frac{1}{m^2} \sum_{\alpha=1}^{m} \sum_{\beta=1}^{m} g_{\alpha\beta}^{\text{hc}}(r) \tag{6.23}$$

Due to the averaging, all segments in a chain are now indistinguishable. The use of an averaged rdf introduces no approximation. Upon introducing a reduced radial

distance $x = r/\sigma$ and potential energy $\tilde{u}(x) = u(x\sigma)/\epsilon$, the perturbation contributions can be recast in the following dimensionless form

$$a_1 = 2\pi\rho^2 m^2 \frac{\epsilon}{kT}\sigma^3 I_1 \tag{6.24}$$

$$a_2 = -\pi\rho^2 m K_0 m^2 \left(\frac{\epsilon}{kT}\right)^2 \sigma^3 \frac{\partial}{\partial\rho}\left(\rho I_2\right)_d \tag{6.25}$$

Here we have introduced the abbreviations I_1 and I_2 for the correlation integrals. For SW chain fluids, these are obtained from the following equations

$$I_1^{\mathrm{SW}}(m, \chi_{\mathrm{R}}, \eta) = -\int_1^{\lambda} g^{\mathrm{hc}}(x\sigma)\, x^2 dx \tag{6.26}$$

$$I_2^{\mathrm{SW}}(m, \chi_{\mathrm{R}}, \eta) = -I_1^{\mathrm{SW}}(m, \chi_{\mathrm{R}}, \eta) \tag{6.27}$$

For LJ chain fluids, the rdf is calculated for an effective hard-chain reference fluid of segment size d. As a result, the correlation integrals become temperature dependent:

$$I_1(m, \chi_{\mathrm{R}}, \eta, T) = \int_1^{\infty} \tilde{u}(x) g_d^{\mathrm{hc}}(x\sigma)\, x^2 dx \tag{6.28}$$

$$I_2(m, \chi_{\mathrm{R}}, \eta, T) = \int_1^{\infty} \tilde{u}^2(x) g_d^{\mathrm{hc}}(x\sigma)\, x^2 dx \tag{6.29}$$

We should note that in the application of the above two equations, a subtle point arises. In a correct application of the concept of an effective segment size to attractive chain fluids, the bond distance between neighbouring segments in a chain molecule should be σ. Therefore, a suitable rdf of the reference fluid would be for a fluid of hard segment diameter d and bond distance σ. Applying a rdf for chains of tangent hard spheres of diameter d and bond distance d, constitutes an approximation. Although this is a commonly employed approximation [68, 69, 73], its effect on calculated thermodynamic properties is difficult to assess *a priori*.

Let us now consider the calculation of the rdf of the hard-chain reference fluid. Although the rdf will clearly have some dependence on the degree of flexibility (χ_{R}) of the chains, we will neglect this dependence and assume the rdf of a fully flexible chain fluid can be used. This approximation seems reasonable, since the effect of intramolecular flexibility is already considered explicitly in the reference contribution to the EoS. Moreover, the approximation is convenient since the rdf of fully flexible tangent hard-sphere chain fluids can be obtained accurately from recently published MC data [218]. In a previous study [71], the rdf was obtained from an integral equation theory of Chiew, which was based on a Percus-Yevick closure (PY2) [219]. We found that (for $m > 2$) this approximate rdf leads to systematically too high values when compared to MC simulations. To illustrate the approximation that comes with the PY2 approach, we calculated the VLE of fully flexible SW- and LJ 8-mers from the 2nd order perturbation theory detailed above, using both the rdf obtained from MC simulations and the PY2 theory. The calculations for the LJ chain fluid are based on the original BH diameter from Eq. (6.8). In Fig. 6.1, the results are compared to MC simulation results of Escobedo and de Pablo [208].

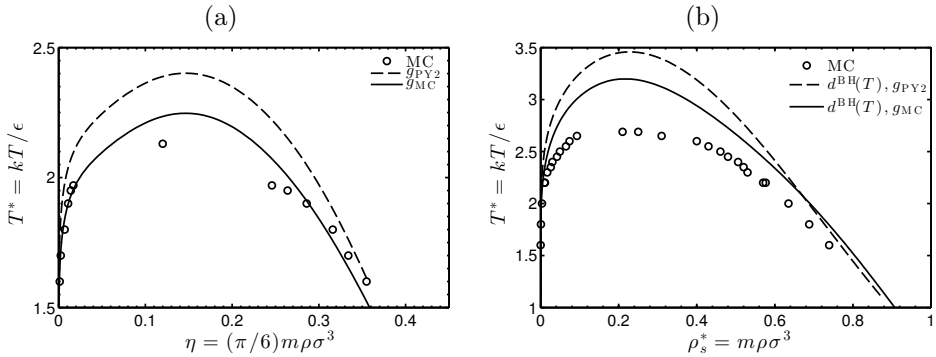

Figure 6.1: The VLE of (a) a fully flexible SW 8-mer fluid, and (b) a fully flexible LJ 8-mer fluid, as obtained from MC simulations [208] (symbols) and a second order Barker-Henderson perturbation theory. Theoretical results are obtained using (1) the Barker-Henderson diameter ($d_{\rm BH}(T)$, Eq. (6.8)) and rdf from the PY2 theory [219] ($g_{\rm PY2}$) as input (dashed line), and (2) the Barker-Henderson diameter and rdf from MC simulations [218] ($g_{\rm MC}$) as input (solid line). The results in this figure show that the incorporation of MC data for the rdf in the calculation of the correlation integrals improves the description of VLE. Furthermore, the results suggest that the original Barker-Henderson diameter calculated from Eq. (6.8) underestimates the effective segment size of the segments in LJ chain fluids.

Due to the overestimation of the rdf, the perturbation terms a_1 and a_2 calculated from the PY2 theory are too negative, leading to a large overestimation of the VL critical temperature and a poor prediction of vapour-liquid coexistence densities. The VLE calculated using MC data for the rdf is clearly in better agreement with the simulated phase envelope. For the SW 8-mer, good agreement with simulation data is obtained. For the LJ 8-mer, however, a significant discrepancy with the VLE as obtained from MC simulations remains. Although a perturbation theory truncated at second order will always result in an overestimation of the VL critical temperature (because density fluctuations characterizing the critical point are only partly described), the overestimation of saturated liquid densities is too pronounced to be attributed to the truncation of the perturbation expansion. Given the high accuracy of the hard-chain reference EoS [128], the reason for the discrepancy must be sought in the perturbation terms or in the link between the hard- and soft repulsive reference system. As the possible sources of error, we therefore identity (1) the LCA approximation used for the 2nd order perturbation term, or (2) the use of the original BH diameter to describe the soft repulsion of LJ chain fluids. As the LCA approximation is known to lead to an underestimation of liquid densities at the low-temperature part of the VLE [234], the overestimation of liquid densities that is observed in Fig. 6.1 (b) must be caused by the use of the BH diameter. In fact, given the large overestimation of the critical temperature, the effective segment size must be underestimated.

6.4.3. New effective segment diameter for LJ chain fluids

The effective segment size should allow a mapping of the properties of a soft repulsive fluid onto those of a hard repulsive fluid. For the original BH diameter from Eq. (6.8), such a mapping was obtained from a scheme in which the Helmholtz energy of a system of soft repulsive spheres (with intermolecular potential defined by Eq. (6.6)) is expanded about the Mayer-f function of a hard-sphere reference system [54]. In this scheme, the BH diameter follows from forcing the first order term in the expansion to zero. Although, in principle, the resulting effective segment size should depend on both temperature and density [54], the density dependence is minor for typical fluid densities of spherical fluids and was therefore not included in the original BH diameter [55].

Evidently, to develop an effective segment size for LJ *chain* fluids, one should find a way to relate a fluid of soft *chains* to that of hard *chains*. In principle, one could opt to establish such a relation by extending the above discussed expansion method to chain fluids. In the present work, however, we take a different approach by directly including simulation data in the development. To start, we consider the low-density limit, for which the effective segment size can be obtained from equating second virial coefficients:

$$B_2^{\mathrm{sc}}(T^*, m, \sigma) = B_2^{\mathrm{hc}}(m, d(T^*, m, \rho_s^* = 0)) \tag{6.30}$$

Here, we have introduced the dimensionless temperature $T^* = kT/\epsilon$ and the shorthand notation 'sc' for 'soft chain'. It is important to note that, unlike the Helmholtz energy contributions in Eq. (6.9), the superscripts 'sc' and 'hc' are here meant as total contributions. For example, B_2^{hc} is the total second virial coefficient of a fluid of hard chains, which includes a hard-sphere contribution and a contribution due to chain formation.

Using a MC integration method (see Chapter 2 for details), we calculated second virial coefficients of hard chains of length m ={1 2 3 5 8 16} and σ = {0.8 0.85 0.9 0.95 0.98 1.0}. For each chain length, a power law in σ was fitted to the results. Next, we calculated second virial coefficients of soft chain fluids of the same chain lengths m at dimensionless temperatures T^* ={0.7 1.0 1.5 2.0 3.0 5.0 7.0 10.0 15.0 20.0}. For each temperature we solved Eq. (6.30) for $d(T^*, m, \rho_s^* = 0)$, the results of which are compared to the original BH diameter in Fig. 6.2. As expected, the results suggest that the effective diameter of the segments in a LJ chain are larger than those of unbonded LJ spheres. For long chains the diameter seems to approach an asymptotic value.

Given that, for $\rho_s^* < 1$, the original BH diameter $d^{\mathrm{BH}}(T^*)$ is known to give an accurate representation of the soft repulsion of LJ spheres [54, 235], the close agreement to our computed $d(T^*, m = 1, \rho_s^* = 0)$ could suggest $d(T^*, m, \rho_s^* = 0)$ is also a good representation of the effective segment size of LJ chains. Unfortunately, this is not the case. Using the GCMC method from Section 6.3, we calculated isothermal pressures of soft chain fluids of length m={1 2 3 4} in the range ρ_s^* =0-1.0 and T^* = 2-20. For tabulated simulation results, the reader is referred to the Supporting Material of Ref. [236]. We compared simulation results to those obtained from the LHrc EoS for the hard-chain reference fluid, calculated using either the

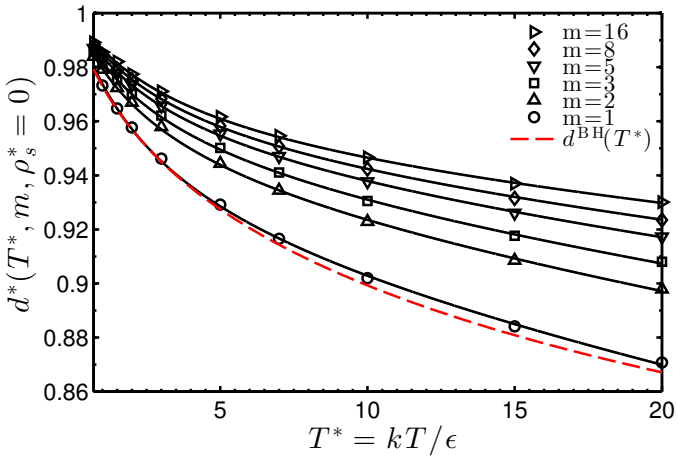

Figure 6.2: The chain-length- and temperature dependence of the low-density limit of the reduced effective segment diameter $d^*(T^*, m, \rho_s^* = 0) = d(T^*, m, \rho_s^* = 0)/\sigma$ of LJ chain fluids. The symbols are obtained from equating second virial coefficients of hard- and soft-chain fluids (see Section 6.4.3 for details); the lines are correlation results from Eq. (6.31). Results for the original Barker-Henderson diameter (Eq. (6.8)) are also included for comparison (dashed line).

original BH diameter $d^{\mathrm{BH}}(T^*)$ or $d(T^*, m, \rho_s^* = 0)$ for the effective segment size, respectively. For all analysed systems, the results show indeed that the use of $d(T^*, m, \rho_s^* = 0)$ leads to a better description of the low-density regime. For larger densities, however, a significant overestimation of simulated pressures is observed. We verified that, for the chain lengths considered here, the hard-chain reference EoS is accurate to within statistical uncertainty of molecular simulations [132, 237]; therefore, we conclude that the observed deviations are due to inaccuracies in the effective segment size. The effective segment size of LJ chain fluids thus needs to be density dependent.

To obtain a closed analytical function for $d(T^*, m, \rho_s^*)$, we adapt a functional form with a temperature dependence as proposed by Cotterman, Schwartz and Prausnitz [238], as

$$\frac{d(T^*, m, \rho_s^*)}{\sigma} = \frac{1 + A(m, \rho_s^*)T^*}{1 + B(m, \rho_s^*)T^* + C(m, \rho_s^*)T^{*2}} \tag{6.31}$$

For the chain-length dependence of the coefficients A, B and C, a functional form as proposed by Hu, Liu and Prausnitz [125] is used:

$$A(m, \rho_s^*) = A_0(\rho_s^*) + A_1(\rho_s^*)\frac{m-1}{m} + A_2(\rho_s^*)\frac{m-1}{m}\frac{m-2}{m} \tag{6.32}$$

$$B(m, \rho_s^*) = B_0(\rho_s^*) + B_1(\rho_s^*)\frac{m-1}{m} + B_2(\rho_s^*)\frac{m-1}{m}\frac{m-2}{m} \tag{6.33}$$

$$C(m, \rho_s^*) = C_0(\rho_s^*) + C_1(\rho_s^*)\frac{m-1}{m} + C_2(\rho_s^*)\frac{m-1}{m}\frac{m-2}{m} \tag{6.34}$$

This chain length dependence distinguishes between nearest- and next-nearest neighbor effects in chain molecules. Moreover, it is capable of reproducing the asymptotic

Table 6.1: The model constants needed to calculate the effective segment size from Eqs. (6.31)-(6.35).

i	0	1	2
α_{0i}	0.30798	0.0051388	0.011117
α_{1i}	0.012390	0.011109	−0.039209
α_{2i}	−0.089339	−0.030677	0.016732
β_{0i}	0.34222	0.033920	−0.016202
β_{1i}	−0.0024993	−0.044614	0.022757
β_{2i}	−0.093741	0.017545	−0.033500
γ_{0i}	0.00096376	0.00037270	0.000083571
γ_{1i}	−0.00043261	−0.00044912	−0.00031474
γ_{2i}	−0.00033133	−0.000041420	0.00044615

behaviour as observed in Fig. 6.2. Regarding the density dependence of the coefficients, a simple quadratic proved to be sufficient:

$$\begin{aligned} A_0(\rho_s^*) &= \alpha_{00} + \alpha_{01}\rho_s^* + \alpha_{02}\rho_s^{*2} \\ A_1(\rho_s^*) &= \alpha_{10} + \alpha_{11}\rho_s^* + \alpha_{22}\rho_s^{*2} \\ &\dots \\ B_0(\rho_s^*) &= \beta_{00} + \beta_{01}\rho_s^* + \beta_{02}\rho_s^{*2} \\ &\dots \\ C_2(\rho_s^*) &= \gamma_{20} + \gamma_{21}\rho_s^* + \gamma_{22}\rho_s^{*2} \end{aligned} \tag{6.35}$$

The model constant α_{i0}, β_{i0}, and γ_{i0} with $i = \{0\ 1\ 2\}$ govern the low-density limit; accordingly, these were correlated to the data for $d(T^*, m, \rho_s^* = 0)$ as obtained from Eq. (6.30). As can be observed in Fig. 6.2, the correlation is excellent. To obtain the remaining model constants, we assumed the LHrc EoS for the reference fluid, and correlated our MC simulation results for the isothermal pressure of soft-chain fluids of length $m = \{1\ 2\ 3\ 4\}$ at various temperatures T^* (see Supporting Material of Ref. [236] for MC data). A very good regression result is obtained, with an average percentage relative deviation per data-point of 0.32% (compared to a deviation of 4.06% if no ρ_s^*-dependence is included). To validate the use of Eq. (6.31) for chain lengths larger than included in the parameter regression, we calculated the isothermal pressure and chemical potential of soft 8-mer fluids for various T^* from GCMC simulations. In Fig. 6.3, we compare simulations to theory. Excellent agreement is obtained, suggesting the chain-length dependence is well correlated. Furthermore, Fig. 6.4 shows that the use of the LHrc EoS for the hard-chain reference fluid in combination with the effective segment size from Eq. (6.31) results in a very good prediction of second virial coefficients. The model constants needed to calculate $d(T^*, m, \rho_s^*)$ from Eq. (6.31) are listed in Table 6.1.

It is important to note that the use of the LHrc EoS in obtaining part of the model constants of Eq. (6.35) does not limit the application of Eqs. (6.31)-(6.35) to this hard-chain reference EoS only. For the chain lengths ($m = \{1\ 2\ 3\ 4\}$) and densities involved in the fitting, the LHrc EoS is as accurate as molecular simulations results; therefore the effective segment size calculated from Eq. (6.31) can be considered general, and can be used in combination with any hard-chain reference EoS.

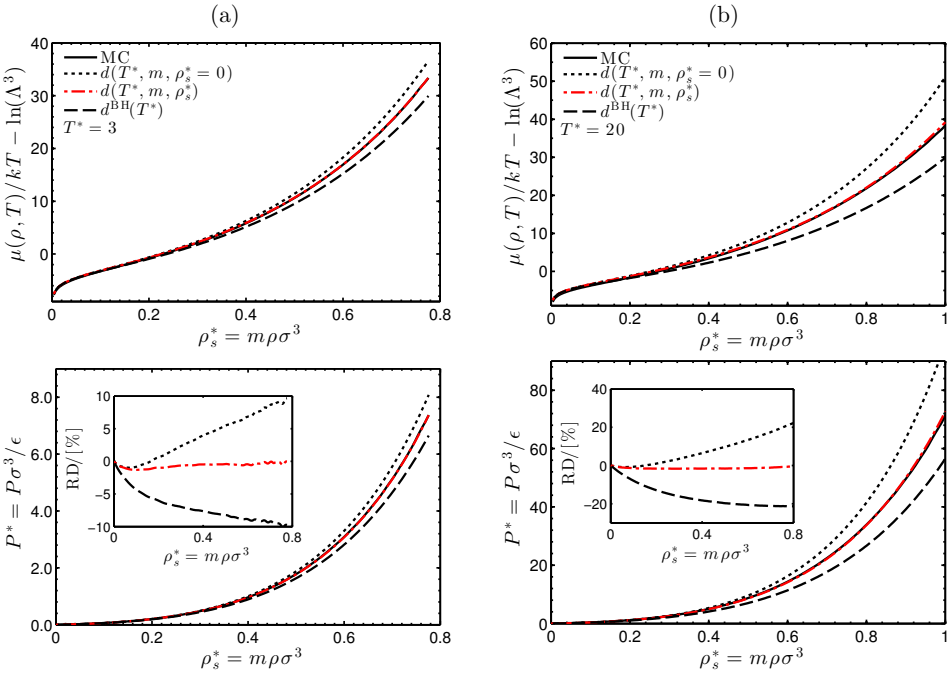

Figure 6.3: Isothermal pressure and density-dependent part of the chemical potential of a soft BH repulsive 8-mer at (a) $T^* = 3$, and (b) $T^* = 20$, as obtained from MC simulations and theory. Theoretical results are obtained from the LHrc EoS, using the newly developed effective segment from Eq. (6.31) (red, dashed-dotted lines), its low density limit (dotted lines), and the Barker-Henderson diameter (dashed lines), respectively. The figure in the inset shows the percentage relative deviation (RD) of the theoretical results to simulation data. Simulation data is provided in tabular form in the Supplementary Material of Ref. [236].

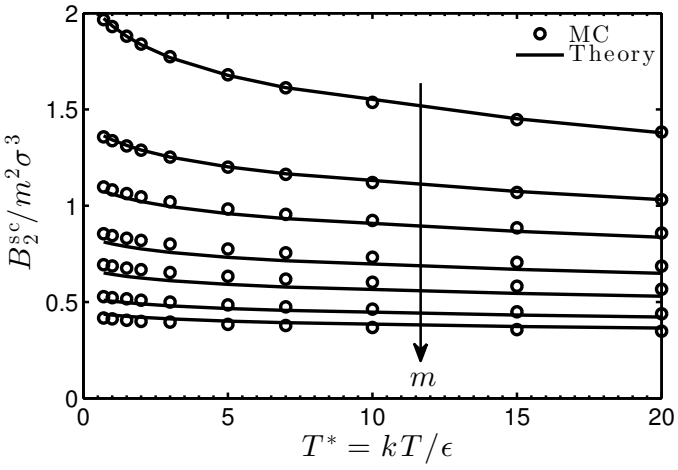

Figure 6.4: The reduced second virial coefficient of soft chain fluids $B_2^{*\mathrm{sc}} = B_2^{\mathrm{sc}}/m^2\sigma^3$ of chain length $m = \{1\ 2\ 3\ 5\ 8\ 16\ 32\}$, as obtained from the LHrc EoS in combination with the effective segment size $d^*(T^*, m, \rho_s^*)$ from Eq. (6.31). Theoretical results (lines) are compared to results obtained from a MC integration method (symbols). For details on the MC method, the reader is referred to Chapter 2 of this thesis.

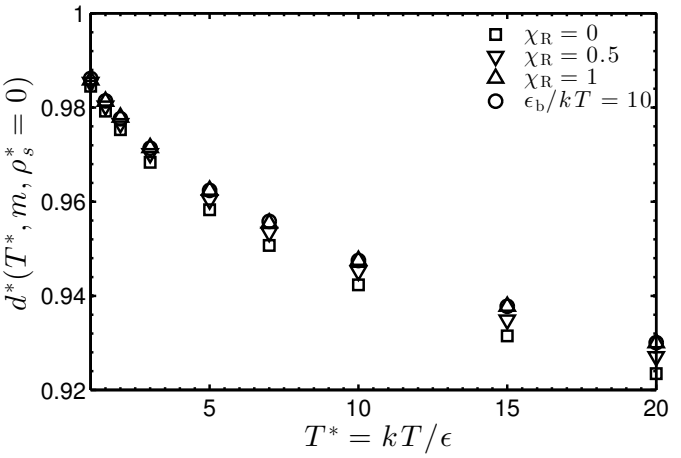

Figure 6.5: The effect of intramolecular flexibility on the low-density limit of the reduced effective segment diameter $d^*(T^*, m, \rho_s^* = 0) = d(T^*, m, \rho_s^* = 0)/\sigma$. Results are shown for linear ($\chi_R = 1$), partially flexible ($\chi_R = 0.5$), fully flexible ($\chi_R = 0$) and semi-flexible ($U_b = \epsilon_b(\theta - \pi)^2$, $\epsilon_b = 10$) chain fluids of length 8. The results are obtained from equating second virial coefficients of hard- and soft-chain fluids (see Section 6.4.3 for details).

Table 6.2: Model constants needed to calculate the coefficients a_i^{SW} (Eq. (6.40)) for calculating the first correlation integral $I_1^{SW}(\eta, m)$ (Eq. (6.36)) of SW chain fluids. The coefficients b_i^{SW} (Eq. (6.41)) needed to calculate the second correlation integral $I_2^{SW}(\eta, m)$ (Eq. (6.37)) are obtained from the exact relation $b_i^{SW} = (i+1)a_i^{SW}$.

i	a_{i0}^{SW}	a_{i1}^{SW}	a_{i2}^{SW}
0	0.79049	-0.59512	-0.15824
1	1.1232	0.49131	-0.10393
2	0.076584	0.88750	0.53747
3	-1.4019	-0.035067	-0.020518
4	-1.9080	-0.72597	-0.51281

To quantify the effect of chain flexibility on the effective segment size, we used the second virial method from Eq. (6.30) to calculate the low-density limit $d(T^*, m, \rho_s^* = 0)$ for linear ($\chi_R = 1.0$), partially flexible ($\chi_R = 0.5$) and semi-flexible (with harmonic bond-bending potential $u_b = \epsilon_b(\theta - \pi)^2$ and $\epsilon_b = 10$) chains of length 8. In Fig. 6.5, we compare the results to those previously calculated for fully flexible ($\chi_R = 0$) 8-mers. The differences are small. While, in principle, the correlation for $d(T^*, m, \rho_s^*)$ from Eq. (6.31) is strictly developed for fully flexible chain fluids, these results suggest it could also provide a reasonable approximation for the effective segment size of chains of different flexibility constraints.

In summary, we propose an accurate EoS for BH-repulsive chain fluids (Eqs. (6.9)-(6.17) and (6.31)), that serves as a reference for the development of an EoS for LJ chains with variable degree of molecular flexibility.

6.4.4. Simplified perturbation terms

It is now our target to obtain simple analytical functions for the correlation integrals from Eqs. (6.28)-(6.29). Since the description of SW chain fluids does not involve the use of any effective segment size, the correlation integrals of SW-chains depend on chain length m and packing fraction η only. For LJ chain fluids, an additional temperature dependence exists.

Using tabulated MC data for the average segment-segment rdf of the hard-chain reference system, taken from Refs. [221] ($m = 1$), [220] ($m = \{2\ 8\}$), and [218]

(m ={3 4 5 6 7 8}), respectively, we calculated the correlation integrals over a range in packing fraction η={0-0.5} (the exact range depending on the MC data for rdf), and dimensionless temperature T^*={0.6 0.8 1.0 1.2 1.4 1.6 1.8 2.0 2.2 2.4 2.8 3.4 3.8 4.2 5 6 8 10 15 20} (only for LJ). In the calculations for LJ chain fluids, the effective segment size was obtained from Eq. (6.31). Moreover, for LJ chain fluids we included additional data for I_2 of a chain molecule of $m = 100000$ at a packing fraction $\eta = 10^{-7}$ in the fitting. The values of I_2 for this case were set to 40% of the PY2 result. The reason for doing this is to avoid non-physical negative values of I_2 for very long ($m > 100$) chain fluids. For both SW and LJ chain fluids, the results were correlated by the following power law in packing fraction

$$I_1^{\mathrm{SW}}(m,\eta) = \sum_{i=0}^{4} a_i^{\mathrm{SW}}(m)\eta^i \tag{6.36}$$

$$I_2^{\mathrm{SW}}(m,\eta) = \sum_{i=0}^{4} b_i^{\mathrm{SW}}(m)\eta^i \tag{6.37}$$

$$I_1^{\mathrm{LJ}}(m,\eta,T^*) = \sum_{i=0}^{4} a_i^{\mathrm{LJ}}(m,T^*)\eta^i \tag{6.38}$$

$$I_2^{\mathrm{LJ}}(m,\eta,T^*) = \sum_{i=0}^{4} b_i^{\mathrm{LJ}}(m,T^*)\eta^i \tag{6.39}$$

where the chain-length dependence of the coefficients a_i and b_i is again obtained from the functional form of Hu, Liu and Prausnitz [125, 128]

$$a_i^{\mathrm{SW}}(m) = a_{io}^{\mathrm{SW}} + a_{i1}^{\mathrm{SW}}\frac{m-1}{m} + a_{i2}^{\mathrm{SW}}\frac{m-1}{m}\frac{m-2}{m} \tag{6.40}$$

$$b_i^{\mathrm{SW}}(m) = b_{io}^{\mathrm{SW}} + b_{i1}^{\mathrm{SW}}\frac{m-1}{m} + b_{i2}^{\mathrm{SW}}\frac{m-1}{m}\frac{m-2}{m} \tag{6.41}$$

$$a_i^{\mathrm{LJ}}(m,T^*) = a_{io}^{\mathrm{LJ}}(T^*) + a_{i1}^{\mathrm{LJ}}(T^*)\frac{m-1}{m} + a_{i2}^{\mathrm{LJ}}(T^*)\frac{m-1}{m}\frac{m-2}{m} \tag{6.42}$$

$$b_i^{\mathrm{LJ}}(m,T^*) = b_{io}^{\mathrm{LJ}}(T^*) + b_{i1}^{\mathrm{LJ}}(T^*)\frac{m-1}{m} + b_{i2}^{\mathrm{LJ}}(T^*)\frac{m-1}{m}\frac{m-2}{m} \tag{6.43}$$

For SW chains, a total of 15 adjustable model constants was used for the fitting (see Table 6.2). For LJ chain fluids, the additional temperature dependence resulted in a total of 31 adjustable model constants. Both the temperature dependence and the model constants are displayed in Table 6.3. As can be observed in Fig. 6.6, the regression result is excellent, with an average relative deviation per data point of 0.3% for I_1^{LJ} and 0.5% for I_2^{LJ}. For SW chain fluids, the results are of similar accuracy. For brevity, the results for I_2 are not included in the Figures. An interesting observation is the decreased temperature dependence of the correlation integrals for longer chain lengths. Intuitively, this result seems correct as for longer chains the shielding of a segment by the other segments in a chain becomes more pronounced, leading to a smaller contribution of the soft intermolecular repulsion to the interactions between molecules.

Table 6.3: Temperature dependence and model constants needed to calculate the coefficients a_i^{LJ}† (Eq. (6.42)) and b_i^{LJ}†† (Eq. (6.43)) for calculating the first correlation integral $I_1^{\mathrm{LJ}}(\eta, m, T^*)$ (Eq. (6.38)) and second correlation integral $I_2^{\mathrm{LJ}}(\eta, m, T^*)$ (Eq. (6.39)) of LJ chain fluids, respectively.

i	$a_{i0}^{\mathrm{LJ}}/b_{i0}^{\mathrm{LJ}}$	$a_{i1}^{\mathrm{LJ}}/b_{i1}^{\mathrm{LJ}}$	$a_{i2}^{\mathrm{LJ}}/b_{i2}^{\mathrm{LJ}}$
0	$p(1)$	$p(11)$	$p(22)$
1	$p(2)+p(3)\sqrt{T^*}$	$p(12)+p(13)\sqrt{T^*}$	$p(23)$
2	$p(4)+p(5)\sqrt{T^*}$	$p(14)+p(15)\sqrt{T^*}$	$p(24)+p(25)\sqrt{T^*}+p(26)T^*$
3	$p(6)+p(7)\sqrt{T^*}+p(8)T^*$	$p(16)+p(17)\sqrt{T^*}+p(18)T^*$	$p(27)+p(28)\sqrt{T^*}+p(29)T^*$
4	$p(9)+p(10)\sqrt{T^*}$	$p(19)+p(20)\sqrt{T^*}+p(21)T^*$	$p(30)+p(31)\sqrt{T^*}$

† $\boldsymbol{p}$ = [-0.8891, -0.7272, 0.02675, -0.6859, 0.8927, 3.432, -1.364, -0.1390, -1.702, 1.269, 0.4016, -0.3407, -0.2923, -0.6860, -0.3161, -3.007, 3.256, 0.01125, 6.271, -3.800, 0.1086, 0.4057, -2.145, 9.963, 0.5556, 0.09979, -20.30, -3.779, -0.1887, 13.53, 5.007]

†† $\boldsymbol{p}$ = [0.4065, 0.6205, -0.02278, -0.02908, -0.4997, 1.008, -0.03263, 0.1068, -3.432, 0.2455, -0.2902, 0.1989, 0.1308, -0.1802, 0.4156, 2.426, -0.6577, -0.1061, -1.999, -0.9246, 0.1546, -0.09634, -0.1705, 0.6318, -0.2604, -0.02258, -0.4699, 0.9034, 0.01521, -0.2431, -0.1696]

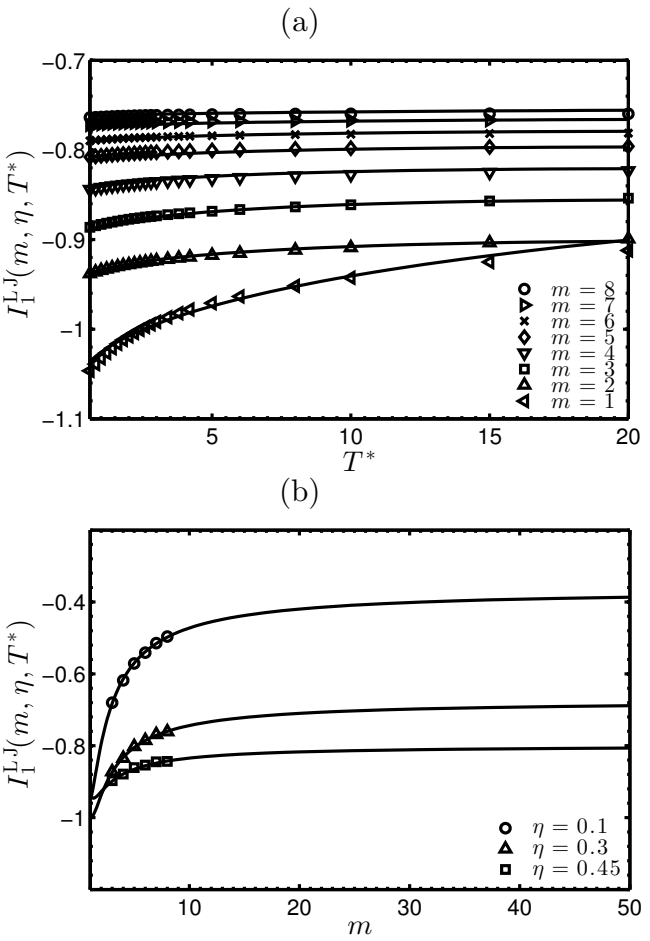

Figure 6.6: The first correlation integral $I_1^{\mathrm{LJ}}(m, \eta, T^*)$ for various chain lengths m, temperatures T^* and packing fractions η. The results in (a) are for $\eta = 0.3$, except for $m = 1$ and $m = 2$ which correspond to $\eta = 0.2618$. The results in (b) are for $T^* = 3.4$. The symbols are obtained from solving the integral from Eq. (6.28) using MC data [218, 220, 221] for the rdf of hard-chain fluids (see Section 6.4.4 for details). The results for $m = 1$ and $m = 2$ correspond to $\eta = 0.2618$. The lines are correlation results from Eq. (6.38). The results for the second correlation integral I_2^{LJ} and the correlation integrals for SW chain fluids are of similar accuracy (not shown for brevity).

6.4.5. Effective segment size and perturbation contribution for mixtures

Let us now extend our results to mixtures. The effective segment size is treated as a pure-component property. Hence, we calculate $d_{ii}(T^*, m, \rho_s^*)$ from Eq. (6.31), using $T^* = kT/\epsilon_{ii}$, $m = m_i$ and $\rho_s^* = \sum_i \rho_i m_i \sigma_{ii}^3$. For the calculation of the perturbation contributions, we assume Van der Waals one-fluid mixing rules [239, 240]. Accordingly, the perturbative part of the Helmholtz energy is mapped onto a pseudo one-component fluid, which is described by the following molecular parameters

$$\bar{\epsilon} = \frac{\sum_i \sum_j \rho_i \rho_j m_i m_j \epsilon_{ij} \sigma_{ij}^3}{\sum_i \sum_j \rho_i \rho_j m_i m_j \sigma_{ij}^3} \tag{6.44}$$

$$\bar{\sigma}^3 = \frac{\sum_i \sum_j \rho_i \rho_j m_i m_j \sigma_{ij}^3}{\sum_i \sum_j \rho_i \rho_j m_i m_j} \tag{6.45}$$

$$\bar{m} = \frac{\sum_i \sum_j \rho_i \rho_j m_i m_j}{\sum_i \sum_j \rho_i \rho_j} \tag{6.46}$$

Using this approach, the two perturbation contributions from Eqs. (6.24)-(6.25) can be written as

$$a_1 = 2\pi\rho^2 \left(\bar{m}^2 \frac{\bar{\epsilon}}{kT} \bar{\sigma}^3 \right) \bar{I}_1 \tag{6.47}$$

$$a_2 = -\pi\rho^2 \bar{m} K_0 \left(\bar{m}^2 \left(\frac{\bar{\epsilon}}{kT} \right)^2 \bar{\sigma}^3 \right) \frac{\partial}{\partial \rho} \left(\rho \bar{I}_2 \right)_d \tag{6.48}$$

where the correlation integrals of the mixture $\bar{I}_1$ and $\bar{I}_2$ are calculated by substituting $\bar{m}$ for m and $T^* = kT/\bar{\epsilon}$ for T^* in Eqs. (6.36)-(6.39).

In the following section we proceed by comparing VLE and isotherms of both SW- and LJ chain fluids as obtained from our simplified perturbation theory to those obtained from molecular simulations. Additionally, the effect of molecular flexibility on the phase behavior is investigated.

6.5 Results and Discussion

6.5.1. Fully flexible SW chains

We start our analysis by comparing theoretical results as obtained from the EoS developed in this chapter to molecular simulation data for the VLE and isotherms of SW chain fluids and their mixtures. SW fluids represent the most basic test of perturbation theory, because the reference fluid is temperature independent.

In Fig. 6.7, we compare the VLE of several fully flexible SW chain fluids as obtained from the perturbation theory to results obtained from molecular simulations [205, 208, 241]. For the regarded chain lengths, very good agreement between theory and simulations is observed. For comparison, we included theoretical results as obtained from the SAFT-VR EoS of Gil-Villegas *et al.* [68]. As for the EoS developed in this work, the SAFT-VR EoS is based on a second order BH perturbation theory with the local compressibility approximation (LCA) for the second order

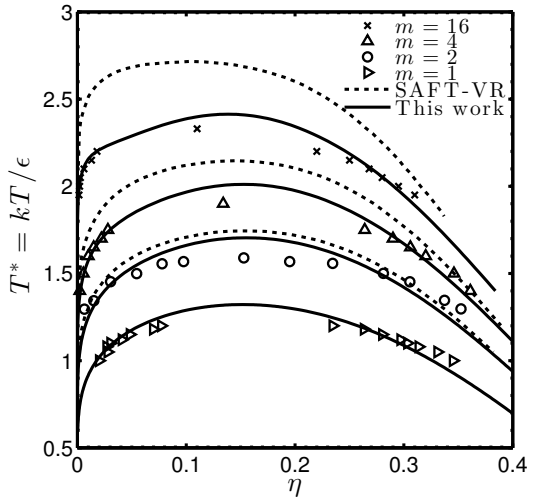

Figure 6.7: The VLE of fully flexible SW chain fluids. The solid lines are results from the perturbation theory developed in this work. The dotted lines are calculations based on the SAFT-VR EoS of Gil-Villegas *et al.* [68]. The symbols are MC simulation results of Vega *et al.* [241] ($m = 1$), Yethiraj and Hall [242] ($m = 2$), and Escobedo and de Pablo. [208] ($m = 4$, $m = 16$).

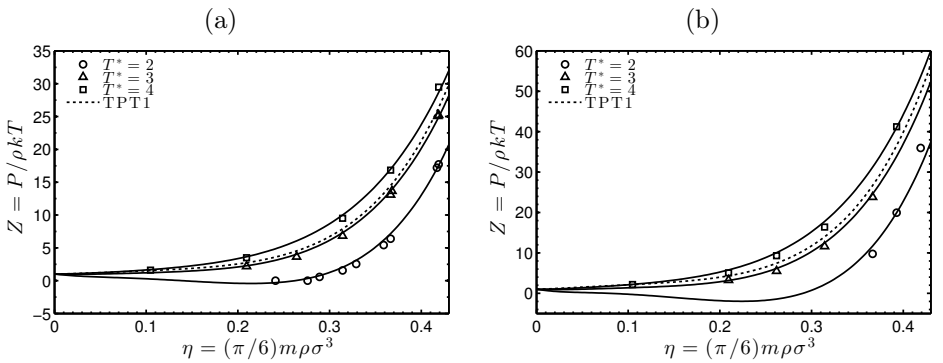

Figure 6.8: Isotherms of (a) a fully flexible SW 8-mer, and (b) a fully flexible SW 16-mer. Lines are results obtained from the perturbation theory developed in this work using the LHrc EoS (solid lines) and the TPT1 EoS (dotted lines) for the hard-chain reference fluid. Symbols are MC data of Escobedo and de Pablo. [208] ($m = 8$) and Tavares *et al.* [207] ($m = 8$, $m = 16$).

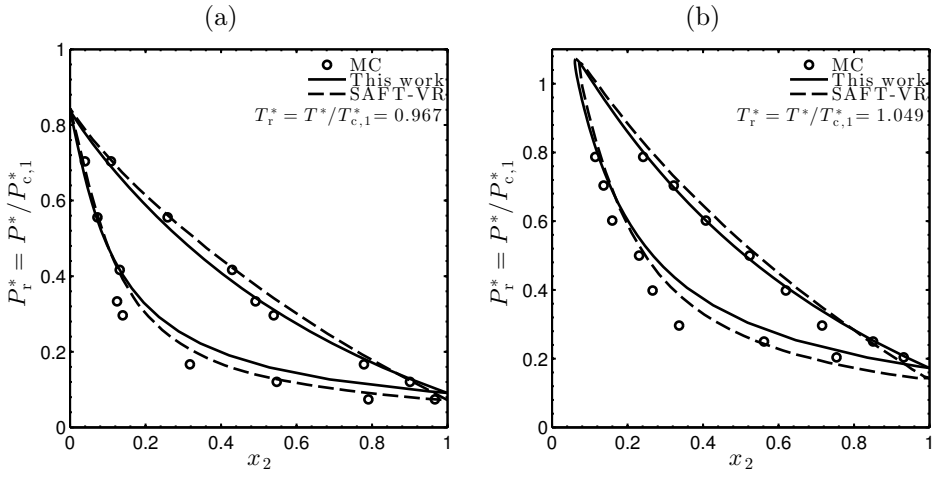

Figure 6.9: Dimensionless pressure ($P^* = P\sigma_{11}^3/\epsilon_{11}$) vs. mole fraction ($x_2$) representation of the VLE of a binary mixture of SW monomers (component 1) and SW dimers (component 2) at a reduced temperature of (a) $T_r^* = T^*/T_{c,1}^* = 0.967$ and (b) $T_r^* = 1.049$, where $T^* = kT/\epsilon_{11}$ and $T_{c,1}$ is the critical temperature of the pure monomeric fluid. Solid lines are results obtained from the perturbation theory developed in this work ($T_{c,1}^* = 1.3219$, $P_{c,1}^* = 0.14270$). Dashed lines are calculations based on the SAFT-VR EoS [74]. Symbols are MC data of Davies *et al.* [74] ($T_{c,1}^* = 1.22$, $P_{c,1}^* = 0.108$).

perturbation contribution. The difference is that the SAFT-VR approach is based on a spherical reference fluid (perturbed-sphere method).

In Fig. 6.8, we proceed by comparing isotherms of SW chain fluids as obtained from the perturbation theory to molecular simulation results [207, 208]. For all temperatures included, good agreement is obtained. For comparison, we included some results obtained from using the TPT1 EoS [59, 122] for the hard-chain reference fluid. As can be observed, the use of this EoS leads to a weaker description of simulation data.

In Figs. 6.9 and 6.10, we analyse the performance of the EoS in describing molecular simulation results [74, 243] for VLE and isotherms of SW-chain fluid mixtures. The VLE are presented in terms of reduced quantities (*i.e.* relative to critical properties). A representation in reduced variables eliminates any inaccuracies introduced by the small overestimation of the pure-component critical properties (see Fig. 6.7). Agreement between simulations and theory is satisfactory and is comparable to that obtained from the SAFT-VR EoS [74].

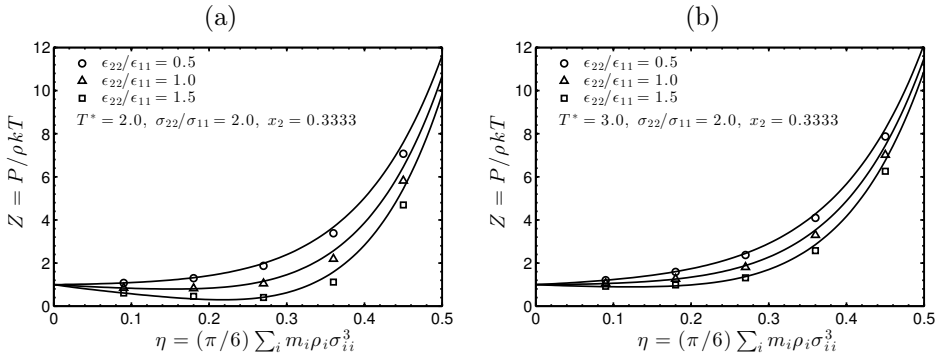

Figure 6.10: Compressibility factor $Z = P/\rho kT$ vs. packing fraction η of several asymmetric binary mixtures of SW monomers (component 1) and SW dimers (component 2) at a dimensionless temperature of (a) $T^* = kT/\epsilon_{11} = 2.0$, and (b) $T^* = 3.0$. Solid lines are results obtained from the perturbation theory developed in this work. Symbols are MD data of Gulati and Hall [243].

6.5.2. Fully flexible LJ chains

In Fig. 6.11, the VLE of fully flexible LJ chain fluids as obtained from the perturbation theory developed in this work is compared to the results from MC simulations [208, 244–248]. For both the vapour-liquid coexistence densities and vapour pressure, we find satisfactory agreement between theory and simulations. Especially the description of vapour pressures is noteworthy. We should stress that, compared to Fig. 6.1, the improved results shown here are a result of the effective segment size from Eq. (6.31). The overall satisfactory agreement between theory and simulation, however, is a result of all three ingredients of the perturbation theory; namely, the accurate EoS for the reference fluid, the effective segment size from Eq. (6.31), and the MC data for the averaged segment-segment rdf of the hard-chain reference fluid. To demonstrate the effect of using a reference EoS different than the LHrc EoS, we included results for the VLE of a LJ 50-mer based on the TPT1 EoS [59] and TPT2 EoS [60] for the hard-chain reference fluid. Especially in the intermediate density region TPT loses some of its accuracy for chains longer than 8 segments. As shown in Fig. 6.11, these inaccuracies result in a rather poor description of the VLE of LJ 50-mers.

As could be expected from a perturbation theory up to second order, the critical temperature is overestimated for all systems considered. For chain lengths $m = 1$ and $m = 2$ we find a small underestimation of coexistence densities in the dense liquid phase. As pointed out by Paricaud [234], discrepancies of this kind are caused by the use of the LCA for the second order perturbation term. The reason these underestimations are not observed for larger chain lengths could be due to the larger overestimation of the critical temperature of these fluids, which leads to a shift of liquid coexistence densities to somewhat larger values. Another reason could be small inaccuracies in the correlation integrals I_1^{LJ} and I_2^{LJ} (Eqs. (6.38)-(6.39)) for chain lengths longer than those used in their development. We observed that, compared to the first correlation integral, the second correlation integral converges more slowly to its asymptotic value at large chain lengths. Therefore it might be that

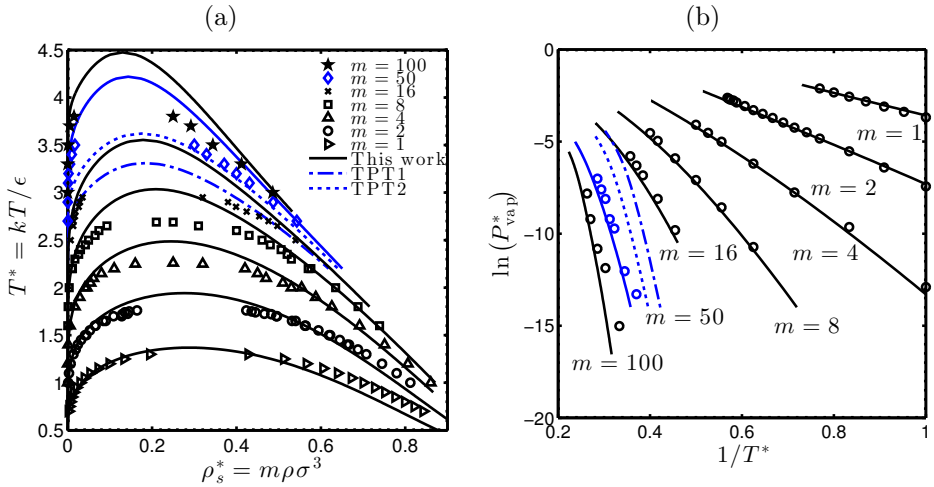

Figure 6.11: The VLE of fully flexible LJ chain fluids of segment number m. Figure (a) shows the coexistence densities, and (b) presents the saturated vapour pressure $P_{\rm vap}^* = P_{\rm vap}\sigma^3/\epsilon$. The solid lines are results from the perturbation theory developed in this work, based on the LHrc EoS for the reference fluid. For comparison we included some results based on the TPT1 EoS (dash-dotted lines) and TPT2 EoS (dotted lines) for the reference fluid. Symbols are MC simulation results of Lotfi *et al.* [244] ($m = 1$), Vega *et al.* [245] ($m = 2$), Dubey *et al.* [246] ($m = 2$), MacDowell *et al.* [247] ($m = 4$, $m = 8$, $m = 16$), Escobedo and de Pablo [208] ($m = 4$, $m = 8$, $m = 16$), and Sheng *et al.* [248] ($m = 50$, $m = 100$). Results for 50-mers are displayed in blue.

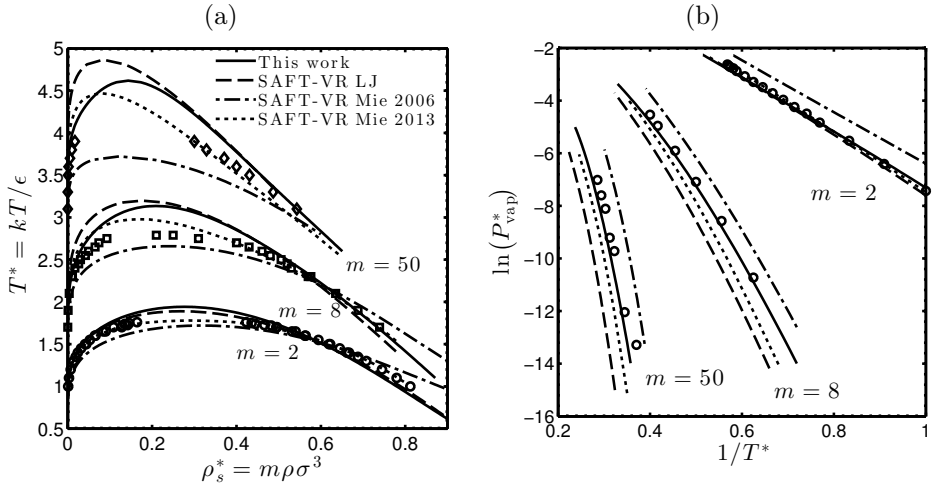

Figure 6.12: The VLE of fully flexible LJ chain fluids of segment number m, as obtained from the perturbation theory developed in this work (solid lines), the SAFT-VR LJ EoS [73] (dashed lines), the SAFT-VR Mie 2006 EoS [69] (dash-dotted lines), the SAFT-VR Mie 2013 EoS [70] (dotted lines), and MC simulations (symbols). Diagram (a) shows the coexistence densities, and (b) presents the saturated vapour pressure $P_{\rm vap}^* = P_{\rm vap}\sigma^3/\epsilon$. For visual clarity, the coexistence temperature in (a) is shifted upwards by 0.1 for $m = 8$, and by 0.4 for $m = 50$. MC simulation results included are those of Vega *et al.* [245] ($m = 2$), Dubey *et al.* [246] ($m = 2$), MacDowell *et al.* [247] ($m = 8$), Escobedo and de Pablo [208] ($m = 8$), and Sheng *et al.* [248] ($m = 50$).

in the development of I_2^{LJ} (Eq. (6.39)), we did not include sufficient MC data for the hard-chain rdf of long chain fluids. Although there is MC data for the rdf of longer ($m = 20$, $m = 50$, $m = 100$) hard-sphere chain fluids available in literature [251], we found that inclusion of this data in the calculation of the correlation integrals leads to irregular scaling behaviour with chain length m. For this reason, we choose not to include additional MC data for the rdf of longer hard-chain fluids in the calculation of the correlation integrals.

It is instructive to compare the results obtained from our perturbed-chain method to those obtained from a perturbation theory based on a spherical reference fluid (perturbed-sphere method). Perturbed-sphere equations of state that were developed on equal grounds as the perturbed-chain EoS presented in this work (*i.e.* 2nd order Barker Henderson theory, LCA for a_2, no correlation to simulation data of attractive chain fluids) are the SAFT-VR LJ EoS of Davies *et al.* [73] and the 2006 version of the SAFT-VR Mie EoS of Lafitte *et al.* [69]. It is noteworthy that other perturbed-sphere methods are available that perform better than SAFT-VR LJ and SAFT-VR Mie 2006. State-of-the-art models, in this respect, are the soft-SAFT EoS of Blas and Vega [67] (which was developed based on the EoS of Johnson and Gubbins [212, 249]) and the 2013 version of the SAFT-VR-Mie EoS of Lafitte *et al.* [70]. For soft-SAFT, the description of the LJ-sphere reference fluid is obtained from an accurate empirical EoS [249]. The SAFT-VR Mie approach describes the LJ-sphere reference fluid based on a third order BH perturbation theory. The second and third order perturbation terms of this approach were parametrized to macroscopic properties, namely to MC results for the VLE of Mie chain fluids. In Fig. 6.12, we compare VLE and vapor pressures as obtained from the SAFT-VR LJ EoS, SAFT-VR Mie 2006 EoS, and SAFT-VR Mie 2013 EoS to those obtained from the EoS developed in this work. As expected, the SAFT-VR Mie 2013 EoS results in the most accurate description of saturated liquid densities and the critical region. For vapor phase properties, however, the perturbation theory developed in this work results in the most faithful description of simulation data.

In Fig. 6.13, we compare isothermal pressures as obtained from the perturbation theory to results from MC simulations [212, 249]. For all temperatures and chain lengths considered, agreement between theory and simulations is excellent. As can be observed in Fig. 6.13 (c), the use of a density-dependent segment size $d(T^*, m, \rho_s^*)$ is essential to come to a reliable description of simulation data. When the original BH diameter $d^{\mathrm{BH}}(T^*)$, or the low-density limit $d(T^*, m, \rho_s^* = 0)$, is used instead, isothermal pressures are under- and overestimated, respectively.

In Figs. 6.14 and 6.15, theoretical predictions for VLE and isothermal pressures of LJ chain fluid mixtures are compared to results obtained from molecular simulations [67, 250]. Given that some of the mixtures involve triple (m, σ and ϵ) asymmetries, agreement between simulations and theory is very satisfactory.

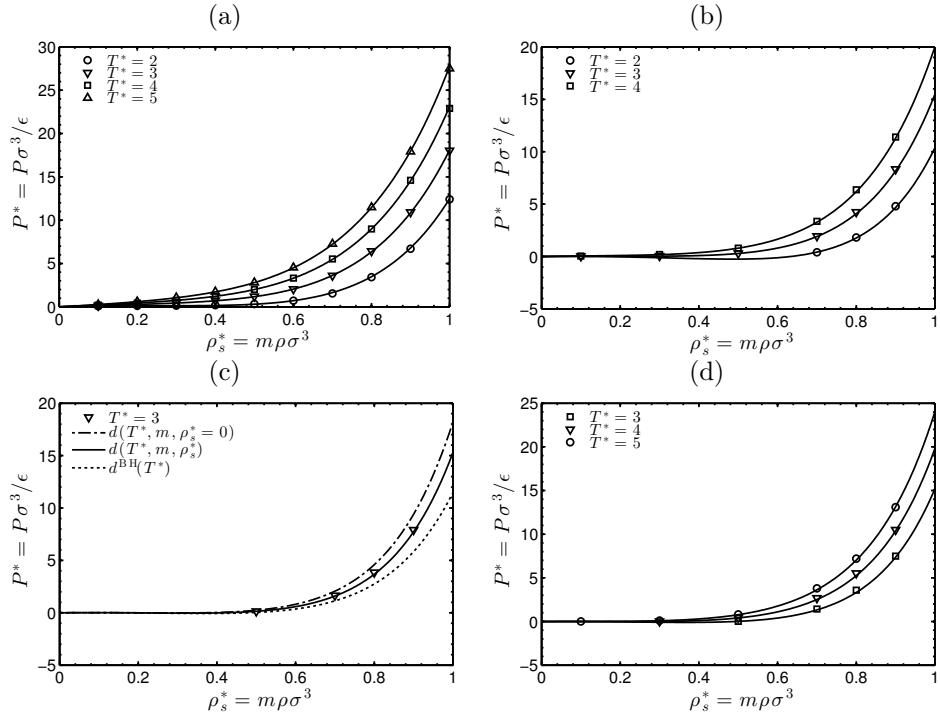

Figure 6.13: Isothermal pressure of fully flexible LJ chain fluids of (a) $m = 2$, (b) $m = 8$, (c) $m = 16$, and (d) $m = 100$. Solid lines are results obtained from the perturbation theory developed in this work. Dotted lines are results obtained from using the original Barker-Henderson diameter $d^{\mathrm{BH}}(T^*)$ instead of Eq. (6.31) to calculate the effective segment size; dash-dotted lines are results obtained from using the low-density limit of Eq. (6.31) $d(T^*, m, \rho_s^* = 0)$ to calculate the effective segment size. For comparison, some results obtained from the SAFT-VR LJ EoS [73] (dashed lines) were included. Symbols are MC data of Johnson and Gubbins. [212, 249]

Figure 6.14: Dimensionless pressure ($P^* = P\sigma_{11}^3/\epsilon_{11}$) vs. mole fraction ($x_1$) representation of the VLE of an asymmetric binary mixture of LJ dimers ($\sigma_{11}/\sigma_{22} = 1.0$, $\epsilon_{11}/\epsilon_{22} = 1.33$) at a reduced temperature of $T_r^* = T^*/T_{c,1}^* = 0.7848$, where $T^* = kT/\epsilon_{11}$ and $T_{c,1}$ is the critical temperature of a pure fluid of component 1. Solid lines are results obtained from the perturbation theory developed in this work ($T_{c,1}^* = 1.9421$, $P_{c,1}^* = 0.10439$). Symbols are MC data of Blas and Vega [67]. For simulation results, the critical properties of the pure fluid of component 1 were obtained from the MC data of Vega *et al.* [245] using conventional scaling laws. We obtain $T_{c,1}^* = 1.784$, $P_{c,1}^* = 0.07784$. Please note that our critical pressure is different than that obtained in the original paper of Vega *et al.* [245] due to an error in their application of the Clausius-Clapeyron equation.

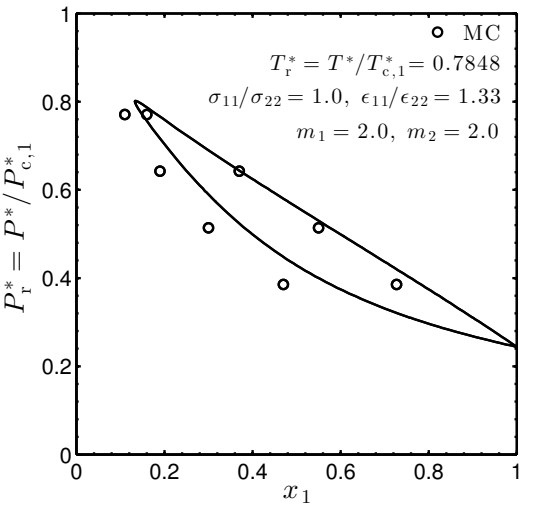

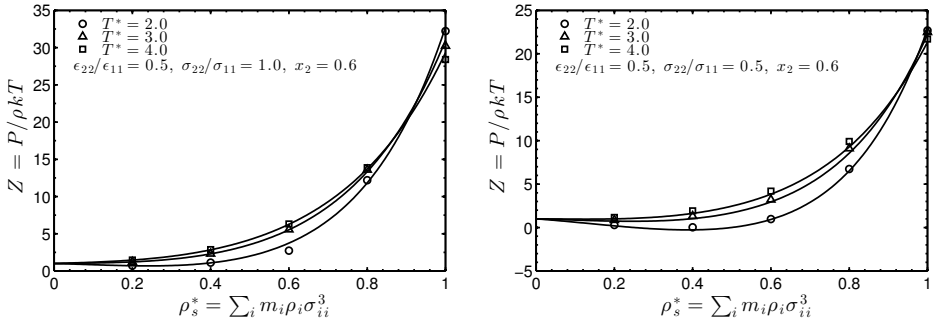

Figure 6.15: Compressibility factor $Z = P/\rho kT$ vs. dimensionless segment density ρ_s^* of two different asymmetric binary mixtures of LJ 4-mers (component 1) and LJ 8-mers (component 2) at several dimensionless temperatures $T^* = kT/\epsilon_{11}$. Solid lines are results obtained from the perturbation theory developed in this work. Symbols are MD data of Reis *et al.* [250].

6.5.3. Effect of molecular flexibility on VLE

We now turn to the effect of molecular flexibility on the VLE. In order to study this, we performed MC simulations to calculate the VLE of fully flexible and rigid linear SW- ($m = 4$) and LJ chain fluids ($m = \{3, 4, 5\}$). For tabulated simulation data, the reader is referred to the Supporting Material of Ref. [236]. In Fig. 6.16 we compare simulation results to those from literature, as obtained by Escobedo and de Pablo [208] (fully flexible SW 4-mers), Galindo *et al.* [216] (rigid linear LJ 5-mers), MacDowell and Blas [247] (fully flexible LJ 4-mers), and Blas *et al.* [252, 253] (fully flexible- and rigid linear LJ 3- 4- and 5-mers). Please note that to allow for a clear distinction of simulation results, the results for LJ 4- and 5-mers are shifted upwards by 0.2 and 0.4 in T^*, respectively. Good agreement between different simulation results is obtained. Upon increasing the rigidity of the chains, our simulations show (1) a widening of the VLE (*i.e.* smaller saturated vapour density, larger saturated liquid density), (2) an increase of the critical temperature T_c, and (3) a decrease of the critical density ρ_c.

In Fig. 6.17, we compare simulation results for fully flexible- and rigid linear SW 4-mers to those obtained from the perturbation theory developed in this work. Both simulations and theory predict an increase of the VL critical temperature and a widening of the VL region with increasing rigidity of the chains. For rigid linear chains, the liquid side of the diagram is more accurately predicted than the vapour side. The reason for this is most probably that our use of the rdf of fully flexible hard-sphere chains in the calculation of the perturbation terms of rigid linear chain fluids is more harsh an approximation at low densities. Altogether, given that the theory only includes the effect of molecular flexibility through the reference fluid, we view the agreement between theory and simulations as very promising. Please note that for other chain lengths than those shown in Fig. 6.17, the theory predicts the same trends with molecular rigidity.

As we show in Fig. 6.18, the effect of flexibility on the VLE of LJ chain fluids is less well described as that of SW chain fluids. As for SW chains, the perturbation theory gives the wrong trend of the critical density with flexibility. For LJ chains, however, the trends of the critical temperature and vapour density with flexibility of the chains are also incorrectly predicted. The theory does capture the effect of molecular flexibility on the liquid densities. The weaker results for the effect of flexibility on the VLE of LJ chain fluids (compared to SW chains) is caused by the use of the effective segment size. One might suspect that a lacking of any χ_R-dependence in $d(T^*, m, \rho_s^*)$ could be the underlying reason. However, the results from Fig. 6.5 suggest the effective segment size of rigid linear chain fluids is somewhat larger than that of fully flexible chains, corresponding to a lower—not higher—critical temperature. A more probable cause of errors is the use of a hard-chain rdf of segment size d and bond-length d in the calculation of the correlation integrals, Eqs. (6.28)-(6.29). Considering a hard-chain fluid with segment diameter d and bond-length d is not strictly correct, because the segment distance should be σ. In future work, we plan to evaluate the effect of this approximation by comparing our perturbation terms to those obtained from MC simulations.

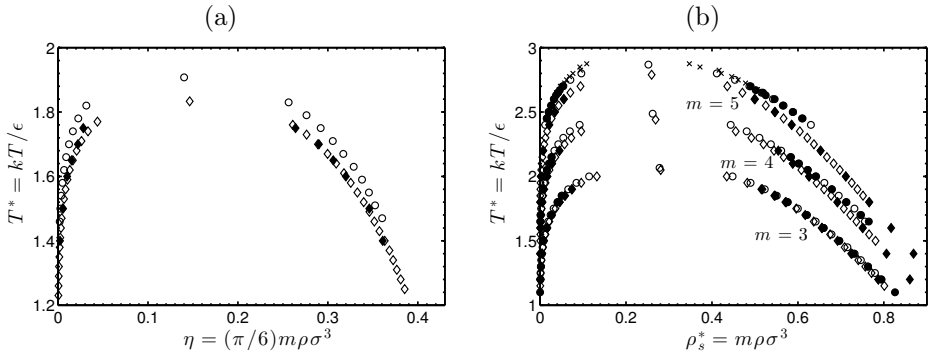

Figure 6.16: The VLE of fully flexible (diamonds) and rigid linear (circles, crosses) SW- (a) and LJ chain fluids (b) as obtained from MC simulations performed in this work (open symbols) and literature (closed symbols, crosses). For visual clarity, the results for LJ chains of $m = 4$ and $m = 5$ are shifted upwards by 0.2 and 0.4, respectively. Literature data included in this figure are those of Escobedo and de Pablo [208] (fully flexible SW 4-mers), MacDowell and Blas [247] (fully flexible LJ 4-mers), Blas *et al.* [252, 253] (fully flexible LJ 3- and 5-mers, rigid linear LJ 3-, 4- and 5-mers) and Galindo *et al.* [216] (rigid linear LJ 5-mers). The data of Galindo *et al.* [216] is shown by the crosses. For tabulated results of the simulations performed in this work, the reader is referred to the Supporting Material of Ref. [236].

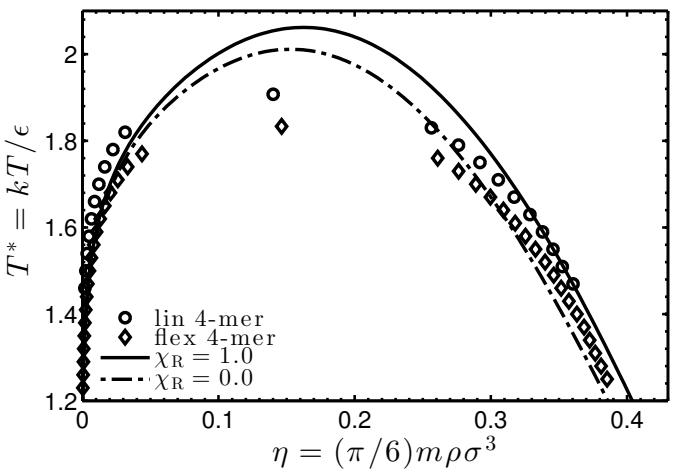

Figure 6.17: The VLE of fully flexible- (diamonds, dash-dotted line) and rigid linear (circles, solid line) SW 4-mers as obtained from the perturbation theory developed in this work (lines) and molecular simulations of this work (symbols).

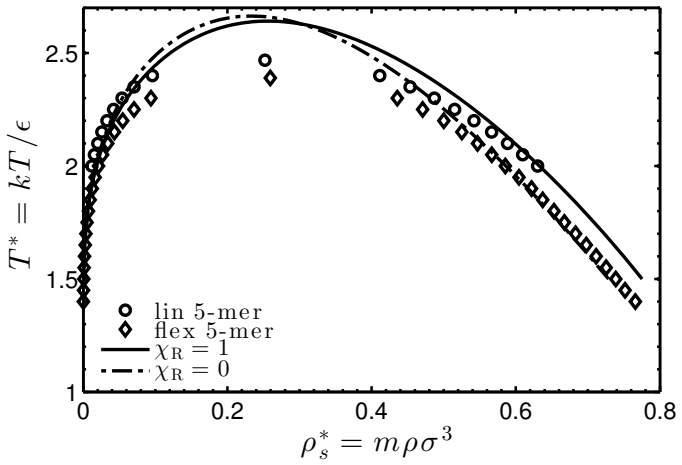

Figure 6.18: The VLE of fully flexible- (diamonds, dash-dotted line) and rigid linear (circles, solid line) LJ 5-mers as obtained from the perturbation theory developed in this work (lines) and molecular simulations of this work (symbols).

6.6 Conclusion

We have developed two new perturbed-chain equations of state for attractive chain fluids with varying degree of flexibility. The two models are for tangent SW- and -LJ chain fluids and their mixtures in isotropic (vapour and liquid) phases. The EoS was derived in the framework of a 2nd order Barker-Henderson perturbation theory. To arrive at a satisfactory comparison between calculated VLE of flexible SW- and LJ chain fluids to those obtained from molecular simulations, some modifications to the original recipe of Barker and Henderson were required. Firstly, it was shown that the original BH diameter is insufficient for approximating the soft repulsion between the segments of LJ chain fluids. A new effective segment size was developed that explicitly incorporates the chain-connectivity of segments. Moreover, the new segment size was shown to be density dependent. Second, it was demonstrated that small inaccuracies in the rdf of the hard-chain reference fluid can lead to significant errors in calculated VLE. We showed that these errors are small if a rdf obtained directly from MC simulations is used. Finally, we showed the importance of using an accurate EoS for the hard-chain reference fluid. In particular, it was shown that commonly used EoS such as TPT1 lead to poor predictions of VLE of long LJ chains. When using the more accurate LH EoS instead, a much better comparison to MC data is obtained.

In Chapter 3, we developed an extension of the LH EoS to partially flexible and rigid linear chain fluids. Using this extended EoS to calculate the reference contribution, it is possible to model the effects of intramolecular flexibility on the VLE of SW- and LJ chain fluids. MC simulations were performed to validate theoretical results. For both SW- and LJ chain fluids, our simulations show the following trends

of the VLE with increased rigidity of the chains: (1) a widening of the VLE (larger saturated liquid density, smaller saturated vapour density), (2) a shift of the critical temperature to higher values, and (3) a shift of the critical density to lower values. For SW chain fluids, theoretical results are in good agreement with results from MC simulations; all trends but that of the critical density were correctly predicted. For LJ chain fluids, the theoretical description captured the widening of the vapour liquid envelope with increasing chain rigidity, but did not capture the shift of critical properties. We suspect that this is due to our application of an effective segment size in the calculation of the perturbation contributions to the EoS. In future work, we plan to test this by comparing the perturbation terms to those obtained from molecular simulations.

In agreement with previous studies on the subject [216, 252–255], the results obtained in this chapter show that the effect of molecular flexibility on the isotropic (vapour-liquid) phase behavior of attractive chain fluids is quite small. If the equation of state is coupled to a suitable description of anisotropic phases (such as solids or liquid crystals), however, it is expected these subtle effects can make the difference for an accurate prediction of phase equilibria (cf. Chapter 3). An extension of the EoS to anisotropic phases will be the subject of the next chapter.

7

An equation of state for describing the isotropic phase, nematic phase and isotropic-nematic phase transition of Lennard-Jones chain fluids

An equation of state (EoS) is developed for describing isotropic-nematic (IN) phase equilibria of LJ chain fluids. The EoS is developed by applying a second order Barker-Henderson perturbation theory to a reference fluid of hard chain molecules. The chain molecules consist of tangentially bonded spherical segments that are allowed to be fully flexible, partially flexible (rod-coil) or rigid linear. The hard-chain reference contribution to the EoS is obtained from the EoS that was developed in part A of this thesis. For the description of the (attractive) dispersive interactions between molecules, we adopt a segment-segment approach. We show that the perturbation contribution for describing these interactions can be divided into an 'isotropic' part, which depends only implicitly on orientational ordering of molecules (through density), and an 'anisotropic' part, for which an explicit dependence on orientational ordering is included (through the nematic order parameter). The isotropic contribution is calculated using the perturbation contribution that was developed in Chapter 6. For the anisotropic contribution we propose an orientation-dependent term, that is simplified to a mean-field form. The perturbation theory is used to study the effect of chain length, molecular flexibility, and attractive interactions on IN phase equilibria of pure LJ chain fluids. Theoretical results for the IN phase equilibrium of rigid linear LJ 10-mers are compared to results obtained from MC simulations in the isobaric-isothermal (NPT) ensemble, and an expanded formulation of the Gibbs-ensemble. Our results show that the anisotropic contribution to the dispersion attraction is irrelevant for LJ chain fluids. Using the isotropic (density-dependent) contribution only ($i.e.$ using a zero'th order expansion of the attractive Helmholtz energy contribution in the nematic order parameter), excellent agreement between theory and simulations is observed. These results suggest that an EoS contribution for describing dispersion interactions in real LCs can be obtained from conventional theoretical approaches designed for isotropic fluids, such as a (PC-)SAFT approach.

Parts of this chapter have been submitted to:
T. van Westen, B. Oyarzún, T.J.H. Vlugt and J. Gross *J. Chem. Phys.* (2015).

7.1 Introduction

As discussed in the introduction chapter of this thesis, the development of nematic-state theories originally evolved along two different paths. The first path, as pioneered by Onsager [109], is based on the premise that intermolecular repulsions are the dominant molecular attribute to mesophase formation; while the second path, as pioneered by Born [256, 257], and later Maier and Saupe [10–12], is based on the view that intermolecular attractions are dominant. While the view that intermolecular repulsions are primarily responsible for nematic ordering seems well-accepted now [19], it should be clear that the rich phase behaviour of thermotropic LCs [32, 43] cannot be interpreted without a detailed account of the different types of attractive interactions in a system (*e.g.* dispersion interactions, dipolar/multipolar interactions, $\pi - \pi$ interactions between aromatic cores, etc.).

Previous studies on attractive mesogens have shown that it is instructive to analyse the effect of certain specific intermolecular interactions separately by studying a suitably chosen model system [19, 258, 259, 259–261]. In the present chapter we focus on dispersion interactions. Therefore, the hard-chain EoS that was developed in part A of this thesis is extended to fluids where the segments of the chains interact with Lennard-Jones potentials. Moreover, the isotropic-nematic phase behaviour of this specific molecular model is studied by means of Monte Carlo (MC) simulations in the isobaric-isothermal (NPT) ensemble, and an expanded formulation [34] of the Gibbs Ensemble (GE) [116, 262].

Our choice for a segment-based approach is somewhat unconventional. In common theoretical approaches for the description of attractive mesogens (see for example the excellent review on generalized Van der Waals theory by Franco-Melgar *et al.* [19]), the attractive interactions are modelled by a molecular-based pair potential that involves an isotropic- (position-dependent) and several anisotropic (orientation-dependent) contributions. Such an approach may at first be more intuitive than a segment-based approach, since any orientation dependence of the attractive Helmholtz energy contribution follows naturally from the theoretical treatment of the pair-potential model. In a segment-based approach, limited knowledge on higher order correlation functions of the segments of the chains forces one to treat such orientation dependencies—if any—from the outset. Here, we show that for LJ chain fluids a reliable description of isotropic-nematic equilibria can be obtained using a dispersive Helmholtz energy contribution that involves no explicit orientation dependence. In principle, this suggests that an accurate theoretical description of the dispersion interactions in real LCs can be obtained from conventional methods that were developed for isotropic fluids (*e.g.* SAFT-like approaches [65, 66]). Since these type of theories are relatively well-developed, this could imply a considerable simplification of the description of anisotropic fluids. We consider this insight as the main finding of this work.

7.2 Molecular model and intermolecular potential

As in previous chapters, a molecule is assumed as a homo-segmented chain of m segments. Molecular flexibility is introduced by the rod-coil model. To model the dispersive pair-interaction between the segments of chains we assume a LJ 12-6 potential (Eq. (6.2)).

7.3 Simulation details

Molecular simulations were conducted for calculating isothermal pressures and isotropic-nematic equilibria of rigid linear Lennard-Jones 10-mers. Isotropic-nematic equilibria were calculated from MC simulations in an expanded formulation of the isometric (NVT) Gibbs-ensemble [34, 116, 262]. For a detailed description of the simulation method, the reader is referred to the recent work of Oyarzun *et al.* [34]. Although the focus of the work of Oyarzun *et al.* was on systems of hard chain molecules, the simulation method was explained for any form of intermolecular pair potential and thus also applies for the LJ chain molecules considered in this work. Here, we provide a brief overview of the method, and list simulation details specific to this work.

As in the usual NVT Gibbs-ensemble [116, 262], two simulation boxes a and b are employed, which are kept in thermodynamic contact by exchanging molecules and volume. In the expanded method as employed in this work, the exchange of molecules is performed gradually by a coordinated coupling/decoupling of a fractional molecule in each simulation box [34]. Similar as in the Continuous Fractional Monte Carlo method of Maginn and co-workers [263–265], the gradual exchange facilitates the transferring of molecules between boxes. The fractional state is characterized by a coupling parameter λ, which simultaneously defines the number of interacting (by Eq. (6.2)) segments of the fractional molecules in both boxes, *i.e.* λ interacting segments in simulation box a and $m - \lambda$ interacting segments in simulation box b. A Monte Carlo cycle is defined by N trial moves, selected from displacement, rotation, reptation, volume change and coupling parameter changes [34], with a relative probability of 100:100:10:1:1000. The number of molecules (N) was typically around 10^3. Maximum displacements, rotations, volume changes and coupling parameter changes were adjusted for a maximum acceptance ratio of 20%. Typically, we used 3×10^6 MC cycles for equilibration, and 1×10^6 for production.

Isotherms were calculated using Monte Carlo (MC) simulations in the isobaric-isothermal (NPT) ensemble [116]. MC moves were the same as for the GEMC simulations, without the use of the coupling parameter move. A number of $N = 500$ molecules was used in each simulation. 3×10^6 MC cycles were required for equilibration and 1×10^6 cycles were used for production.

For all simulations, the LJ interactions were evaluated for segments of different chains and segments within the same chain that are separated by two or more bonds. Interactions were truncated at 2.5σ and standard long-ranged tail corrections were applied [116]. Isotropic initial configurations were generated in a cubic box, whereas nematic initial configurations were started from a rectangular box with a typical ratio of edge lengths equal to 1:1.1:1.2. The phase type was monitored by

calculation of the nematic order parameter S_2, which was defined in Eq. (1.2).

7.4 Theory

7.4.1. Equation of state

As in Chapter 6, we apply a perturbation approach to develop the EoS of nematic LJ chain fluids. Accordingly, the Helmholtz energy A of a system of N molecules at a temperature T is calculated from a reference contribution (A_0), caused by repulsive interactions between molecular cores, and a perturbative contribution (A^{pert}), caused by attractive interactions, as

$$\frac{\beta A}{V} = a = a_0 + a^{\text{pert}} \tag{7.1}$$

Here, β^{-1} is the product of Boltzmann's constant k with absolute temperature T, and $a = \beta A/V$ is a reduced Helmholtz energy density.

To calculate the reference contribution to the EoS (a_0) we employ the truncated form of the Vega-Lago rescaled Onsager theory that was developed in Chapter 5 of this thesis. The residual Helmholtz energy of the isotropic fluid that is required in this approach is obtained from the LHrc EoS from Chapter 3. Since, in contrary to our analysis from Chapters 3 and 5, we are here concerned with softly repulsive fluids, the reference EoS is calculated using the effective segment size that was developed in Chapter 6.

To account for attractive dispersion interactions between the segments of LJ chain molecules, the perturbation contribution from Eq. (7.1) is divided into an isotropic- and anisotropic part, according to

$$a^{\text{pert}} = a^{\text{pert}}_{\text{iso}} + a^{\text{pert}}_{\text{aniso}} \tag{7.2}$$

By definition it follows that

$$a^{\text{pert}}_{\text{aniso}} = \Delta_{\text{I}\to\text{N}|_{\rho,T}} a^{\text{pert}} = a^{\text{pert}} - a^{\text{pert}}_{\text{iso}} \tag{7.3}$$

It is important to note that the anisotropic term defined as such should not be confused with a contribution due to an anisotropic intermolecular potential (as for example in Ref. 19). Instead, it reflects the difference between a nematic and (hypothetical) isotropic fluid of the same density and temperature, as the operator $\Delta_{\text{I}\to\text{N}|_{\rho,T}}$ indicates. The anisotropic contribution therefore solely encompasses the effect of orientational ordering on the attractive Helmholtz energy of a system at fixed density. The density change that accompanies a phase transition from an isotropic to an orientationally ordered (nematic) phase is captured by the isotropic contribution.

The isotropic contribution $a^{\text{pert}}_{\text{iso}}$ is calculated using the 2nd order BH perturbation theory from Chapter 6. Since the BH approach involves no particular assumptions regarding the nature of the phase [55, 126], the same procedure as in Chapter 6 can in principle be applied to nematic fluids. To first order, the anisotropic disper-

sion contribution of a pure fluid is thus calculated as

$$\tilde{a}^{\text{pert}}_{\text{aniso}} = \Delta_{\text{I}\to\text{N}|_{\rho,T}} \tilde{a}^{\text{pert}} = \frac{2\pi\rho}{kT} \sum_{\alpha=1}^{m} \sum_{\beta=1}^{m} \int_{\sigma}^{\infty} u(r) \Delta_{\text{I}\to\text{N}|_{\rho,T}} g^{\text{hc}}_{d,\alpha\beta}(r) r^2 \mathrm{d}r \tag{7.4}$$

As for the isotropic perturbation contribution, we can now introduce an averaged segment-segment rdf (Eq. (6.23)), and by introducing dimensionless quantities $x = r/\sigma$ and $\tilde{u}(x) = u(x\sigma)/\epsilon$, we obtain

$$\tilde{a}^{\text{pert}}_{\text{aniso}} = 2\pi\rho \left(m^2 \frac{\epsilon}{kT} \sigma^3 \right) \Delta_{\text{I}\to\text{N}|_{\rho,T}} I_1 \tag{7.5}$$

$$\Delta_{\text{I}\to\text{N}|_{\rho,T}} I_1 = \int_{1}^{\infty} \tilde{u}(x\sigma) \Delta_{\text{I}\to\text{N}|_{\rho,T}} g^{\text{hc}}_{d}(x\sigma) x^2 \mathrm{d}x \tag{7.6}$$

The integral $\Delta_{\text{I}\to\text{N}|_{\rho,T}} I_1$ over the difference of the correlation function of an isotropic and nematic fluid of the same temperature and density depends on the molecular architecture (m,χ_{R}), density (ρ), temperature (T), and the degree of orientational order of the nematic phase. To proceed, some approximations are required. We take a Van der Waals approach, *i.e.* the dependence of $\Delta_{\text{I}\to\text{N}|_{\rho,T}} I_1$ on temperature is neglected, and the dependence on density is treated at the mean-field level. These approximations are reasonable because the relevant density range is limited and because temperature acts on the rdf of the isotropic and nematic fluid in a similar manner (*i.e.* through the effective segment size). Furthermore, we assume the dependence of $\Delta_{\text{I}\to\text{N}|_{\rho,T}} I_1$ on the degree of orientational order can be decoupled from all other dependencies. Specifically, we assume $\Delta_{\text{I}\to\text{N}|_{\rho,T}} I_1$ scales with the orientational order parameter (S_2) squared. Given that S_2 varies between zero (isotropic phase) and unity (perfect nematic phase), we can expand $\Delta_{\text{I}\to\text{N}|_{\rho,T}} I_1$ in S_2^2, according to

$$\tilde{a}^{\text{pert}}_{\text{aniso}} = -2\pi\rho \left(m^2 \frac{\epsilon}{kT} \sigma^3 \right) a^{\text{mf}} \left\{ \xi_1 S_2^2 + \xi_2 S_2^4 + \xi_3 S_2^6 + \ldots \right\} \tag{7.7}$$

Here, a^{mf} is an mean-field integration constant, and ξ_i are expansion parameters of order i. We analyze the expansion up to first order, leading to the following result for the anisotropic dispersion contribution

$$\tilde{a}^{\text{pert}}_{\text{aniso}} = -2\pi\rho \left(m^2 \frac{\epsilon}{kT} \sigma^3 \right) \xi^{\text{LC}} S_2^2 \tag{7.8}$$

$\xi^{\text{LC}} = a^{\text{mf}} \xi_1$ is a (positive) parameter which can be interpreted as a measure for the effect of orientational ordering on the dispersive Helmholtz energy contribution of a system at a specified density and temperature. In the present work, ξ^{LC} is considered as a constant. In the Onsager Trial Function approximation, the order parameter becomes an explicit function of the variational parameter α, and is calculated as [18]

$$S_2 = 1 - \frac{3\coth(\alpha)}{\alpha} + \frac{3}{\alpha^2} \tag{7.9}$$

Table 7.1: GEMC results for the isotropic-nematic equilibrium of rigid linear LJ 10-mers. We show dimensionless temperature $T^* = kT/\epsilon$, pressure $P^* = P\sigma^3/\epsilon$, isotropic and nematic coexistence densities $\rho^*_{\mathrm{s,I}}$ and $\rho^*_{\mathrm{s,N}}$ (where $\rho^*_s = \rho m \sigma^3$), and the nematic order parameter S_2.

T^*	P^*	$\rho^*_{\mathrm{s,I}}$	$\rho^*_{\mathrm{s,N}}$	S_2
6	0.83	0.420	0.582	0.899
7	1.17	0.423	0.544	0.851
8	1.57	0.439	0.537	0.830
9	1.92	0.438	0.527	0.805
10	2.30	0.444	0.523	0.788

7.4.2. Solving the phase equilibrium

Phase equilibrium between two phases A and B follows from equality of temperature T, pressure P, and chemical potential μ in both phases, according to $T^{\mathrm{A}} = T^{\mathrm{B}}$, $P^{\mathrm{A}} = P^{\mathrm{B}}$, $\mu^{\mathrm{A}} = \mu^{\mathrm{B}}$. The pressure and chemical potential are obtained from the reduced Helmholtz energy $\tilde{a}$ as $\beta P/N = -\left(\partial \tilde{a}/\partial V\right)_{NT}$ and $\beta\mu = \tilde{a} + Z$, where $Z = \beta P/\rho$ is the compressibility factor.

To calculate the pressure and chemical potential of a nematic fluid, one first has to find the equilibrium degree of orientational order, as characterized by α. For a specified temperature and density, α_{eq} follows from a minimization of the total Helmholtz energy, as calculated from Eq. (7.1). It can therefore be obtained self-consistently from the EoS by solving the following non-linear equations

$$\left(\frac{\partial a}{\partial \alpha}\right)_{T\rho,\alpha=\alpha_{\mathrm{eq}}} = 0 \tag{7.10}$$

$$\left(\frac{\partial^2 a}{\partial \alpha^2}\right)_{T\rho,\alpha=\alpha_{\mathrm{eq}}} > 0 \tag{7.11}$$

A modified Newton-Raphson method [194] was used to solve this problem.

7.5 Results and Discussion

7.5.1. Comparison to molecular simulations

For a proper evaluation of the perturbation theory developed in this chapter, GEMC simulations were performed for a system of rigid linear LJ 10-mers at several dimensionless temperatures T^*. The simulation results are presented in Table 7.1. For the temperatures included, the simulations indicate the existence of isotropic-nematic phase equilibrium only. We performed two additional simulations for a lower temperature, $T^* = 4$ and $T^* = 5$. For these temperatures, no stable nematic phase was found. Although the results suggests the formation of a solid or smectic phase; no definite conclusions could be made.

In Fig. 7.1, we compare simulation results to predictions from the perturbation theory. In agreement with simulations, the theory predicts coexistence of isotropic and nematic phases, without the appearance of a vapor-liquid equilibrium. At high temperatures, the effect of the attractive interactions decreases and the isotropic-nematic-equilibrium increasingly resembles that of the corresponding hard-chain fluid of effective segment size d. At lower temperatures, the effect of attractive interactions becomes more pronounced, leading to a significant widening of the phase envelope.

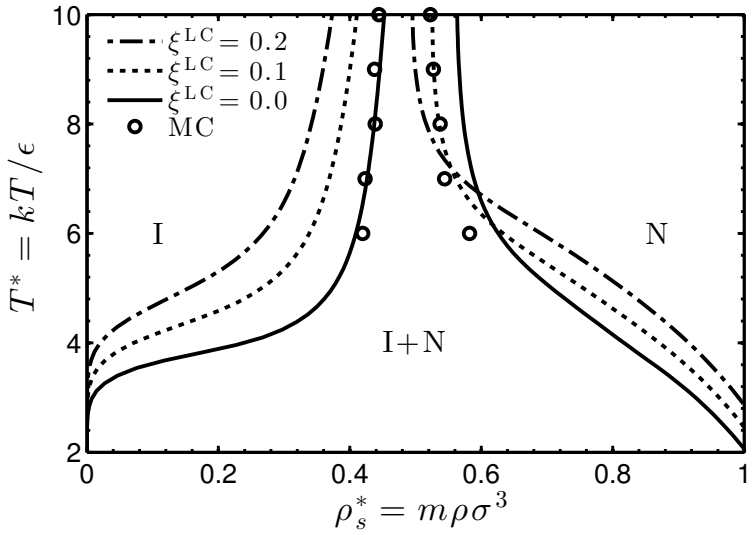

Figure 7.1: The phase diagram of rigid linear LJ 10-mers as obtained the perturbation theory developed in this chapter (lines) for different values of the anisotropic parameter ξ^{LC}. Comparison to results obtained from GEMC simulations (symbols).

To analyse the effect of the anisotropic dispersion contribution on the EoS, theoretical results are included for several values of the anisotropic parameter ξ^{LC}. Our results clearly show that for $\xi^{LC} = 0$, the best agreement between simulations and theory is obtained. For the isotropic coexistence densities, agreement is quantitative. Due to small inaccuracies in the description of the purely repulsive reference system (Chapter 4), nematic coexistence densities and the density difference at the phase transition are slightly overestimated.

A further evaluation of the perturbation theory is included in Fig. 7.2, where we compare predicted isothermal pressures and nematic order parameters (at $T^* = 7$) to results obtained from NPT MC simulations. Agreement between theory and simulations is very satisfactory. As for the isotropic-nematic equilibria, the best agreement is obtained if the anisotropic parameter ξ^{LC} is set to zero. Theoretical results for other values of ξ^{LC} were not included for clarity.

Given the good agreement between simulations and theory for $\xi^{LC} = 0$, we conclude that the difference between the dispersive Helmholtz energy contribution of an isotropic and nematic fluid is mainly caused by the density difference between both phases. The (direct) effect of orientational ordering on the attractive contribution to the EoS (as reflected by ξ^{LC}) is very small, and can be neglected.

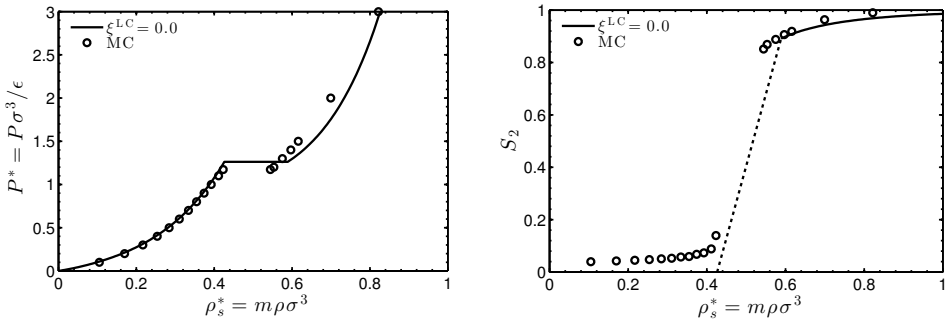

Figure 7.2: Isothermal pressure ($P^* = P\sigma^3/\epsilon$) and nematic order parameter (S_2) of a system of rigid linear LJ 10-mers at a temperature $T^* = 7$, as obtained from the perturbation theory (solid lines) and NPT MC simulations (symbols). The simulated coexistence points were obtained from expanded GEMC simulations. The dotted line connects the isotropic and nematic coexistence points as obtained from the theory. Note that theoretical results are calculated based on the isotropic dispersion contribution only (*i.e.* $\xi^{\mathrm{LC}} = 0.0$).

7.5.2. Theoretical analysis of phase equilibria

We continue with a theoretical analysis of phase equilibria. Given the results from the previous section, only the isotropic perturbation contribution is considered ($\xi^{\mathrm{LC}} = 0$).

In Fig. 7.3, we show a typical phase diagram. The system under consideration is a rigid linear LJ 5-mer. Three types of phase equilibria are observed. At high temperatures, the effect of the attractive intermolecular interactions is negligible; hence, in analogy to systems of purely repulsive molecules [52, 140, 146], only an isotropic-nematic equilibrium is present. As the temperature is decreased, the attractions become more prominent, leading to a widening of the isotropic-nematic region. Moreover, the attractions between the molecules stabilize the nematic phase, thereby shifting the isotropic-nematic transition to lower densities. The soft repulsion of the molecules (as described by the effective segment size $d(T^*, m, \rho_s^*)$) enhances this effect. At lower temperatures a vapor-liquid equilibrium appears. When the temperature is decreased further, the vapor-liquid and liquid-nematic equilibria coincide, leading to a vapor-liquid-nematic triple point. At temperatures below the triple point, only a stable vapor-nematic equilibrium is obtained. Using the classification scheme of Varga *et al.* [266], the phase behaviour sketched in Fig. 7.3 is defined as Type I behaviour. Other systems for which Type I behaviour was predicted from theory are, for example, hard spherocylinders- [195, 267], hard ellipsoids- [266, 267], and hard disks equipped with isotropic square-well attractions [20]. Type I behaviour was also observed in molecular simulation studies of Gay-Berne fluids [268] or solutions of hard rod-like colloids in a solvent of spherical, ideal polymer particles. Effectively, these colloid-polymer systems can be considered as pseudo one-component systems of attractive colloids due to polymer-induced depletion interactions [94].

In Fig. 7.4, we analyze the effect of the chain length m on the phase equilibria of rigid linear LJ chain fluids. An increase in chain length results in an increase

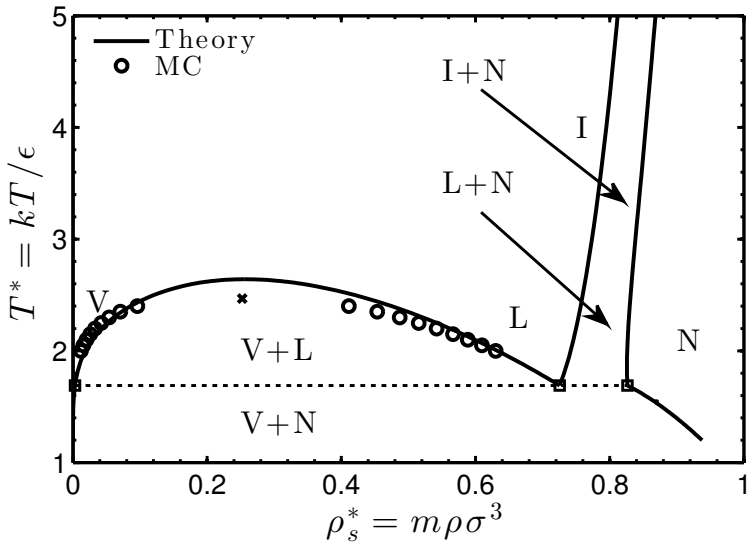

Figure 7.3: The vapor-liquid (VL), liquid-nematic (LN), isotropic-nematic (IN) and vapor-nematic (VN) equilibria of a system of rigid linear LJ 5-mers. Lines are results from the theory developed in this work ($\xi_{\mathrm{LC}} = 0$), symbols are MC data for VLE from Chapter 6. The vapor-liquid critical point estimated from the MC data is drawn by the cross. The VLN triple point as obtained from the theory is denoted by the squares, which are connected by the dotted line. We should stress that the theory does not include a description of solid or smectic phases. In fact, for the system analyzed here, the LNE is most likely metastable with respect to a liquid-solid equilibrium [216].

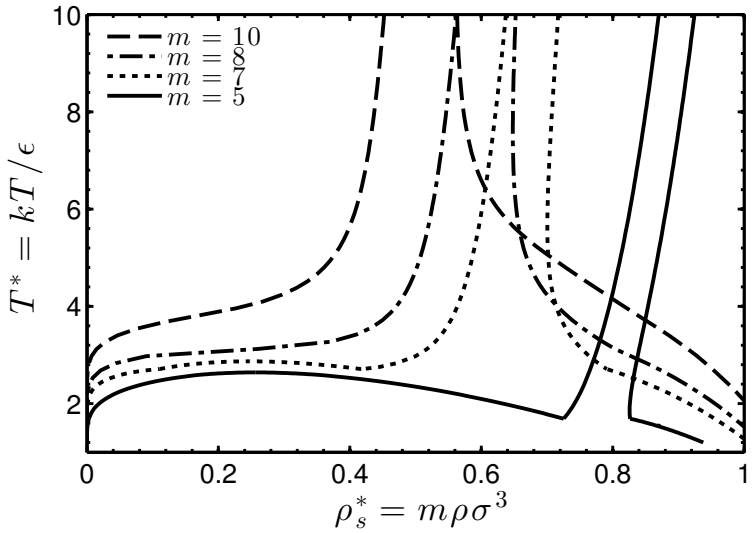

Figure 7.4: The effect of chain length m on the phase diagram of rigid linear LJ chain fluids ($\xi_{\mathrm{LC}} = 0$). Phase equilibria as in Figs. 7.1 and 7.3.

of the vapor-liquid-nematic triple-point temperature. The reason is a stabilization of the nematic phase, resulting from an increased anisotropy of the pair-excluded volume of the molecules. The vapor-liquid critical temperature is less affected by the increase in chain length. Therefore, beyond a certain chain length, the vapor-liquid equilibrium becomes metastable and a single isotropic-nematic equilibrium is obtained. Disappearing (metastable) vapor-liquid equilibria were predicted in several previous theoretical studies on pure-component systems of attractive mesogens [20, 20, 162, 195, 266, 267] and this phase diagram is classified as Type II [266]. Experimentally, Type II behaviour is observed in solutions of polypeptides in DMF [269]. Given that the size of the solvent molecules relative to the polypeptides is very small, these systems can be considered as pseudo one-component systems of attractive macromolecules. Therefore, they present a relevant reference case for our present discussion on pure-component systems. Also, Type II behaviour was confirmed by molecular simulations of hard spherocylinders with polymer induced attractive interactions [94].

When the chain length is increased to very large values (~ 35), an additional nematic-nematic equilibrium arises at the high-temperature part of the phase diagram (see Fig. 7.5). The reason is that, due to the large anisotropy of the molecules, the nematic phase forms at very low density. As a result, the mechanism that normally underlies the vapor-liquid equilibrium, *i.e.* condensation, can now prevail in the anisotropic part of the phase diagram, leading to an equilibrium between a low- and high-density nematic phase. The nematic-nematic equilibrium can thus be interpreted as a Van der Waals-like "vapor-liquid" equilibrium in the anisotropic phase. This type of behaviour, referred to as Type III behaviour [266], was initially predicted from a lattice theory for solutions of rigid polymers by Flory and co-workers [13, 270]. Later, the same behaviour was predicted from several Onsager-based approaches [20, 162, 195, 266, 267]. Experimentally, the existence of Type III behaviour is observed for solutions of poly(γ-benzyl-L-glutamate) (PBLG) [269, 271, 272], -polysaccharide Schizophyllan [273, 274], and -hexa-alkylbenzene derivatives of discotic LCs [275]. Very recently, Wu *et al.* [20] successfully used a coarse-grained representation for PBLG in the framework of an Onsager-Van der Waals theory to correlate the experimental data of the system of PBLG in dimethylformamide [269].

In Fig. 7.6, we analyze the effect of intramolecular flexibility on the phase behaviour by comparing the phase diagram of a rigid linear LJ 10-mer, a 10-9 rod-coil, a 10-8 rod-coil and a 10-7 rod-coil. It can be observed that on making the molecules partially flexible, the nematic phase is destabilized and therefore shifted to higher density. The reason is a less anisotropic pair-excluded volume of molecules of increased flexibility (Chapter 2). Another aspect that can be observed is that the density difference at the isotropic-nematic equilibrium (for specified T^*) decreases with increased flexibility of the chains. The same result was found in Chapter 4 for systems of purely repulsive chain molecules.

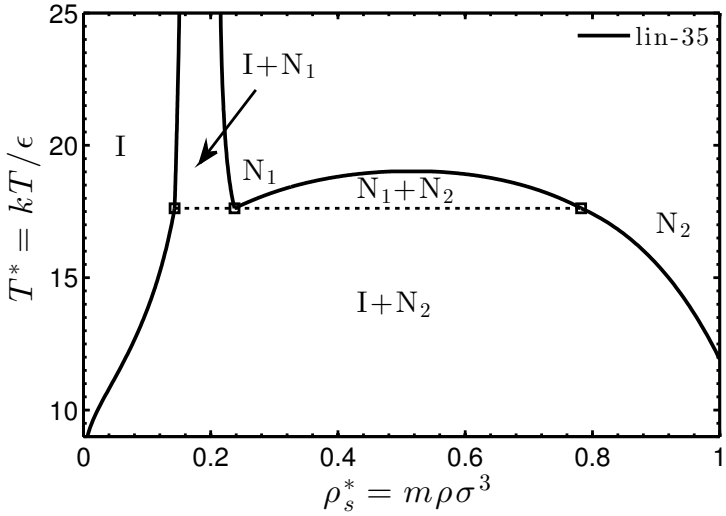

Figure 7.5: The phase diagram of a rigid linear LJ 35-mer ($\xi_{\mathrm{LC}} = 0$). Due to the large chain length, a phase equilibrium between two nematic phases (N_1 and N_2) is established. The isotropic-nematic-nematic (I-N_1N_2) triple point is denoted by the squares, which are connected by the dotted line.

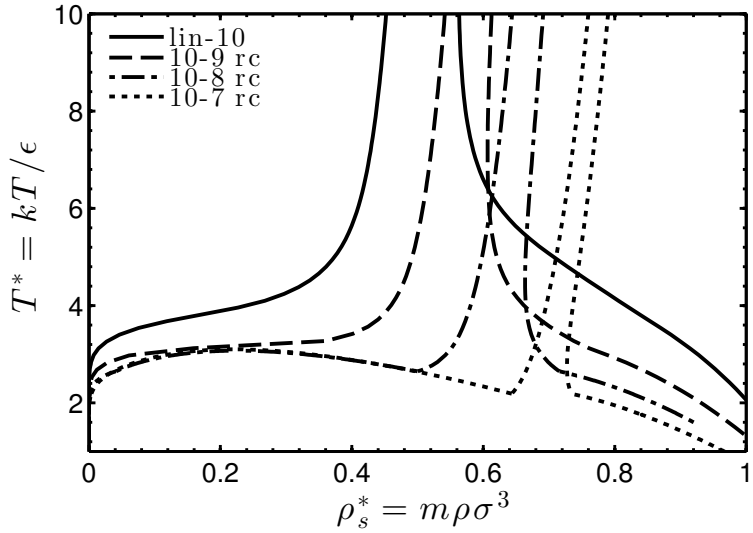

Figure 7.6: The effect of partial molecular flexibility on the phase diagram of LJ m-m_{R} rod-coil fluids ($\xi_{\mathrm{LC}} = 0$). With increasing flexibility of the molecules, the isotropic-nematic equilibrium is destabilized and shifted to higher densities. Moreover, the density difference at the isotropic-nematic phase transition decreases with increased flexibility of the chains. Phase equilibria as in Figs. 7.1 and 7.3.

7.6 Conclusion

We developed an EoS for describing the isotropic-nematic phase equilibrium of LJ chain fluids. The EoS was developed by combining the EoS for the hard-chain reference fluid from Chapters 4-5 with the isotropic dispersion contribution from Chapter 6. Theoretical results for the isotropic-nematic equilibrium of rigid linear LJ 10-mers were compared to results obtained from expanded NVT GEMC simulations. Excellent agreement was observed. The perturbation contribution of an orientationally ordered phase is in our approach expressed as that of a (hypothetical) randomly oriented fluid of same density, plus an anisotropic part, namely the Helmholtz energy contribution for the transition from the randomly oriented fluid to the ordered fluid at constant density. Our study shows, that the anisotropic part is small and can be neglected. This result implies that a reliable description of the dispersion interactions of real nematic LCs can be obtained from a theoretical approach designed for isotropic fluids, such as a (PC-)SAFT approach [65, 66, 72]. Given the relative maturity of such isotropic-fluid theories, this could lead to a considerable simplification of the description of anisotropic fluids. Other types of interactions, which clearly depend on the orientation of molecules, such as multipolar interactions, could be added as a separate contribution to the EoS (*e.g.* along the lines of Ref. 19).

Appendix A: The excluded volume for chains of different length

In this appendix, we derive an equation for the excluded volume of two linear homonuclear tangent hard sphere chains of arbitrary chain length m_1 and m_2 and segment size σ. The starting point is the result of Williamson and Jackson [118] for the excluded volume of linear chains of equal chain length m from Eq. (2.12). Central in their analysis is a decomposition of the excluded volume of two chains with perpendicular orientation (*i.e.* $\gamma = \pi/2$) into a central part and the excluded volume of the chains in a parallel orientation (*i.e.* $\gamma = 0$), where the latter is available in analytical form. For values of γ between the parallel and perpendicular limits the decomposition is still valid, however for this case the volume of the central part is a function of γ, *i.e.*

$$V_{\mathrm{ex}}(\gamma, m) = V_{\mathrm{ex}}^{||}(m) + V_{\mathrm{c}}(\gamma, m) \tag{7.12}$$

From a graphical representation of the excluded volume (see Figs. 4 (a), 4 (b) and 5 of Ref. [118] for details) Williamson and Jackson show that the volume of the central region is equal to $(m-1)^2$ times the central region of the corresponding excluded volume of two dimers $V_{\mathrm{c}}(\gamma; m = 2)$ [118]. Since the exact expression of $V_{\mathrm{c}}(\gamma; m = 2)$ involves some lengthy integrals, a simple linear function of $\sin(\gamma)$ was fitted to the numerical results to obtain

$$V_{\mathrm{c}}(\gamma, m) = 3.5339(m-1)^2 \sin(\gamma) \tag{7.13}$$

For chains of arbitrary chain length m_1 and m_2, one can easily see from Fig. 5 of Ref. [118] that the central region should correspond to $(m_1 - 1)(m_2 - 1)$ times the central region of the dimers, leading to

$$V_{\mathrm{c}}(\gamma, m_1, m_2) = 3.5339(m_1 - 1)(m_2 - 1) \sin(\gamma) \tag{7.14}$$

Eq. (7.13) is a special case of this general result for mixtures.

For the parallel orientation, the excluded volume (large overlapping spheres of diameter 2σ) of several pairs of linear chains (small spheres of diameter σ) is shown in Fig. A.1 . The volume of the overlap region of the large spheres, marked in gray, is identical for all cases and, as derived by Williamson and Jackson, is given by

$$V_{\mathrm{overlap}} = \frac{5}{2} V_s \tag{7.15}$$

Here, V_s is the volume of a sphere of diameter σ. Fig. A.1 shows that the excluded volume of two linear chains in a parallel orientation depends on the average chain length $\bar{m}_{12}$ (Eq. (2.21)) rather than on m_1 and m_2 separately, and we find a general $\bar{m}_{12}$-dependence as

$$V_{\mathrm{ex}}^{||}(\bar{m}_{12}) = (2\bar{m}_{12} - 1)V_S - 2(\bar{m}_{12} - 1)V_{\mathrm{overlap}} \tag{7.16}$$

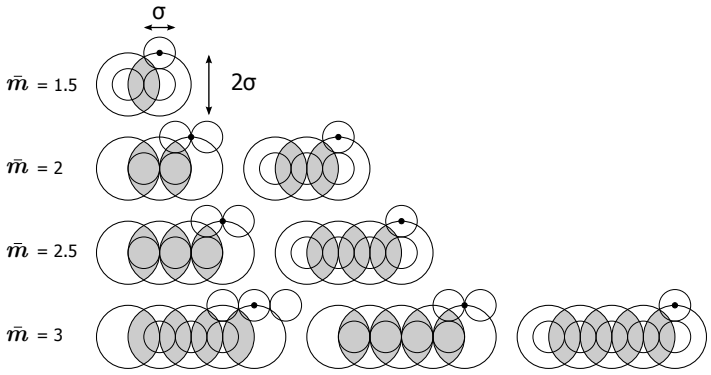

Figure A.1: The pair-excluded volume of linear homonuclear tangent hard-sphere chains (of segments size σ) in a parallel orientation for different average chain lengths $\bar{m}_{12}$ (Eq. (2.21)). The large overlapping spheres with diameter 2σ (overlap region marked gray) make up the excluded volume.

Here $V_S = 8V_s$ is the volume of the large spheres that make up the excluded volume. Using Eq. (7.15) we obtain the exact result

$$\frac{V_{\text{ex}}^{||}(\bar{m}_{12})}{V_{\bar{m}_{12}}} = \frac{11\bar{m}_{12} - 3}{\bar{m}_{12}} \tag{7.17}$$

where $V_{\bar{m}_{12}}$ is the molecular volume of a chain of $\bar{m}_{12}$ spheres of diameter σ. The final result for the excluded volume of two chains of arbitrary chain length m_1 and m_2 is then

$$\frac{V_{\text{ex}}(\gamma)}{V_{\bar{m}_{12}}} = \frac{11\bar{m}_{12} - 3}{\bar{m}_{12}} + 3.5339\frac{(m_1 - 1)(m_2 - 1)}{\bar{m}_{12}}\sin(\gamma) \tag{7.18}$$

It is important to note that we have not introduced any approximations in extending Eq. (2.12) to this general result for mixtures.

Appendix B: A recursive TPT2 EoS for partially flexible chains

To use TPT2 to describe partially flexible chain fluids, we combined the recursive TPT2 equation that was developed by Phan *et al.* [137] with the work of Müller and Gubbins [134] on the triplet correlation function. For clarity, we give a brief summary of the equations in this section.

As shown by Phan *et al.* [137], the chain contribution of TPT2 can be obtained from that of TPT1 [63] upon adding an additional term:

$$\frac{A^{\mathrm{ch}}_{\mathrm{TPT2}}}{NkT} = \frac{A^{\mathrm{ch}}_{\mathrm{TPT1}}}{NkT} - \sum_{i}^{N_C} x_i \ln[J_2(m_i, \boldsymbol{\lambda}_i)] \tag{7.19}$$

Here, J_2 is a quantity that includes the three-body correlations in a fluid (in the terminology of Phan *et al.* [137] it is defined as $I_2(M)/g(\sigma)^{M-1}$). The $\boldsymbol{\lambda}_i$-vector effectively contains the triplet correlation function of all $m-2$ triplets in a chain of component i. For a specific triplet j with a rigid bond-angle θ_b, λ_j is given by [134]

$$\lambda_j^{\mathrm{rig}} = \frac{g^{(3)}_{\mathrm{hs}}(\sigma, \sigma, 2\sigma \sin(\theta_b/2))}{[g_{\mathrm{hs}}(\sigma)]^2} - 1 \tag{7.20}$$

Here, $g^{(3)}_{\mathrm{hs}}$ is the triplet correlation function of three tangentially bonded hard spheres of diameter σ. Since it is generally difficult to obtain $g^{(3)}_{\mathrm{hs}}$, Müller and Gubbins [134] defined a different triplet correlation function g_0 as

$$g_0 = \frac{g^{(3)}_{\mathrm{hs}}(\sigma, \sigma, 2\sigma \sin(\theta_b/2))}{[g_{\mathrm{hs}}(\sigma)]^2} \tag{7.21}$$

Based on an integral equation approach of Attard [276], Attard and Stell [277] reported tabulated values for g_0 which were correlated by Müller and Gubbins [134] using the following analytical expression

$$g_0 = \frac{1 + a\eta + b\eta^2}{(1-\eta)^3} \tag{7.22}$$

Here, a and b depend on the bond-angle θ_b. For a bond-angle of 180°, $a = -2.9643$ and $b = 2.5575$. For other bond-angles, the values of a and b were tabulated by Müller and Gubbins [134]. For fully flexible bonds, λ_j is calculated as [134]

$$\lambda_j^{\mathrm{flex}} = \frac{2}{3} \int_{\pi/3}^{\pi} \lambda_i^{\mathrm{rig}} \sin(\theta_b) d\theta_b \tag{7.23}$$

Using Eqs. (7.20)-(7.22), Müller and Gubbins [134] evaluated the above integral numerically and fitted the results to the following function

$$\lambda_j^{\mathrm{flex}} = 0.233633\eta(1 + 0.472\eta) \tag{7.24}$$

This function can be used for a packing fraction up to 0.47. For the case that all triplets in all chain molecules in the mixture are bound by the same flexibility constraints (*i.e.* $\lambda_j = \lambda$), $J_2(m_i, \boldsymbol{\lambda}_i)$ can be calculated as [137]

$$J_2(m_i, \lambda) = \frac{1}{\sqrt{1+4\lambda}} \left[\left(\frac{1+\sqrt{1+4\lambda}}{2} \right)^{m_i} - \left(\frac{1-\sqrt{1+4\lambda}}{2} \right)^{m_i} \right] \tag{7.25}$$

When this is substituted in Eq. (7.19), the common algebraic form of TPT2 is retained. In Chapter 3, this algebraic form is used to describe linear or fully flexible m-mers. For the more general case, where different flexibility constraints can be defined for all bond-angles in a molecule, Phan *et al.* showed that $J_2(m_i, \boldsymbol{\lambda}_i)$ is calculated from [137]

$$\begin{aligned} J_2(m_i, \lambda_1, \ldots, \lambda_{m_i-2}) &= J_2(m_i - 1, \lambda_1, \ldots, \lambda_{m_i-3}) \\ &\quad + \lambda_{m_i-2} J_2(m_i - 2, \lambda_1, \ldots, \lambda_{m_i-4}) \\ J_2(m = 4, \lambda_1, \lambda_2) &= 1 + \lambda_1 + \lambda_2 \\ J_2(m = 3, \lambda_1) &= 1 + \lambda_1 \\ J_2(m = 2) &= 1 \end{aligned} \tag{7.26}$$

In the main text, the above recursive equation is used to describe partially flexible chain fluids. It can be shown that Eq (7.25) is a special case of this general result.

Appendix C: The decoupling approximation

In this appendix, the Onsager Vega-Lago (OVL) theory is derived based on Parsons' decoupling approximation [49]. Although, originally, Parsons considered rigid molecules (hard rods) only, his method is also perfectly valid for nonrigid chain molecules.

Assuming pairwise additive intermolecular interactions, the compressibility factor $Z = \beta P/\rho$ of an inhomogeneous system of anisotropic, nonrigid chain molecules can be obtained from the pressure equation as [54]

$$Z = 1 - \frac{\beta}{6\rho V} \iiint r_{12} \frac{\partial \phi(\boldsymbol{r}_{12}, \tilde{\boldsymbol{\omega}}_1, \tilde{\boldsymbol{\omega}}_2)}{\partial r_{12}} g(\boldsymbol{r}_{12}, \tilde{\boldsymbol{\omega}}_1, \tilde{\boldsymbol{\omega}}_2) \rho(\tilde{\boldsymbol{r}}_1) \rho(\tilde{\boldsymbol{r}}_2) d\tilde{\boldsymbol{r}}_1 d\tilde{\boldsymbol{r}}_2 \tag{7.27}$$

Here, $g(\boldsymbol{r}_{12}, \tilde{\boldsymbol{\omega}}_1, \tilde{\boldsymbol{\omega}}_2)$ is the pair distribution function of molecules 1 and 2. The intermolecular potential is defined as

$$\phi(\boldsymbol{r}_{12}, \tilde{\boldsymbol{\omega}}_1, \tilde{\boldsymbol{\omega}}_2) = \begin{cases} \infty & \text{when } r_{12} < \sigma(\hat{\boldsymbol{r}}_{12}, \tilde{\boldsymbol{\omega}}_1, \tilde{\boldsymbol{\omega}}_2), \\ 0 & \text{when } r_{12} \geq \sigma(\hat{\boldsymbol{r}}_{12}, \tilde{\boldsymbol{\omega}}_1, \tilde{\boldsymbol{\omega}}_2). \end{cases} \tag{7.28}$$

where $\sigma(\hat{\boldsymbol{r}}_{12}, \tilde{\boldsymbol{\omega}}_1, \tilde{\boldsymbol{\omega}}_2)$ is the conformation-dependent contact distance. This contact distance is a function of the conformations of molecules 1 and 2 and the orientational unit vector $\hat{\boldsymbol{r}}_{12}$ between the molecule's centers of mass.

Since we are concerned with describing nematic phases, the single-molecule density can be factorized into a uniform number density and a conformational distribution as $\rho(\tilde{\boldsymbol{r}}) = \rho f(\tilde{\boldsymbol{\omega}})$ to obtain

$$Z = 1 - \frac{\beta}{6} \rho \iiint r_{12} \frac{\partial \phi(\boldsymbol{r}_{12}, \tilde{\boldsymbol{\omega}}_1, \tilde{\boldsymbol{\omega}}_2)}{\partial r_{12}} g(\boldsymbol{r}_{12}, \tilde{\boldsymbol{\omega}}_1, \tilde{\boldsymbol{\omega}}_2) f(\tilde{\boldsymbol{\omega}}_1) f(\tilde{\boldsymbol{\omega}}_2) d\boldsymbol{r}_{12} d\tilde{\boldsymbol{\omega}}_1 d\tilde{\boldsymbol{\omega}}_1 \tag{7.29}$$

The analogue of Onsager's original second virial theory for nonrigid molecules is obtained from the above equation by inserting the low-density limit of the pair distribution function and integrating the pressure over the volume. To extend the Onsager result to higher densities, Parsons used an improved approximation for the pair distribution function which is usually referred to as the 'decoupling approximation'. By writing both the intermolecular potential and the pair distribution function as a function of a reduced intermolecular separation $y = r_{12}/\sigma(\hat{\boldsymbol{r}}_{12}, \tilde{\boldsymbol{\omega}}_1, \tilde{\boldsymbol{\omega}}_2)$, all translational and conformational dependencies can be decoupled, according to

$$Z = 1 - \frac{\beta}{6} \rho \int y^3 \frac{\partial \phi(y)}{\partial y} g(y) dy \iiint \sigma^3 f(\tilde{\boldsymbol{\omega}}_1) f(\tilde{\boldsymbol{\omega}}_2) d\hat{\boldsymbol{r}}_{12} d\tilde{\boldsymbol{\omega}}_1 d\tilde{\boldsymbol{\omega}}_2 \tag{7.30}$$

The conformational part of this integral can be rewritten in terms of the pair-

excluded volume, by writing

$$V_{\mathrm{ex}}(\tilde{\boldsymbol{\omega}}_1,\tilde{\boldsymbol{\omega}}_2) = \int \left(1-\exp\left[-\beta\phi(\boldsymbol{r}_{12},\tilde{\boldsymbol{\omega}}_1,\tilde{\boldsymbol{\omega}}_2)\right]\right) d\boldsymbol{r}_{12} \tag{7.31}$$
$$= \int_{r_{12}=0}^{r_{12}=\sigma(\hat{\boldsymbol{r}}_{12},\tilde{\boldsymbol{\omega}}_1,\tilde{\boldsymbol{\omega}}_2)} \int r_{12}^2 dr_{12} d\hat{\boldsymbol{r}}_{12}$$
$$= \frac{1}{3}\int \sigma(\hat{\boldsymbol{r}}_{12},\tilde{\boldsymbol{\omega}}_1,\tilde{\boldsymbol{\omega}}_2)^3 d\hat{\boldsymbol{r}}_{12}$$

To deal with the discontinuity of the intermolecular potential in the translational integral, a cavity correlation function $Y(y) = g(y)\exp(\beta\phi)$ can be introduced as [54]

$$\int y^3 \frac{\partial\phi(y)}{\partial y} g(y) dy = -\frac{1}{\beta}\int y^3 \frac{\partial \exp(-\beta\phi(y))}{\partial y} Y(y) dy \tag{7.32}$$

For the hard, purely repulsive molecules considered in this work, the Boltzmann factor is a Heaviside step-function, the derivative of which is a Dirac delta function. Accordingly, the translational integral can be reduced to

$$\int y^3 \frac{\partial\phi(y)}{\partial y} g(y) dy = -\frac{1}{\beta} g(1^+) \tag{7.33}$$

Here, $g(1^+)$ is the value of the pair distribution function in the limit of contact approaching from above (contact value theorem) [54]. Inserting Eqs. (7.31) and (7.33) in Eq. (7.30) one obtains

$$Z = 1 + \frac{1}{2}\rho g(1^+) \iiint V_{\mathrm{ex}}(\tilde{\boldsymbol{\omega}}_1,\tilde{\boldsymbol{\omega}}_2) f(\tilde{\boldsymbol{\omega}}_1) f(\tilde{\boldsymbol{\omega}}_2) d\tilde{\boldsymbol{\omega}}_1 d\tilde{\boldsymbol{\omega}}_2 \tag{7.34}$$

Using Eq. (2.6), this result can be recast in the form of a virial

$$Z = 1 + g(1^+) B_2[f(\tilde{\boldsymbol{\omega}})]\rho \tag{7.35}$$

Finally, integration over density gives the residual Helmholtz energy

$$\frac{\beta A^{\mathrm{res}}}{N} = \int \frac{Z-1}{\rho} d\rho$$
$$= B_2[f(\tilde{\boldsymbol{\omega}})] \int g(1^+) d\rho \tag{7.36}$$

Let us now assume that $g(1^+)$ of the system being described can be approximated by that of a reference system of the same molecular volume at the same packing fraction. Assuming the virial from Eq. (7.40) is valid for the given reference system (note that this is only exact for a system of hard spheres) we can write

$$g(1^+) \approx g_{\mathrm{ref}}(1^+) = \left(\frac{Z_{\mathrm{ref}}-1}{\rho}\right)\frac{1}{B_{2,\mathrm{ref}}} \tag{7.37}$$

Substitution in Eq. (7.40) and integrating the compressibility leads to the following result for the residual Helmholtz energy of a nematic fluid

$$\frac{\beta A^{\mathrm{res}}}{N} = \frac{\beta A^{\mathrm{res}}_{\mathrm{ref}}}{N}\frac{B_2[f(\tilde{\boldsymbol{\omega}})]}{B_{2,\mathrm{ref}}} \tag{7.38}$$

Appendix D: Generalization of the Onsager-Vega-Lago theory to mixtures

In this appendix, the mixture version of the OVL theory, as presented in Sec. 5.2, is derived based on Parsons' decoupling approximation [49]. Starting from the pressure equation for mixtures of nonrigid chain molecules [54], one can follow the same derivation as presented in Appendix C for pure-component systems, and use the decoupling approximation to derive the following virial for the compressibility factor of a nematic fluid mixture

$$Z = 1 + \sum_i \sum_j x_i x_j g_{ij}(1^+) B_{2,ij}[f(\boldsymbol{\omega})]\rho \tag{7.39}$$

Here, $g_{ij}(1^+)$ is the radial distribution function (rdf) of two molecules of type i and j at contact. We now introduce an averaged rdf $g_{\rm av}(1^+)$, according to

$$Z = 1 + g_{\rm av}(1^+) \sum_i \sum_j x_i x_j B_{2,ij}[f(\boldsymbol{\omega})]\rho \tag{7.40}$$

$$= 1 + g_{\rm av}(1^+) \bar{B}_2\left[f(\boldsymbol{\omega})\right] \rho \tag{7.41}$$

Assuming $g_{\rm av}(1^+)$ of the nematic fluid can be approximated by that of the isotropic fluid at the same density, one can write

$$g_{\rm av}(1^+) \approx g_{\rm av,iso}(1^+) = \left(\frac{Z_{\rm iso} - 1}{\rho}\right) \frac{1}{\bar{B}_{2,\rm iso}} \tag{7.42}$$

which, when substituted in Eq. (7.40), leads to a generalized OVL theory for nematic fluid mixtures, according to

$$Z = 1 + Z_{\rm iso}^{\rm res} \frac{\bar{B}_2\left[f(\boldsymbol{\omega})\right]}{\bar{B}_{2,\rm iso}} \tag{7.43}$$

It is important to note that, compared to pure component systems, the above derived result for mixtures is more approximate. The reason is that, due to the averaging of the rdf over all components in the mixture, part of the many-fluid behavior is lost. The accurate comparison of theory and molecular simulation results obtained in this work (see Sec. 5.3.1 and 5.3.3), however, suggests that the larger part of this behavior is retained by considering all individual pair-interactions of the fluid mixture in the second virial coefficient.

Bibliography

[1] G. R. Luckhurst and G. W. Gray, *Molecular physics of liquid crystals* (Academic Press, London, 1979).

[2] S. Chandrasekhar, *Liquid crystals*, 2nd ed. (Cambridge University Press, Cambridge, 1992).

[3] P. G. de Gennes and J. Prost, *The physics of liquid crystals*, 2nd ed. (Oxford University Press, Oxford, 1993).

[4] P. J. Collings, *Liquid crystals. Nature's delicate phase of matter*, 2nd ed. (Princeton University Press, Princeton, 2002).

[5] C. M. Care and D. J. Cleaver, Computer simulation of liquid crystals, Rep. Prog. Phys. **68**, 2665 (2005).

[6] H. Zocher, Uber freiwillige Strukturbildung in Solen, Z. Anorg. Chem. **147**, 91 (1925).

[7] F. C. Bawden, N. W. Pirie, J. D. Bernal, and I. Frankuchen, Liquid crystalline substances from virus-infected plants, Nature **138**, 1051 (1936).

[8] I. Langmuir, The role of attractive and repulsive forces in the formation of tactoids, thixotropic gels, protein crystals and coacervates, J. Chem. Phys. **6**, 873 (1938).

[9] L. Onsager, The effect of shape on the interaction of colloidal particles, Ann. N.Y. Acad. Sci. **51**, 627 (1949).

[10] W. Maier and Z. Saupe, Eine einfache molekulare Theorie des nematischen kristallinflüssigen Zustandes, Naturforsch. **13a**, 564 (1958).

[11] W. Maier and Z. Saupe, Eine einfache molekular statistische Theorie der nematischen kristallinflüssigen Phase. Teil I., Naturforsch. **14a**, 882 (1959).

[12] W. Maier and Z. Saupe, Eine einfache molekular statistische Theorie der nematischen kristallinflüssigen Phase. Teil II., Naturforsch. **15a**, 287 (1960).

[13] P. J. Flory, Phase equilibria in solutions of rod-like particles, Proc. R. Soc. Lond. A **234**, 73 (2012).

[14] W. M. Gelbart and B. A. Baron, Generalized van der Waals theory of the isotropic–nematic phase transition, J. Chem. Phys. **66**, 207 (1977).

[15] B. A. Baron and W. M. Gelbart, Molecular shape and volume effects on the orientational ordering of simple liquid crystals, J. Chem. Phys. **67**, 5795 (1977).

[16] M. A. Cotter, Hard spherocylinders in an anisotropic mean field: simple model for a nematic liquid crystal, J. Chem. Phys. **66**, 1098 (1977).

[17] M. A. Cotter, Generalized van der Waals theory of nematic liquid crystals: an alternative formulation, J. Chem. Phys. **66**, 4710 (1977).

[18] M. Franco-Melgar, A. J. Haslam, and G. Jackson, A generalisation of the Onsager trial-function approach: describing nematic liquid crystals with an algebraic equation of state, Mol. Phys. **106**, 649 (2008).

[19] M. Franco-Melgar, A. J. Haslam, and G. Jackson, Advances in generalised van der Waals approaches for the isotropic-nematic fluid phase equilibria of thermotropic liquid crystals-an algebraic equation of state for attractive anisotropic particles with the Onsager trial function, Mol. Phys. **107**, 2329 (2009).

[20] L. Wu, G. Jackson, and E. A. Müller, Liquid crystal phase behaviour of attractive disc-like particles, Int. J. Mol. Sci. **14**, 16414 (2013).

[21] L. Wu, E. A. Müller, and G. Jackson, Understanding and describing the liquid-crystalline states of polypeptide solutions: a coarse-grained model of PBLG in DMF, Macromolecules **47**, 1482 (2014).

[22] C. Blanc, D. Coursault, and E. Lacaze, Ordering nano- and microparticles assemblies with liquid crystals, Liquid Crystal Reviews **1**, 83 (2013).

[23] J. Gross and P. Jansens, A method for the removal of a gas from a process gas stream by means of liquid crystals, patent application: "Wo2008147181-a1/nl2000654-c2" (2008).

[24] M. de Groen, T. J. H. Vlugt, and T. W. de Loos, Phase behavior of liquid crystals with CO_2, J. Phys. Chem. B **116**, 9101 (2012).

[25] M. de Groen, H. Matsuda, T. J. H. Vlugt, and T. W. de Loos, Phase behaviour of the system 4'-pentyloxy-4-cyanobiphenyl + CO_2, J. Chem. Thermodynamics **59**, 20 (2013).

[26] M. de Groen, B. C. Ramaker, T. J. H. Vlugt, and T. W. de Loos, Phase behavior of liquid crystal + CO_2 mixtures, J. Chem. Eng. Data **116**, 9101 (2012).

[27] G. T. Rochelle, Amine scrubbing for CO_2 capture, Science **325**, 1652 (2009).

[28] P. D. Vaidya and E. Y. Kenig, CO_2-alkanolamine reaction kinetics: a review of recent studies, Chem. Eng. Technol. **30**, 1467 (2007).

[29] B. Smit, J. R. Reimer, C. M. Oldenburg, and I. C. Bourg, *Introduction to carbon capture and sequestration* (Imperial College Press, London, 2014).

[30] J. D. Seader and E. J. Henley, *Separation process principles*, 2nd ed. (Wiley, Hoboken, 2006).

[31] *Gas sweetening* (Dow Chemical Company, Midland, 1998).

[32] G. W. Gray, *Thermotropic liquid crystals* (John Wiley & Sons, Chichester, 1987).

[33] T. van Westen, T. J. H. Vlugt, and J. Gross, The isotropic-nematic and nematic-nematic phase transition of binary mixtures of tangent hard-sphere chain fluids: an analytical equation of state, J. Chem. Phys. **140**, 034504 (2014).

[34] B. Oyarzún, T. van Westen, and T. J. H. Vlugt, Isotropic-nematic phase equilibria of hard-sphere chain fluids - pure components and binary mixtures, J. Chem. Phys. **142**, 064903 (2015).

[35] M. de Groen, T. J. H. Vlugt, and T. W. de Loos, Binary and ternary mixtures of liquid crystals with CO_2, submitted to AIChE J. (2015).

[36] O. Odele and S. Macchietto, Computer aided molecular design: a novel method for optimal solvent selection, Fluid Phase Equilibria **82**, 47 (1993).

[37] F. E. Pereira, E. Keskes, A. Galindo, G. Jackson, and C. S. Adjiman, Integrated solvent and process design using a SAFT-VR thermodynamic description: High-pressure separation of carbon dioxide and methane, Computers and Chemical Engineering **35**, 474 (2011).

[38] A. Bardow, K. Steur, and J. Gross, Continuous-molecular targeting for integrated solvent and process design, Ind. Eng. Chem. Res. **49**, 2834 (2010).

[39] B. Oyarzún, A. Bardow, and J. Gross, Integration of process and solvent design towards a novel generation of CO_2 absorption capture systems, Energy Procedia **4**, 282 (2011).

[40] C. S. Adjiman, A. Galindo, and G. Jackson, Molecules matter: The expanding envelope of process design, Proceedings of the 8th International Conference on Foundations of Computer-Aided Process Design **35**, 55 (2014).

[41] L. Lin, A. H. Berger, R. L. Martin, J. Kim, J. A. Swisher, K. Jariwala, C. H. Rycroft, A. S. Bhown, M. W. Deem, M. Haranczyk, and B. Smit, In *silico* screening of carbon-capture materials, Nature Materials **11**, 633 (2012).

[42] J. Kim, L. Lin, J. K. Stolaroff, B. Smit, and R. D. Aines, New materials for methane capture from dilute and medium-concentration sources, Nature Communications **4**, 1694 (2013).

[43] P. J. Collings and M. Hird, *Introduction to liquid crystals* (Taylor & Francis, Bristol, 1997).

[44] L. D. Landau and E. M. Lifshitz, *Statistical phyiscs*, 3rd ed. (Pergamon, New York, 1980).

[45] S. I. Sandler, *An introduction to applied statistical thermodynamics* (Wiley, Hoboken, 2011).

[46] R. G. Horn and T. E. Faber, Alignment in nematic liquid crystals: a comparison between the results of experiments at high pressure and predictions based on mean field theories, Naturforsch. **368**, 199 (1979).

[47] T. Hino and J. M. Prausnitz, A perturbed hard-sphere-chain equation of state for nematic liquid crystals and their mixtures with polymers, Liquid Crystals **22**, 317 (1997).

[48] J. E. Mayer and M. G. Mayer, *Statistical Mechanics*, 7th ed. (Wiley, New York, 1940) Chap. 13.

[49] J. Parsons, Nematic ordering in a system of rods, Phys. Rev. A **19**, 1225 (1979).

[50] S. D. Lee, A numerical investigation of nematic ordering based on a simple hard-rod model, J. Chem. Phys. **87**, 4972 (1987).

[51] S. D. Lee, The Onsager-type theory for nematic ordering of finite-length hard ellipsoids, J. Chem. Phys. **89**, 7036 (1988).

[52] C. Vega and S. Lago, Isotropic-nematic transition of hard polar and nonpolar molecules, J. Chem. Phys. **100**, 6727 (1994).

[53] T. Boublík, C. Vega, and M. Diaz-Penã, Equation of state of chain molecules, J. Chem. Phys. **93**, 730 (1990).

[54] J. P. Hansen and I. R. McDonald, *Theory of simple liquids*, 3rd ed. (Academic Press, London, 2006).

[55] J. A. Barker and D. Henderson, Perturbation theory and equation of state for fluids. II. A succesful theory of liquids, J. Chem. Phys. **47**, 4714 (1967).

[56] M. S. Wertheim, Fluids with highly directional attractive forces. I. Statistical thermodynamics, J. Stat. Phys. **35**, 19 (1984).

[57] M. S. Wertheim, Fluids with highly directional attractive forces. II. Thermodynamic perturbation theory and integral equations, J. Stat. Phys. **35**, 35 (1984).

[58] M. S. Wertheim, Fluids with highly directional attractive forces. III. Multiple attraction sites, J. Stat. Phys. **42**, 459 (1986).

[59] M. S. Wertheim, Fluids with highly directional attractive forces. IV. Equilibrium polymerization, J. Stat. Phys. **42**, 477 (1986).

[60] M. S. Wertheim, Thermodynamic perturbation theory of polymerization, J. Chem. Phys. **87**, 7323 (1987).

[61] W. G. Chapman and K. E. Gubbins, Theory and simulation of associating liquid mixtures, Fluid Phase Equilibria **29**, 337 (1986).

[62] G. Jackson, W. G. Chapman, and K. E. Gubbins, Phase equilibria of associating fluids: spherical molecules with multiple bonding sites, Mol. Phys. **65**, 1 (1988).

[63] W. G. Chapman, G. Jackson, and K. E. Gubbins, Phase equilibria of associating fluids: chain molecules with multiple bonding sites, Mol. Phys. **65**, 1057 (1988).

[64] W. G. Chapman, K. E. Gubbins, G. Jackson, and M. Radosz, New reference equations of state for associating liquids, Ind. Eng. Chem. Res. **29**, 1709 (1990).

[65] E. A. Müller and K. E. Gubbins, Molecular-based equations of state for association fluids: a review of SAFT and related approaches, Ind. Eng. Chem. Res. **40**, 2193 (2001).

[66] S. P. Tan, H. Adidharma, and M. Radosz, Recent advances and applications of statistical associating fluid theory, Ind. Eng. Chem. Res. **47**, 8063 (2008).

[67] F. J. Blas and L. F. Vega, Thermodynamic behaviour of homonuclear and heteronuclear Lennard-Jones chains with association sites from simulation and theory, Mol. Phys. **92**, 135 (1997).

[68] A. Gil-Villegas, A. Galindo, P. J. Whitehead, S. J. Mills, G. Jackson, and A. N. Burgess, Statistical associating fluid theory for chain molecules with attractive potentials of variable range, J. Chem. Phys. **106**, 4168 (1997).

[69] T. Lafitte, D. Bessieres, M. M. Piñeiro, and J. Daridon, Simultaneous estimation of phase behavior and second-derivative properties using the statistical associating fluid theory with variable range approach, J. Chem. Phys. **124**, 024509 (2006).

[70] T. Lafitte, A. Apostolakou, C. Avendãno, A. Galindo, C. S. Adjiman, E. A. Müller, and G. Jackson, Accurate statistical associating fluid theory for chain molecules formed from Mie segments, J. Chem. Phys. **139**, 154504 (2013).

[71] J. Gross and G. Sadowski, Application of perturbation theory to a hard-chain reference fluid: an equation of state for square-well chains, Fluid Phase Equilibria **168**, 183 (2000).

[72] J. Gross and G. Sadowski, Perturbed-Chain SAFT: an equation of state based on a pertubation theory for chain molecules, Ind. Eng. Chem. Res. **40**, 1244 (2001).

[73] L. A. Davies, A. Gil-Villegas, and G. Jackson, Describing the properties of chains of segments interacting via soft-core potentials of variable range with the SAFT-VR approach, International Journal of Thermophysics **19**, 675 (1998).

[74] L. A. Davies, A. Gil-Villegas, G. Jackson, S. Calero, and S. Lago, Phase equilibria of a square-well monomer-dimer mixture: Gibbs ensemble computer simulation and statistical associating fluid theory for potentials of variable range, Phys. Rev. E **57**, 2035 (1998).

[75] W. G. Chapman, K. E. Gubbins, G. Jackson, and M. Radosz, New reference equations of state for associating liquids, Ind. Eng. Chem. Res. **29**, 1709 (1990).

[76] J. Gross and G. Sadowski, Application of the perturbed-chain SAFT equation of state to associating systems, Ind. Eng. Chem. Res. **41**, 5510 (2002).

[77] J. Gross and J. Vrabec, An equation-of-state contribution for polar components: dipolar molecules, AIChE Journal **52**, 1194 (2006).

[78] J. Gross, An equation-of-state contribution for polar components: quadrupolar molecules, AIChE Journal **51**, 2556 (2005).

[79] L. F. Cameretti and G. Sadowski, Modeling of aqueous electrolyte solutions with perturbed-chain statistical associated fluid theory, Ind. Eng. Chem. Res. **44**, 3355 (2005).

[80] J. M. A. Schreckenberg, S. Dufal, A. J. Haslam, C. S. Adjiman, G. Jackson, and A. Galindo, Modelling of the thermodynamic and solvation properties of electrolyte solutions with the statistical associating fluid theory for potentials of variable range, Mol. Phys. **112**, 2339 (2014).

[81] T. van Westen, T. J. H. Vlugt, and J. Gross, Determining force field parameters using a physically based equation of state, J. Phys. Chem. B **115**, 7872–7880 (2011).

[82] C. S. Schacht, T. J. H. Vlugt, and J. Gross, Using an analytic equation of state to obtain quantitative solubilities of CO_2 by molecular simulation, J. Phys. Chem. Lett. **2**, 393 (2011).

[83] C. Avendaño, T. Lafitte, A. Galindo, C. S. Adjiman, G. Jackson, and E. A. Müller, SAFT-γ force field for the simulation of molecular fluids. 1. A single-site coarse grained model of carbon dioxide, J. Phys. Chem. B **115**, 11154 (2011).

[84] T. Lafitte, C. Avendaño, V. Papaioannou, A. Galindo, C. S. Adjiman, G. Jackson, and E. A. Müller, SAFT-γ force field for the simulation of molecular fluids. 3. Coarse grained models of benzene and hetero-group models of n-decylbenzene, Mol. Phys. **110**, 1189 (2012).

[85] A. F. Ghobadi and J. R. Elliott, Adapting SAFT-γ perturbation theory to site-based molecular dynamics simulation. I. Homogeneous fluids, J. Chem. Phys. **139**, 234104 (2013).

[86] M. Dijkstra and D. Frenkel, Simulation study of the isotropic-to-nematic transitions of semiflexible polymers, Phys. Rev. E **51**, 5891 (1995).

[87] M. Franco-Melgar, *Developing a molecular-based equation of state for engineering applications of fluid-phase equilibria and orientational ordering in liquid crystal systems.*, Ph.D. thesis, Imperial College of Science, Technology and Medicine (2006).

[88] T. van Westen, T. J. H. Vlugt, and J. Gross, An analytical approximation for the orientation-dependent excluded volume of tangent hard sphere chains of arbitrary chain length and flexibility, J. Chem. Phys. **37**, 044906 (2012).

[89] G. W. Gray, *Thermotropic liquid crystals* (John Wiley & Sons, Chichester, 1987) Chap. 2.

[90] P. J. Flory, Statistical thermodynamics of semi-flexible chain molecules, Proc. R. Soc. Lond. A **234**, 60 (1956).

[91] J. S. van Duijneveldt and M. P. Allen, Computer simulation study of a flexible-rigid-flexible model for liquid crystals, Mol. Phys. **92**, 855 (1997).

[92] C. McBride, C. Vega, and L. G. MacDowell, Isotropic-nematic phase transition: influence of intramolecular flexibility using a fused hard sphere model, Phys. Rev. E **64**, 011703 (2001).

[93] C. McBride and C. Vega, A Monte Carlo study of the influence of molecular flexibility on the phase diagram of a fused hard sphere model, J. Chem. Phys. **117**, 10370 (2002).

[94] P. Bolhuis and D. Frenkel, Tracing the phase boundaries of hard spherocylinders, J. Chem. Phys. **106**, 666 (1997).

[95] D. Frenkel and R. Eppenga, Monte-Carlo study of the isotropic-nematic transition in a fluid of thin hard disks, Phys. Rev. Lett. **49**, 1089 (1982).

[96] R. Eppenga and D. Frenkel, Monte-Carlo study of the isotropic and nematic phases of infinitely thin hard platelets, Mol. Phys. **52**, 1303 (1984).

[97] D. Frenkel and B. M. Mulder, The hard ellipsoid-of-revolution .1. Monte-Carlo simulations, Mol. Phys. **55**, 1171 (1985).

[98] A. Samborski, G. T. Evans, C. P. Mason, and M. P. Allen, The isotropic to nematic liquid-crystal transition for hard ellipsoids - an Onsager-like theory and computer-simulations, Mol. Phys. **81**, 263 (1994).

[99] C. McBride, M. Wilson, and J. Howard, Molecular dynamics simulations of liquid crystal phases using atomistic potentials, Mol. Phys. **93**, 955 (1998).

[100] A. R. Khokhlov, Liquid crystalline ordering in the solution of semiflexible macromolecules, Phys. Lett. A **68**, 135 (1978).

[101] A. R. Khokhlov and S. A. N., Liquid crystalline ordering in the solution of long persistent chains, Physica A **108**, 546 (1981).

[102] A. R. Khokhlov and S. A. N., Liquid crystalline ordering in the solution of partially flexible macromolecules, Physica A **112**, 605 (1982).

[103] H. Fynewever and A. Yethiraj, Phase behavior of semiflexible tangent hard sphere chains, J. Chem. Phys. **108**, 1636 (1997).

[104] K. M. Jaffer, S. B. Opps, D. E. Sullivan, B. G. Nickel, and L. Mederos, The nematic-isotropic phase transition in semiflexible fused hard-sphere chain fluids, J. Chem. Phys. **114**, 3314 (2001).

[105] P. P. F. Wessels and B. M. Mulder, Nematic homopolymers: from segmented to wormlike chains, Soft Materials **1**, 313 (2003).

[106] R. Diplock, D. E. Sullivan, K. M. Jaffer, and S. B. Opps, Nematic-isotropic phase transition in diblock fused-sphere chain fluids, Phys. Rev. E **69**, 062701 (2004).

[107] P. P. F. Wessels and B. M. Mulder, Isotropic-to-nematic transition in liquid-crystalline heteropolymers: I. Formalism and main-chain liquid-crystalline polymers, J. Phys.: Condens. Matter **18**, 9335 (2006).

[108] T. Jiang and J. Wu, Isotropic-nematic phase transition in athermal solutions of rod-coil diblock copolymers, J. Chem. Phys. **127**, 034902 (2007).

[109] L. Onsager, Minutes of the meeting of the New England section held at Hartford, Connecticut, October 24, 1942, Phys. Rev. **62**, 558 (1942).

[110] M. Dennison, M. Dijkstra, and R. van Roij, Phase diagram and effective shape of semiflexible colloidal rods and biopolymers, Phys. Rev. Lett. **106**, 208302 (2011).

[111] M. Dennison, M. Dijkstra, and R. van Roij, The effects of shape and flexibility on bio-engineered fd-virus suspensions, J. Chem. Phys. **135**, 144106 (2011).

[112] M. G. Martin and J. I. Siepmann, Transferable potentials for phase equilibria. 1. United-atom description of n-alkanes, J. Phys. Chem. B **102**, 2569 (1998).

[113] M. N. Rosenbluth and A. W. Rosenbluth, Monte-Carlo calculation of the average extension of molecular chains, J. Chem. Phys. **23**, 356 (1955).

[114] D. Frenkel and B. Smit, Unexpected length dependence of the solubility of chain molecules, Mol. Phys. **75**, 983 (1992).

[115] D. Frenkel, G. C. A. M. Mooij, and B. Smit, Novel scheme to study structural and thermal properties of continuously deformable molecules, J. Phys.: Condens. Matter **4**, 3053 (1992).

[116] D. Frenkel and B. Smit, *Understanding molecular simulation: from algorithms to applications*, 2nd ed. (Academic Press, San Diego, 2002).

[117] G. J. Vroege and H. N. W. Lekkerkerker, Phase transitions in lyotropic colloidal and polymer liquid crystals, Rep. Prog. Phys. **55**, 1241 (1992).

[118] D. C. Williamson and G. Jackson, Excluded volume for a pair of linear chains of tangent hard spheres with an arbitrary relative orientation, Mol. Phys. **86**, 819 (1995).

[119] T. Kihara, Convex molecules in gaseous and crystalline states, Adv. Chem. Phys. **5**, 147 (1963).

[120] C. Vega and S. Lago, Linear hard sphere models. Virial coefficients and equation of state, Mol. Phys. **82**, 1233 (1994).

[121] T. van Westen, B. Oyarzún, T. J. H. Vlugt, and J. Gross, An equation of state for the isotropic phase of linear, partially flexible and fully flexible tangent hard-sphere chain fluids, Mol. Phys. **112**, 919 (2014).

[122] W. G. Chapman, G. Jackson, and K. E. Gubbins, Phase equilibria of associating fluids: chain molecules with multiple bonding sites, Mol. Phys. **65**, 1057 (1988).

[123] H. G. Honnell and C. K. Hall, A new equation of state for athermal chains, J. Chem. Phys. **90**, 1841 (1989).

[124] Y. Zhou and G. Stell, Chemical association in simple models of molecular and ionic fluids. III. The cavity function, J. Chem. Phys. **96**, 1507 (1992).

[125] Y. Hu, H. Liu, and J. M. Prausnitz, Equation of state for fluids containing chainlike molecules, J. Chem. Phys. **104**, 396 (1996).

[126] J. A. Barker and D. Henderson, Perturbation theory and equation of state for fluids: the square-well potential, J. Chem. Phys. **47**, 2856 (1967).

[127] J. D. Weeks, D. Chandler, and H. C. Andersen, Role of repulsive forces in determining the equilibrium structure of simple liquids, J. Chem. Phys. **54**, 5237 (1971).

[128] H. Liu and Y. Hu, Molecular thermodynamic theory for polymer systems Part II. Equation of state for chain fluids, Fluid Phase Equilibria **122**, 75 (1996).

[129] J. I. Siepmann and D. Frenkel, Configurational bias Monte Carlo: a new sampling scheme for flexible chains, Mol. Phys. **75**, 59 (1992).

[130] D. Frenkel, G. C. A. M. Mooij, and B. Smit, Novel scheme to study structural and thermal properties of continuously deformable molecules, J. Phys.: Condens. Matter **3**, 3053 (1991).

[131] N. F. Carnahan and K. E. Starling, Equation of state for nonattracting rigid spheres, J. Chem. Phys. **51**, 635 (1969).

[132] D. J. Tildesley and W. B. Street, An equation of state for hard dumbell fluids, Mol. Phys. **4**, 85 (1980).

[133] M. D. Amos and G. Jackson, BHS theory and computer simulations of linear heteronuclear triatomic hard-sphere molecules, Mol. Phys. **74**, 191 (1991).

[134] E. A. Müller and K. E. Gubbins, Simulation of hard triatomic and tetratomic molecules, Mol. Phys. **80**, 957 (1993).

[135] A. Yethiraj, K. G. Honnell, and C. K. Hall, Monte Carlo calculation of the osmotic second virial coefficieint of off-lattice athermal polymers, Macromolecules **25**, 3979 (1992).

[136] B. Oyarzún, T. van Westen, and T. J. H. Vlugt, The phase behavior of linear and partially flexible hard-sphere chain fluids and the solubility of hard spheres in hard-sphere chain fluids, J. Chem. Phys. **138**, 204905 (2013).

[137] S. Phan, E. Kierlik, and M. L. Rosinberg, Equations of state for hard chain molecules, J. Chem. Phys. **99**, 5326 (1993).

[138] C. Vega, C. McBride, and L. G. MacDowell, Liquid crystal phase formation for the linear tangent hard sphere model from Monte Carlo simulations, J. Chem. Phys. **115**, 4203 (2001).

[139] H. G. Honnell and C. K. Hall, Theory and simulation of hardchain mixtures: Equations of state, mixing properties, and density profiles near hard walls, J. Chem. Phys. **95**, 4481 (1991).

[140] T. van Westen, B. Oyarzún, T. J. H. Vlugt, and J. Gross, The isotropic-nematic phase transition of tangent hard-sphere chain fluids - pure components, J. Chem. Phys. **139**, 034505 (2013).

[141] X. Wen, R. B. Meyer, and D. L. D. Caspar, Observation of smectic-A ordering in a solution of rigid-rod-like particles, Phys. Rev. Lett. **63**, 2760 (1989).

[142] S. D. Zhang, P. A. Reynolds, and J. S. Duijneveldt, Phase behavior of mixtures of colloidal platelets and nonadsorbing polymers, J. Chem. Phys. **117**, 9947 (2002).

[143] L. Wu, H. H. Wensink, G. Jackson, and E. A. Müller, A generic equation of state for liquid crystalline phase of hard-oblate particles, Mol. Phys. **110**, 1269 (2012).

[144] S. C. McGrother, D. C. Williamson, and G. Jackson, A re-examination of the phase diagram of hard spherocylinders, J. Chem. Phys. **104**, 6755 (1996).

[145] E. de Miguel and E. M. del Río, Equation of state for hard Gaussian overlap particles, J. Chem. Phys. **118**, 1852 (2003).

[146] D. C. Williamson and G. Jackson, Liquid crystalline phase behavior in systems of hard-sphere chains, J. Chem. Phys. **108**, 10294 (1998).

[147] D. Chandler and L. R. Pratt, Nonrigid molecules in condensed phases, J. Chem. Phys. **65**, 2925 (1976).

[148] L. R. Pratt and D. Chandler, Interaction site cluster series for the Helmholtz free energy and variational principle for chemical equilibria and intramolecular structures, J. Chem. Phys. **66**, 147 (1977).

[149] M. A. Cotter and D. E. Martire, Statistical mechanics of rodlike particles. I. A scaled particle treatment of a fluid of perfectly aligned rigid cylinders, J. Chem. Phys. **52**, 1902 (1970).

[150] M. A. Cotter, Hard-rod fluid: Scaled Particle Theory revisited, Phys. Rev. A **10**, 625 (1974).

[151] T. Boublík and I. Nezbeda, Equation of state for hard dumbbells, Ch. Phys. Lett. **46**, 315 (1977).

[152] T. Boublík, The equation of state of linear hard interaction site model fluids, Mol. Phys. **44**, 1369 (1981).

[153] T. Boublík, Equation of state of linear fused hard-sphere models, Mol. Phys. **68**, 191 (1989).

[154] A. Isihara, Theory of anisotropic colloid solutions, J. Chem. Phys. **19**, 1142 (1951).

[155] G. Lasher, Nematic ordering of hard rods derived from a scaled particle treatment, J. Chem. Phys. **53**, 4141 (1970).

[156] J. Herzfeld, A. E. Berger, and J. W. Wingate, A highly convergent algorithm for computing the orientation distribution functions of rodlike particles, Macromolecules **17**, 1718 (1984).

[157] H. N. W. Lekkerkerker, P. Coulon, R. Van Der Haegen, and R. Deblieck, On the isotropic-liquid crystal phase separation in a solution of rodlike particles of different lengths, J. Chem. Phys. **80**, 3427 (1984).

[158] S. Lee and R. B. Meyer, Computations of the phase equilibrium, elastic constants, and viscosities of a hardrod nematic liquid crystal, J. Chem. Phys. **84**, 3443 (1986).

[159] D. Williamson and G. Jackson, Monte Carlo annealing technique for the minimization of the Onsager free energy functional, Mol. Phys. **83**, 603 (1994).

[160] R. W. D. Nickalls, A new approach to solving the cubic: Cardan's solution revealed, The Mathematical Gazette **77**, 354 (1993).

[161] A. Wulf and A. G. De Rocco, Statistical mechanics for long semiflexible molecules: a model for the nematic mesophase, J. Chem. Phys. **55**, 12 (1971).

[162] A. R. Khokhlov and S. A. N., On the theory of liquid-crystalline ordering of polymer chains with limited flexibility, J. Stat. Phys. **38**, 161 (1985).

[163] D. B. Dupré and S. Yang, Liquid crystalline properties of persistent polymer chains, J. Chem. Phys. **94**, 7466 (1991).

[164] M. Esposito and G. T. Evans, Isotropic, nematic and smectic A phases in fluids of hard spherocylinders, Mol. Phys. **83**, 835 (1994).

[165] F. Alavi and F. Feyzi, The equation of state of flexible chains of tangent hard spheres at high-density region from simulation and thermodynamic pertubation theory, J. Chem. Phys. **138**, 024903 (2013).

[166] F. J. Blas, E. Sanz, C. Vega, and A. Galindo, Fluid-solid equilibria of flexible and linear rigid tangent chains from Wertheim's thermodynamic perturbation theory, J. Chem. Phys. **119**, 10958 (2003).

[167] M. Schadt, Liquid crystal materials and liquid crystal displays, Annu. Rev. Mater. Sci. **27**, 305 (1997).

[168] R. Eelkema and B. L. Feringa, Amplification of chirality in liquid crystals, Org. Biomol. Chem. **4**, 3729 (2006).

[169] N. Tamaoki, Cholesteric liquid crystals for color information technology, Adv. Mater. **13**, 1135 (2001).

[170] D. Dutta, A. Fruitwala, A. Kohli, and R. A. Weiss, Polymer blends containing liquid crystals: a review, Polymer Engineering and Science **30**, 1005 (1990).

[171] N. Kapernaum, C. S. Hartley, J. C. Roberts, R. P. Lemieux, and F. Giesselmann, Molecular length distribution and the formation of smectic phases, Beilstein Journal of Organic Chemistry **65**, 1 (2009).

[172] N. Kapernaum, C. S. Hartley, J. C. Roberts, F. Schoerg, D. Krueerke, R. P. Lemieux, and F. Giesselmann, Systematic variation of length ratio and the formation of smectic A and smectic C phases, ChemPhysChem **11**, 2099 (2010).

[173] T. Itou and A. Teramoto, Triphase equilibrium in aqueous solutions of the rodlike polysaccharide schizophyllan, Macromolecules **17**, 1419 (1984).

[174] T. Itou and A. Teramoto, Multi-phase equilibrium in aquaeous solutions of the triple-helical polysacchardie, schizophyllan, Polym. J. (Tokyo, Jpn.) **16**, 779 (1984).

[175] P. A. Buining and H. N. W. Lekkerkerker, Isotropic-nematic phase separation of a dispersion of organophylic boehmite rods, J. Phys. Chem. **97**, 11510 (1993).

[176] P. J. Flory and A. Abe, Statistical thermodynamics of mixtures of rodlike particles. 1. Theory for polydisperse systems, Macromolecules **11**, 1119 (1978).

[177] T. Odijk and H. N. W. Lekkerkerker, Theory of the isotropic-liquid crystal phase separation for a solution of bidisperse rodlike macromolecules, J. Phys. Chem. **89**, 2090 (1985).

[178] G. J. Vroege and H. N. W. Lekkerkerker, Theory of the isotropic-nematic-nematic phase separation for a solution of bidisperse rodlike particles, J. Phys. Chem. **97**, 3601 (1993).

[179] S. Varga, A. Galindo, and G. Jackson, global fluid phase behavior in binary mixtures of rodlike and platelike molecules, J. Chem. Phys. **117**, 7207 (2002).

[180] A. Galindo, A. J. Haslam, S. Varga, G. Jackson, and A. G. Vanakaras, The phase behavior of a binary mixture of rodlike and disclike mesogens: Monte Carlo simulation, theory, and experiment, J. Chem. Phys. **119**, 5216 (2003).

[181] G. Cinacchi, L. Mederos, and E. Velasco, Liquid-crystal phase diagrams of binary mixtures of hard spherocylinders, J. Chem. Phys. **121**, 3854 (2004).

[182] S. Varga, K. R. Purdy, A. Galindo, S. Fraden, and G. Jackson, Nematic-nematic phase separation in binary mixtures of thick and thin hard rods: results from Onsager-like theories, Phys. Rev. E **72**, 051704 (2005).

[183] G. Cinacchi, Y. Martínez-Ratón, L. Mederos, and E. Velasco, Smectic, nematic, and isotropic phases in binary mixtures of thin and thick hard spherocylinders, J. Chem. Phys. **124**, 234904 (2006).

[184] A. Cuetos, B. Martínez-Haya, S. Lago, and L. F. Rull, Use of Parsons-Lee and Onsager theories to predict nematic and demixing behavior in binary mixtures of hard rods and hard spheres, Phys. Rev. E **75**, 061701 (2007).

[185] J. Philips and M. Schmidt, Bulk phase behavior of binary hard platelet mixtures from density functional theory, Phys. Rev. E **81**, 041401 (2010).

[186] F. A. Escobedo and J. J. de Pablo, Monte Carlo simulation of athermal mesogenic chains: Pure systems, mixtures, and constrained environments, J. Chem. Phys. **106**, 9858 (1997).

[187] P. J. Camp and M. P. Allen, Hard ellipsoid rod-plate mixtures: Onsager theory and computer simulations, Physica A **229**, 410 (1996).

[188] P. J. Camp, M. P. Allen, P. G. Bolhuis, and D. Frenkel, Demixing in hard ellipsoid rod-plate mixtures, J. Chem. Phys. **106**, 9270 (1997).

[189] H. H. Wensink, G. J. Vroege, and H. N. W. Lekkerkerker, Isotropic-nematic density inversion in a binary mixture of thin and thick hard platelets, J. Phys. Chem. B **105**, 10610 (2001).

[190] M. Dijkstra and R. van Roij, Entropy-driven demixing in binary hard-core mixtures: from hard spherocylinders towards hard spheres, Phys. Rev. E **56**, 5594 (1997).

[191] G. Nounesis, S. Kumar, S. Pfeiffer, R. Shahidhar, and C. W. Garland, Experimental observation of a transition between two uniaxial nematic liquid crystal phases, Phys. Rev. Lett. **73**, 565 (1994).

[192] K. R. Purdy, S. Varga, A. Galindo, G. Jackson, and S. Fraden, Nematic phase transitions in mixtures of thin and thick collodial rods, Phys. Rev. Lett. **94**, 057801 (2005).

[193] F. M. van der Kooij, D. van der Beek, and H. N. W. Lekkerkerker, Isotropic-nematic phase separation in suspensions of polydisperse colloidal platelets, J. Phys. Chem. B **105**, 1696 (2001).

[194] W. H. Press, S. A. Teukolsky, W. T. Vetterling, and B. P. Flannery, *Numerical recipes in Fortran 77* (Cambridge University Press, Cambridge, 1992).

[195] M. Franco-Melgar, A. J. Haslam, and G. Jackson, A generalisation of the Onsager trial-function approach: describing nematic liquid crystals with an algebraic equation of state (vol 106, pg 649, 2008), Mol. Phys. **110**, 3107 (2012).

[196] S. M. Walas, *Phase equilibria in chemical engineering* (Butterworth Publishers, Stoneham, 1985).

[197] S. I. Sandler, *Chemical, biochemical, and engineering thermodynamics*, 4th ed. (Wiley, Hoboken, 2006).

[198] T. Bose, C. D. Mukherjee, M. K. Roy, and M. Saha, A molecular mean field theory of re-entrant phases, Mol. Cryst. Liq. Cryst. **126**, 197 (1985).

[199] N. V. Madhusudana and J. Rajan, A simple molecular theory of double re-entrance exhibited by highly polar compounds, Liquid Crystals **7**, 31 (1990).

[200] A. Prasad and M. K. Das, Orientational order parameters of a binary mixture showing both induced smectic and re-entrant nematic phases, Phase Transitions **82**, 780 (2009).

[201] A. Prasad and M. K. Das, Refractive index and orientational order parameter of a polar-polar binary system showing induced smectic A and re-entrant nematic phases, Phase Transitions **83**, 1072 (2010).

[202] N. Kapernaum, F. Knecht, C. S. Hartley, J. C. Roberts, R. P. Lemieux, and F. Giesselmann, Formation of smectic phases in binary liquid crystal mixtures with a huge length ratio, Beilstein Journal of Organic Chemistry **8**, 1118 (2012).

[203] J. Chang and S. I. Sandler, An equation of state for the hard-sphere chain fluid: theory and Monte Carlo simulation, Chem. Eng. Sci. **49**, 2777 (1994).

[204] D. Ghonasgi and W. G. Chapman, A new equation of state for hard chain molecules, J. Chem. Phys. **100**, 6633 (1994).

[205] A. Yethiraj and C. K. Hall, Generalized Flory equations of state for square-well chains, J. Chem. Phys. **95**, 8494 (1991).

[206] M. Banaszak, Y. C. Chiew, and M. Radosz, Thermodynamic perturbation theory: sticky chains and square-well chains, Phys. Rev. E **48**, 3769 (1993).

[207] F. W. Tavares, J. Chang, and S. I. Sandler, Equation of state for the square-well chain fluid based on the dimer version of Wertheim's perturbation theory, Mol. Phys. **86**, 1451 (1995).

[208] F. A. Escobedo and J. J. de Pablo, Simulation and prediction of vapour-liquid equilibria for chain molecules, Mol. Phys. **87**, 347 (1996).

[209] F. W. Tavares, J. Chang, and S. I. Sandler, A completely analytic aquation of state for the square-well chain fluid of variable well width, Fluid Phase Equilibria **140**, 129 (1997).

[210] J. Cui and J. E. Elliott, Phase envelopes for variable width square well chain fluids, J. Chem. Phys. **114**, 7283 (2001).

[211] M. Lee, C. McCabe, and P. T. Cummings, Square-well chain molecules: a semi-empirical equation of state and Monte Carlo simulation data, Fluid Phase Equilibria **221**, 63 (2004).

[212] J. K. Johnson, E. A. Müller, and K. E. Gubbins, Equation of state for Lennard-Jones chains, J. Phys. Chem. **98**, 6413 (1994).

[213] M. Banaszak, Y. C. Chiew, R. O'Lenick, and M. Radosz, Thermodynamic perturbation theory: Lennard-Jones chains, J. Chem. Phys. **100**, 3803 (1994).

[214] D. Ghonasgi and W. G. Chapman, Prediction of the properties of model polymer solutions and blends, AIChE J. **40**, 878 (1994).

[215] E. A. Müller, L. F. Vega, and K. E. Gubbins, Theory and simulation of associating fluids: Lennard-Jones chains with association sites, Mol. Phys. **83**, 1209 (1994).

[216] A. Galindo, C. J. Vega, E. Sanz, L. G. MacDowell, and E. de Miguel, Computer simulation study of the global phase behavior of linear rigid Lennard-Jones chain molecules: comparison with flexible models, J. Chem. Phys. **120**, 3957 (2004).

[217] T. W. Cochran and Y. C. Chiew, Perturbed-chain equation of state for the solid phase, J. Chem. Phys. **124**, 224901 (2006).

[218] F. Alavi and F. Feyzi, A new perturbed-chain equation of state for square-well chains in fluid and solid phases, J. Chem. Phys. **139**, 074104 (2013).

[219] Y. C. Chiew, Percus-Yevick integral equation theory for athermal hard-sphere chains. II. Average intermolecular correlation functions, Mol. Phys. **73**, 359 (1991).

[220] J. Chang and S. I. Sandler, The correlation functions of hardsphere chain fluids: comparison of the Wertheim integral equation theory with the Monte Carlo simulation, J. Chem. Phys. **102**, 437 (1995).

[221] J. Kolafa, S. Labik, and A. Malijevsky, Radial distribution function of the hard sphere fluid, Presented at 18th IUPAC ICCT, Beijing, China, August 17-21, 2004, MD data can be found at http://www.vscht.cz/fch/software/hsmd/ .

[222] H. A. Lorentz, Ueber die Anwendung des Satzes vom Virial in der kinetischen Theorie der Gase, Ann. Phys. **12**, 127 (1881).

[223] D. C. R. Berthelot, Sur le mélange de gaz, Hebd. Séanc. Acad. Sci. Paris **126**, 1703 (1898).

[224] P. Virnau and M. Möller, Calculation of free energy through successive umbrella sampling, J. Chem. Phys. **120**, 10925 (2004).

[225] V. K. Shen and J. R. Errington, Metastability and instability in the Lennard-Jones fluid investigated by transition-matrix Monte Carlo, J. Phys. Chem. B **108**, 19595 (2004).

[226] J. R. Errington, Direct calculation of liquid-vapor phase equilibria from transition matrix Monte Carlo simulation, J. Chem. Phys. **118**, 9915 (2003).

[227] N. B. Wilding and M. Müller, Liquid-vapor asymmetry in pure fluids: a Monte Carlo simulation study, J. Chem. Phys. **102**, 2562 (1995).

[228] N. B. Wilding, Simulation studies of fluid critical behavior, J. Chem. Phys. **9**, 585 (1997).

[229] A. Z. Panagiotopoulos, Monte Carlo methods for phase equilibria of fluids, J. Phys.: Condens. Matter **12**, R25 (2000).

[230] A. Hemmen, J. Gross, and A. Z. Panagiotopoulos, Grand canonical Monte Carlo simulations and histogram reweighting for phase equilibria supported by an analytic equation of state - transferable anisotropic Mie-potential for ethers, submitted to J. Phys. Chem. B (2015).

[231] K. E. Gubbins, W. R. Smith, M. K. Tham, and E. W. Tiepel, Perturbation theory for the radial distribution function, Mol. Phys. **22**, 1089 (1971).

[232] T. Boublík, Hard sphere equation of state, J. Chem. Phys. **53**, 471 (1970).

[233] G. Mansoori, N. F. Carnahan, K. E. Starling, and T. W. Leland, equilibrium thermodynamic properties of the mixture of hard spheres, J. Chem. Phys. **54**, 1523 (1971).

[234] P. Paricaud, A general perturbation approach for equation of state development: applications to simple fluids, ab initio potentials, and fullerenes, J. Chem. Phys. **124**, 154505 (2006).

[235] Y. Tang, Role of the Barker–Henderson diameter in thermodynamics, J. Chem. Phys. **116**, 6694 (2002).

[236] T. van Westen, T. J. H. Vlugt, and J. Gross, On the vapor-liquid equilibrium of attractive chain fluids of variable degree of molecular flexibility, in preparation .

[237] R. Dickman and C. K. Hall, High density Monte Carlo simulations of chain molecules: Bulk equation of state and density profile near walls, J. Chem. Phys. **89**, 3168 (1988).

[238] R. L. Cotterman, B. J. Schwarz, and J. M. Prausnitz, Molecular thermodynamics for fluids at low and high densities. Part I: pure fluids containing small or large molecules, AIChE J. **32**, 1787 (1986).

[239] T. W. Leland, P. S. Chappelear, and B. W. Gamson, Prediction of vapor-liquid equilibria from the corresponding states principle, Inst. Chem. Eng. J. **8**, 482 (1962).

[240] T. W. Leland, J. S. Rowlinson, and G. A. Sather, Statistical thermodynamics of mixtures of molecules of different sizes, Trans. Faraday Soc. **64**, 1447 (1968).

[241] L. Vega, E. de Miguel, L. F. Rull, G. Jackson, and I. A. McLure, Phase equilibria and critical behavior of squarewell fluids of variable width by Gibss ensemble Monte Carlo simulations, J. Chem. Phys. **96**, 2296 (1992).

[242] A. Yethiraj and C. K. Hall, Square-well diatomics: bulk equation of state, density profiles near walls, virial coefficients and coexistence properties, Mol. Phys. **72**, 619 (1991).

[243] H. S. Gulati and C. K. Hall, Fluids and fluid mixtures containing square-well diatomics: equations of state and canonical molecular dynamics simulation, J. Chem. Phys. **107**, 3930 (1997).

[244] A. Lotfi, J. Vrabec, and J. Fischer, Vapour liquid equilibria of the Lennard-Jones fluid from the NpT plus test particle method, Mol. Phys. **76**, 1319 (1992).

[245] C. Vega, C. McBride, F. J. Blas, and A. Galindo, The phase diagram of the two center Lennard-Jones model as obtained from computer simulation and Wertheim's thermodynamic perturbation theory, J. Chem. Phys. **118**, 10696 (2003).

[246] G. S. Dubey, S. O'Shea, and P. A. Monson, Vapour-liquid equilibria for two centre Lennard-Jones diatomics and dipolar diatomics, Mol. Phys. **80**, 997 (1993).

[247] L. G. MacDowell and F. J. Blas, Surface tension of fully flexible Lennard-Jones chains: role of long-range corrections, J. Chem. Phys. **131**, 074705 (2009).

[248] Y. Sheng and A. Z. Panagiotopoulos, Monte Carlo calculation of phase equilibria for a bead-spring polymeric model, Macromolecules **27**, 400 (1994).

[249] J. K. Johnson, J. A. Zollweg, and K. E. Gubbins, The Lennard-Jones equation of state revised, Mol. Phys. **78**, 591 (1993).

[250] R. A. Reis, M. L. L. Paredes, M. Castier, and F. W. Tavares, Evaluation of mixing and combining rules for asymmetric Lennard–Jones chain mixtures: effect of segment diameter, energy interaction, and chain length, Fluid Phase Equilibria **259**, 123 (2007).

[251] A. Yethiraj and C. K. Hall, Monte Carlo simulations and integral equation theory for microscopic correlations in polymeric fluids, J. Chem. Phys. **96**, 797 (1992).

[252] F. J. Blas, A. Ignacio Moreno-Ventas Bravo, J. M. Míguez, M. M. Piñeiro, and L. G. MacDowell, Vapor-liquid interfacial properties of rigid-linear Lennard-Jones chains, J. Chem. Phys. **137**, 084706 (2012).

[253] F. J. Blas, A. I. Moreno-Ventas Bravo, J. Algaba, F. J. Martínez-Ruiz, and L. G. MacDowell, Effect of molecular flexiblity of Lennard-Jones chains on vapor-liquid interfacial properties, J. Chem. Phys. **140**, 114705 (2014).

[254] G. A. Chapela and J. Alejandre, Liquid-vapor interfacial properties of vibrating square well chains, J. Chem. Phys. **135**, 084126 (2011).

[255] G. A. Chapela, E. Díaz-Herrera, J. C. Armas-Pérez, and J. Quintana-H, Effect of flexibility on liquid-vapor coexistence and surface properties of tangent linear vibrating square well chains in two and three dimensions, J. Chem. Phys. **138**, 224509 (2013).

[256] M. Born, On anisotropic fluids. The test of a theory of fluid crystals and of electrical Kerr effects in fluids., Sits. Phys. Maths. **25**, 614 (1916).

[257] M. Born, Electron theory of natural optic rotation processes in isotropic and anisotropic liquids, Ann. Phys. **55**, 177 (1918).

[258] S. C. McGrother, A. Gil-Villegas, and G. Jackson, The liquid-crystalline phase behaviour of hard spherocylinders with terminal point dipoles, J. Phys.: Condens. Matter **8**, 9649 (1996).

[259] A. Gil-Villegas, S. C. McGrother, and G. Jackson, Reaction-field and Ewald summation methdos in Monte Carlo simulations of dipolar liquid crystals, Mol. Phys. **92**, 723 (1997).

[260] S. C. McGrother, A. Gil-Villegas, and G. Jackson, The effect of dipolar interactions on the liquid crystalline phase transitions of hard spherocylinders with central longitudinal dipoles, Mol. Phys. **95**, 657 (1998).

[261] J. S. Duijneveldt, A. Gil-Villegas, G. Jackson, and M. P. Allen, Simulation study of the phase behavior of a primitive model for thermotropic liquid crystals: rodlike molecules with terminal dipoles and flexible tails, J. Chem. Phys. **112**, 9092 (2000).

[262] A. Z. Panagiotopoulos, Direct determination of phase coexistence properties of fluids by Monte-Carlo simulation in a new ensemble, Mol. Phys. **61**, 813 (1987).

[263] W. Shi and E. J. Maginn, Continuous Fractional Component Monte Carlo: an adaptive biasing method for open system atomistic simulations, J. Chem. Theory Comput. **3**, 1451 (2007).

[264] W. Shi and E. J. Maginn, Improvement in molecule exchange efficiency in Gibbs ensemble Monte Carlo: development and implementation of the continuous fractional component move, J. Comp. Chem. **29**, 2520 (2008).

[265] A. Torres-Knoop, S. P. Balaji, T. J. H. Vlugt, and D. Dubbeldam, A comparison of advanced Monte Carlo methods for open systems: CFCMC vs CBMC, J. Chem. Theory Comput. **10**, 942 (2007).

[266] S. Varga, D. C. Williamson, and I. Szalai, Square-well fluid based decoupling approximation for system of hard non-spherical particles with spherical square-wells, Mol. Phys. **96**, 1695 (1999).

[267] D. Garcia, D. C. Williamson, and A. Martinez-Richa, Effects of molecular geometry on liquid crystalline phase behaviour: isotropic-nematic transition, Mol. Phys. **98**, 179 (2000).

[268] E. de Miguel, E. M. del Río, J. T. Brown, and M. P. Allen, Effect of the attractive interactions on the phase behavior of the Gay–Berne liquid crystal model, J. Chem. Phys. **105**, 4234 (1996).

[269] W. G. Miller, C. C. Wu, E. L. Wee, G. L. Santee, J. H. Rai, and K. G. Goebel, Thermodynamics and dynamics of polypeptide liquid crystals, Pure Appl. Chem. **38**, 37 (1974).

[270] M. Warner and P. J. Flory, The phase equilibria in thermotropic liquid crystalline systems, J. Chem. Phys. **73**, 6327 (1980).

[271] E. L. Wee and W. G. Miller, Liquid crystal-isotropic phase equilibria in the system poly-γ-benzyl-α,L-glutamate-dimethylformamide, J. Phys. Chem. **75**, 1446 (1971).

[272] A. Hill and A. M. Donald, Gelation in the poly (γ-Benzyl-L-Glutamate)-benzyl alchol system, Mol. Cryst. Liq. Cryst. **153**, 395 (1987).

[273] T. Itou and A. Teramoto, Multi-phase equilibrium in aqueous solutions of the triple-helical polysaccharide, schizophyllan, Polymer Journal **16**, 779 (1984).

[274] T. Inoue, S. Ogata, M. Kakimoto, and Y. Imai, Triphase equilibrium in aqueous solutions of the rodlike polysaccharide schizophyllan, Macromolecules **17**, 1419 (1984).

[275] D. Vijayaraghavan and S. Kumar, Effect of slow cooling on a discotic nematic liquid crystal: evidences for nematic–nematic transitions, Mol. Cryst. Liq. Cryst. **452**, 11 (2006).

[276] P. Attard, Spherically inhomogeneous fluids. I. Percus-Yevick hard spheres: osmotic second virial coefficients and triplet correlation functions, J. Chem. Phys. **91**, 3072 (1989).

[277] P. Attard and G. Stell, Three-particle correlations in a hard-sphere fluid, Ch. Phys. Lett. **189**, 128 (1992).

Summary

We developed an equation of state (EoS) for describing the isotropic- and nematic fluid-phase behaviour of a prototypical model for liquid crystal (LC) molecules of prolate type. The molecular model assumes a LC molecule as a chain of equally-sized tangent spheres, the interaction of which is described by a Lennard-Jones potential. To model the typical structure of real (thermotropic) LC molecules, one part of the chain is allowed in a rigid linear conformation (referred to as 'rod'), while the remaining part is fully flexible (referred to as 'coil'). By changing the ratio 'rod' to 'coil', the flexibility of a rod-coil molecule can be varied.

The EoS was developed using a perturbation theory. The description of the repulsive reference fluid (part A of this thesis) was obtained from combining a novel hard-chain EoS for isotropic fluids (Chapter 3) with a Vega-Lago rescaled Onsager theory (Chapter 4-5) and an accurate analytical approximation for the orientation-dependent pair-excluded volume of rod-coil molecules (Chapter 2). Due to the use of the Onsager trial function for describing the orientational distribution function, the reference EoS could be recast to a compact analytical form. Theoretical results for the isotropic-nematic phase equilibrium and nematic order parameter of hard rod-coil molecules were extensively tested against results obtained from molecular simulations. Both, for pure-component systems and mixtures, excellent agreement was obtained.

In part B of this thesis, we extended the reference model with a Lennard-Jones potential for describing dispersion interactions between the segments of chains. A Helmholtz energy contribution for describing these interactions was developed by applying a second order perturbation theory of Barker and Henderson. Perturbation terms were calculated using a novel effective segment diameter for chain fluids (Chapter 6). The radial distribution function as required in the perturbation theory was obtained from Monte Carlo simulations of fully flexible chain fluids. Theoretical results for phase equilibria (*e.g.* vapour-liquid, vapour-nematic, liquid-nematic) of LJ chains with variable degree of molecular flexibility were compared to results obtained from molecular simulations. Overall, an accurate comparison was obtained. Especially the accurate description of isotropic-nematic equilibria (Chapter 7) is noteworthy. Given that the perturbation terms involve no explicit dependence on the orientation of molecules we conclude that an EoS contribution for describing dispersion interactions in real LCs can be obtained from conventional theoretical methods designed for isotropic fluids, such as a (PC-)SAFT approach.

Samenvatting

In dit werk ontwikkelen we een toestandsvergelijking voor het beschrijven van het isotrope- en nematische fase-gedrag van een prototype model voor een (prolaat) vloeibaar kristal. Het moleculaire model beschrijft de moleculen van een vloeibaar kristal (nematogenen) als ketens van identieke bollen, wiens interactie wordt beschreven met een Lennard-Jones potentiaal. Om de typische moleculaire structuur van echte (thermotrope) nematogenen te modelleren is een deel van de keten vastgelegd in een rigide lineaire configuratie (waaraan gerefereerd wordt als 'rod'), terwijl de rest van de keten volledig flexibel is en dus alle configuraties kan aannemen (waaraan gerefereerd wordt als 'coil'). Door de ratio 'rod' ten opzichte van 'coil' te veranderen kan de flexibiliteit van een rod-coil molecuul gevarieerd worden.

De toestandsvergelijking is ontwikkelt door middel van een perturbatietheorie. De beschrijving van de repulsieve referentie-fluid (deel A van dit proefschrift) is verkregen door het combineren van een nieuwe toestandsvergelijking voor de isotrope fase van harde-keten-moleculen (Hoofdstuk 3) met een Vega-Lago geschaalde Onsager-theorie (Hoofdstuk 4 en 5) en een nauwkeurige analytische benadering voor het oriëntatie-afhankelijke uitgesloten volume van twee rod-coil moleculen (Hoofdstuk 2). Door gebruik te maken van de Onsager-trial-functie kon de toestandsvergelijking voor de referentie-fluid herschreven worden tot een compacte, analytische vorm. Theoretische resultaten voor het evenwicht tussen de isotrope en nematische fase en de orde-parameter bij evenwicht zijn uitgebreid vergeleken met resultaten verkregen uit moleculaire simulaties. Zowel voor systemen met maar één component als voor mengsels van meerdere componenten vinden we goede overeenstemming tussen theorie en simulaties.

In deel B van dit proefschrift wordt het referentie-model uitgebreid met een Lennard-Jones potentiaal voor het beschrijven van (dispersieve) attractieve interacties tussen de segmenten van de ketenmoleculen. Een Helmholtz-energie bijdrage voor het beschrijven van deze interacties is ontwikkelt door een tweede-orde perturbatietheorie van Barker en Henderson toe te passen. De perturbatie-bijdragen zijn berekend op basis van een nieuwe effectieve segmentgrootte voor ketenmoleculen (Hoofdstuk 6). The radiale verdeelfunctie is verkregen uit Monte Carlo simulaties voor volledig flexibele ketenmoleculen. Theoretische resultaten voor faseevenwichten (*e.g* damp-vloeistof, damp-nematisch, vloeistof-nematisch) van LJ ketenmoleculen met variabele graad van moleculaire flexibiliteit zijn uitgebreid vergeleken met resultaten verkregen uit moleculaire simulaties. Theorie en simulaties zijn in goede overeenstemming. Vooral de nauwkeurige beschrijving van het isotroop-nematisch evenwicht (Hoofdstuk 7) is opmerkelijk. Gegeven dat de perturbatie-bijdragen niet expliciet afhangen van de oriëntaties van de ketenmoleculen, kan er geconcludeerd worden dat een Helmholtz-energie bijdrage voor het beschrijven van dispersie interacties in echte vloeibare kristallen verkregen kan worden uit conventionele methodes zoals ontwikkelt voor gewone (isotrope) vloeistoffen, zoals een (PC-)SAFT aanpak.

Curriculum Vitæ

Thijs van Westen

12-12-1986 Born in Middelharnis, The Netherlands.

Education

1998–2004 Pre-university education (*cum laude*)
RGO, Middelharnis

2004–2010 Master of Science, Chemical Engineering
Delft University of Technology
Thesis: Using a physically-based equation of state for fitting force field parameters
Supervisors: Prof. Joachim Gross, dr. Thijs J. H. Vlugt

Professional

2005-2009 Chemistry teacher
SSL/University of Leiden
Chemistry training course for high-school students.

2010 Internship
Infochem, London
Project: Extending the Multiflash phase equilibrium simulator by adding the polar and polarisable terms of the Helmholtz energy to the in-house PC-SAFT code

2010–2014 Phd student
Delft University of Technology
Thesis: The development of an equation of state for nematic liquid crystals: Towards a molecular-based description
Promotors: Prof. Joachim Gross, Prof. Thijs J. H. Vlugt

List of Journal Publications

10. **Oyarzún, B.**; van Westen, T.; Vlugt, T. J. H., *Liquid-crystal phase equilibria of Lennard-Jones chains*, in preparation

9. **van Westen, T.**; Oyarzún, B.; Vlugt, T. J. H.; Gross, J., *An analytical equation of state for describing isotropic-nematic phase equilibria of Lennard-Jones chain fluids with variable degree of molecular flexibility*, J. Chem. Phys. **142**, 244903 (2015)

8. **van Westen, T.**; Vlugt, T. J. H.; Gross, J., *On the vapor-liquid equilibrium of attractive chain fluids with variable degree of molecular flexibility*, J. Chem. Phys. **142**, 224504 (2015)

7. **Oyarzún, B.**; van Westen, T.; Vlugt, T. J. H., *Isotropic-nematic phase equilibria of hard-sphere chain fluids—Pure components and binary mixtures*, J. Chem. Phys. **142**, 064903 (2015)

6. **van Westen, T.**; Oyarzún, B.; Vlugt, T. J. H.; Gross, J., *An equation of state for the isotropic phase of linear, partially flexible and fully flexible tangent hard-sphere chain fluids*, Mol. Phys. **112**, 919–928 (2014)

5. **van Westen, T.**; Vlugt, T. J. H.; Gross, J., *The isotropic-nematic and nematic-nematic phase transition of binary mixtures of tangent hard-sphere chain fluids—An analytical equation of state*, J. Chem. Phys. **140**, 034504 (2014)

4. **Oyarzún, B.**; van Westen, T.; Vlugt, T. J. H., *The phase behavior of linear and partially flexible hard-sphere chain fluids and the solubility of hard spheres in hard-sphere chain fluids*, J. Chem. Phys. **138**, 204905 (2013)

3. **van Westen, T.**; Oyarzún, B.; Vlugt, T. J. H.; Gross, J., *The isotropic-nematic phase equilibrium of tangent hard-sphere chain fluids—Pure components*, J. Chem. Phys. **139**, 034505 (2013)

2. **van Westen, T.**; Vlugt, T. J. H.; Gross, J., *An analytical approximation for the orientation-dependent excluded volume of tangent hard sphere chains of arbitrary chain length and flexibility*, J. Chem. Phys. **137**, 044906 (2012)

1. **van Westen, T.**; Vlugt, T. J. H.; Gross, J., *Determining force field parameters using a physically based equation of state*, J. Phys. Chem. B **115**, 7872–7880 (2011).

Acknowledgement

Doing a PhD can at times be a frustrating endeavour: on the practical side, the work is generally slow and requires a great deal of patience and perseverance; on the social side, the benefit of the work you are doing is not always known beforehand, and is usually not easily explained to a broad audience. The latter especially applied to the work performed in this thesis. Telling people you are trying to describe the phase behaviour of hard-sphere chains simply doesn't do it at birthdays and other social gatherings. In that respect, Lennard-Jones chains don't do much better. Perhaps the work of the theoretician is not meant for the limelights...

Besides these small struggles at the social front, I experienced my PhD as a wonderful experience. Being part of the quest for new knowledge is exciting and challenging. It is intriguing, that many of the complex phenomena occurring in nature are explained by a handful of laws which can be formulated in a simple mathematical form. The observation that phenomena as complex as self-organization of molecules, particles, or even organisms, can be explained by the mere basic laws of energy conservation and entropy maximization is astonishing, and for me, clearly shows the power of the scientific method.

In these last couple of years, I have had the pleasure to work with—and learn from—some very talented people. First and foremost, I'd like to thank my supervisors: Joachim Gross and Thijs Vlugt.

Joachim, you truly have been a mentor. Our collaboration started already during my studies, and I hope will stand for years to come. I'd like to thank you for bringing fundamentals into the curriculum at the time of my studies in Delft, for introducing me to the wonderful field of statistical mechanics, for being the supervisor of my MSc thesis, and (hopefully) soon, for being the promotor of my PhD thesis. You are a constant inspiration. The enthusiasm with which you approach your lectures, research, and life in general, should be an example for everyone. I really enjoyed our weekly Friday-afternoon-Skype sessions (which usually put me in a good mood for the weekend), and the regular trips to your group in Stuttgart, including playing football with you and your friends, and our (un)productive evening sessions. I heard you recently switched from football to karate. Some would say that after reaching a certain age you should leave such things for the younger—but I leave that for you to decide.

Thijs, I have learned a great many things from you. I still remember the day I walked into your office for a crash-course on molecular simulations. Three sessions of an hour proved sufficient to produce a first paper on the subject. This doesn't show the field of molecular simulations is a simple one; it shows that when you put some effort into something things tend to work out. Our collaboration has always been productive; I hope we can continue working together. I have come to know you as an excellent scientist, a fast thinker, and a man with a weakness for theme parks like de Efteling. Up till now, you still have the world-speed-record in e-mail answering; I hope you can maintain your pole position. I wish you all the best with

little Sophie.

Another indispensable force during my PhD was Bernardo Oyarzun. Bernardo, I can honestly say that without your extensive work on molecular simulations this thesis would have been much less convincing. Thanks for the fruitful collaboration; I hope we will continue to do so in the near future. I should also thank you for the many discussions we had on classical thermodynamics. I know I'm not the most easily convinced (some would call it stubborn), but I must admit you were usually in the right. Besides work-related things, I'd like to thank you for two 'awesome' road-trips through the USA. Driving without a plan: not for me as you know; however, a dear memory.

Besides my direct colleagues, I'd like to thank the others at ETh, Process&Energy, and the Stuttgart group. Special thanks to Theo de Loos, Dick Bedeaux, Brian, Sayee, Sondre, Mahinder, Pablo, and Mariette, for helpful discussions and making the office a better place. I wish you all the best.

This also seems the place to thank other teachers that have been an inspiration. Prof. Harrie van den Akker, thanks to teachers like you Universities primarily remain institutes of education instead of mere institutes of science. I won't easily forget your lectures on transport phenomena, in which iterative calculations were simply done on the chalkboard. Happy days! Meneer Leijdens, you were the one that introduced me to chemistry. In your classes I came to realize the natural sciences were the path to go. Thanks for that!

This acknowledgement would not be complete without thanking my dear family and friends. I consider myself lucky with some life-long friendships; the Flakkee-connection seems one that is not easily broken. I'd also like to thank the people from KMT81, the student house a resided in Delft. Besides getting a second education (not always for the good), I made some solid friendships there, for which I'm grateful. Finally, I'd like to thank all the friends I made in Rotterdam these last couple of years. Dear friends, you provide my quality of life; and I thank you for it.

Dear parents, beste ouders (en tegenwoordig opa & oma), dit lijkt me het juiste moment om jullie te bedanken voor de geweldige en liefdevolle opvoeding die jullie mij hebben gegeven. Mijn jongere jaren zijn vrijwel onbezorgd geweest, en dit is vooral aan jullie te danken. Jullie hebben mij altijd in staat gesteld om mijn dromen en doelen te verwezenlijken, zelfs als jullie jezelf daarvoor weg moesten cijferen. Ik ben er van overtuigd dat deze onvoorwaardelijke steun mij heeft gebracht tot waar ik nu ben. Als Manouk en ik onze Lucas net zo'n fijne jeugd kunnen geven als jullie mij, dan ben ik (en waarschijnlijk Lucas later ook) een tevreden man. Liefs, Thijs.

Willem, grote broer, beste vriend. Alhoewel je waarschijnlijk liever door je platencollectie gaat dan door dit proefschrift, hoop ik dat dit dankwoord je toch bereikt. Zonder al te sentimenteel te worden wil ik je zeggen dat ik erg dankbaar ben voor onze vriendschap. Ik denk dat deze uniek is en dat we daar best trots op mogen zijn.

Lieve Manouk, mijn liefde. Jij bent degene die het meest heeft meegekregen van het proces dat geleid heeft tot dit proefschrift. Bedankt voor al je geduld en inlevingsvermogen. Ik weet dat het niet altijd makkelijk is om mijn partner te zijn, toch voelt jouw liefde als onvoorwaardelijk; hier ben ik je ontzettend dankbaar voor.

We hebben onlangs een kleine bekroning gekregen op onze 8 jaar samen. Bij het schrijven van dit stukje ligt hij naast me in de box te brabbelen, wat een heerlijk ventje! Met veel liefde, Thijs.